“Visualization of dopaminergic signaling in the retina with optogenetic sensors”

Von der Fakultät für Mathematik, Informatik und Naturwissenschaften der RWTH Aachen University zur Erlangung des akademischen Grades einer Doktorin der Naturwissenschaften genehmigte Dissertation

vorgelegt von

Master of Science
Anna Sieben

aus Hagen

Berichter: Universitätsprofessor Dr. Frank Müller

Universitätsprofessor Dr. Marc Spehr

Tag der mündlichen Prüfung: 31.05.2016

Diese Dissertation ist auf den Internetseiten der Universitätsbibliothek online verfügbar.

Content

Zusammenfassung V

Abstract VII

Abbreviations IX

1. Introduction 1

1.1. The retina and phototransduction 1

1.2. The dopaminergic system in the retina 4
1.2.1. Dopaminergic amacrine cells 4
1.2.2. Dopamine receptors 5
1.2.3. Dopamine's role in light adaptation 7

1.3. Genetically encoded biosensors 9
1.3.1. FRET-based biosensors 9
1.3.1.1. Biosensors for the detection of changes in the cAMP/PKA cascade 10
1.3.1.2. TN-L15: A FRET-based biosensor for the detection of changes in $[Ca^{2+}]_i$ 12
1.3.2. Detection of neurotransmitter release with synapto-pHluorin 12
1.3.3. Sensors based on permutated GFP 13

1.4. The chemical Ca^{2+} indicator Fluo-4 14

1.5. Objective of the study 14

2. Materials and Methods 16

2.1. Animals 16

2.2. General buffers and solutions 16

2.3. Molecular biology 19
2.3.1. Plasmids 19
2.3.2. Kits 19
2.3.3. Transformation of competent cells 19
2.3.4. DNA isolation 20
2.3.5. Quantification of nucleic acids 20
2.3.6. Restriction digestion 21
2.3.7. Ligation 21
2.3.8. Separation of nucleic acids in agarose gels 22
2.3.9. Isolation of DNA fragments from preparative agarose gels 23
2.3.10. Driving gene expression by the TH promoter 23

2.4. Cell culture 27
2.4.1. Stable cell line culture 27
2.4.1.1. Human Embryonic Kidney 293 cells 27
2.4.1.2. Splitting and seeding cells 27
2.4.1.3. Coating coverslips with Poly-L-Lysine 28
2.4.1.4. Liposome-mediated transfection 28
2.4.1.5. AAV transduction 28
2.4.2. Primary culture of dissociated retinal neurons 29

2.4.2.1. Preparation of coverslips 29
2.4.2.2. Isolation of retinae 29
2.4.2.3. Dissociation of isolated retinae 29
2.4.2.4. AVV transduction 30
2.4.2.5. Liposome-mediated transfection 30
2.4.2.6. Fixation of cultured cells 31
2.5. Ocular Injections 31
2.5.1. Equipment/Micro injection system 31
2.5.2. Anesthesia 32
2.5.3. Operation procedure 32
2.5.4. *In vivo* electroporation 33
2.6. Preparation of living slices of the retina 33
2.6.1. Setting up the vibratome 33
2.6.2. Isolation of the retina 34
2.6.3. Preparation and embedding of the retina 34
2.6.4. Transferring retinal slices into the imaging chamber 34
2.7. Widefield-Imaging 35
2.7.1. Imaging setup 35
2.7.2. Perfusion chamber 35
2.7.3. Ca^{2+}-imaging with Fluo-4 and GCaMP3.0 35
2.7.3.1. Loading of the cells with Fluo-4 35
2.7.3.2. Data acquisition 35
2.7.3.3. Data evaluation 36
2.7.4. FRET- based imaging 36
2.7.4.1. TN-L15 imaging in isolated retinal wholemounts 36
2.7.4.2. FRET-based imaging in cultured cells 37
2.7.4.3. Data acquisition 37
2.7.4.4. Data evaluation 37
2.8. Immunochemistry 38
2.8.1. Antibody staining of cultured cells 38
2.8.2. Antibody staining of retinal cryosections 38
2.8.2.1. Fixation and cryoprotection of retinae 38
2.8.2.2. Cryosectioning 38
2.8.2.3. Staining procedure 38
2.8.3. Antibody staining of retinal wholemounts 39
2.8.4. Antibodies 39
2.9. Confocal Microscopy 41
2.10. Pharmaceuticals 42
2.11. Software 43
3. Results 44
3.1. Immunocytochemical analysis of the dopaminergic system in retinal cultured neurons 44
3.1.1. Identification of retinal cell types that are targets for dopaminergic modulation 44
3.1.2. Identification of D1R downstream signaling molecules in retinal cultured neurons .48
3.2. Using FRET-based biosensors for the visualization of the cAMP/PKA pathway 51

3.2.1. Characterization of EPAC1-camps and AKAR4 in HEK293 cells 51
3.2.2. Using EPAC1-camps and AKAR4 in cultured retinal neurons 53
3.2.2.1. DA induced changes in $[cAMP]_i$ and PKA activity 53
3.2.2.2. Comparison of EPAC1-camps and AKAR4 56
3.2.2.3. The DA-induced increase in PKA activity is due to activation of D1Rs 57
3.2.2.4. Does the same neuron express both types of DRs? 60
3.3. Impact of DA on $[Ca^{2+}]_i$ in cultured retinal neurons 63
3.3.1. DA triggers a change in $[Ca^{2+}]_i$ in cultured retinal neurons 63
3.3.2. Involvement of different dopamine receptor types 67
3.3.2.1. D1Rs are partly involved in the increase in $[Ca^{2+}]_i$ 68
3.3.2.2. Are D2Rs involved in DA-induced changes in $[Ca^{2+}]_i$? 70
3.3.3. Investigation of the classical DR signaling pathway 72
3.3.3.1. The role of external Ca^{2+} in DA-induced changes in $[Ca^{2+}]_i$ 72
3.3.3.2. Role of Ca^{2+}-channels in DA-induced changes in $[Ca^{2+}]_i$ 74
3.3.3.3. PKA is a mediator of DA-induced increase in $[Ca^{2+}]_i$ 77
3.3.3.4. Influence of phosphatases PP1 and PP2A 78
3.3.3.5. The role of Gβγ in DA-induced changes in $[Ca^{2+}]_i$ 80
3.3.4. Investigation of alternative pathways 81
3.3.4.1. Does blockade of SERCA affect DA-induced changes in $[Ca^{2+}]_i$? 82
3.3.4.2. The role of phospholipase C 84
3.4. Investigation of dopaminergic signaling *in vivo* 86
3.4.1. Towards the visualization of DA release 87
3.4.1.1. Does the TH promoter yield cell type-specific expression of GFP? 87
3.4.1.2. The sensor synapto-pHluorin is expressed in retinal neurons 90
3.4.2. Using AAVs as gene shuttles to express sensor proteins 91
3.4.2.1. AAV2-GFP infects target neurons of dopaminergic signaling in culture 92
3.4.2.2. AAV2-GFP infects target neurons of dopaminergic signaling *in vivo* 93
3.4.2.3. Does AAV2 infect dopaminergic neurons *in vivo*? 96
3.4.3. Viral expression of the FRET-based cAMP sensor EPAC1-camps 97
3.4.3.1. AAV2-mediated expression of EPAC1-camps in cultured cells 97
3.4.3.2. Is EPAC1-camps expressed *in vivo* after viral infection with AAV2? 100
3.4.4. Alternative approach: *in vivo* electroporation 103
3.4.5. Impact of dopaminergic signaling on $[Ca^{2+}]_i$ in GCs of the intact retina 105
3.4.5.1. DA altered $[Ca^{2+}]_i$ in TN-L15-positive GCs 106
3.4.5.2. Is there a correlation between the type of GC and type of response to DA? 108
3.4.5.2.1. Large GCs responded with a decrease in $[Ca^{2+}]_i$ 108
3.4.5.2.2. Differentiation between ON- and OFF-GCs via L-AP4 111
3.4.5.3. Are the DA-induced changes in $[Ca^{2+}]_i$ due to a network response or due to direct action at GCs? 114
3.4.5.3.1. Role of the excitatory input in DA-induced changes in $[Ca^{2+}]_i$ 114
3.4.5.3.2. Role of the inhibitory input in DA-induced changes in $[Ca^{2+}]_i$ 116

4. Discussion 120

4.1. DA modulates the intracellular concentration of second messengers 120
4.1.1. Activation of D1Rs induces an increase in $[cAMP]_i$ and PKA activity 120
4.1.2. DA changes $[Ca^{2+}]_i$ in retinal cultured neurons 122

4.1.2.1. The DA-induced increase in $[Ca^{2+}]_i$ is caused by the interplay of different parameters 122
4.1.2.2. The origin of the DA-induced decrease in $[Ca^{2+}]_i$ is still undefined 125
4.2. Application of genetically encoded sensors *in vivo* 127
4.2.1. Expression of FRET-based biosensors in the intact retina 127
4.2.2. Cell-specific expression of sensor proteins 129
4.2.3. AAV troubleshooting 130
4.3. DA modulates $[Ca^{2+}]_i$ in GCs of the intact retina 131
4.3.1. GCs of the decrease type 131
4.3.1.1. Are GCs of the decrease type ON-alpha-GCs? 131
4.3.1.2. Is the DA-triggered decrease in $[Ca^{2+}]_i$ in GCs due to a network response? 135
4.3.2. GCs of the increase type 138
4.3.2.1. Are GCs of the increase type W3 GCs? 138
4.3.2.2. Is the DA-triggered increase in $[Ca^{2+}]_i$ in GCs due to a network response? 139
4.4. How do changes in second messenger concentrations affect signal processing in the retinal network? 140
4.5. Outlook 144
References 146
Appendix 160
Acknowledgements 166

Zusammenfassung

Die Netzhaut kann sich an Lichtintensitäten adaptieren, die mehrere Größenordnungen überspannen. Dopamin (DA) ist ein Neuromodulator, der von einem Amakrinzelltyp in der Retina freigesetzt wird und dem bereits in den frühen 80er Jahren eine bedeutende Rolle bei der Licht-Adaptation zugesprochen wurde. DA vermittelt seine Wirkung über G-Protein gekoppelte Rezeptoren (GPCRs), die in zwei Familien unterteilt werden: Die D1-Familie (D1R), deren Aktivierung zu einer Steigerung der Adenylatzyklase (ACy)-Aktivität führt und die D2-Familie (D2R), deren Aktivierung eine Verringerung der ACy-Aktivität bewirkt. Der DA-Rezeptor-vermittelte (DR) Signalweg ist also auch an die Regulierung der Proteinkinase A (PKA)-Aktivität gekoppelt. Neben diesem klassischen cAMP (zyklisches Adenosinmonophosphat)/PKA-vermittelten Signalweg wurden Alternativwege beschrieben, die unter anderem zu einer Veränderung in der intrazellulären Konzentration des zentralen sekundären Botenstoffes Calcium ($[Ca^{2+}]_i$) führen können. Bislang sind viele verschiedene Wirkungen von DA in der Retina bekannt, allerdings sind die zu Grunde liegenden Signalwege weitgehend ungeklärt. Um ein besseres Verständnis dieser Mechanismen zu erlangen, sollten in der vorliegenden Arbeit sowohl die Regulation der DA-Freisetzung als auch DA-vermittelte Signalwege in Zielzellen untersucht werden. Als Modell diente die Mausretina.

Um die Freisetzung von DA aus den dopaminergen Amakrinzellen zeitlich aufgelöst zu detektieren, sollte der genetisch-codierte Sensor Synapto-pHluorin spezifisch in diesen Zellen exprimiert werden. Zu Testzwecken wurde zunächst ein Konstrukt kloniert, in dem die Expression des Markerproteins GFP (grün-fluoreszierendes Protein) durch den Tyrosinhydroxylase (TH)-Promoter kontrolliert wird. Nach Expression dieses Konstrukts in HEK293-Zellen und retinalen Kulturen ergab sich, dass der Promoter nicht die erwartete Spezifität aufwies: GFP wurde in TH-negativen Zellen exprimiert. Die Auswirkung von DA auf die intrazelluläre cAMP-Konzentration in Zielzellen wurde unter Verwendung der genetisch codierten Förster-Resonanz-Energie-Transfer (FRET)-Sensoren EPAC1-camps und AKAR4 untersucht. Zunächst wurden die Sensoren sowohl in HEK293-Zellen als auch in retinalen Kulturen via Lipofektamin-Transfektion exprimiert und charakterisiert. Beide Sensoren ermöglichten es, die Produktion und den Abbau von cAMP nach Stimulation von GPCRs zu verfolgen. Mittels pharmakologischer Methoden wurde gezeigt, dass die Aktivierung von D1R zu einem Anstieg in der PKA-Aktivität in einer Population von retinalen Neuronen führte.

In Ca^{2+}-Imaging-Experimenten mit Fluo-4 beladenen Zellen in Kultur wurde gezeigt,

dass DA die $[Ca^{2+}]_i$ in etwa 20% der Zellen verändert. Es wurden verschiedene Antworttypen gefunden. Pharmakologische Untersuchungen gaben Hinweise darauf, dass an dem DA-vermittelten Anstieg im $[Ca^{2+}]_i$ sowohl der klassische D1R/PKA-Signalweg als auch alternative Signalwege beteiligt sind. Bislang konnte kein DR-Typ identifiziert werden, der den DA-induzierten Abfall in $[Ca^{2+}]_i$ vermittelt.

Um genetisch-codierte Sensoren in der intakten Retina anzuwenden, wurde die Methode des viralen Gentransfers etabliert. Adeno-assoziierte Viren (AAVs) dienten dabei als Gen-Fähren. Es wurde gezeigt, dass AAV2 sowohl *in vitro* als auch *in vivo* Neuronen transduzierte, die durch DA reguliert werden. Dopaminerge Amakrinzellen hingegen wurden nicht infiziert. Auch die virale Expression des EPAC1-camps Sensors war nicht erfolgreich, obwohl kleinere Sensoren wie GCaMP3.0 funktionell mit dieser Methode exprimiert werden konnten.

Unter Verwendung einer transgenen Mauslinie, die den genetisch-codierten Ca^{2+}-Sensor TN-L15 in Ganglienzellen (GC) exprimiert, wurde gezeigt, dass DA die $[Ca^{2+}]_i$ in ~50% der GC beeinflusst. Es wurden verschiedene Antworttypen gefunden. Mittels pharmakologischer und fluoreszenzmikroskopischer Methoden wurde nachgewiesen, dass GC verschiedener Antworttypen sich morphologisch (Somagröße) und physiologisch (ON-/OFF-Typ) unterscheiden. Gezielte Blockade des exzitatorischen oder inhibitorischen Eingangs gab Hinweise darauf, dass ein Teil des DA-Effekts auf direkte Wirkung von DA an der GC, ein Teil auf die präsynaptische Wirkung von DA im retinalen Netzwerk zurückgeht.

Abstract

The retina is able to adapt to light intensities that range over several orders of magnitude. Dopamine (DA) is a neuromodulator that is released by one amacrine cell type in the retina. In the early eighties, DA was already discussed to play a central role in light adaptation processes. DA exerts it effects via G-protein coupled receptors (GPCRs), which were grouped into two families: the D1-family (D1R), whose activation leads to an increase in adenylate cyclase (ACy) activity, and the D2-family (D2R), whose activation reduces the activity of the ACy. Thus, these DA-receptor (DR)-mediated pathways are coupled to the regulation of protein kinase A (PKA) activity. Besides this classical cyclic adenosine monophosphate (cAMP)/PKA cascade, multiple alternative pathways have been described which amongst others may lead to changes in the intracellular concentration of the central second messenger calcium ($[Ca^{2+}]_i$). Up to now, in the retina multiple effects of DA are known but the underlying mechanisms are still unresolved. To gain a better comprehension of these mechanisms, the present study was designed to investigate the regulation of DA release as well as the DA-mediated pathways in target cells. The mouse retina served as model system.

To monitor the release of DA in the retina in a time-resolved manner, the genetically-encoded sensor synapto-pHluorin should specifically be expressed in dopaminergic amacrine cells. For test purposes, a construct was cloned in which the expression of the marker protein GFP (green fluorescent protein) was controlled by the tyrosine hydroxylase (TH) promoter. Expression of this construct in HEK293 cells and retinal neurons in culture revealed that the promoter did not exhibit the expected specificity: GFP was expressed in TH-negative cells.

The impact of DA on the intracellular cAMP concentration ($[cAMP]_i$) in target cells was investigated using the genetically-encoded Förster-resonance-energy-transfer (FRET)-based sensors EPAC1-camps and AKAR4. Initially, the two sensors were expressed in HEK293 cells and in cultured retinal neurons via Lipofectamine-transfection and were characterized. Both sensors made it possible to visualize production and degradation of cAMP after stimulation of GPCRs. Using a pharmacological approach, it was shown that the activation of D1R triggered an increase in PKA activity in a population of retinal neurons.

In Ca^{2+}-imaging experiments with Fluo-4-loaded cultured retinal neurons, it was demonstrated that DA alters $[Ca^{2+}]_i$ in about 20% of cells. Different response types were

found. Pharmacological investigations led to the assumption that the classical D1R/PKA-pathway as well as alternative pathways participate in DA-induced increases in $[Ca^{2+}]_i$. The DR-type mediating the DA-induced decrease in $[Ca^{2+}]_i$ could not be identified, yet. In order to employ genetically-encoded sensors in the intact retina, the method of viral gene transfer was established. Adeno-associated viruses (AAVs) served as gene-shuttles. It was shown that AAV2 transduced neurons *in vitro* as well as *in vivo* that are regulated by DA. However, dopaminergic amacrine cells were never infected. In addition, viral expression of EPAC1-camps was not successful in retinal neurons although smaller sensors such as GCaMP3.0 could be functionally expressed with this method. Under the use of a transgenic mouse line that expresses the genetically-encoded Ca^{2+}-sensor TN-L15 in ganglion cells (GC), it was shown that DA influences $[Ca^{2+}]_i$ in ~50% of GCs. Different response types were found. Using pharmacological and fluorescence-microscopical methods it was proven that GCs of distinct response types differed morphologically (soma size) and physiologically (ON-/OFF-type). Selective blockade of the excitatory or inhibitory input to GCs indicated that a part of the DA-effect was based on a direct action of DA at the GC itself, while another part was based on the presynaptic effect of DA in the retinal network.

Abbreviations

$[Ca^{2+}]_i$	intracellular calcium concentration
$[cAMP]_i$	intracellular cAMP concentration
⌀	diameter
°C	degree celsius
AAV	adeno-associated virus
AC	amacrine cell
ACh	acetylcholine
ACy	adenylate cyclase
AKAR4	A kinase activity reporter 4
AM	acetoxymethyl ester
Amp	ampicillin
AMPA	α-amino-3-hydroxy-5-methyl-4-isoxazolepropionic acid
AMPA-R	AMPA receptor
BC	bipolar cell
BD	binding domain
bidest	double-distilled
bp	base pair
BPF	band pass filter
Ca^{2+}	calcium
CaBP	calcium-binding protein-28 kDa
CaCh	calcium channel
CAG	cytomegalovirus-actin-globin hybrid (promoter)
CaM	calmodulin
CaMKII	Ca^{2+}/calmodulin-dependent protein kinase II
cAMP	cyclic adenosine monophosphate
CBP	CREB-binding protein

cDNA	complementary DNA
CFP	cyan fluorescent protein
CGP54626	[S-(R*,R*)]-[3-[[1-(3,4-Dichlorophenyl)ethyl]amino]-2-hydroxypropyl](cyclohexylmethyl) phosphinic acid
CI	confidence interval
CMF-Hank's	calcium-magnesium-free Hank's
CMV	cytomegalovirus (promoter)
CNQX	6-cyano-7-nitroquinoxaline-2,3-dione
CNS	central nervous system
CPA	cyclopiazonic acid
cpEGFP	circularly permutated eGFP
cpVenus	circularly permutated Venus (fluorophore)
CRE	cAMP-response element
CREB	Ca^{2+}/cAMP-response element binding protein
Cy2, Cy3, Cy5	carbocyanin derivatives
DA	dopamine
D-AP5	(2R)-amino-5-phosphonovaleric acid
DARPP-32	dopamine- and cAMP-regulated phosphoprotein
DIV	day(s) *in vitro*
DMEM	Dulbecco´s modified eagle medium
DMSO	dimethyl sulfoxide
DNA	desoxyribonucleic acid
DR	dopamine receptor
DXR	dopamine receptor type X
e.g.	*exempli gratia* (for example)
EC_{50}	half maximal effective concentration
eCFP	enhanced cyan fluorescent protein
Eco RI	restriction enzyme from *Escherichia coli* X

EDTA	ethylenediaminetetraacetic acid
EMCCD	electron multiplying charge-coupled-device
endo	endogenous
EPAC	exchange protein activated by cAMP
ER	endoplasmatic reticulum
ES	extracellular solution
et al.	*et alii* (and others)
EtOH	ethanol
eYFP	enhanced yellow fluorescent protein
FBS	fetal bovine serum
Fig.	figure
FP	fluorescent protein
FRET	Förster-resonance energy transfer or fluorescence-resonance energy transfer
GABA	γ-Aminobutyric acid
GAD	glutamic acid decarboxylase
GC	ganglion cell
GCaMP	genetically encoded Ca^{2+}-sensor
GCL	ganglion cell layer
GFP	green fluorescent protein
G_i	inhibitory G-protein
GlyT	glycine transporter
$G_o\alpha$	α-subunit of inhibitory G-protein
GPCR	G-protein coupled receptors
G_q	PLC-coupled G-protein
G_s	stimulatory G-protein
Gβγ	βγ-subunit of a G-protein
HC	horizontal cell

HCN	hyperpolarization-activated cyclic nucleotide-gated cation channel
HEK293	human embryonic kidney cells 293
HEPES	2-[4-(2-hydroxyethyl)piperazin-1-yl]ethanesulfonic acid
Hin	restriction enzyme from *Haemophilus influenzae*
hrs	hours
i.e.	*id est* (that is)
iGluR	ionotropic glutamate receptor
IMBX	3-isobutyl-1-methylxanthine
INL	inner nuclear layer
ipGC	intrinsically photosensitive ganglion cell
ISBN	International Standard Book Number
KAR	kainate receptor
kDa	kilo Dalton
L-AP4	2-Amino-4-phosphonobutyric acid
LB	lysogeny broth
LED	light-emitting diode
M13	myosine light-chain kinase 13
MC	Müller cell
MEM	minimal essential medium
mGluR	metabotropic glutamate receptor
min	minute
MIP	maximal intensity projection
n	number
n.s.	not significant
NA	noradrenaline
NCX	Na^+/Ca^{2+} exchanger

NKH477	N,N-Dimethyl-(3R,4aR,5S,6aS,10S,10aR,10bS)-5-(acetyloxy)-3-ethenyldodecahydro-10,10b-dihydroxy-3,4a,7,7,10a-pentamethyl-1-oxo-1H-naphtho[2,1-b]pyran-6-yl ester β-alanine hydrochloride
NMDA	*N*-Methyl-D-aspartate
norm.	normalized
ONL	outer nuclear layer
p.a.	*pro analysi*, for analysis
PA	paraformaldehyde
PB	phosphate buffer
PBS	phosphate buffered saline
PCR	polymerase chain reaction
PDE	phosphodiesterase
PDL	poly-D-lysine
PKA	protein kinase A
PKARIIβ	protein kinase A, regulatory subunit Iiβ
PKC	protein kinase C
PKCα	protein kinase C, α isoform
PKCε	protein kinase C, ε isoform
PLC	phospholipase C
PLL	poly-L-lysine
PMCA	plasma membrane Ca^{2+} ATPase
pp.	pages
PP1	phosphatase 1
PP2A	phosphatase 2A
PR	photoreceptor
Px	postnatal day x
RB	rod bipolar
RNA	ribonucleic acid

ROI	region of interest
RT	room temperature
Sal	restriction enzyme from *Streptomyces albus* G
Ser	Serine
SERCA	sarco-/endoplasmatic reticulum calcium ATPase
SybII	synaptobrevin 2
TAE	TRIS-Acetat-EDTA (buffer)
TE	TRIS-EDTA (buffer)
TH	tyrosine hydroxylase
Thr75	threonine 75
TN-L15	troponin C-based Ca^{2+}-sensor
TPMPA	(1,2,5,6-Tetrahydropyridin-4-yl)methylphosphinic acid
U	units (enzymatical)
UV	ultra violet
VAMP-2	vesicular membrane protein 2
vGlut1	vesicular glutamate transporter 1
vp	virus particles
w/	with
WPRE	Woodchuck hepatitis virus (WHP) posttranscriptional regulatory element
Xba	restriction enzyme from *Xanthomonas campestris pv. badrii*
YFP	yellow fluorescent protein

The usual abbreviations of the *International System of Units* (SI) were used. Multiples and fractions of units were specified by metric prefixes.

1. Introduction

Vision is our most important remote sense. It enables orientation during daylight as well as during night, it enables us to collect food or recognize predators, in short: it ensures our survival. Vision provides us with an enormous amount of information which is reflected by the fact that about 30-40% of our cortex is involved in the analysis of visual information. But before visual information reaches the cortex, it is extensively pre-processed and filtered by the highly complex neuronal network of the retina.

1.1. The retina and phototransduction

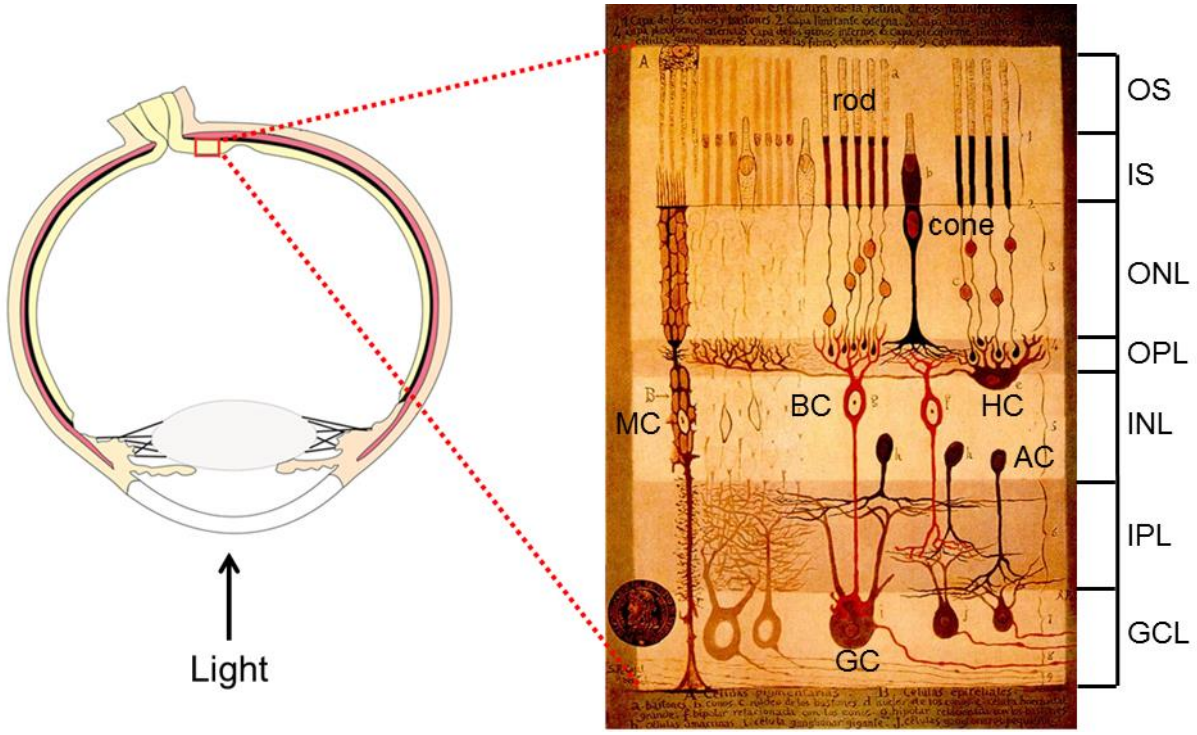

Fig. 1.1.1: Cellular organization of the retina. (Left) Cross-section through the eye ball. Picture from A. Mataruga, ICS-4, FZ-Jülich. **(Right)** Schematic drawing of a vertical section through the mammalian retina from Santiago Ramon y Cajal (1900) which he produced based on Golgi-stained retinae. Different cell types are labeled in the picture: cones and rods with the inner (IS) and outer segments (OS); HC, horizontal cell; BC, bipolar cell; AC, amacrine cell; GC, ganglion cell; MC, müller cell. In addition, the following layers are depicted: ONL, outer nuclear layer; OPL, outer plexiform layer; INL, inner nuclear layer; IPL, inner plexiform layer; GCL, ganglion cell layer. The arrow indicates how light enters the eye. It first has to cross the whole thickness of the retina to be detected by the PRs.

The retina is a 200 µm thick (Wässle, 2004), highly layered neuronal tissue that is lining the inner surface of the posterior portion of the eye. Two types of photoreceptors (PR), rods and cones, detect light at wavelengths of 400-750 nm. Before this light can be captured, it must pass through the whole thickness of the retina as the PRs lie farthest from the incoming light (Fig. 1.1.1). The somata of these PRs form the outer nuclear layer (ONL). The light signal is converted into an electrical signal in the outer segments

(OS) of the PRs (Wässle, 2004). In the outer plexiform layer (IPL), PR transfer the signal to bipolar cells (BC) via glutamatergic synapses. The somata of BCs and Müller cells (MC), the major glial cell type in the retina, are located in the inner nuclear layer (INL). In the second synaptic layer, the inner plexiform layer (IPL), BCs pass on the signal to the output neurons of the retina, the ganglion cells (GC). This vertical pathway is modulated by laterally acting pathways which mainly involve horizontal cells (HC) and amacrine cells (AC) both of whose somata are located within the INL. HCs both receive from and act upon the PRs they contact (for review see Wässle, 2004 and Thoreson and Mangel, 2012). ACs are axon-less cells that make synaptic contacts with BCs, GCs and one another (for review see Masland, 2012a). Finally, GCs collect and integrate all the information coming from the retinal network and send it to the brain via the optic nerve.

Both types of PRs are depolarized in darkness resulting in a sustained release of glutamate from the synaptic terminal. Upon light-onset, PRs hyperpolarize due to the closure of ion channels causing a reduction in glutamate release from the PR synapses (reviewed in Müller and Kaupp, 1998 and Baylor, 1996). This light-triggered reduction in glutamate release in turn alters the activity of the postsynaptic BCs. The mouse retina contains at least 11 different types of cone-driven BCs and one type of rod-driven BC (Wässle *et al.*, 2009; for review see Masland, 2012a and Euler *et al.*, 2014). According to their light responses, these types of BCs can be functionally categorized into ON-BCs and OFF-BCs. OFF-BCs depolarize at light-offset and thus follow the light response of PRs whereas ON-BCs depolarize at light-onset by inverting the PR response (Fig. 1.1.2). Cone-driven BC types 1 to 4 belong to the OFF-type, types 5 to 9 and the rod BC are ON-BCs (reviewed in Euler *et al.*, 2014). The response polarity of each BC is determined by the expression of distinct types of glutamate receptors on their dendrites. OFF-BCs express ionotropic glutamate receptors such as kainate receptors (KAR) or α-amino-3-hydroxy-5-methyl-4-isoxazolepropionic acid receptors (AMPA-R) whereas ON-BCs express the metabotropic glutamate receptor 6 (mGluR6) (Nakajima *et al.*, 1993; reviewed in Brandstätter and Hack, 2001). Both, ON- and OFF-BCs pass on their signal to GCs via glutamatergic synapses in a sign-conserving way: OFF-BCs synapse onto OFF-GCs and ON-BCs contact ON-GCs (Peichl, 1992). The result of which is that OFF-GCs are hyperpolarized and ON-GCs are depolarized at light-onset (Fig. 1.1.2).

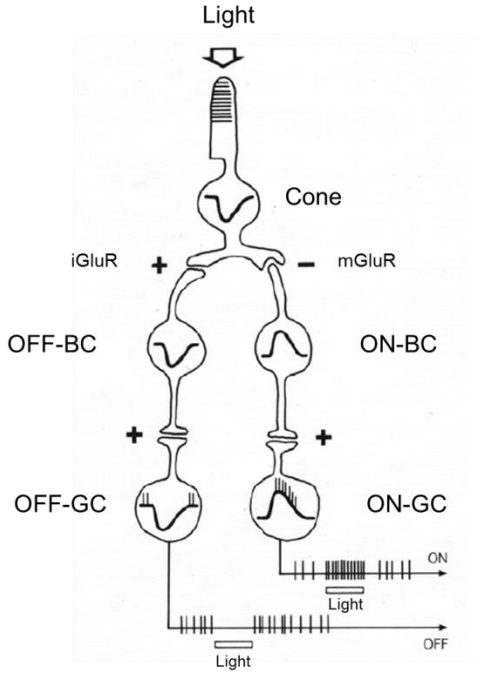

Fig. 1.1.2: The response of cone PRs is fed into two separated channels: the ON- and the OFF-pathway. Schematic depiction of the ON- and OFF-pathway in the retina. Light-induced hyperpolarization of cones induces a hyperpolarization in OFF-BCs and a depolarization in ON-BCs due to the distinct expression of ionotropic (iGluR) or metabotropic glutamate receptors (mGluR), respectively. The BCs transfer the signal to OFF- and ON-GCs in a sign-conserving way. Figure modified from Peichl, 1992.

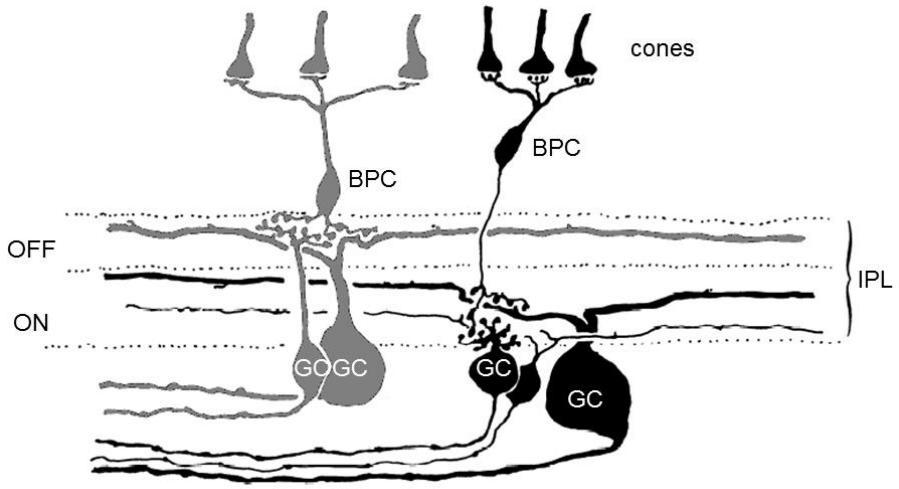

Fig. 1.1.3: BCs synapse onto GCs in distinct sublaminae of the IPL. Schematic drawing of the connections between ON-BCs/ON-GCs and OFF-BCs/OFF-GCs. Cone-driven ON-BCs synapse onto ON-GCs in the ON-sublamina of the IPL (black pathway) whereas cone-driven OFF-GCs synapse onto OFF-GCs in the OFF-sublamina of the IPL (grey pathway). Figure modified from Nelson *et al.*, 1978.

Besides their physiology, BC types can be identified by their stratification level in the IPL. The mammalian IPL can be divided into two sublayers: the ON-sublamina and the OFF-sublamina. In the ON-sublamina, ON-BCs synapse onto ON-GCs whereas OFF-BCs make contacts to OFF-GCs in the OFF-sublamina (Fig. 1.1.3).

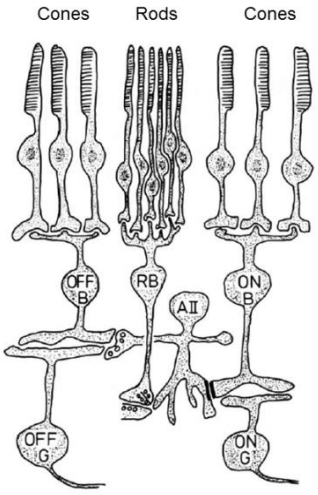

Fig. 1.1.4: Rod PRs use a detour to relay their signals onto GCs. Rods transfer their signal to rod BCs (RB) which are ON-BCs. RBs do not synapse onto GCs but make contacts with AII ACs (AII). AII ACs are electrically coupled to ON-BCs (here ON B) and make inhibitory synapses onto OFF-BCs (here OFF B). Thus, AII ACs serve as a link between rods and GCs. Figure modified from Wässle and Boycott, 1991.

Several pathways have been described for rods. In the classical pathway, rods pass on their signal to rod BCs which are ON-BCs. The axons of rod BCs (RB) were found to terminate close to GC perikarya but do not make direct output synapses onto GCs (Fig. 1.1.4). Instead, at each output synapse they contact two types of ACs, which in most cases are the small-field, glycinergic AII AC and usually a wide-field putative GABAergic AC, such as the A17 cell (for review see Wässle and Boycott, 1991). AII ACs are electrically coupled to ON-BCs (via gap junctions) and make inhibitory chemical synapses onto OFF-BCs (Fig. 1.1.4). Thus, rod BCs use a detour by feeding their signals into the cone bipolar pathways in order to relay the rod signal to GCs (for review see Wässle, 2004). Besides the classical rod pathway two alternative pathways have been described. One route is through gap junctions between rods and cones and the other via synapses between rods and certain OFF-cone BCs (for review see Wässle, 2004).

1.2. The dopaminergic system in the retina

1.2.1. Dopaminergic amacrine cells

Amongst 30 different types of ACs (for review see Masland, 2001), there is only one population in the mouse retina that is known to synthesize and release DA (Wulle and Schnitzer, 1989; Versaux-Botteri *et al.*, 1984). Dopaminergic neurons can be immunohistochemically detected by an antibody directed against tyrosine hydroxylase (TH), the rate-limiting enzyme of the catecholamine biosynthetic pathway (Nguyen-

Legros, 1988). TH-positive cells are regularly distributed throughout the retina and appear at low density of roughly 30 cells/mm^2 in adult retinae of mice (Wulle and Schnitzer, 1989; Versaux-Botteri *et al.*, 1984). At P6, TH-positive cells are found for the first time (Wulle and Schnitzer, 1989). The cell bodies of dopaminergic cells have a diameter of 12-15 µm (Wulle and Schnitzer, 1989; Versaux-Botteri *et al.*, 1984) and are found within the layer of ACs at the border of the INL and IPL (Witkovsky, 2004). They form a dense dendritic plexus that is lining the border of INL and IPL (Fig. 1.2.1). From this network of processes, other fine processes spread out towards the inner (Fig. 1.2.1, arrow) as well as the outer retina (Fig. 1.2.1, arrowhead). That is why TH-positive ACs are often described as interplexiform cells (Gallego, 1971; Witkovsky *et al.*, 2008).

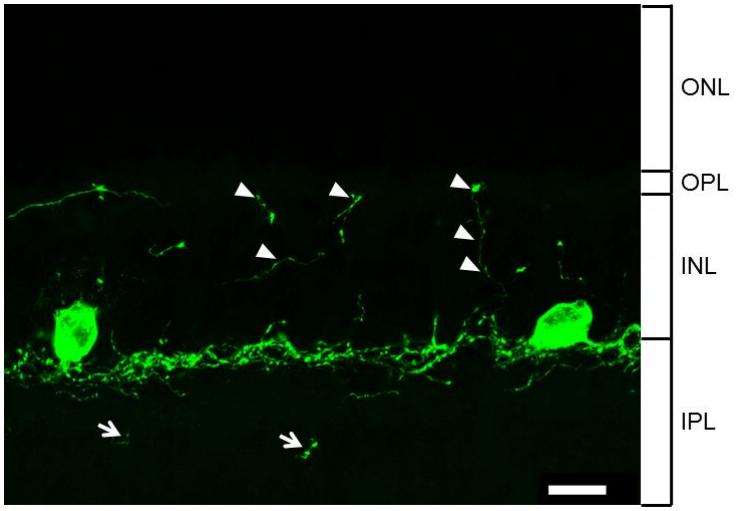

Fig. 1.2.1: Dopaminergic ACs in a vertical section of the mouse retina. Confocal image of a vertical cryosection from mouse retina that was stained with an antibody directed against tyrosine hydroxylase, the rate-limiting enzyme in the biosynthesis of dopamine. Fine processes spread towards the OPL (arrowheads) and INL (arrows). Scale bar 15 µm.

This morphology suggests that DA is released throughout the retina where it acts as a paracrine transmitter at the majority of cells. But it has also been shown that TH-positive neurons make real synapses onto AII ACs (Voigt and Wässle, 1987; Völgyi *et al.*, 2014) which are the link between the rod and the cone pathway. TH-positive ACs have an intrinsic spike firing rate that is controlled by excitatory as well as inhibitory inputs which they receive from bipolar and other ACs (Witkovsky, 2004).

1.2.2. Dopamine receptors

There are five different types of dopamine receptors (D1R-D5R) that are grouped into two families: the D1R-family including D1R and D5R and the D2R-family which comprises D2R-D4R. Dopamine receptors are members of the seven transmembrane domain G protein-coupled receptor family that display amino acid sequence

conservation within the transmembrane domains (Missale *et al.*, 1998). The five types of DRs differ in their affinity for DA: The D3R subtype displays the highest affinity for DA followed by D5R. The D1R exhibits the lowest affinity for DA amongst all DRs (Strange and Neve, 2013; Missale *et al.*, 1998). DRs vary in the type of G-protein they are coupled to, suggesting that they activate different signaling cascades. In a classical view, activation of D1Rs and D2Rs changes the activity of ACy in opposing ways: activation of D1Rs leads to a rise in ACy activity and thus an increase in $[cAMP]_i$. In contrast to that, activation of D2Rs induces an inhibition of ACy followed by a reduction in cAMP synthesis (Fig. 1.2.2).

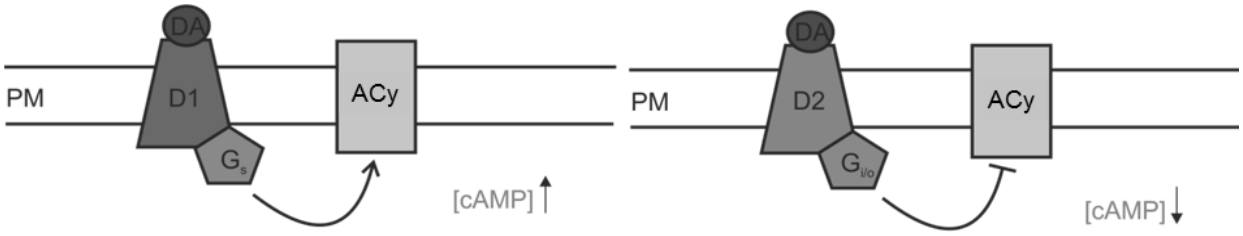

Fig. 1.2.2: D1Rs and D2Rs couple to ACy. Activation of D1Rs leads to an increase in ACy activity followed by a rise in $[cAMP]_i$. In contrast, stimulation of D2Rs inhibits ACy and thereby reduces $[cAMP]_i$.

However, both (D1R- and D2R-) signaling pathways trigger a change in the activity of the cAMP-dependent protein kinase A (PKA) through the described changes in $[cAMP]_i$. Activated PKA phosphorylates a huge variety of downstream targets such as ion channels, GPCRs or cytoplasmic proteins *e.g.* dopamine- and cAMP-regulated phosphoprotein (DARPP-32) and thereby modulates the cells' physiology. Besides these classical ways of action, other downstream signaling molecules are discussed to be involved in DR-signaling. One such alternative pathway for D1-like receptor-signaling is phospholipase C (PLC)-mediated mobilization of intracellular Ca^{2+} (Neve *et al.*, 2004). As for the D2R, alternative signaling via Gβγ has been proposed (Neve *et al.*, 2004).

In the retina, DRs are expressed in a variety of different cell populations. Using specific antibodies for D1R and D2R it was found, that in the mouse retina both types of DRs are abundantly expressed in both synaptic layers (Fig. 1.2.3) as also shown for D1Rs in a variety of other mammals (Nguyen-Legros *et al.*, 1997). In immunohistochemical studies of mouse retinae it could be shown that D1Rs are expressed in the somata and the axon terminal systems of type 5 and 7 BCs (ON-BCs) but not in type 1-3 cone BCs and rod BCs (Usai, 2014). Veruki and Wässle concluded that HCs, at least three types of cone BCs and a small number of ACs were immunolabelled for D1R in the rat retina (Veruki and Wässle, 1996). There is also evidence for the expression of D1R on rat retinal GCs

(Hayashida *et al.*, 2009). The dopaminergic AC itself possesses D2Rs which function as autoreceptor (Veruki, 1997; Rashid *et al.*, 1993; Wang *et al.*, 1997). In addition, it has been demonstrated that PRs in the mouse retina possess D4Rs (Cohen *et al.*, 1992). The D5Rs are not found in the retina but seem to be expressed in the retinal pigment epithelium (Versaux-Botteri *et al.*, 1997).

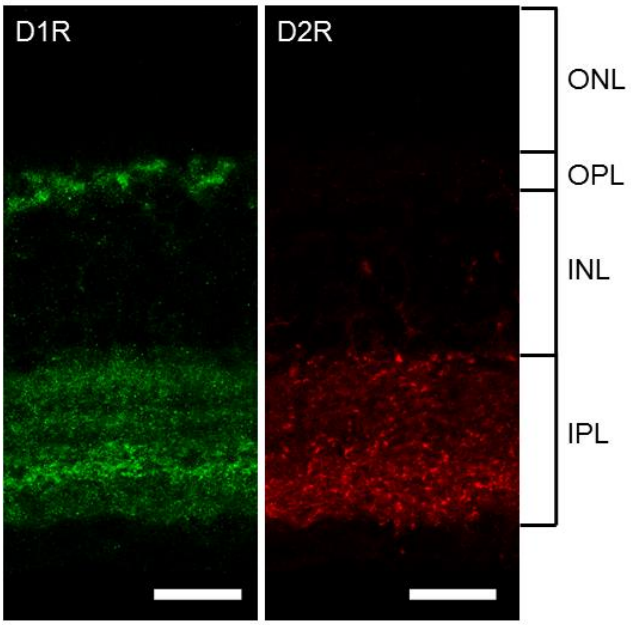

Fig. 1.2.3: Dopamine receptors are expressed in the synaptic layers of the mouse retina. Confocal images of vertical cryosections of a mouse retina which were stained with antibodies against D1R (green) and D2R (red). Strongest expression of the D1R was found in both synaptic layers whereas D2R immunoreactivity was detected only in the IPL. Scale bar 15 µm.

The situation gets more complex by the fact that DRs can exist as dimers. Dopamine receptors have been shown to form homo-dimer and also hetero-dimers that exhibit divergent pharmacological and cell signaling properties (for review see Perreault *et al.*, 2011). Ogata and colleagues provided the first evidence that DA activates a receptor in adult mammalian retinal neurons that is distinct from classical D1Rs and D2Rs and most likely a D2-D5 heteromeric receptor (Ogata *et al.*, 2012). Further evidence for alternative signaling pathways of heteromeric DRs was found in heterologous expression systems (So *et al.*, 2005; Chun *et al.*, 2013).

1.2.3. Dopamine's role in light adaptation

The retina has the striking feature that it enables vision in different light conditions: from a starry night to a bright sunny day (Fig. 1.2.4). These different light intensities stretch over the enormous range of more than ten orders of magnitude on a logarithmic scale (Rodieck, 1998). In this broad range of light intensities vision is made possible by adaptation processes which in the retina take place on every level of retinal processing,

the single PR cell as well as in the entire network. These adaptation processes are mediated by the orchestration of a variety of neurotransmitters and second messenger cascades, amongst them adenosine (Ribelayga and Mangel, 2005), nitric oxide (Djamgoz *et al.*, 2000) and DA (Witkovsky, 2004). Rods are highly sensitive to single photons and mediate vision in scotopic conditions. Cones are less sensitive to light and mediate vision in photopic conditions (Wässle and Boycott, 1991; Wässle, 2004). Vision in mesopic conditions is based on the activity of both PR types (Fig. 1.2.4).

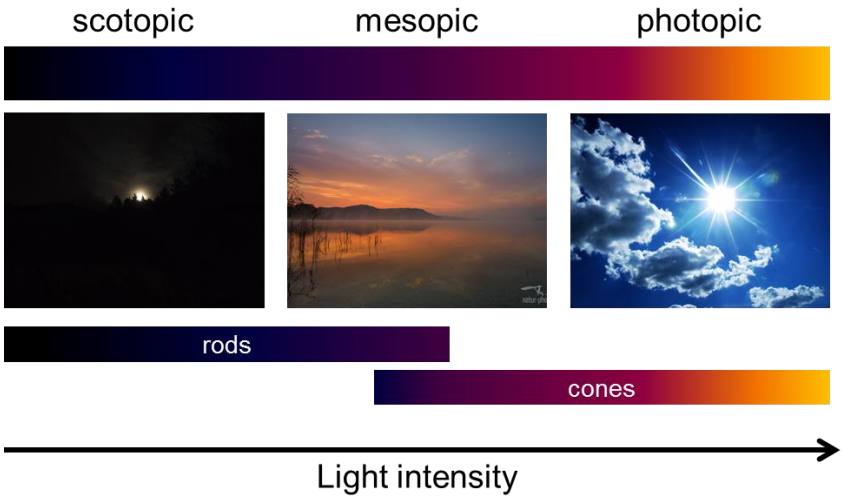

Fig. 1.2.4: The retina works in a broad range of light intensities. The retina enables vision at different light intensities: in a starry night (scotopic), in dusk and dawn (mesopic), and in bright sunlight (photopic). Rods mediate vision in scotopic condition whereas cones are the dominant active type in photopic conditions. In mesopic conditions, both PR types are involved in the detection of light. Internet sources for images are indicated in the appendix.

It has been demonstrated that besides adaptation in the single PR cell a network adaptation takes place. This is where -besides others- DA becomes involved. DA release is higher in light than in darkness (Witkovsky, 2004; Bauer *et al.*, 1980). In PRs, DA acts through D4Rs resulting in dephosphorylation of connexins and thus an uncoupling of PRs. Similar DA-dependent regulation of cell-to-cell coupling has been found in AII ACs (Hampson *et al.*, 1992; Bloomfield and Völgyi, 2009; Kothmann *et al.*, 2009). Both these mechanisms of uncoupling may act to prevent contamination of the photopic cone signals by saturated rod signals (Kothmann *et al.*, 2009; Li and O'Brien, 2012; for review see Bloomfield and Völgyi, 2009).

In addition to DA's role as regulator of cell-to-cell coupling it has been shown in the retina and in other parts of the central nervous system (CNS) that it also exhibits a modulatory role in the regulation of glutamate and GABA receptors. Snyder and colleagues found that D1R activation increases the phosphorylation of a subunit of NMDA-type glutamate receptors in medium spiny neurons of the *nucleus accumbens*

(Snyder *et al.*, 1998). Feigenspan and colleagues demonstrated that DA induced an increase of GABA-induced whole-cell currents in ACs of rat retina (Feigenspan and Bormann, 1994). Furthermore, it has been demonstrated that DA increases $[Ca^{2+}]_i$ in synaptic terminals of BCs which may potentiate the release of neurotransmitters and thus modulate the throughput from PRs to GCs (Heidelberger and Matthews, 1994). All these findings indicate that DA has a modulatory role contributing to a change in the physiology of its downstream targets.

1.3. Genetically encoded biosensors

Genetically-encoded biosensors are valuable tools for the detection of changes in the intracellular concentration of second messengers or changes in neurotransmission with high spatial and temporal resolution. They have the great advantage that they can be applied from single cells up to whole organisms, that they can be specifically expressed in defined groups of cells or tissues and that they can be recorded without a requirement for exogenous co-factors (Miesenböck *et al.*, 1998). They are applied in isolated cells (Dunn, 2006) and intact tissue (Mironov *et al.*, 2009; Lelito and Shafer, 2012; Heim *et al.*, 2007). The biosensors are based on the usage of fluorescent proteins (FP) such as green fluorescent protein (GFP) from *Aequorea victoria* that exhibit variable properties: some of them are pH-sensitive, some change their fluorescence emission upon conformational changes and others are designed as such that they enable energy transfer from one to another (reviewed in Ai, 2015).

1.3.1. FRET-based biosensors

One group of genetically encoded biosensors is based on a physical process called Förster-resonance energy transfer or fluorescence-resonance energy transfer, short FRET. During FRET, energy is transferred non-radiatively from an excited molecular fluorophore (the donor) to another fluorophore (the acceptor) (Sekar and Periasamy, 2003). One precondition for an efficient energy transfer between the two fluorophores is that the emission spectrum of the donor fluorophore overlaps with the excitation spectrum of the acceptor fluorophore. The second precondition is that the two fluorophores are within 2-10 nm of one another (reviewed in Broussard *et al.*, 2013). These FRET-based biosensors are always constructed according to the same principle: they are composed of a binding domain (BD) that interacts with the cellular compound that is to be detected. This BD is flanked by two FPs (Fig. 1.3.1). The two most often used

FPs that serve as FRET-pair are the cyan fluorescent protein (CFP) and the yellow fluorescent protein (YFP) or derivatives of these two proteins. FRET-based biosensors exist in two conformational states: state 1 where the two FPs are far away from each other preventing an energy transfer between one another and state 2 where the FPs are in close proximity allowing energy transfer to take place (Fig. 1.3.1).

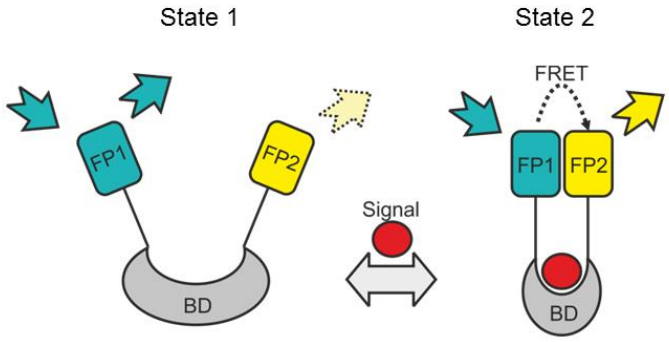

Fig. 1.3.1: Basic mechanism of FRET-based biosensors. FRET-based biosensors are composed of a binding domain (BD) which is flanked by two fluorescent proteins (FPs) designed for FRET. Upon presence of a signal, the conformation of the sensor changes enabling energy transfer from the donor (FP1) to the acceptor (FP2). Excitation of the donor fluorophore in this state leads to an increased emission signal of the acceptor fluorophore.

The switch between these two states is a cellular compound that interacts with the BD. This interaction triggers a conformational change in the sensor protein altering the distance between the two fluorophores. Excitation of the donor fluorophore (FP1) in state 1 results in a higher emission signal of FP1 than of the acceptor (FP2). In state 2, excitation of FP1 leads to an energy transfer to FP2 resulting in an increase in the emission signal of FP2 and a decrease in the emission signal of FP1. Thus, experiments with FRET-based sensors rely on measuring the amount of acceptor protein emission after excitation of the donor (Broussard *et al.*, 2013). The degree of FRET can be measured by various approaches, of which the most popular is represented by simple ratiometry (Sprenger and Nikolaev, 2013). In this approach, the donor fluorophore is excited with a specific wavelength and the emission signals of both fluorophores, the donor and the acceptor, are detected simultaneously. The signals are depicted as the ratio in fluorescence intensity of donor/acceptor or acceptor/donor.

1.3.1.1. Biosensors for the detection of changes in the cAMP/PKA cascade

As it has been described in 1.2, the classical way of DA-downstream signaling involves stimulation of DRs which in turn alters the activity of ACy and thus $[cAMP]_i$. There are various genetically encoded sensors that are used for the detection of changes in $[cAMP]_i$ (reviewed in Gorshkov and Zhang, 2014 and Sprenger and Nikolaev, 2013). In

2004, two independent groups published a FRET-based cAMP-sensor which they called EPAC (Ponsioen *et al.*, 2004; Nikolaev *et al.*, 2004). Both groups utilized the cAMP-BD of the exchange protein activated by cAMP 1 (Epac1) as key element of the sensor. Both sensors were devoid of any catalytic or targeting domains that might interfere with intracellular regulatory processes. In the present study, the sensor EPAC1-camps generated by Nikolaev and colleagues was used. The cAMP-BD of EPAC1-camps is flanked by the two FPs enhanced-YFP (eYFP) and enhanced-CFP (eCFP) (Fig. 1.3.2). At low cAMP concentrations, the two FPs are in close proximity to each other. Upon binding of cAMP, the distance between the two FPs is enhanced. Thus, a decrease in YFP emission and a mirror-reversed increase in CFP emission indicates an increase in $[cAMP]_i$. Fluorometric measurements determined an EC_{50} value of 2.35±0.42 µM for the EPAC1-camps sensor (Nikolaev *et al.*, 2004).

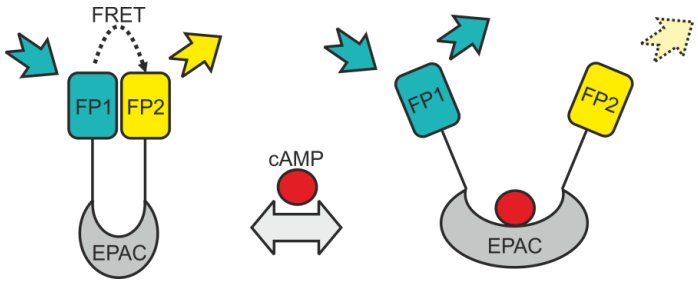

Fig. 1.3.2: Mechanism of the FRET-based biosensor EPAC1-camps. EPAC1-camps is composed of the cAMP-BD of the EPAC1 protein which is flanked by two FPs eCFP (FP1) and eYFP (FP2) which serve as FRET-pair. Upon binding of cAMP (red ball) to the BD (grey), the conformation of the sensor changes leading to a decrease in the energy transfer from the donor (FP1) to the acceptor (FP2).

PKA is activated by cAMP and thus a downstream signaling protein of DRs. In 2001, the Zhang lab published the first A-kinase activity reporter (AKAR) consisting of fusions of eCFP, a phosphoamino acid BD (14-3-3τ), a PKA-specific phosphorylatable peptide sequence, and YFP (Zhang *et al.*, 2001). In 2010, they developed an improved sensor called AKAR4 which yields a maximal change in YFP/CFP of 58±1.7% in HEK293 cells stimulated with isoproterenol to elicit a rise in $[cAMP]_i$ (Depry *et al.*, 2011). In the present study this AKAR4 sensor was used to visualize changes in PKA activity. When PKA activity is low, the two FPs are far away from each other. Due to the phosphorylation of the PKA-specific peptide sequence by PKA, the phosphoamino acid BD and the phosphorylated PKA-specific peptide sequence interact with each other inducing a conformational change in the AKAR4 sensor protein. This conformational change results in an increase in energy transfer as the two FPs are in close proximity to each other (Fig. 1.3.3). An increase in YFP fluorescence and a mirror-reversed decrease in CFP fluorescence thus indicate an increase in PKA activity.

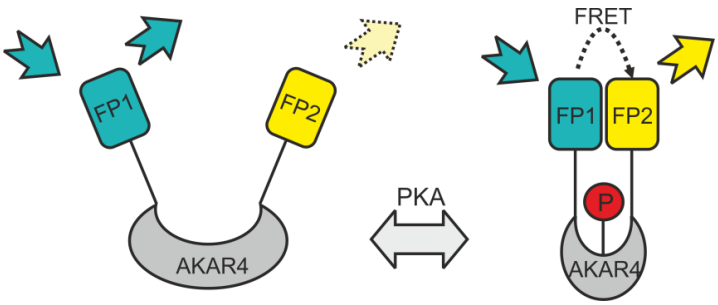

Fig. 1.3.3: Mechanism of the FRET-based biosensor AKAR4. AKAR4 is composed of a PKA-specific peptide sequence and a phosphoamino acid BD which are flanked by the two FPs cerulean (FP1) and cpVenus (FP2) which serve as FRET-pair. Phosphorylation (red ball) of the PKA-specific peptide sequence (grey) induces a conformational change in the sensor protein leading to an increase in the energy transfer from the donor (FP1) to the acceptor (FP2).

1.3.1.2. TN-L15: A FRET-based biosensor for the detection of changes in $[Ca^{2+}]_i$

The FRET-based Ca^{2+}-sensor TN-L15 is based on truncated chicken skeletal muscle troponin C in which the N-terminal amino acid residues 1–14 are deleted. This Ca^{2+}-binding protein is sandwiched between the two FPs CFP and Citrine (Heim and Griesbeck, 2004). Binding of Ca^{2+} to the troponin C variant increases the energy transfer from the donor (CFP) to the acceptor (YFP). Thus, an increase in the YFP emission signal and a mirror-reversed decrease in CFP emission signal indicates an increase in $[Ca^{2+}]_i$ (see Fig. 1.3.1). The TN-L15 sensor exhibits a dissociation constant of 1.2 µM for Ca^{2+}. Maximal ratio changes of 100% were detected within cells expressing TN-L15 (Heim and Griesbeck, 2004).

1.3.2. Detection of neurotransmitter release with synapto-pHluorin

The first pH-sensitive genetically encoded biosensor was introduced by Miesenböck and colleagues in 1998. The sensor is based on a pH-sensitive GFP (pHluorin) that is fused to the luminal side of vesicular membrane protein (VAMP-2)/synaptobrevin II (SybII) which gave it the name synapto-pHluorin. When the pH-sensitive GFP is excited at a wavelength of 488 nm, the emission at 508 nm is more than 15-fold higher at pH 7.5 than at pH 5.5 (Miesenböck *et al.*, 1998; see fig. 1.3.4 A). Miesenböck and colleagues further demonstrated that the sensor is well suited for the visualization of neurotransmission. Under resting conditions, the lumen of a vesicle has a low pH of about 5.5 and thus the fluorescence emission of the GFP is low (Fig. 1.3.4 B, resting). Upon stimulation of a neuron, vesicles are exocytosed resulting in an increase in the pH and in turn to an increase in the fluorescence emission of the pHluorin (Fig. 1.3.4 B, exocytosis). Upon endocytosis, the lumen of the vesicle is re-acidified resulting in a loss of pHluorin fluorescence emission (Fig. 1.3.4 B, endocytosis). Thus, an increase in

synapto-pHluorin fluorescence emission is an indicator for the release of synaptic vesicles containing neurotransmitters such as DA from the neuron.

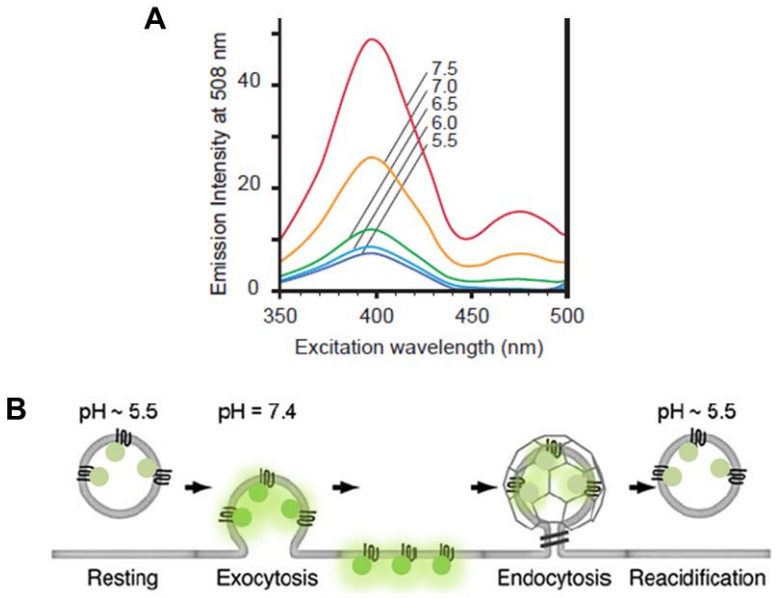

Fig. 1.3.4: Synapto-pHluorin can be used for the visualization of neurotransmitter release. (A) Fluorescence excitation spectrum of pHluorin. Modified from Miesenböck *et al.*, 1998. **(B)** Fluorescence emission is low at low pH inside the vesicle lumen. Upon exocytosis, pHluorin fluorescence emission is increased. Modified from Royle *et al.*, 2008.

1.3.3. Sensors based on permutated GFP

In 1999, Baird and colleagues set the basis for the development of a large group of biosensors (Baird *et al.*, 1999). They showed that several rearrangements or insertions within GFPs, in which the amino and carboxyl portions are interchanged and rejoined with a short spacer connecting the original termini, still become fluorescent (Baird *et al.*, 1999). These so called circular permutations have altered pKa values and altered orientations of the chromophore. In addition, they demonstrated that it is possible to insert foreign proteins such as CaM into GFP without impairing its fluorescence. Based on these findings, the first Ca^{2+}-biosensor called GCaMP was developed (Nakai *et al.*, 2001). GCaMPs are composed of CaM which serves as Ca^{2+}-BD, a circularly permutated GFP (cpEGFP) and the CaM-binding peptide myosine light-chain kinase M13 (Fig. 1.3.5; Nakai *et al.*, 2001). In the Ca^{2+}-unbound state GCaMP fluorescence is low. Binding of Ca^{2+} to CaM leads to an interaction between CaM and M13. This in turn induces a conformational change which results in a 4.5-fold fluorescence increase.

In 2009 an improved GCaMP sensor was published (Tian *et al.*, 2009). This GCaMP3 exhibited increased baseline fluorescence, increased dynamic range and higher affinity for Ca^{2+}. Further modifications of the original GCaMP have now resulted in greatly

improved **Ca^{2+}-**probes, such as GCaMP6 and GCaMP7 which exhibit an excellent signal-to-noise ratio and sensitivity (reviewed in Ai, 2015).

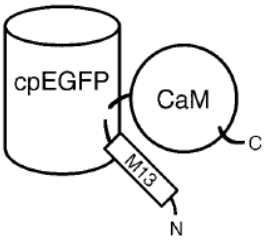

Fig. 1.3.5: Schematic depiction of the Ca^{2+}-sensor GCaMP. GCaMP is composed of a CaM which serves as Ca^{2+}-BD, a CaM-binding peptide myosine light-chain kinase M13 and a circulary permutated GFP. Ca^{2+}-binding to CaM induces a conformational change in the GFP leading to an increase in fluorescence intensity. Image taken from Nakai *et al.*, 2001.

1.4. The chemical Ca^{2+} indicator Fluo-4

There is a huge amount of chemical indicators for a variety of ions (Ca^{2+}, Mg^{2+}, Cl^- or Zn^{2+}) which are used for the investigation of signaling pathways in cell culture or acute tissue preparations. Compared to genetically encoded biosensors, these chemical indicators have the great advantage of easy handling as they can be introduced into cells by passive diffusion, do not require transfection or transduction procedures, and make it possible to image many cells simultaneously. However, they have the big disadvantage that they cannot be targeted to specific cell types or tissues.

The chemical Ca^{2+}-indicator Fluo-4-AM (Invitrogen) is a well-established indicator to monitor changes in $[Ca^{2+}]_i$. Due to the protection of its charged groups by acetoxymethyl (AM) esters Fluo-4-AM is able to cross the plasma membrane by passive diffusion. Once it is inside the cell, the AM-esters are cleaved-off by esterases preventing the dye from exiting the cell again. In the Ca^{2+}-unbound state fluorescence emission of Fluo-4 is low. Upon binding of Ca^{2+} ions fluorescence emission is increased about 100-fold. Thus, an increase in fluorescence emission reflects an increase in $[Ca^{2+}]_i$.

1.5. Objective of the study

Dopamine is released upon light onset and is discussed to be a key player in mediating light adaptation in the retina. There exists a huge amount of episodic knowledge about DA's actions in the retina including the modulation of the activity of ion channels, transmitter systems and gap-junctional coupling (for review see Witkovsky, 2004). However, many important details about the underlying pathways are still unresolved.

The intention of this study was to contribute to a better understanding of the underlying pathways of DA's action in the retina - on the level of the dopaminergic ACs as well as on the level of target cells. To this end, above all imaging experiments using genetically encoded sensors were to be employed. In this study, the mouse retina served as model system.

Until now, the light-induced release of DA from the retina was only investigated by studying the release of radioactively labeled DA (Kramer, 1971; Bauer *et al.*, 1980). My aim was to establish a new method that would make it possible to visualize DA release in a high local and temporal resolution. One part of the project was the attempt by means of molecular cloning, to specifically express the sensor synapto-pHluorin that visualizes neurotransmission in dopaminergic ACs under control of the cell type-specific TH promoter.

In order to investigate DA-induced signaling pathways in target cells, the retinal primary culture was chosen as model system and was characterized by immunocytochemistry. To visualize changes in $[cAMP]_i$, the FRET-based biosensors EPAC1-camps and AKAR4 were first characterized in HEK293 cells and later expressed in the retinal cell culture via Lipofectamine-transfection. To dissect the underlying pathways involved in DA-induced changes in the cAMP/PKA-cascade, a pharmacological approach was applied. There is only little known about DA's impact on $[Ca^{2+}]_i$ of postsynaptic cells. In order to investigate whether and how DA regulates $[Ca^{2+}]_i$ in retinal neurons, Ca^{2+}-imaging experiments in Fluo-4-loaded cultured cells were conducted. A pharmacological approach was applied to dissect the underlying pathways of DA-induced changes in $[Ca^{2+}]_i$.

The knowledge from the experiments in culture had to be transferred to the intact retinal tissue. As the retina is a highly complex system, experimental procedures and analysis were more difficult and required the establishment of new methods. As Lipofectamine-transfection is not applicable for the *in vivo* expression of sensor proteins, adeno-associated viruses (AAVs) were used as gene-shuttles. To deliver these viruses to the retina, the method of intraocular injections had to be established. Immunohistochemistry was used to characterize AAV-infected retina. To unravel the impact of DA on $[Ca^{2+}]_i$ in the output neurons of the retina, a transgenic mouse line that expresses the Ca^{2+}-sensor TN-L15 in GCs was utilized.

2. Materials and Methods

2.1. Animals

Neonatal C57Bl/6 mice at the age of postnatal day 1 (P1) to P4 were used for retinal dissociated cultures. Injections were performed in C57Bl/6 mice at P6 to P8. Mice were obtained from Charles River (Sulzfeld, Germany) or from the own live-stock breeding at the Forschungszentrum Jülich. Transgenic mice expressing the genetically encoded Ca^{2+}-sensor TN-L15 (gift from Dr. O. Griesbeck, MPI for Neurobiology, Martinsried, Germany) were also taken from the own live-stock breeding from the animal facility at the Forschungszentrum Jülich.

2.2. General buffers and solutions

Chemicals and reagents with purity grade *pro analysi* (*p.a.*) were purchased from AppliChem (Darmstadt, Germany), Biozym (Hessisch Oldendorf, Germany), Enzo (Lörrach, Germany), GE Healthcare (Freiburg, Germany), Merck (Darmstadt, Germany), MWG-Biotech (Ebersberg, Germany), Qiagen (Hilden, Germany) and Sigma-Aldrich (Munich, Germany). Materials for cell line culture and primary cell and tissue culture were ordered from GIBCO (Invitrogen, Germany). All solutions were prepared with bi-distilled water. Solutions were sterilized by filtration or autoclaving for 20 min at 121°C, when necessary.

10 % sucrose:	10% Sucrose with 0.05% NaN_3 dissolved in 0.1 M PB
30 % sucrose:	30% Sucrose with 0.05% NaN_3 dissolved in 0.1 M PB
4% Low melt agarose:	4 g of Low Melt Agarose (Peqlab, 35-2020) were dissolved in 100 ml Hank's
Agarose:	Roth, 2267.3
Ames high K^+:	20 mM potassium bicarbonate added; pH adjusted to 7.4 with sodium bicarbonate while bubbling with a gas mixture of 95% O_2 and 5% CO_2

Ames medium:	pH adjusted to 7.4 with sodium bicarbonate while bubbling with a gas mixture of 95% O_2 and 5% CO_2 (Sigma-Aldrich, A1420)
Ampicillin (Amp):	100 mg/ml in H_2O (AppliChem, A0839)
Aqua Polymount:	Polyscience, 18606
BBS (2x):	50 mM BES, 280 mM NaCl, 1.5 mM Na_2HPO_4 x 2 H_2O; pH adjusted with 2 N NaOH; sterile filtered.
$CaCl_2$ (1 M):	dissolved in H_2O and sterile filtered
Chemiblocker (C) 5%:	diluted 1:20 with 0.1 M PB (EMD Millipore, 2170)
CMF-Hank's:	Ca^{2+}-Magnesium-free Hank's (Sigma-Aldrich, H6648) buffered with 10 mM HEPES (1 M; sterile filtered; pH adjusted to 7.4 with NaOH) to pH 7.4
Competent bacteria:	TOP10F (Invitrogen)
CT:	5% C with 0.5 % Triton X
CTA:	5% C with 0.5 % Triton X and 0.05 % NaN_3
DH10:	500 ml DMEM (GIBCO, 41090-028) supplemented with 10% FBS (GIBCO, 10270-106) and 1% Antibiotic/Antimycotic (100X; GIBCO, 15240-062)
$DMEM_{neuro}$:	DMEM (GIBCO, 61965-026) supplemented with 1% Antibiotic-Antimycotic (100X; GIBCO, 15240-062), 1% Sodium-Pyruvate (Sigma Aldrich, S8636), 25 mM HEPES (1 M; sterile filtered), 1% N2 Supplement (GIBCO, 17502-048) and 10% Fetal Bovine Serum (GIBCO, 10270-106).
DNA-Ladder:	λDNA/*Eco*RI+*Hind*III Marker (Thermo Fisher Scientific, SM0191)

ES_{neuro}:	145 mM NaCl, 5 mM KCl, 1 mM $CaCl_2$ x $2H_2O$, 1 mM $MgCl_2$ x $6H_2O$, 10 mM HEPES, 10 mM D-Glucose x H_2O; pH 7.4
ES_{normal}:	120 mM NaCl, 5 mM KCl, 2 mM $CaCl_2$ x $2H_2O$, 2 mM $MgCl_2$ x $6H_2O$, 10 mM HEPES, 10 mM D-Glucose x H_2O; pH 7.4
Fixative:	4% Paraformaldehyde (PA) in PB
Fluo4-AM:	Invitrogen, F14201; dissolved in dimethyl sulfoxide (DMSO) to a final concentration of 2 mM
Hank's:	136.89 mM NaCl, 5.36 mM KCl, 1.25 mM $CaCl_2$ x $2H_2O$, 0.81 mM $MgCl_2$ x $6H_2O$, 10 mM HEPES, 5.55 mM D-Glucose x H_2O adjusted to pH 7.4
HEPES:	1 M in H_2O bidest adjusted to pH 7.4 with NaOH
Laminin:	10 µg/ml (Invitrogen, L2020) in H_2O
LB agar:	5 g/l NaCl, 2 g/l $MgSO_4$ x 7 H_2O, 10 g/l NZ amine, 5 g/l yeast extract, 7.5 g/l Agarose
LB medium:	1% Baktotrypton, 0.5% yeast extract, 1% NaCl
M10:	500 ml MEM (GIBCO, 41090-028) supplemented with 10% FBS (GIBCO, 10270-106), 1% Antibiotic/Antimycotic (100X; GIBCO, 15240-062) and 1% MEM not essential amino acids (GIBCO, 11140-035)
OPTI-MEM:	Gibco, 51985-026
Papain:	(Worthington, LK003178) dissolved in CMF-Hank's to 20 U/ml
PB:	81 mM Na_2HPO_4, 19 mM NaH_2PO_4 with pH 7.4
PBS:	130 mM NaCl, 7 mM Na_2HPO_4, 3 mM NaH_2PO_4 with pH 7.4

PDL:	0.1 mg/ml (Sigma, P6407) in H_2O
SYBR® Safe DNA Stain:	Invitrogen, S33102
TAE buffer:	40 mM Tris/Acetate pH 7.5, 1 mM EDTA
TE buffer:	10 mM Tris/HCl pH 7.5, 1 mM EDTA; pH 8.0
Transfection reagent:	Lipofectamine 2000 (Invitrogen, 11668-019)
Trypsine w/ EDTA:	Gibco, 25300-054

2.3. Molecular biology

2.3.1. Plasmids

p156rrlSybIIpHluorin:	Dr. R. Guzman, ICS-4, FZ-Jülich
pcDNA3.1(-)	Invitrogen, V795-20
pEGFP-N1:	Clontech, 632469
TH Promoter:	SwitchGear Genomics, S722286

2.3.2. Kits

Miniprep:	NucleoSpin Plasmid (Macherey-Nagel, 740588-250)
Gel and PCR Clean-up:	NucleoSpin Gel and PCR Clean-up (Macherey-Nagel, 740609-250)
Maxiprep:	QIAGEN Plasmid Maxi Kit (Qiagen, 12165)
Ligation:	Rapid DNA Ligation Kit (Thermo Fisher Scientific, K1422)
PCR:	KOD Hot Start DNA Polymerase (Merck Millipore, 71086)

2.3.3. Transformation of competent cells

For multiplying DNA, competent bacteria (TOP10F, Invitrogen) were transformed with plasmid DNA which conveys them with a resistance to different selection antibiotics

such as ampicillin (Amp). The process of transformation, meaning the uptake of free DNA from the environment, results in a change of the genotype of the bacteria.

Competent TOP10F cells, stored at -80 °C, were gently thawed on ice. Fifty µl of competent bacteria were incubated with 5 µl of plasmid DNA for 20 min on ice. Then, 200 µl LB medium was added and the bacteria were further incubated for 30 min at 37 °C. Following, bacteria were seeded on LB agar plates containing appropriate selection antibiotics (Amp) using a fire polished glass pipette. The plates were incubated overnight at 37 °C. The next day, clones were picked with an autoclaved toothpick and grown in 5 ml LB medium containing 1:1000 diluted selection antibiotics (Amp: 100 µg/ml) overnight in a roller shaker at 37 °C. These mini-cultures were further used for DNA isolation (see 2.3.4) or for the inoculation of a maxi-culture. For the inoculation of a maxi-culture, a mini-culture was transferred to 500 ml LB medium containing 1:1000 diluted selection antibiotics (Amp: 100 µg/ml). These cultures were incubated overnight in a shaker at 37 °C. The next morning, the maxi-culture was used for DNA isolation (see 2.3.4).

2.3.4. DNA isolation

Bacterial cultures, mini- or maxi-cultures (see 2.3.3), were pelleted using a centrifuge. According to the manufacturer´s protocol, mini-cultures were pelleted for 30 s at 11000 rpm in an Eppendorf centrifuge 5425 and maxi-cultures for 15 min at 6000 rpm in a Sorvall Evolution RC centrifuge (rotor SLA-3000). For minipreps, the DNA was isolated with the NucleoSpin Plasmid kit (Macherey-Nagel) according to the manufacturer´s protocol. DNA was eluted in H_2O when used for further processing (2.3.6 and 2.3.7) and in TE buffer when stored for longer time. Maxipreps were prepared with the QIAGEN Plasmid Maxi Kit (Qiagen) according to the manufacturer´s protocol. DNA was eluted in TE buffer.

2.3.5. Quantification of nucleic acids

For determination of deoxyribonucleic acid (DNA) concentrations ([DNA]), the spectrometer NanoDrop (Thermo Fisher Scientific) was used. Before quantification of the [DNA], the device had to be blanked with H_2O or TE, depending on which solution was used for DNA elution (see 2.3.4). DNA maximally absorbs light of 260 nm. Thus, measuring the absorbance of the sample at 260 nm is an indicator for the concentration of DNA: the higher the absorbance the higher [DNA]. As the sample could be

contaminated with proteins, ribonucleic acid (RNA) or other compounds, sample purity ratios at 260/280 nm (for proteins) and 260/230 nm (organic compounds) were determined. Ideally, 260/230 nm should be 1.5-1.8 and 260/280 nm ≥ 1.8.

2.3.6. Restriction digestion

The most useful tools for the modification of plasmids are restriction enzymes. These enzymes recognize specific palindromic DNA sequences of 4-8 base pairs and hydrolyze the covalent bond between base pairs.

For control digestions, a total reaction volume of 10 µl was used (Table 2.3.1). For preparative gels, a total reaction volume of 40 µl was used (Table 2.3.1). Restriction digestions were carried out for 30-60 min at 37 °C. All FastDigest restriction enzymes and the reaction buffers were purchased from Thermo Fisher Scientific.

Table 2.3.1: Composition of the restriction digestion mixture.

	Control gel	**Preparative gel**
Fast Digest Enzyme 1	0.2 µl	1 µl
Fast Digest Enzyme 2	0.2 µl	1 µl
10x FastDigest Green Buffer	1 µl	4 µl
DNA	1 µg	4 µg
H_2O bidest	ad 10 µl	ad 40 µl
Total volume	10 µl	40 µl

2.3.7. Ligation

The process of DNA ligation is an enzyme catalyzed reaction that serves to connect two pieces of DNA, a vector and an insert, via the formation of phosphodiester bonds.
The ligation was carried out using the Rapid DNA Ligation Kit (Thermo Fisher Scientific) which is composed of T4 DNA Ligase (5 u/µl) and 5X Rapid Ligation Buffer. The vector DNA and insert DNA were mixed with the 5X Rapid Ligation Buffer and the T4 DNA Ligase according to the manufacturer´s protocol (Table 2.3.2). For correct determination of the necessary amount of insert DNA, which was applied at 3:1 molar excess of vector DNA, the ligation calculator from the University of Düsseldorf (http://www.insilico.uni-duesseldorf.de/Lig_Input.html) was used. The ligation mixture was incubated at 22 °C

for 5 min. Five µl of the ligation reaction were used for the transformation of competent bacteria (2.3.3.).

Table 2.3.2: Composition of the DNA ligation mixture.

Linearized vector DNA	50 ng
Insert DNA (at 3:1 molar excess over vector)	variable
5X Rapid Ligation Buffer	4 µl
T4 DNA Ligase	1 µl
H_2O bidest, nuclease-free	Ad 20 µl
Total volume	20 µl

2.3.8. Separation of nucleic acids in agarose gels

In order to analyze the restriction pattern of DNA, the whole volume of the restriction reaction (2.3.6) was loaded onto agarose gels. These gels serve as molecular sieves allowing the separation of linearized DNA fragments according to their length. The size of the pores in the agarose gel depends on the amount of agarose used. Thus, the higher the amount of agarose, the smaller DNA fragments can be separated (Table 2.3.3; taken from www.promega.de).

Table 2.3.3: Resolution of linear DNA on agarose gels.

% of agarose	Optimum resolution for linear DNA
1.0	500 – 10.000 bp
1.5	200 – 3.000 bp
2.0	50 – 2.000 bp

As the size of the constructs generated in this project ranges between 5000 bp - 8000 bp, 1% -1.5% agarose gels were used for the separation of DNA fragments. Gels were made from freshly molten agarose (in TAE buffer; 60 °C). In order to visualize DNA bands, the agarose was mixed with SYBR® Safe DNA Gel Stain (1X; Invitrogen, S33102). Liquid agarose was poured into a gel carrier harboring a molder for sample bags. After solidification of the gel, samples were applied into the sample bags. The electrophoresis was conducted in TAE buffer at 90-120 V.

SYBR® Safe intercalates into nucleic acids and has fluorescence excitation maxima at 280 nm and 502 nm and an emission maximum at 530 nm. It was excited at 280 nm and detected at 530 nm using the Biorad Gel DocTM XR+ System (Bio-Rad, Munich). Gel images were optimized using Image Lab software (Bio-Rad) and Image J (NIH).

For determination of the size of the separated DNA fragments, the DNA ladder λDNA/*Eco*RI+*Hind*III Marker (Thermo Fisher Scientific) was run in parallel.

2.3.9. Isolation of DNA fragments from preparative agarose gels

Often, single DNA fragments obtained from restriction digestion are either used as insert DNA for cloning into new vector backbones or as vector DNA serving as recipient DNA for new inserts. Those fragments have to be isolated from the agarose gel.
The separated DNA fragments were visualized with UV-light using the Biorad Gel DocTM XR+ System (Bio-Rad). Pieces of agarose, harboring the DNA fragment of interest, were cut out with a fresh scalpel blade and transferred into a 1.5 ml tube. DNA was isolated from the agarose gel pieces using the NucleoSpin Gel and PCR Clean-up (Macherey-Nagel) according to the manufacturer´s protocol. The DNA was eluted in H_2O and used for further cloning steps.

2.3.10. Driving gene expression by the TH promoter

For placing the TH promoter (SwitchGear Genomics, S722286) in front of the gene of interest, suitable restriction sites (*Sal*I and *Xba*I) were needed to be inserted into the TH promoter DNA by polymerase chain reaction (PCR) using the primers AAAAAAGTCGACGAGCTCACGCGTGGCGTCTCCTTAGAGA (sense) and AAAAAATCTAGACTCTTACCATGATGGCCTCTGCCTGCTTGGC (antisense) (Eurofins, MWG Operon). The PCR was carried out according to the protocol of the KOD Hot Start DNA Polymerase Kit (Merck Millipore) with the parameters listed in table 2.3.4 and 2.3.5.

The PCR product was purified using the NucleoSpin® Gel and PCR Clean-up Kit (Macherey-Nagel) and eluted in H_2O.
In the next steps, the CMV promoter of the plasmid pcDNA3.1(-) was replaced by the modified TH promoter. pcDNA3.1(-) served as vector backbone. In a first step, the CMV promoter of pcDNA3.1(-) was removed by restriction digestion (2.3.6) with *Mlu*I and *Xba*I. The same enzymes were used to cut the modified TH promoter DNA. The digested DNA was separated in a preparative agarose gel (2.3.8). Fragments of interest were cut out of the agarose gel with a scalpel blade and eluted from the gel (2.3.9). The size of the

resulting fragments was verified by running a 1% agarose gel (Fig. 2.3.1). Following, pcDNA3.1(-) vector was ligated with the TH promoter (2.3.7). The obtained ligation products were transformed in TOP10F competent cells which were grown on Amp-containing LB agar plates over night at 37 °C (2.2.2). The next day, clones were picked and grown in Amp-containing LB medium over night at 37°C in a shaker to propagate the plasmid DNA. The DNA was isolated (2.3.4) and its identity verified by restriction analysis (2.3.6) with *Mlu*I and *Xba*I (Fig. 2.3.2) and by sequencing (data not shown) with the primers GACCGACAATTGCATGAAGAA (sense) and ACCGAGCTCGGATCCACTAGT (antisense). Clone #1 of the new construct, called pcTH, was used for further cloning.

Table 2.3.4: Composition of PCR reaction mixture for modification of the TH promoter.

Component	Volume	Final concentration
10x Buffer for KOD Hot Start DNA Polymerase	5 µl	1 x
25 mM $MgSO_4$	3 µl	1.5 mM
dNTPs (2 mM each)	5 µl	0.2 mM each
H_2O	32.5 µl	-
Sense Primer (10 µM in H_2O)	1.5 µl	0.3 µM
Antisense Primer (10 µM in H_2O)	1.5 µl	0.3 µM
Template DNA (10 ng)	1.0 µl	-
KOD Hot Start DNA Polymerase (1 U/µl)	1 µl	0.02 U/µl
Total reaction volume	50 µl	-

Table 2.3.5: PCR cycling conditions for inserting restriction sites for *Sal*I and *Xba*I into the TH promoter.

Step	Settings
Polymerase activation	95°C for 2 min
Denature	95°C for 20 s
Annealing	60°C for 20 s
Extension	70°C for 20 s
25 cycles	

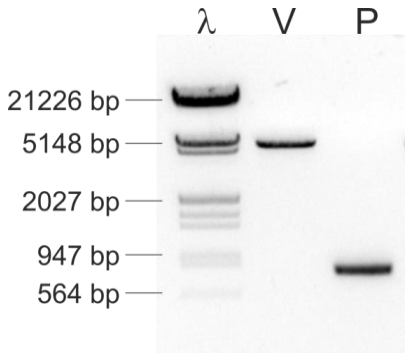

Fig. 2.3.1: Restriction of pcDNA3.1 and TH promoter resulted in expected fragment sizes. pcDNA3.1(-) served as vector (V). As expected, restriction with *Mlu*I and *Xba*I resulted in a fragment of 4740 bp. Restriction of the modified TH promoter (P) resulted in a fragment of 770 bp. The marker λ-*Eco*RI/*Hind*II served as DNA ladder.

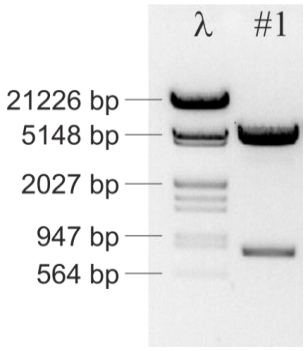

Fig. 2.3.2: Restriction of the vector pcTH confirmed its correctness. Clone #1 of the pcTH vector was tested for its correctness. Restriction with *Mlu*I and *Xba*I resulted in two fragments: 770 bp and 4740 bp. The marker λ- *Eco*RI/*Hind*II served as DNA ladder.

In the following, EGFP was inserted into the new pcTH vector construct. For this reason, Vector DNA (pcTH#1) and insert DNA (taken from pEGFP-N1) were both restriction digested (2.3.6) with *Eco*RI and *Afl*II for 1 hour at 37°C. Fragments were separated in a 1.5% preparative gel and vector and insert fragments of interest were cut out with a scalpel blade (2.3.8; Fig. 2.3.3, ---).

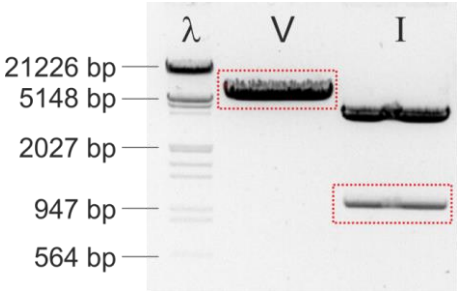

Fig. 2.3.3: Restriction of pcTH and pEGFP-N1 with *Eco*RI and *Afl*II. pcTH#1 served as vector (V; 5466 bp), the EGFP of pEGFP-N1 served as insert (I; 1010 bp). The marker λ-*Eco*RI/*Hind*II served as DNA ladder. Red-marked bands were cut out with a scalpel blade.

Isolated fragments were extracted from the gel (2.3.9) and their concentration determined by using the NanoDrop device (2.3.5). The vector pcTH#1 (5466 bp) and the insert EGFP (1010 bp) were assembled by ligation (2.3.7). TOP10F competent cells were

transformed with the resulting construct called "pcTH-EGFP" and grown on Amp-containing LB agar plates over night at 37°C (2.3.3). The next day, clones were picked and multiplied in Amp-containing LB medium overnight at 37 °C in a shaker. DNA was isolated the next day (2.3.4). The correct insertion of the EGFP-insert into the vector backbone (pcTH) was verified by restriction digestion (2.3.6) with *Eco*RI and *Afl*II (Fig. 2.3.4). Clone #4 of the new construct (pcTH-EGFP) was positive and used for further experiments.

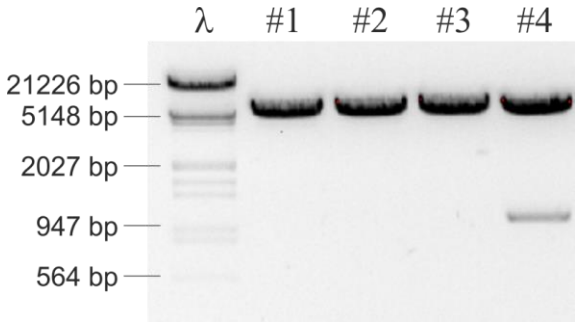

Fig. 2.3.4: Restriction of new construct pcTH-EGFP with *Eco*RI and *Afl*II. Restriction with *Eco*RI and *Afl*I resulted in a fragment of 1010 bp (GFP) and 5466 bp only in clone #4. The marker λ-*Eco*RI/*Hind*II served as DNA ladder.

In the last step, the DNA fragment coding for the synapto-pHluorin sensor was inserted into the pcTH vector construct. In order to do so, vector DNA (pcTH#1) and the insert DNA (taken from p156rrlSybIIpHluorin) were both restriction digested (2.3.6) with *Xba*I and *Eco*RI for 2.5 hrs at 37 °C. Fragments were separated in a preparative gel (2.3.8) and vector and insert fragments were cut out with a scalpel blade (2.3.9; Fig. 2.3.5, ---).

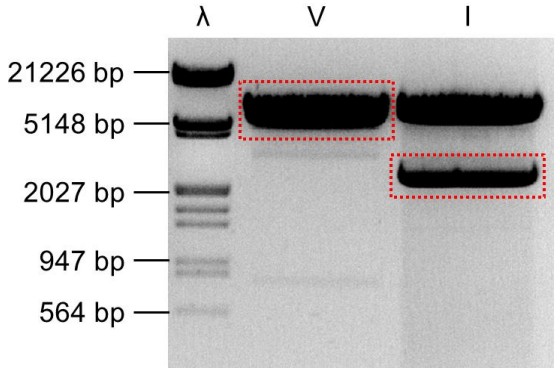

Fig. 2.3.5: Restriction of pcTH and p156rrlSybIIpHluorin with *Xba*I and *Eco*RI. pcTH#1 served as vector (V; 5471 bp), the CDS of p156rrlSybIIpHluorin served as insert (I; 2354 bp). The marker λ-*Eco*RI/*Hind*II served as DNA ladder. Red-marked bands were cut out with a scalpel blade.

The DNA was eluted from the agarose gel (2.3.9). The concentration was determined by the NanoDrop device (2.3.5). The vector (pcTH#1) and the insert (SynpH) were assembled by ligation (2.3.7). TOP10F cells were transformed with the new construct "pcTH-SynpH" and grown on Amp-containing LB agar plates over night at 37 °C (2.3.3).

Clones were picked the next day and multiplied in Amp-containing LB medium over night at 37 °C in a shaker. The next day, DNA was isolated from cells (2.3.4). To check, whether the synapto-pHluorin is inserted correctly into the pcTH vector, the eluted DNA was restriction digested with *Xba*I and *Eco*RI (2.3.6). Six out of 10 clones were positive (Fig. 2.3.6). Clone #4 was used for further studies.

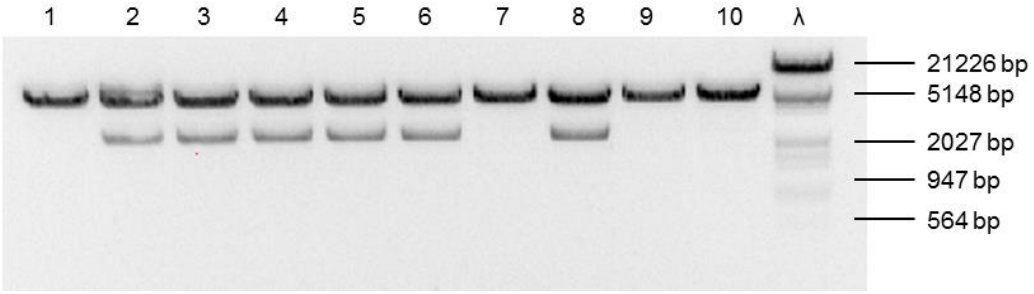

Fig. 2.3.6: Restriction of pcTH-SynpH with *Xba*I and *Eco*RI. Clone 2-6 and clone 8 were verified to be correct clones as restriction resulted in two fragments of expected lengths: 2354 bp and 5471 bp. The marker λ-*Eco*RI/*Hind*II served as DNA ladder.

The sequence and the vector maps for both newly generated constructs (pcTH-EGFP and pcTH-SynpH) are provided in the appendix.

2.4. Cell culture

2.4.1. Stable cell line culture

2.4.1.1. Human Embryonic Kidney 293 cells

Human Embryonic Kidney 293 cells (HEK293) are originally derived from human embryonic kidney cells. They were generated by transformation with adenovirus 5 (Graham *et al.*, 1977). HEK293 cell were cultured in DH10 or M10 medium at 37°C, 5% CO_2 and 95% humidity in 10 cm culture dishes. The whole culture medium was exchanged every second day. Cells were splitted twice a week when confluency of 90% was reached.

2.4.1.2. Splitting and seeding cells

Cells, cultured in 10 cm dishes, were incubated in 1 ml of trypsine w/ EDTA at 37 °C until the cells detached from the culture dish. The activity of trypsine was stopped by adding 5 ml warm DH10 medium. Cells were dissociated by pipetting the solution up and down. To completely remove the trypsine, the cell suspension was centrifuged for 5 min at 200 g. Following, the supernatant was removed and the pellet resuspended in 5 ml of DH10 medium. The cell number was determined by a Neubauer-hemocytometer.

For maintenance, cells were seeded at a density of 8×10^5 in DH10 medium. After 30 passages, cells were discarded and a new aliquot thawed for further culturing. For long-term-storage, cells were harvested from a 10 cm plate when they were in the logarithmic growth-phase. About 2×10^6 cells per ml medium with 10% DMSO were frozen in liquid nitrogen.

2.4.1.3. Coating coverslips with Poly-L-Lysine

Single sterile glass coverslips were placed in each well of the multiwell plate. A poly-L-lysine (PLL) stock solution (1 mg/ml) was diluted 1:10 with H_2O. Each coverslip was covered with 500 µl of the 1:10 PLL solution. Coating was carried out for 2 hours at room temperature (RT) or overnight at 4°C. After coating, the PLL solution was aspirated off the coverslips. Then, coverslips were washed twice with H_2O bidest and dried before cells were plated.

2.4.1.4. Liposome-mediated transfection

Cells were seeded such that they reached a density of 4×10^5 cells/coverslip on the day of transfection. The transfection mixture was prepared as follows: 100 µl OPTI-MEM plus 1 µl Lipofecatmine 2000 reagent and DNA (concentration dependent on construct) per well were mixed and vortexed for 30 s. The culture medium was reduced to 200 µl, and 100 µl of the transfection mixture were added to each well. Cells were incubated for 1 hour at 37 °C. Afterwards, the whole transfection mixture was replaced by 500 µl fresh culture medium. Cells were further incubated at 37 °C and 5% CO_2 until they were used for measurements the next day.

2.4.1.5. AAV transduction

HEK293 cells growing in M10 medium were seeded onto PLL-coated coverslips with a density of $\mathbf{1 \times 10^4}$ cells per well. One day later, cells were transduced with AAV2sub-EPAC1-camps. The virus stock was diluted in M10 to a final concentration of $\sim 2.1 \times \mathbf{10^8}$ virus particles (vp) per ml. After removal of the incubation medium, 350 µl of the virus dilution was added to each well (final concentration: $\sim \mathbf{7.35 \times 10^7}$ vp per well). Cells were further incubated at 37 °C and 5% CO_2. Every second day, 100 µl of fresh M10 medium were added to each well to always provide cells with fresh nutrients. The cells were cultured for another five days and then splitted. In order to do so, culture medium was replaced by 250 µl trypsine w/ EDTA per well. After the cells detached from the glass coverslip, the activity of trypsine was blocked by adding 500 µl M10 medium.

Twohundredfifty µl of the resuspended cells were transferred to a new well harboring a PLL-coated coverslip. The total volume of the well was adjusted to 500 µl. Before using the cells for imaging experiments on the following day, cells were washed twice in fresh M10 medium in order to remove the virus.

2.4.2. Primary culture of dissociated retinal neurons

2.4.2.1. Preparation of coverslips

The day before plating the cells, sterile coverslips (⌀13 mm) were coated with poly-D-lysine (PDL). The coverslips were placed onto a piece of parafilm (Bemis Company Inc., Oshkosh, WI) in a petri dish to prevent spilling of the liquid. Each coverslip was covered with 150 µl of a 0.1 mg/ml PDL stock solution and incubated at RT overnight. To ensure complete sterility, UV-light was turned on for 2 hours. On the day of dissociation, PDL solution was aspirated off the coverslips which were in turn washed twice with sterile water. Subsequently, each dried coverslip was covered with 150 µl of a 10 µg/ml laminin stock solution. Incubation was carried out for 2-6 hours at RT.

2.4.2.2. Isolation of retinae

Retinae were taken from neonatal mouse pups (C57BL/6) at the age of P1 to P4. Neonatal pups were sacrificed by decapitation. The whole preparation procedure was carried out under semi-sterile conditions (instruments and surfaces were disinfected with 70 % EtOH). Eyes were quickly enucleated and transferred into sterile 37 °C warm Hank´s solution. The eyeball was locally opened by a fine injection needle. Following, the eyeball was cut open along the *ora serrata* using fine scissors. Upon that, the lens, cornea and vitreous body were separated from the eye cup harboring the retina. The retina was exposed by carefully removing the eyecup and cutting the optic nerve. Using a small spoon, 2-6 isolated retinae were transferred into a 1.5 ml Eppendorf tube filled with 1 ml of 37 °C warm Hank´s solution.

2.4.2.3. Dissociation of isolated retinae

The following steps were carried out under sterile conditions in a laminar flow hood. The retinae were briefly centrifuged and the Hank's solution removed carefully. One ml of 37 °C warm Ca^{2+}-Mg^{2+}-free Hank's solution (CMF-Hank's) was added to the retinae. The tissue was incubated for 10 min at 37 °C in the water bath. Then, CMF-Hank's solution was removed carefully and replaced by an activated papain solution (activation was carried out by dissolving the papain powder in CMF-Hank's (20 U/ml)). After an

incubation time of 20-30 min at 37 °C in the water bath, the papain solution was removed and the retinae were washed twice with pre-warmed $DMEM_{neuro}$ to inactivate the papain. Cells were dissociated in 1 ml fresh $DMEM_{neuro}$ by pipetting the solution up and down several times. The cell number was determined in a hemocytometer. Before seeding the cells, the laminin solution was removed from the coverslips (but coverslips were not completely dried). Three hundred thousand cells were plated per coverslip (still on the parafilm) in a total volume of 150 µl. To let the cells attach to the coated surface of the coverslip, cells were incubated at 37 °C for 1 hour. Then, the coverslips were transferred into a 24-well plate and the total volume per well was adjusted to 500 µl.

2.4.2.4. AVV transduction

Two days after seeding the cells (2 DIV), retinal dissociated neurons were transduced with AVVs that were serving as gene shuttles. Virus stocks were synthesized and kindly provided by Prof. A. Baumann's group (ICS-4, FZ Jülich; Table 2.4.1).

Table 2.4.1: Viruses used in this thesis.

Serotype	Protein	Stock concentration (vp/µl)	Application
AAV2sc	GFP	1.66 - 1.78 x 10^9	*In vivo* and *in vitro*
AAV2sc	GCaMP3.0	1.16 x 10^9	*In vivo*
AAV2sub	EPAC1-camps	7.39 x 10^7	*In vivo* and *in vitro*

sc: self-complementary; sub: psub201 vector backbone (Samulski *et al.*, 1987)

The virus stocks were diluted in $DMEM_{neuro}$ to a final concentration of 3.3×10^9 vp per ml. After removal of the incubation medium, 300 µl of the virus dilution was added to each well (final concentration: 1×10^9 vp per well). Cells were further incubated at 37 °C and 5% CO_2. Every second day, 100 µl of fresh $DMEM_{neuro}$ were added to each well to always provide cells with fresh nutrients. Depending on the used virus type, cells were incubated for further 3-7 days to ensure complete expression of the gene of interest. Before using the cells for imaging, the whole virus suspension was removed and cells were washed twice with fresh $DMEM_{neuro}$.

2.4.2.5. Liposome-mediated transfection

On 2 to 5 DIV, retinal neurons were transiently transfected by using Lipofectamine® 2000 transfection reagent. A mixture of 100 µl OPTI-MEM, 1 µl Lipofectamine 2000 transfection reagent and DNA (concentration dependent on construct; Table 2.4.2) was

prepared per well that should be transfected. The mixture was vortexed shortly. The culture medium in each well was reduced to 200 µl. Then, 100 µl of the transfection mixture were added to each well. Transfection was carried out for 1 hour at 37°C and 5% CO_2. After incubation, cells were washed with pre-warmed fresh $DMEM_{neuro}$ once and further incubated in fresh $DMEM_{neuro}$ until used for experiments.

Table 2.4.2: cDNA used for transient transfection of retinal cultures and HEK293 cells (2.4.1.14).

Construct name	Backbone	Coded protein	Origin
AKAR4	pcDNA3	PKA activity sensor AKAR4	Dr. S. Mehta, Johns Hopkins University
D1R-GFP	pCMV6-AC-GFP	GFP-tagged D1R	Origene, MG226226
EPAC1-camps	pcDNA3.1	cAMP-sensor EPAC1-camps	Prof. Lohse, Univ. Würzburg
pcTH-EGFP	pcDNA3.1	TH-driven EGFP	See 2.3.10
pcTH-SynpH	pcDNA3.1	TH-driven synapto-pHluorin	See 2.3.10
pEGFP-N1	pcDNA3.1	Enhanced GFP	Clontech, 632469
p156rrlSybIIpHluorin	p156rrl	Synapto-pHluorin	Dr. R. Guzman, ICS-4, FZ-Jülich

2.4.2.6. Fixation of cultured cells

Before fixation, the incubation medium was removed. Fixation with 4% PA was carried out for 5 min at RT and stopped by washing the cells with 0.1 M PB twice. Fixed cells were stored at 4 °C in PB.

2.5. Ocular Injections

The ultimate aim of my project was to express sensor proteins in the intact retinal tissue of living mice. As the application of Lipofectamine-transfection is restricted to the culture system, alternative methods had to be found. One of them is AAV-mediated gene transfer which was already described for the retinal culture system (2.4.2.4). In order to use AAVs for infection of neurons *in vivo*, we established the method of ocular injections.

2.5.1. Equipment/Micro injection system

To inject minimal volumes of virus or DNA solution precisely into the eye of newborn mouse pups a micro-injection system was used. This system was composed of a

33 gauge beveled needle (WPI, Germany) connected to a 10 µl NanoFil syringe (WPI, Germany) via a polyethylene tube (ID 0.38 mm; AgnoTho´s AB, Sweden).

2.5.2. Anesthesia

Five to 8 day old mouse pups (C57Bl/6) were anesthetized by subcutaneous injection of an anesthetic cocktail according to the protocol of Preißel (Preißel, 2006; Table 2.5.1). The anesthetic cocktail was composed of Medetomidin (Domitor©, Pfizer), Midazolam (Dormicum©, Hoffman-LaRoche AG) and Fentanyl (Fentanyl-Janssen©, Janssen GmbH) (Preißel, 2006), the antidote cocktail of Atipamezol (Antisedan©, Pfizer, Karlsruhe), Flumazenil (Anexate©, Hoffman-LaRoche AG) and Naloxon (Narcanti©, Janssen GmbH) (Table 2.5.1). Mice were anesthetized with 10 µl of the anesthetic cocktail per g body weight. Approximately 6 min after injection of the anesthetic cocktail, the pups did not show any reflexes and the ocular injection could be started. Directly after the operation, 10 µl of the antidote cocktail per g body weight were injected subcutaneously.

Table 2.5.1: Composition of anesthetics and antidote for anesthesia of mouse pups.

Substance	Volume (µl)	Final concentration
Anesthetics		
Meditomidin	50	1 mg/ml
Midazolam	100	1mg/ml
Fentanyl	100	0.1 mg/ml
Sodium-Chloride solution	750	-
Antidote		
Atipamezol	50	5 mg/ml
Flumazenil	500	0.1 mg/ml
Naloxon	300	0.4 mg/ml
Sodium-Chloride solution	150	-

2.5.3. Operation procedure

The whole operation procedure was carried out under a dissecting microscope (Leica Microsystems, Germany). The pups were kept warm by a warming pad (42 °C) and were continuously provided with fresh oxygen. Before exposing the eye, Xylocain gel

(AstraSeneca GmbH, Wedel, Germany) was applied to the skin covering the eye in order to locally anaesthetize the operation area. The eye was exposed by cutting along the fused junctional epithelium using a scalpel blade. To enable insertion of the injection needle (33 gauge, beveled, WPI) a small hole was made at the *ora serrata* using a 20 gauge beveled needle (Braun). Then the injection needle was inserted through the hole until a slight resistance could be sensed. Upon that, the injection needle was withdrawn minimally until it could be seen through the lens. Half a microliter of virus stock (for AAV-mediated gene-transfer; see table 2.4.1) or DNA solution (for electroporation) were injected. After about 5 s, the injection needle was carefully withdrawn from the eye. The antidote was given directly after the operation procedure was finished. To prevent inflammation, the wound (of the cover skin) was covered with antibiotics (Refobacin Augensalbe, Merck). The pups were observed during the wake-up phase. During that, they were constantly kept warm and provided with fresh oxygen. Around 10 min after operation, the pups could be given back to the mother. The condition of the injected pups was checked daily in order to make sure that they did not suffer from pain.

2.5.4. *In vivo* electroporation

Directly after the injection of DNA (2.5.3), mouse pups were subjected to electroporation. To this end, the head of the pup was carefully placed between two tweezertrodes (BTX Harvard Apparatus) that were soaked in 0.1 M PB in order to ensure full conductivity. The positive electrode was always placed onto the injected eye. Five square wave pulses of 50 ms duration, 950 ms interval and 80 or 100 V were given by a pulse generator (ECM830, BTX Harvard Apparatus). Immediately after electroporation, the antidote was given and the injected eye was smeared with antibiotics (Refobacin Augensalbe, Merck). In the following, pups were treated as described in 2.5.3.

2.6. Preparation of living slices of the retina

2.6.1. Setting up the vibratome

The chamber of the vibratome (VT 100 S, Leica Biosystems) was filled with ice cold and oxygenated (mixture of 5% CO_2 and 95% O_2) Ames solution. The knife holder was equipped with a razor blade (Personna Platinum Chrome, Mühle, Germany).

2.6.2. Isolation of the retina

Untreated or injected mice were deeply anaesthetized with isofluorane and decapitated using scissors. Eyes were quickly enucleated and transferred into 4 °C Hank´s solution. The eyeball was locally opened by a fine injection needle. Following, the eyeball was cut open along the *ora serrata* using fine scissors. Upon that, the lens, cornea and vitreous body were separated from the eye cup harboring the retina. The retina was exposed by carefully removing the eyecup and cutting the optic nerve.

2.6.3. Preparation and embedding of the retina

Before starting the sectioning procedure, 4% low melt agarose (Peqlab, 35-2020) was dissolved in Hank's solution by heating it up to 80 °C in a water bath under continuous stirring. Lowering of the temperature to 38 °C was started when the air bubbles had vanished. The agarose was kept at 38 °C until usage. Retinae from adult untreated or injected C57Bl/6 mice were prepared as described in 2.6.2. After the retina had been isolated, edges were carefully cut with a scalpel blade in order to simplify flattening of the retina. Then, the retina was moved to the tip of a spatula GC side up. The retina was flattened with fine brushes and subsequently carefully dried with small pieces of filter paper. After that, a 3 cm petridish was filled with liquid agarose (38 °C). The retina was vertically inserted into the agarose and carefully detached from the spatula using a brush. In order to fasten up the solidification of the agarose, the 3 cm dish was placed onto crushed ice for about 2 min. After solidification, the agarose was cut into a trapezium containing the retina and fixed with instant glue onto the specimen disc in a way that the retina was vertically oriented relative to the razor blade. Two hundred µm thick slices were cut at a speed/frequency of 7 and were collected from the chamber using a brush. The retinal slices were transferred into oxygenated Ames solution at RT and kept there until used for imaging. The whole procedure was carried out in room light.

2.6.4. Transferring retinal slices into the imaging chamber

Retinal sections were transferred with a brush to a custom-made perfusion chamber (2.7.2) that was filled with oxygenated Ames solution. Slices were fixed with a custom-made harp (U-shaped wire covered with nylon strings) and mounted onto the imaging setup.

2.7. Widefield-Imaging

2.7.1. Imaging setup

Microscope:	Examiner.Z1 (upright) Lens: 40x/1.0 water	Zeiss
LEDs:	Colibri (420 nm, 470nm)	Zeiss
Camera:	iXon (Model No. DV885JCS-VP; cooled EMCCD)	Andor Technology
Filter-sets:	Filter set 47 (489047-0000) Filter set 38 (1031-346)	Zeiss

2.7.2. Perfusion chamber

A custom made perfusion chamber was used for all imaging experiments. Imaging objects were placed into the center of the perfusion chamber and continuously perfused with solution using a gravity-driven multichannel perfusion system. The solution entered the chamber via a plastic tube and was aspirated through a second plastic tube by a roller pump. Cells were perfused at a flow rate of 3-4 ml/min in order to exchange the medium in a maximal time range of 30 s.

2.7.3. Ca^{2+}-imaging with Fluo-4 and GCaMP3.0

2.7.3.1. Loading of the cells with Fluo-4

For visualizing changes in $[Ca^{2+}]_i$ in neurons, cells were loaded with the synthetic Ca^{2+}-indicator Fluo-4 AM (Invitrogen). The loading solution was composed of 4 µl Fluo-4-AM (2 mM in DMSO) per ml ES_{neuro}. Cells growing on glass coverslips were incubated in 500 µl/well of the loading solution for 20-30 min at RT in the dark. After loading, cells were directly transferred to the custom-made imaging chamber and continuously superfused with solution via a gravity-driven perfusion system.

2.7.3.2. Data acquisition

Fluo-4 has an excitation maximum at 494 nm and an emission maximum at 506 nm in the Ca^{2+}-bound state (Invitrogen). GCaMP3.0 has an excitation maximum at 497 nm and an emission maximum at 513 nm in the Ca^{2+}-bound state (Shigetomi *et al.*, 2013). The setup was adjusted to these criteria as such, that Fluo-4 and GCaMP3.0 were excited at a

wavelength of 470 nm at an LED intensity of 2-5%. The exciting light was passed through a band pass filter (BPF) for 470/40 nm (Carl Zeiss, Germany). Excitation and emission light were separated by a dichroic mirror FT 495 (Carl Zeiss, Germany). The emission light was passed through a BPF 525/50 nm (Carl Zeiss, Germany) and was finally detected by an iXon camera (Andor Technology). The cells were continuously exposed to excitation light. Images were recorded at 0.5-1 Hz and stored as stacks of TIF files.

2.7.3.3. Data evaluation

Using ImageJ software (NIH), original data were processed by defining regions of interest (ROI). To cancel out variations in cell thickness, total dye concentration and illumination heterogeneities, the fluorescence signal was expressed as relative fluorescence change dF/F which is defined as follows:

$$\frac{\Delta F}{F} = \frac{(F - F0)}{F0}$$

F denotes the background-subtracted fluorescence level after a stimulus and F0 denotes the background-subtracted pre-stimulus fluorescence level (Yuste, 2005). The background signal was calculated from a ROI positioned in the background of the image movie. Diagrams were generated and statistical analysis was conducted in Origin 8.0 and/or SigmaPlot. Differences were considered as not significant (n.s) at $p>0.5$, as weakly significant at $p^{*}\leq 0.05$, as moderately significant at $p^{**}\leq 0.01$, and as highly significant at $p^{***}\leq 0.001$ when compared to control.

2.7.4. FRET- based imaging

2.7.4.1. TN-L15 imaging in isolated retinal wholemounts

Retinae of adult TN-L15 mice were isolated as described in 2.6.2 and cut into three pieces each. One third of the retina was used for each single imaging experiment. The remaining pieces were kept in oxygenated Ames solution in darkness until they were used for imaging. One piece of retina was transferred into the imaging chamber with the PRs facing the bottom of the chamber and fixed with a custom made harp (U-shaped

wire covered with nylon strings). During the whole measurement, the retinal piece was perfused with oxygenated Ames solution with or without desired agents.

2.7.4.2. FRET-based imaging in cultured cells

Cells, growing on glass coverslips and expressing the EPAC1-camps or AKAR4 sensor after transient transfection with Lipofectamine 2000 or after viral infection with AAV2, were carefully transferred into the custom-made imaging chamber. During the whole measurement, cells were continuously perfused with ES with or without desired agents (ES_{neuro} for cultured retinal neurons and ES_{normal} for HEK293 cells).

2.7.4.3. Data acquisition

The fluorophores CFP and YFP have an excitation/emission maximum of 435/485 nm and 508/524 nm, respectively. Sensors were excited at a wavelength of 420 nm with a LED intensity between 2-8 %. The excitation and emission light was separated by a dichroic mirror FT 455 (Carl Zeiss, Germany). Following, the emission light was passed through an image splitter (505 nm) which separated CFP emission light from YFP emission light. Both, the CFP and YFP emission light were detected by the same iXon camera (Andor Technology). The cells were always exposed to excitation light. Images were captured at 0.5 Hz and stored as stacks of TIF-files.

2.7.4.4. Data evaluation

The recorded data were processed using a software plugin based on Matlab (Mathworks) which was programmed by Dr. Dai (ICS-4, FZ Jülich). The background-subtracted fluorescence level of well-defined ROIs was determined within the program and the ratio between YFP and CFP was calculated for each ROI. A change in the ratio between the two fluorophores indicates a change in the intracellular concentration of the second messengers cAMP (FRET sensor: EPAC1-camps), a change in PKA activity (FRET-sensor: AKAR4) or a change in $[Ca^{2+}]_i$ (FRET sensor: TN-L15). Diagrams were generated and statistical analysis was conducted in Origin 8.0 and/or SigmaPlot. Differences were considered as not significant (n.s) at $p>0.5$, as weakly significant at $p^{*}\leq0.05$, as moderately significant at $p^{**}\leq0.01$, and as highly significant at $p^{***}\leq0.001$ when compared to control.

2.8. Immunochemistry

2.8.1. Antibody staining of cultured cells

The staining procedure was carried out in two steps. First, fixed cells (2.4.2.6) on glass coverslips were incubated with primary antibodies (Table 2.8.1; in CTA) for 1 hour at RT. After that, fixed cells were washed twice with 0.1 M PB for 10 min. Second, cells were incubated with fluorescent-labeled secondary antibodies (Table 2.8.2; in CT) for 30 min at RT in the dark. Again, fixed cells were washed twice in 0.1 M PB for 10 min. Finally, coverslips were embedded in a small drop of Aqua Polymount (Polysciences, Warrington, USA). Stained cultures were stored at 4 °C.

2.8.2. Antibody staining of retinal cryosections

2.8.2.1. Fixation and cryoprotection of retinae

Retinae were isolated as described in 2.6.2 but were still protected by the eyecup. Retinae and eyecups were fixed for 30 min in 4% PA at RT. After fixation, the tissue was washed twice with 0.1 M PB for 10 min. Fixed retinae inside the eyecups were cryoprotected by infiltration with 10% sucrose for one hour following an overnight cryoprotection in 30% sucrose.

2.8.2.2. Cryosectioning

The cryoprotected retinae were isolated from the eyecup and flattened on a glass slide covered with a piece of parafilm. Sucrose solution was removed with a filter paper. Retinae were covered with NEG50TM and immediately frozen in the cryostat (Thermo Fisher Scientific, Microm HM 560) at -50 °C. Frozen retinae were mounted on a specimen stage (-15 °C; Thermo Fisher Scientific) and cut into 18 µm vertical sections with a blade (-20 °C). Cryosections were collected on Superfrost plus glass slides (J1800AMNZ, Thermo Fisher Scientific) and either directly used for antibody stainings or stored at -20 °C until usage.

2.8.2.3. Staining procedure

Retina sections (2.8.2.2) were pre-incubated in CTA for 15 min. After this, CTA was removed and the primary antibodies (Table 2.8.1), diluted in CTA, were added. Incubation was carried out over night at RT in a moist chamber. The following day, retinal sections were washed in 0.1 M PB for 10 min at RT. Following, secondary antibodies (Table 2.8.2), diluted in CT, were applied to the sections and incubated for 1 hour in the dark at RT. After this, the sections were again washed in 0.1 M PB for 10 min

and then covered with a drop of Aqua Polymount and a glass coverslip (VWR, 631-0144). The stained sections were stored at 4 °C.

2.8.3. Antibody staining of retinal wholemounts

The staining procedure was carried out in two steps. Fixed retinal wholemounts (2.8.2.1) were incubated in primary antibodies (Table 2.8.1; in CTA) for a minimum of 24 hrs at RT. Following, the wholemounts were washed twice in 0.1 M PB for 10-20 min. Second, incubation in secondary antibodies (Table 2.8.2) for a minimum of 6 hrs at RT in the dark followed. Again, retinal wholemounts were washed twice in 0.1 M for 10-20 min. Following, the retinae were embedded in Aqua Polymount (Polysciences, Warrington, USA) and covered with a glass coverslip (VWR, 631-0144).

2.8.4. Antibodies

Table 2.8.1: Primary antibodies used in this project. Abbreviations: ch- chicken; gp- guinea pig; gt- goat; ms- mouse; rb- rabbit; rt- rat

1st antibody	Antigen	Host	Dilution	Origin
AB5585	Recoverin	rb	1:2000	Chemicon, ab5585
CaBP	Calbindin	rb	1:2000	Abcam, ab11426
D1mono	Dopamine receptor 1	rt	1:500	Sigma, d187
GFP	Green fluorescent protein	ch	1:1000	Chemicon, ab16901
		rb	1:8000	Abcam, ab290
Glycine	Glycine	rt	1:3000	Pow *et al.*, 1995
GlyT1	Glycine transporter 1	gt	1:2000	Chemicon, ab1770
Goα	G-protein o	ms	1:16000	Chemicon, mab3073
HCN2α E2	HCN2	rb	1:500	AG Müller, Dr. A. Mataruga, ICS-4
PKARIIb	Protein kinase A	rb	1:500	Chemicon, ab1614
		ms	1:2000	BD Biosciences, p54720
PKCα	Protein kinase C alpha	rb	1:2000	Santa Cruz, sc208

1st antibody	Antigen	Host	Dilution	Origin
Rec, K2	Recoverin	rb	1:1000	Dr. K. Koch, ICS-4
TH	Tyrosine hydroxylase	ms	1:500	Sigma, t2928
		ch	1:500	Neuromics, ch23006
vGlut1	Vesicular glutamate transporter 1	gp	1:30000	Chemicon, ab5905

Table 2.8.2: Secondary antibodies used in this project. Abbreviations: ch- chicken; d- donkey; gp- guinea pig; gt- goat; ms- mouse; rb- rabbit; rt- rat

2nd antibody	Dilution	Origin
gt anti rt A488	1:500	Invitrogen, A11006
gt anti rb A488	1:500	Invitrogen, A11034
d anti gt Cy2	1:400	Dianova, 705-225-147
d anti gp Cy2	1:400	Dianova, 706-225-148
d anti rb Cy2	1:400	Dianova, 711-225-152
d anti ms Cy3	1:100	Dianova, 715-165-150
d anti rb Cy3	1:100	Dianova, 711-165-152
d anti rt Cy3	1:500	Dianova, 712-165-153
d anti rb Dy649	1:500	Dianova, 711-495-152
d anti rt Cy5	1:200	Dianova, 712-175-153
gt anti ch Dy549	1:800	Dianova, 103-505-155

TO-PRO®3 staining was conducted during the incubation of the secondary antibodies. TO-PRO®3 was applied in a dilution of 1:1000.

2.9. Confocal Microscopy

Immunohisto- or cytochemically treated samples were analyzed with a confocal laser scanning microscope (TCS SP5 II, Leica Microsystems, Germany). Leica LAS AF software was used to control the intensity of lasers and filter settings. The microscope was equipped with an Argon laser, generating the wavelength 458 nm (for CFP) and 488 nm (for Cy2 and GFP), and three Helium-Neon lasers, generating the wavelength 543 nm (for Cy3), 594 nm (for Alexa594) and 633 nm (for Cy5, Alexa647, DyLight649, TO-PRO®3).

In many cases, serial pictures of different focal planes were obtained (so-called stacks). The settings were selected such that the distance between different focal planes was about 1 µm. To rule out cross-talk between fluorescence detection channels in multiple stained samples, the sequential scanning mode was used. In addition, well defined band pass filters of 465 - 490 nm for CFP, 500 - 540 nm for Cy2 and GFP, 555 - 605 nm for Cy3, 610 - 635 nm for Alexa594, and 650 - 750 nm for Cy5, Alexa647, DyLight649, TO-PRO®3 were used. All fluorescence micrographs were artificially colored. The recorded stacks were converted into 2D images in ImageJ (tool: “Maximum Intensity Projection”, MIP). Each pixel of the output MIP-image depicts the maximum value over all images in the stack at the perpendicular pixel location (ImageJ, NIH). Pictures of cultured cells or vertical sections of the retina were acquired with 20x/0.70 oil or 63x/1.32-0.6 oil immersion objectives at an image resolution of 1024x1024 pixels. In order to improve the resolution, every image was scanned 4 times. The resulting value per pixel was finally averaged over the sum of measurements (tool: “line average”). Overviews of retinal wholemounts were acquired with a 10x/0.30 air objective at an image resolution of 512x512 pixels (line average: 2). As the whole flattened retina is larger than the field of view, the “stitching tool” (Leica) was used. This tool acquires stacks of images at different positions of the sample. MIP images were generated from each stack. Finally, all MIP-images from the different positions were assembled to one single picture.

2.10. Pharmaceuticals

Table 2.10.1: Pharmaceuticals used in this project.

Pharmaceutical	Stock	Biological function	Distributor
Calyculin A	100 µM	Phosphatase 1 and 2A inhibitor	Research Biochemicals Inc., C-149
CGP54626	5 mM in DMSO	$GABA_B$-receptor antagonist	Tocris, 1088
6-Cyano-7-nitroquinoxaline-2,3-dione (CNQX)	20 mM in H_2O	AMPA/kainate receptor antagonist	Tocris, 1045
Cyclopiazonic acid (CPA)	100 mM in DMSO	SERCA inhibitor	Sigma-Aldrich, C1530
D-(-)-2-Amino-5-phosphonopentanoic acid (D-AP5)	20 mM in H_2O	NMDA receptor antagonist	Tocris, 0106
Dopamine hydrochloride	10 mM in H_2O	Dopamine receptor agonist	Sigma Aldrich, H8502
Eticlopride	26.5 mM in H_2O	D2-receptor antagonist	Sigma-Aldrich, E101
Gallein	50 mM DMSO	Gβγ inhibitor	Tocris, 3090
H89	20 mM in H_2O	Protein kinase A inhibitor	Tocris, 2910
3-Isobutyl-1-methylxanthin (IBMX)	500 mM in DMSO	Phosphodiesterase inhibitor	Sigma-Aldrich, I-5879
L-(+)-2-Amino-4-phosphonobutyric acid (L-AP4)	50 mM in NaOH	mGluR6 agonist	Tocris, 0103
Nimodipine	10 mM in DMSO	L-type Ca^{2+}-channel blocker	Sigma-Aldrich, N149
NKH477	10 mM in DMSO	Adenylate cyclase activator	BioTrend, BS0123
Noradrenaline	100 mM in H_2O	Agonist at adrenoreceptor	Sigma-Aldrich, A0937
Picrotoxin	50 mM in DMSO	$GABA_A$-receptor antagonist	Sigma-Aldrich, P1675
Quinpirole	20 mM in H_2O	D2-receptor agonist	Sigma-Aldrich, Q102

Pharmaceutical	Stock	Biological function	Distributor
SCH 23390	10 mM in H_2O	D1-receptor antagonist	Sigma-Aldrich, D054
SKF 38939	10 mM in H_2O	D1-receptor agonist	Sigma-Aldrich, D047
Strychnine	10 mM in H_2O	Glycine-receptor antagonist	Sigma-Aldrich, S8753
(1,2,5,6-Tetrahydropyridin-4-yl)methylphosphinic acid (TPMPA)	20 mM in H_2O	$GABA_C$ antagonist	Tocris, 1040
ω-Conotoxin GVIA	0.329 mM in H_2O	N-type Ca^{2+}-channel blocker	Tocris, 1085

2.11. Software

Table 2.11.1: Software used in this project.

Software	Purpose	Producer
Andor Solis X-1707	Data aquisition	Andor
Corel Draw X6	Image processing	Corel
Exel Professional Plus 2010	Data analysis	Microsoft
Image J	Data analysis, Image processing	National Institutes of Health (NIH)
LAS AF	Data acquisition, Image processing	Leica
Ligation Calculation	Ligation calculation	http://www.insilico.uni-duesseldorf.de
Matlab	FRET data analysis	The MathWorks
Origin Pro 7	Statistical analysis, Diagrams	OriginLab
Power Point Professional Plus 2010	Image processing	Microsoft
SigmaPlot10	Statistical analysis	Systat Software GmbH
Vector NTI	Sequence analysis Restriction analysis Plasmid construction	Life Technologies
Word Professional Plus 2010	Word processing	Microsoft

3. Results

3.1. Immunocytochemical analysis of the dopaminergic system in retinal cultured neurons

3.1.1. Identification of retinal cell types that are targets for dopaminergic modulation

It is well known from literature that DA modulates the activity of a huge number of cells in the retina (Nguyen-Legros, 1999). As a lot of cell types have been found to express specific types of DRs, the first part of this chapter focuses on the identification of retinal cell types in the culture system that could be targets for dopaminergic modulation. Hampson and co-workers showed that one such effect of DA-signaling is the uncoupling of AII ACs in the rabbit retina via D1Rs (Hampson *et al.*, 1992). Further studies revealed that dopaminergic cells directly synapse onto AII ACs (Voigt and Wässle, 1987; Völgyi *et al.*, 2014). Nevertheless, immunoreactivity for D1Rs was not found in AII ACs of rat and mouse retina (Veruki and Wässle, 1996; Nguyen-Legros, 1997). In order to test whether this is also true for retinal dissociated neurons in culture, fixed cells were stained with anti-glycine transporter 1 (GlyT1) which was shown to be a suitable marker for glycinergic and thus AII ACs in the rat retina (Menger *et al.*, 1998).

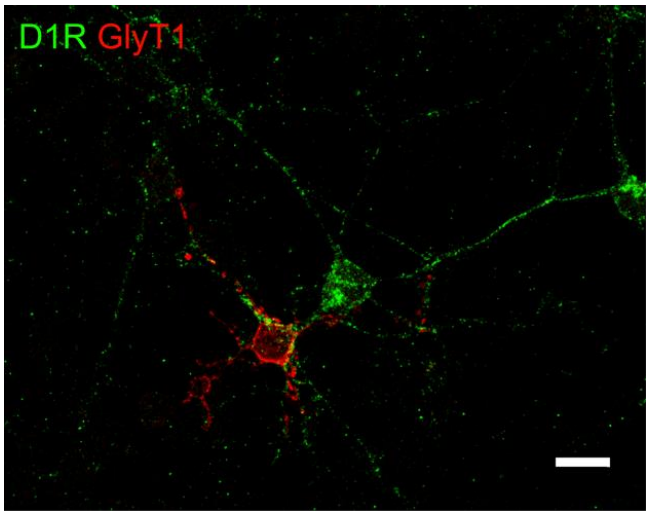

Fig. 3.1.1: D1R-expressing neurons in culture were not glycinergic. Retinal dissociated neurons in culture were fixed and stained with anti-D1R (green) and anti-GlyT1 (red) which labels glycinergic cells. A co-localization was never observed. Scale bar 10 µm.

Confocal images of cultures stained with anti-GlyT1 revealed that this antibody labeled neurons with a round soma that exhibited about 4 primary dendrites spanning only a few micrometers (Fig. 3.1.1, red). These dendrites branched out into many fine processes. In contrast to that, D1R-positive neurons had a square-like soma with up to 3 long primary processes that did not show a high branching (Fig. 3.1.1, green). D1R-

positive neurons were not positive for GlyT1 (Fig. 3.1.1), indicating that glycinergic cells in my culture system did not express D1Rs. In assumption that most of these GlyT1-positive neurons in the culture are AII ACs (Menger *et al.*, 1998), this finding is in line with previous publications that did not find immunoreactivity for D1Rs in AII ACs (Veruki and Wässle, 1996; Nguyen-Legros, 1997).

Another type of retinal neuron that had been shown to be a target for dopaminergic modulation are HCs. Zhang and colleagues showed that activation of D1Rs leads to a reduction in horizontal receptive field size in primates (Zhang *et al.*, 2011). Furthermore, it was demonstrated that DA decreases the gap junction permeability between HCs via the activation of D1Rs in turtle retina (Piccolino *et al.*, 1984). Based on these findings it was tested here, whether murine HCs in culture express D1Rs. Fixed cells were stained with anti-D1R and an antibody that was directed against the Ca^{2+}-binding protein-28 kD (CaBP). Anti-CaBP was shown to be a suitable marker for HCs in the mouse retina (Haverkamp and Wässle, 2000).

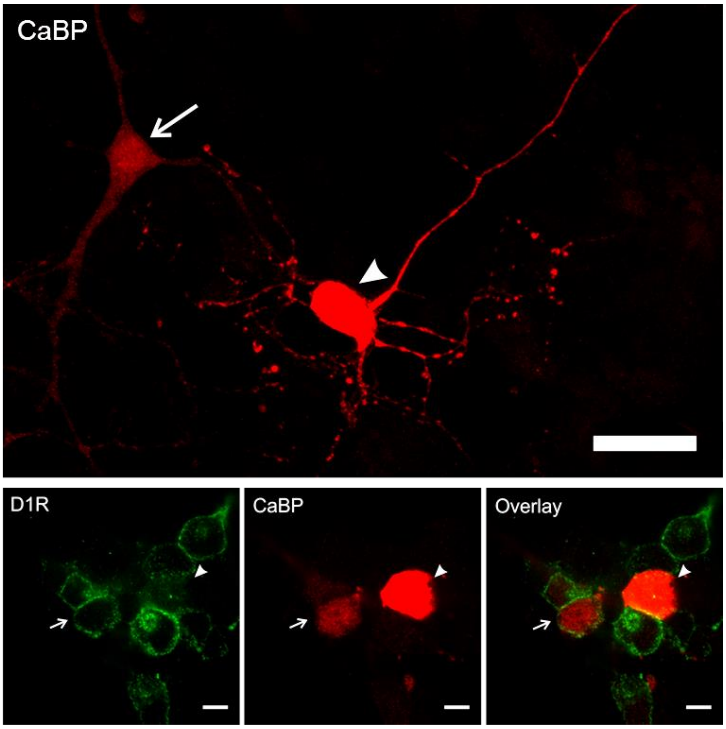

Fig. 3.1.2: Weakly CaBP-positive cells expressed D1Rs. (A) Retinal dissociated neurons in culture were fixed at DIV8 and stained with anti-CaBP (red). Scale bar 25 µm. Two types of neurons are positive for CaBP: cells that were strongly immunoreactive for CaBP (arrowhead) and cells that showed weak CaBP-immunoreactivity (arrow). **(B)** Neurons were stained with anti-D1R (green) and anti-CaBP (red). The two types of CaBP-positive cells differed in the expression of D1Rs: Strongly CaBP-positive cells were negative for D1Rs (arrowhead) and weakly CaBP-positive cells were positive for D1Rs (arrow). Scale bars 5 µm.

Two different types of CaBP-positive cells were found (Fig. 3.1.2 A, arrow and arrowhead) that differed in their strength of CaBP-immunoreactivity and in their

morphology. Neurons strongly positive for CaBP (Fig. 3.1.2 A, arrowhead) had a huge soma and many primary dendrites that arborized into fine processes. In some cases, these cells exhibited one long axon-like process. On the other hand there were cells that were only weakly positive for CaBP (Fig. 3.1.2 A, arrow). These cells had a smaller square-like soma and a few thick non-arborized primary processes. From literature it is known that mice and rats have only one type of HC (Masland, 2001), thus these two observed CaBP-positive cell types cannot both be HCs. In stainings of vertical cryo-sections of the mouse retina, CaBP not only labels HCs but also a significant number of ACs. The strength of staining differed between these two cell populations: HCs were strongly immunoreactive for CaBP whereas ACs were only faintly labeled (Haverkamp and Wässle, 2000). Thus, my findings suggest that strongly labeled CaBP-positive neurons in my culture are HCs while the weakly labeled neurons are ACs.

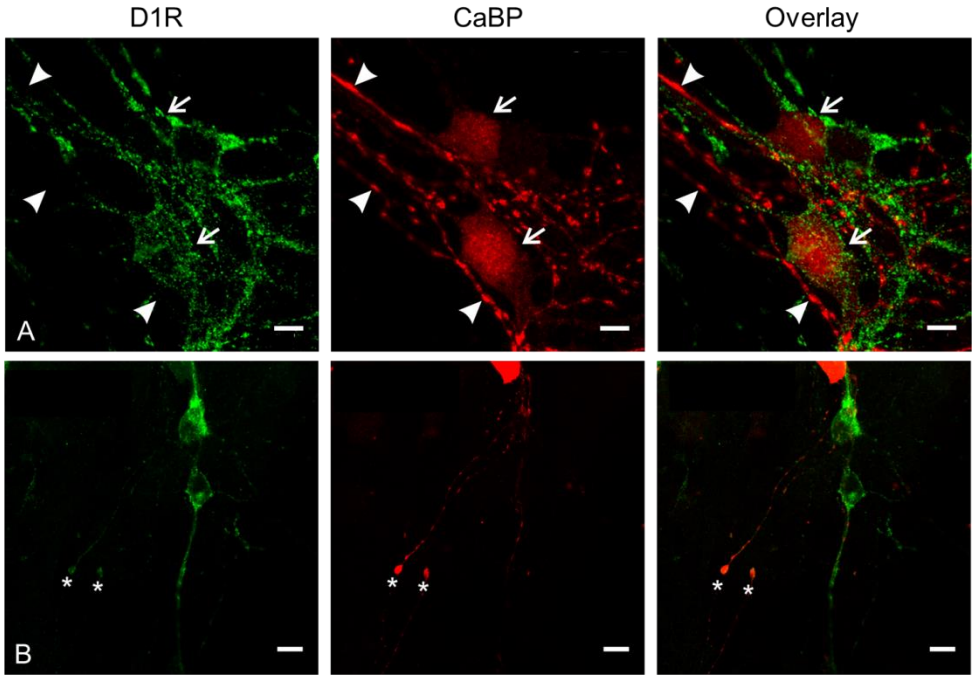

Fig. 3.1.3: In the majority of strongly CaBP-positive neurons D1Rs were not expressed in fine processes. Retinal dissociated neurons in culture were fixed at DIV9 and stained with anti-D1R (green) and anti-CaBP (red). **(A)** Most processes of the strongly CaBP-positive cells were not immunoreactive for anti-D1R (arrowhead) whereas the somata of weakly CaBP-positive cells were positive for anti-D1R (arrow). Scale bar 5 µm. **(B)** D1R co-localization was found in some endtips of strongly CaBP-positive neurons (asterisk). Scale bar 10 µm.

These two different types of CaBP-positive cells did not only differ in their morphology and strength of immunoreactivity for anti-CaBP but they also differed in the expression of D1Rs. Doublestaining with anti-D1R and anti-CaBP revealed that only those neurons that were weakly positive for CaBP expressed D1Rs in their soma (Fig. 3.1.2 B, arrow). The somata of those neurons that were strongly positive for CaBP were found to be

negative for D1Rs (Fig. 3.1.2 B, arrowhead).

As immunohistochemical analysis of macaque, rat, mouse, and hamster retinae showed D1R expression especially in HC processes (Nguyen-Legros, 1999), the fine processes of strongly CaBP-positive neurons in culture were investigated. The somata of weakly CaBP-positive cells were again found to be positive for D1Rs (Fig. 3.1.3 A, arrow). Most often it was observed that the dendrites of strongly CaBP-positive neurons (Fig. 3.1.3 A, arrowhead) were negative for D1Rs (Fig. 3.1.3 A, green). However, in some of the strongly CaBP-positive neurons D1R immunoreactivity was found in the endtips (Fig. 3.1.3 B, asterisk) or processes (not shown).

It has been shown that PRs possess D4Rs (Cohen *et al.*, 1992). The existence of D1Rs in PRs had never been reported (Cohen *et al.*, 1992; Nguyen-Legros, 1997; Nguyen-Legros, 1999). In order to identify PRs, an antibody against recoverin that brightly labels PR cells but shows also faint labeling in type 2 cone BCs in mouse retina (Haverkamp *et al.*, 2003; Biswas *et al.*, 2014) was used. Like PRs, type 2 BCs were found to be negative for D1Rs (Veruki and Wässle, 1996) making it improbable to find a co-localization of anti-Recoverin and anti-D1R. Analysis of confocal images of retinal cultures stained with anti-D1R and anti-Recoverin supported this notion: none of the recoverin-positive cells (Fig. 3.1.4, arrowhead) did show immunoreactivity for D1Rs (Fig. 3.1.4, arrow).

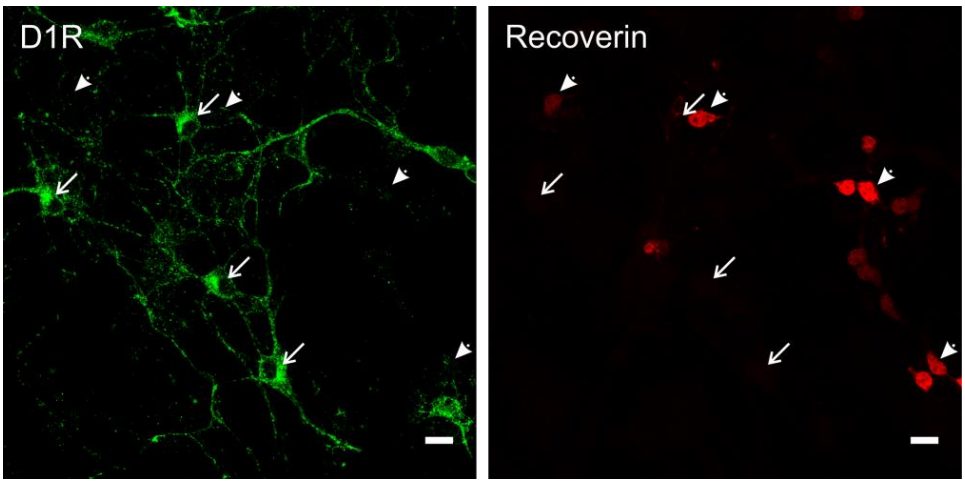

Fig. 3.1.4: Recoverin-positive neurons in culture did not express D1Rs. Retinal dissociated neurons in culture were fixed at DIV8 and stained with anti-D1R (green) and anti-Recoverin (AB5585, red). No co-localization was found between D1R-positive neurons (arrow) and recoverin-positive cells (arrowhead). Scale bar 10 µm.

In summary, all these results indicate that the culture system is a well suited system to study dopaminergic signaling pathways in the retina as most results fit to previous published data.

3.1.2. Identification of D1R downstream signaling molecules in retinal cultured neurons

As it is well accepted that D1Rs couple to G_s leading to an activation of Acy and thus to an increase in $[cAMP]_i$ and PKA activity (Beaulieu and Gainetdinov, 2011), it was investigated whether D1R-positive retinal neurons in culture are also positive for PKA. Fixed retinal dissociated neurons were stained with anti-D1R and anti-PKARIIβ, an antibody directed against the regulatory subunit IIβ of PKA. Analysis of confocal images revealed that some D1R-positive neurons were positive for PKARIIβ (Fig. 3.1.5, arrow). In addition, there were PKARIIβ-positive neurons that showed a dim staining for anti-D1R (Fig. 3.1.5, arrowhead) and some D1R-positive neurons that did not express PKARIIβ (Fig. 3.1.5, asterisk).

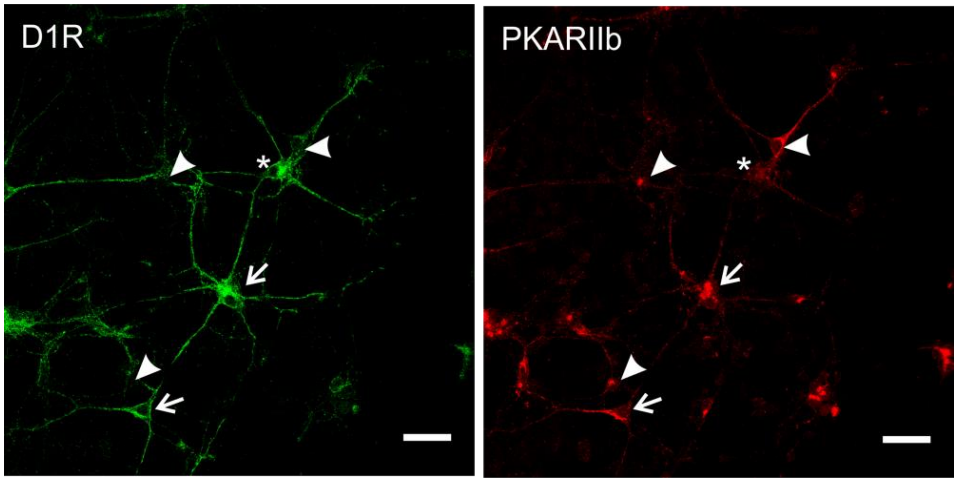

Fig. 3.1.5: Retinal dissociated neurons in culture expressed D1Rs and were positive for PKA. Retinal dissociated neurons in culture were fixed at DIV8 and stained with anti-D1R (green) and anti-PKARIIb (red). Three groups of neurons were found: cells that were positive for PKARIIβ that showed dim staining for D1R (arrowhead), neurons that were only positive for D1R (asterisk) and others that exhibited immunoreactivity for both D1R and PKARIIβ (arrow). Scale bar 25 µm.

As anti-PKARIIβ in sections of mouse retina labels two types of cells- namely type 3b bipolar and some amacrine cells (Mataruga *et al.*, 2007)- it was investigated whether the D1R/PKARIIβ-positive neurons were bipolar or amacrine cells. In order to distinguish between bipolar and amacrine cells, an antibody directed against the vesicular glutamate transporter 1 (vGlut1) was used. This antibody is well suited for the identification of BC terminals (Johnson *et al.*, 2004), as all types of BCs in the retina use glutamate as neurotransmitter. VGluT1 staining was found to be punctiform indicating that this antibody labeled glutamatergic synapses (Fig. 3.1.6, red). In most samples tested, no co-localization of vGluT1 and D1R was found (Fig. 3.1.6). Only occasionally, co-localization between D1R and vGlut1 was observed (data not shown). This indicates that most of the D1R-positive neurons in culture were ACs.

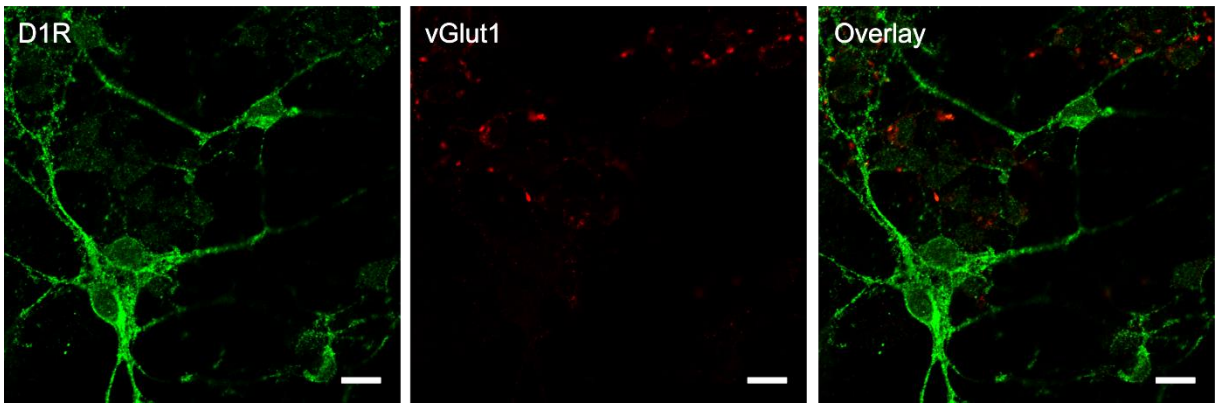

Fig. 3.1.6: Most of the D1R-positive neurons in culture were not positive for vGlut1. Retinal dissociated neurons in culture were fixed at DIV8 and stained with anti-D1R (green) and anti-vGlut1 (red). No co-localization of D1R-positive and vGlut1-expressing cells was found indicating that D1R-positive neurons were not BCs. Scale bar 10 µm.

In literature it is still under discussion whether the activation of D1Rs can also result in activation of the PLC cascade (Neve *et al.*, 2004). If so, downstream signaling will involve the activation of G_q-proteins and in turn lead to a change in the activity of protein kinase C (PKC) (Beaulieu and Gainetdinov, 2011). It has already been shown that DA selectively activates PKCα- and PKCε-isoforms in renal epithelial cells via the activation of D1Rs (Nowicki *et al.*, 2000). In order to test whether D1R-positive retinal neurons in culture express PKCα, cells were stained with anti-D1R and anti-PKCα. Some of the D1R-positive neurons were also positive for PKCα (Fig. 3.1.7, arrow). In addition, there were PKCα-positive neurons that were not immunoreactive for D1R (Fig. 3.1.7, arrowhead) and others that were positive for D1R but negative for PKCα (Fig. 3.1.7, asterisk).

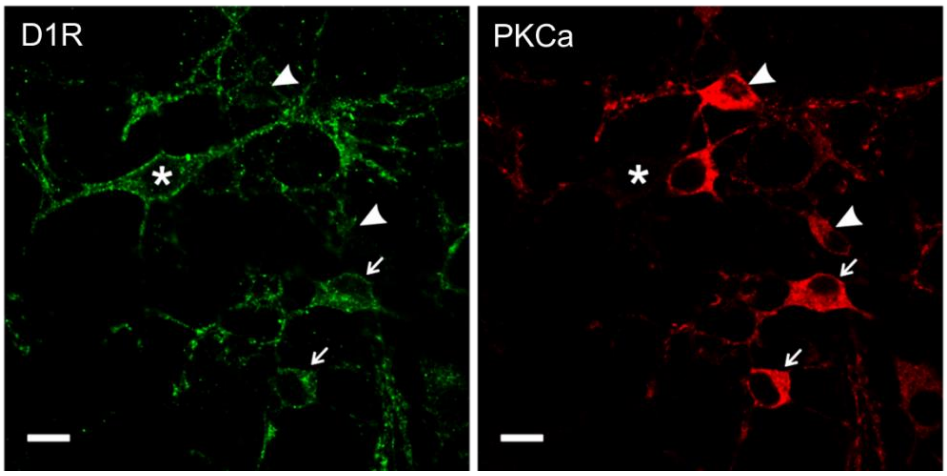

Fig. 3.1.7: Some D1R-positive neurons were also positive for PKCα. Retinal dissociated neurons in culture were fixed at DIV8 and stained with anti-D1R (green) and anti-PKCα (PKCa, red). Three groups of neurons were found: cells that were only positive for D1Rs (asterisk), others that only expressed PKCα (arrowhead) and some cells that were positive for both, D1Rs and PKCα (arrow). Scale bar 10 µm.

It has already been mentioned that the well-accepted D1R-triggered pathway involves the activation G_s (Beaulieu and Gainetdinov, 2011). On the other hand it has also been

suggested that D1Rs can couple to the PTX-sensitive $G_o\alpha$ (Kimura *et al.*, 1995; Hille, 1994). Furthermore, it is known that D2-like receptors interact with PTX sensitive $G_i\alpha$ and $G_o\alpha$ proteins and that activation of D2Rs independently of cAMP inhibits Ca^{2+} conductance via $G_o\alpha$ (Nguyen-Legros, 1999). Thus, the existence of $G_o\alpha$ proteins in the retina is of essential importance, as both DR families could exert their effects via these proteins. Due to this reason it was tested whether retinal neurons in culture express $G_o\alpha$-protein. It was found that a significant number of neurons do express this type of G-protein (Fig. 3.1.8, red). Anti-$G_o\alpha$-positive neurons showed staining at the plasma membrane and in their processes. Different types of neurons expressed $G_o\alpha$, as neurons with different soma sizes and varying process structure were found to be positive for $G_o\alpha$. Staining with anti-D1R revealed that some of the D1R-positive neurons were also positive for $G_o\alpha$ (Fig. 3.1.8, arrows). In addition, there were neurons that were only positive for $G_o\alpha$ (Fig. 3.1.8, arrowhead) and others that were only positive for D1R but did not show the $G_o\alpha$-specific membrane staining (Fig. 3.1.8, asterisk).

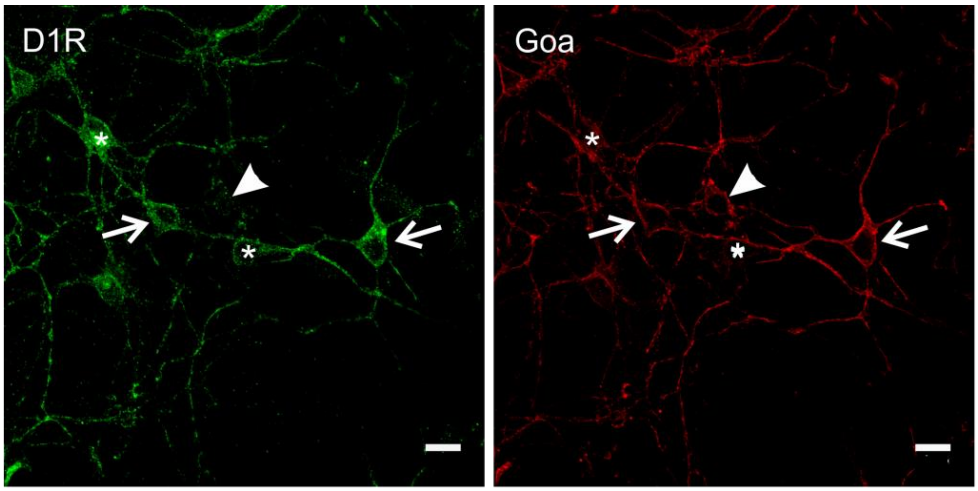

Fig. 3.1.8: Some D1R-expressing neurons in culture were positive for $G_o\alpha$. Retinal dissociated neurons in culture were fixed at DIV8 and stained with anti-D1R (green) and anti-$G_o\alpha$ (red). Three groups of neurons were found: cells that were only positive for D1Rs (asterisk), others that only expressed $G_o\alpha$ (arrowhead) and some cells that were positive for both, D1Rs and $G_o\alpha$ (arrow). Scale bar 10 µm.

In summary, the findings in this chapter demonstrate that all three G-protein coupled pathways could be induced by stimulation of D1Rs in the retinal culture system: the G_s-mediated pathway as some D1R-positive neurons express PKA, the G_q-mediated pathway as some of the D1R-positive neurons showed immunoreactivity for PKC and the $G_{i/o}$ mediated pathway as a fraction of the D1R-positive neurons were found to express $G_o\alpha$. These findings are in line with previous studies which have demonstrated that D1Rs couple to different types of G-proteins (Kimura *et al.*, 1995). Unfortunately, it

could not be tested whether other types of DRs are also present in the culture system as the respective antibodies did not yield specific labeling patterns in the culture system.

3.2. Using FRET-based biosensors for the visualization of the cAMP/PKA pathway

From the classical view, DA-dependent signaling is associated with the regulation of $[cAMP]_i$ and PKA through two families of G-protein coupled receptors (Beaulieu and Gainetdinov, 2011; Neve *et al.*, 2004). In order to investigate dopaminergic signaling on the basis of this signaling cascade, the two FRET-based biosensors EPAC1-camps (Nikolaev *et al.*, 2004) and AKAR4 (Depry *et al.*, 2011) were tested for their suitability. Finally, these two biosensors were used to examine dopaminergic signaling in cultured retinal neurons.

3.2.1. Characterization of EPAC1-camps and AKAR4 in HEK293 cells

To test whether the FRET-based cAMP sensor EPAC1-camps is applicable for the detection of DA-induced changes in $[cAMP]_i$, HEK293 cells were transiently co-transfected with cDNA coding for the EPAC1-camps sensor and for a GFP-tagged D1R (D1R-GFP). One day after transfection, cells were imaged and stimulated for 1 min with 0.5 µM DA. The cell shown in fig. 3.2.1 responded with a decrease in YFP fluorescence and a mirror-reversed increase in CFP fluorescence to stimulation with DA. This was to be expected, as binding of cAMP to the EPAC1-camps sensor reduces the efficiency of FRET between the two fluorophores CFP and YFP (Nikolaev *et al.*, 2004). The response started with a delay of about 15 s, which can be attributed to the lag in the perfusion system. The amplitude of the change in fluorescence was reached shortly after the stimulation was stopped and the signal started to recover back to baseline 1 min later (Fig. 3.2.1 A). In the following, the EPAC1-camps signal was depicted as the ratio CFP/YFP by dividing the CFP fluorescence intensity by the YFP fluorescence intensity (Fig. 3.2.1 B). All values were normalized to the CFP/YFP ratio during the first 20 s of the recording. The increase in the ratio of CFP/YFP, which is due to a cAMP-induced reduction of FRET, indicates a rise in $[cAMP]_i$. For control, HEK293 cells were transfected with the EPAC1-camps sensor only (data not shown). Stimulation of these cells with 0.5 µM DA did not elicit any change in CFP/YFP confirming the finding that the DA-induced changes in co-transfected HEK293 cells were due to the activation of D1R-GFP.

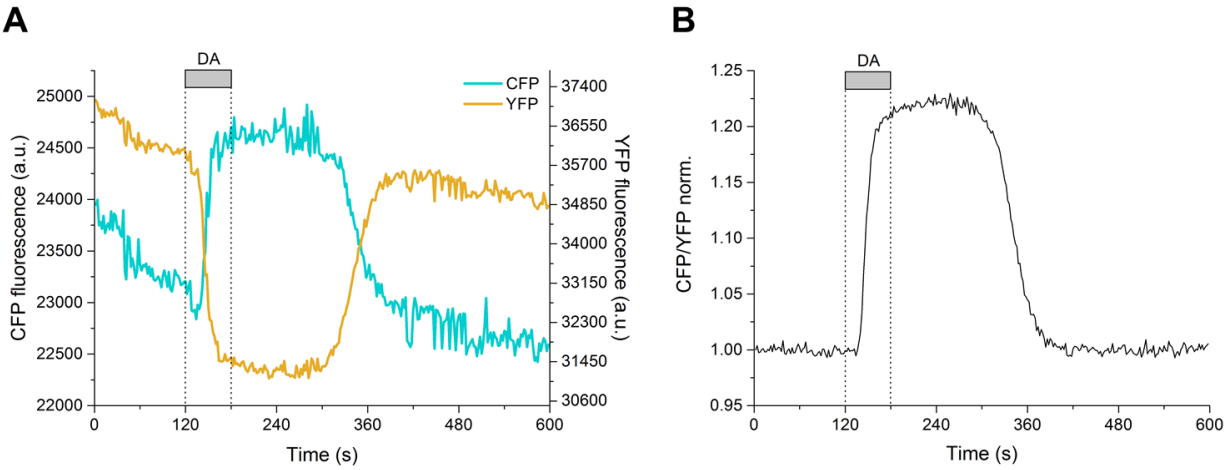

Fig. 3.2.1: DA-induced changes in $[cAMP]_i$ were detected by EPAC1-camps in D1R-GFP-expressing HEK293 cells. (A) Stimulation of HEK293 cells co-expressing EPAC1-camps and D1R-GFP (Lipofectamine-transfection) with 0.5 µM DA resulted in a mirror-reversed change in the fluorescence of the two fluorophores CFP and YFP. **(B)** The increase in the ratio of CFP/YFP indicates an increase in $[cAMP]_i$ upon stimulation with 0.5 µM DA.

AKAR4 is a PKA activity sensor and thus an indirect reporter for changes in $[cAMP]_i$. In order to test whether AKAR4 is suitable to detect DA-induced changes in PKA activity, HEK293 cells were transiently co-transfected with cDNA coding for AKAR4 and D1R-GFP. One day after transfection, cells were imaged and stimulated for 1 min with 0.5 µM DA. The cell shown in fig. 3.2.2 responded with an increase in YFP fluorescence and a mirror-reversed decrease in CFP fluorescence to stimulation with DA.

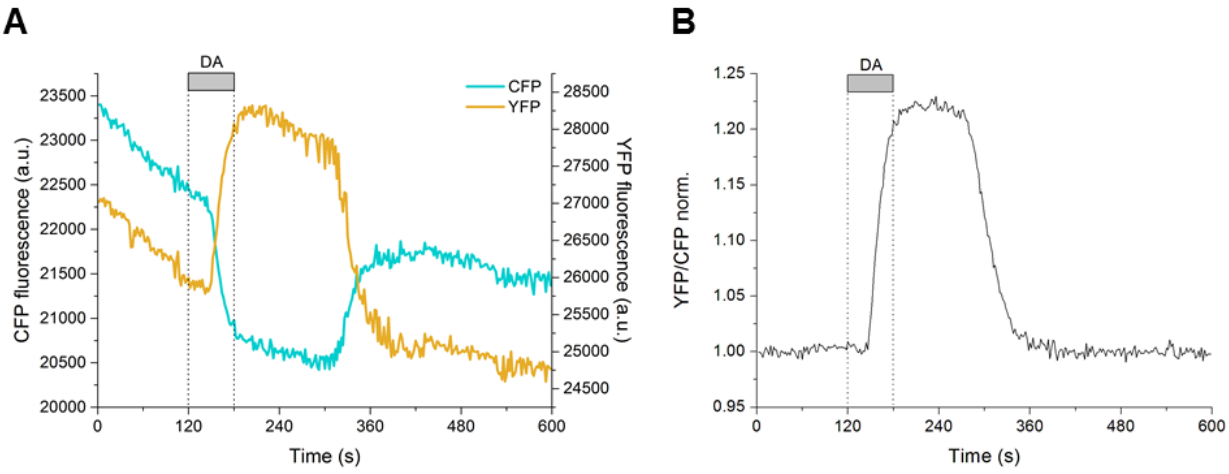

Fig. 3.2.2: AKAR4 detected DA-induced changes in PKA activity in D1R-GFP-expressing HEK293 cells. (A) Stimulation of HEK293 cells co-expressing AKAR4 and D1R-GFP (Liofectamine-transfection) with 0.5 µM DA resulted in a mirror-reversed change in the fluorescence of the two fluorophores YFP and CFP. **(B)** The increase in the ratio of YFP/CFP indicates an increase in PKA activity upon stimulation with 0.5 µM DA.

This is to be expected, as phosphorylation of the AKAR4-consensus sequence by PKA increases the efficiency of FRET between the two fluorophores CFP and YFP (Depry *et al.*, 2011). The change in the fluorescence of the two fluorophores reached amplitude shortly after the stimulation was stopped and started to recover back to baseline 1 min

later (Fig. 3.2.2 A). In the following, the AKAR4 signal was depicted as the ratio YFP/CFP by dividing the YFP fluorescence intensity by the CFP fluorescence intensity (Fig. 3.2.2 B). All values were normalized to the YFP/CFP ratio during the first 20 s of the recording. The increase in the ratio of YFP/CFP reflects the phosphorylation of the AKAR4 sensor and thus indicates a gain in PKA activity induced by an increase in $[cAMP]_i$.

As both sensors EPAC1-camps and AKAR4 reliably detect DA-induced changes in the cAMP/PKA-signaling cascade in HEK293 cells, they were further used to examine dopaminergic signaling in retinal dissociated neurons in culture.

3.2.2. Using EPAC1-camps and AKAR4 in cultured retinal neurons

3.2.2.1. DA induced changes in $[cAMP]_i$ and PKA activity

In the retinal culture characterized in chapter 3.1, DRs are expressed in a substantial number of neurons. In a first step it was investigated whether DA induces changes in $[cAMP]_i$ in these neurons in culture. For this purpose, retinal neurons were transiently transfected with cDNA coding for EPAC1-camps. The day after transfection, cells were used for imaging experiments. Neurons responded to stimulation with 5 µM DA with an increase in the ratio of CFP/YFP indicating a DA-induced increase in $[cAMP]_i$ (Fig. 3.2.3 A). The responses of neurons varied in the onset of the response, the time point of peaking, the steepness of the curve and the amplitude (Fig. 3.2.3 A). In cell 2 and 3 the ratio CFP/YFP reached amplitude still during stimulation with DA, whereas cell 1 peaked 1 min after the stimulus was stopped. The response of cell 2 immediately recovered back to baseline whereas the response of cell 3 decreased in two phases. The signal of cell 2 and cell 3 almost returned to baseline 2 min after the stimulus was stopped. In contrast to that, the signal of cell 1 did not completely recover back to baseline.

In total, 49 EPAC1-camps-expressing neurons (from 8 cultures) were stimulated with 5 µM DA. Only 37% (n=18) of these neurons responded with an increase in CFP/YFP. Following, the response amplitudes ($d(CFP/YFP)_{Max}$) triggered by the DA stimulus were calculated by determination of dF_{Max}/F in a time interval of 300 s after start of the stimulus. Fifty % of the neurons responded with a maximal increase in CFP/YFP ranging between 0.04 and 0.09 (Fig. 3.2.3 B, black box). The mean maximal increase of all neurons was 0.07±0.015 (±95% Confidence Interval (CI); Fig. 3.2.3 B, dotted line). There

were quite diverse response amplitudes: the highest amplitude was 0.13 while the minimal amplitude was 0.03 (Fig. 3.2.3 B).

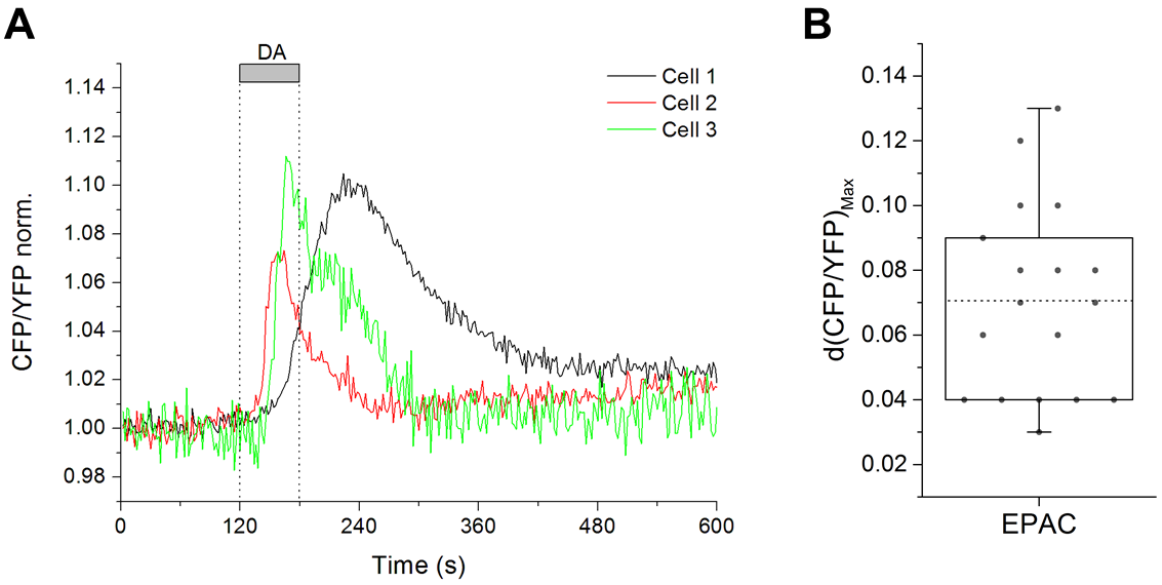

Fig. 3.2.3: DA induced changes in $[cAMP]_i$ in retinal neurons. (A) Three neurons in retinal dissociated culture expressing EPAC1-camps after transient transfection were stimulated with 5 µM DA. The cells reacted with an increase in $[cAMP]_i$ which was implied by an increase in the ratio of CFP/YFP. The three cells differed in their response kinetics. **(B)** The maximal change in CFP/YFP upon DA application was determined for each neuron (n=18) and data were plotted as box plot. Each dot represents $d(CFP/YFP)_{Max}$ of one cell. Fifty percent of the cells had a maximal change in CFP/YFP between 0.04 and 0.09 (black box). The mean (dotted line) was 0.07±0.015 (±95% CI). One neuron responded with a maximal change in CFP/YFP which was 0.03 and one with a maximal change of 0.13. The whiskers above and below the box indicate the 95th and 5th percentiles, respectively.

To further examine the downstream signaling processes of DRs in the retina, retinal dissociated neurons in culture were transiently transfected with cDNA coding for the FRET based sensor AKAR4 which detects changes in PKA activity (1.3.1.1). These neurons were stimulated with 5 µM DA for 1 min. Fig. 3.2.4 A shows the responses of three AKAR4-expressing neurons that responded to stimulation with DA with an increase in YFP/CFP. The responses of the neurons differed in the onset of the response, in the steepness of the curve, in the time point of peaking and in the amplitude of the response. Six min after the stimulus was stopped, all neurons recovered almost back to baseline.

In total, 80 AKAR4-expressing neurons (from 10 cultures) were stimulated with 5 µM DA for 1-3 min. Ninety two percent (n=74) of these neurons responded with an increase in YFP/CFP to stimulation with DA. Fifty six cells (1 min application) of these 74 cells that responded to stimulation with DA were further analyzed. Following, the response amplitudes ($d(YFP/CFP)_{Max}$) triggered by the DA stimulus were calculated by determination of dF_{Max}/F in a time interval of 300 s after start of the stimulus. Fifty % of

neurons (n=54) responded with a maximal increase in YFP/CFP ranging between 0.16 and 0.5 (Fig. 3.2.4 B, black box). The mean maximal increase of all neurons was 0.35±0.07 (±95% CI; Fig. 3.2.4 B, dotted line). There were also neurons with extreme responses into both directions: one neuron responded with a maximal change in YFP/CFP of only 0.03 whereas one neuron responded with a maximal change in YFP/CFP of more than 1.3 (Fig. 3.2.4 B).

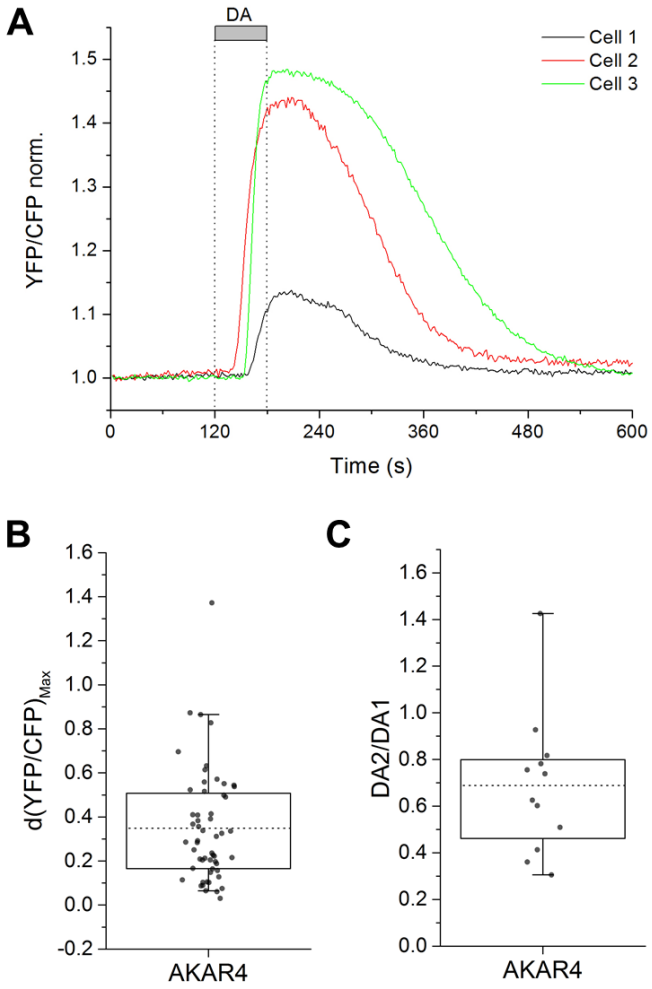

Fig. 3.2.4: DA induced an increase in PKA activity in cultured retinal neurons. (A) Retinal dissociated neurons were transfected with cDNA coding for AKAR4. Stimulation with 5 µM DA resulted in an increase in YFP/CFP indicating an increase in PKA activity. **(B)** The maximal change in YFP/CFP upon DA application was determined for each of the 56 neurons and data were plotted as box plot. Each dot represents $d(YFP/CFP)_{Max}$ of one cell. Fifty percent of the cells had a maximal change in YFP/CFP between 0.16 and 0.5 (black box). The mean (dotted line) was 0.35±0.075 (±95% CI). One neuron responded with a maximal change in YFP/CFP which was 0.03 and one with a maximal change of 1.37. The whiskers above and below the box indicate the 95th and 5th percentiles, respectively. **(C)** The ratio DA2/DA1 was plotted as box plot. Each dot represents DA2/DA1 of one cell (n=12). Fifty percent of the cells had a ratio between 0.45 and 0.8 (black box). The mean (dotted line) was 0.69. One neuron exhibited a DA2/DA1 which was 0.3 and another with 1.43. The whiskers above and below the box indicate the 95th and 5th percentiles, respectively.

For the following experiments it was quite important to test whether the neurons responded reversibly and repeatedly to subsequent stimulation with DA. Thus, AKAR4-

expressing cells (n=12) were stimulated twice with 5 µM DA and washed in between with ES_{neuro}. Following, the response amplitudes were compared with each other by calculating the ratio DA2/DA1. The average response amplitude triggered by the first DA application was about two-fold higher (DA1: 0.3±0.13; ±95% CI) than the response induced by the second application of DA (DA2: 0.18±0.08; ±95% CI). This reduction in the response amplitudes was reflected in the average ratio DA2/DA1 that was 0.69±0.19 (±95% CI; Fig. 3.2.4 C; dotted line).

3.2.2.2. Comparison of EPAC1-camps and AKAR4

In the previous chapter it was shown that EPAC1-camps and AKAR4 detect DA-induced changes in $[cAMP]_i$ and subsequent changes in PKA activity. The DA-induced responses appeared to vary from cell to cell with differences in amplitudes and kinetics. This variation was observed with both sensors (Fig. 3.2.3 and 3.2.4). One interpretation could be that different types of neurons show distinct responses which may differ due to the variable composition and numbers of DRs.

When comparing the experiments using EPAC1-camps and AKAR4 as sensors, clear differences were observed. First, the expression level of AKAR4 in retinal neurons in culture was higher compared to EPAC1-camps making it easier to detect transfected neurons in the microscope. Second, it appeared that more neurons survived the expression of AKAR4 than expression of EPAC1-camps. This may be due to the fact that expression of EPAC1-camps led to the buffering of cAMP molecules and thus an interference with the cAMP homeostasis of the neuron. In experiments with EPAC1-camps-expressing neurons only 37% of cells responded with a change in CFP/YFP to stimulation with DA whereas the number of responding AKAR4-expressing neurons was significantly higher (92%). This difference may have variable reasons. First, it cannot be ruled out that sensors may exist in a non-functional conformation in neurons of the culture and that this occurs more often in the case of EPAC1-camps than in the case of AKAR4. Second, as AKAR4 experiments were conducted at a later stage in the project than EPAC1-camps experiments, I may have gained more experience in identifying neurons that express DRs solely based on cellular morphology and appearance. This may have biased the search for neurons in culture to be recorded in favor of cells that respond to DA. Finally, AKAR4 may be more sensitive than EPAC1-camps. While one cAMP molecule can only bind one EPAC1-camps sensor molecule, one activated PKA molecule can phosphorylate many AKAR4 sensor molecules. In fact, comparison of the

average signal amplitude of DA-induced changes of YFP/CFP in AKAR4-expressing neurons (0.35±0.07; ±95% CI; n= 56) and DA-induced changes of CFP/YFP in EPAC1-camps-expressing neurons (mean: 0.07±0.015; ±95% CI; n= 18) revealed that AKAR4 granted more robust and larger signals. Thus, AKAR4 serves as an adequate replacement for EPAC1-camps for the investigation of DR downstream signaling in retinal neurons.

3.2.2.3. The DA-induced increase in PKA activity is due to activation of D1Rs

As function of AKAR4 relies on PKA-mediated phosphorylation and, hence on PKA activity, the PKA-specific antagonist H89 (Varella *et al.*, 1997) should block AKAR4 responses. Seven retinal neurons (from 2 cultures) transiently expressing AKAR4 after Lipofectamine-transfection, were stimulated with 5 µM DA for 1 min followed by a wash out phase. Following, cells were perfused with 25 µM H89 for 3-10 min in order to block PKA activity. Still during blockade of PKA, cells were stimulated with 5 µM DA for a second time. This second application was again followed by a wash out phase. Cells responded with an increase in YFP/CFP to the first stimulation with DA indicating a DA-triggered increase in PKA activity. When PKA was blocked by H89, stimulation with DA did not elicit an increase in YFP/CFP verifying that the previously observed change in YFP/CFP is indeed due to activation of PKA (Fig. 3.2.5 A).

As D1Rs positively couple to ACy leading to an increase in $[cAMP]_i$, it was assumed that the observed increase in PKA activity upon DA stimulation is due to the activation of D1Rs. In order to test for this, AKAR4-expressing neurons were first stimulated for 1 min with 5 µM DA. After a washout phase, cells were stimulated with 100 nM of the D1R-specific agonist SKF38393 (for review see Seeman and Van Tol, 1994) for 1 min. All neurons responded with an increase in YFP/CFP to both agonists (Fig. 3.2.5 B). When D1Rs were blocked by 100 nM of the D1R-specific antagonist SCH23390 (for review see Seeman and Van Tol, 1994) stimulation with DA did not cause an increase in YFP/CFP (Fig. 3.2.5 C). These findings verified that the previously observed increase in YFP/CFP is indeed due to activation of D1Rs.

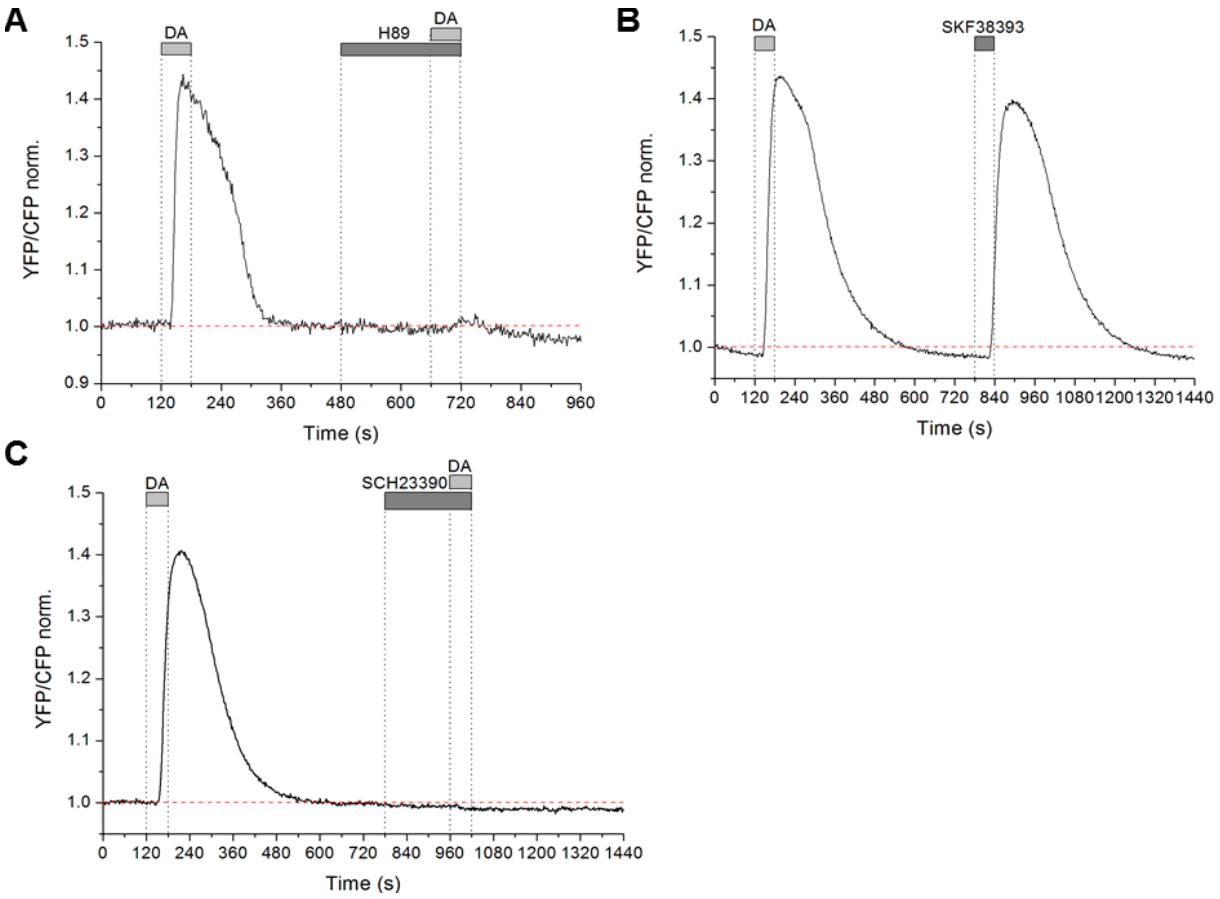

Fig. 3.2.5: The DA-induced increase was due to the activation of the D1R/PKA-cascade. Retinal cultured neurons were transfected with cDNA coding for AKAR4. The next day, neurons were used for imaging experiments. **(A)** Stimulation with 5 µM DA resulted in an increase in YFP/CFP that could be blocked by the PKA-specific inhibitor H89 (25 µM). **(B)** Stimulation with 5 µM DA resulted in an increase in YFP/CFP that was mimicked by the D1R-specific agonist SKF38393 (100 nM). **(C)** D1Rs were blocked by perfusion of 100 nM SCH23390, a specific D1R-antagonist. Blockade of D1Rs abolished the DA-induced increase in YFP/CFP.

In order to find out whether D2Rs are also involved in DA-induced changes in the activity of PKA, AKAR4-expressing neurons were stimulated with 5 µM DA for 1 min followed by a wash-out phase. After that, cells were stimulated for 1 min with 100 nM of the D2R-specific agonist quinpirole (for review see Seeman and Van Tol, 1994). After stimulation with quinpirole, cells were washed and again stimulated for 1 min with DA. The neuron depicted in fig. 3.2.6 A responded to both DA stimulations with an increase in YFP/CFP but did not show any change in YFP/CFP when stimulated with the D2R-specific agonist quinpirole. The D2R-specific antagonist eticlopride (100 nM) did not suppress the DA-induced rise in YFP/CFP (Fig. 3.2.6 B).

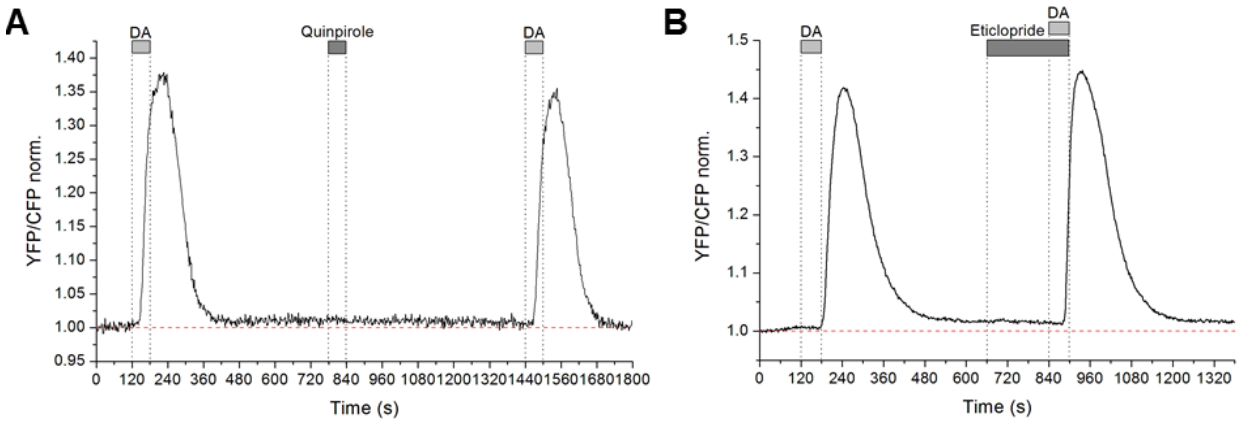

Fig. 3.2.6: D2Rs were not involved in DA-induced changes in PKA activity. Retinal cultured neurons were transfected with cDNA coding for AKAR4. The day after transfection, cells were used for imaging experiments. **(A)** Stimulation with 5 µM DA resulted in an increase in YFP/CFP whereas the D2R- specific agonist quinpirole (100 nM) did not alter YFP/CFP. **(B)** D2Rs were blocked by perfusion with 100 nM eticlopride, a D2R-specific antagonist. The DA-induced increase in YFP/CFP was not blocked by eticlopride.

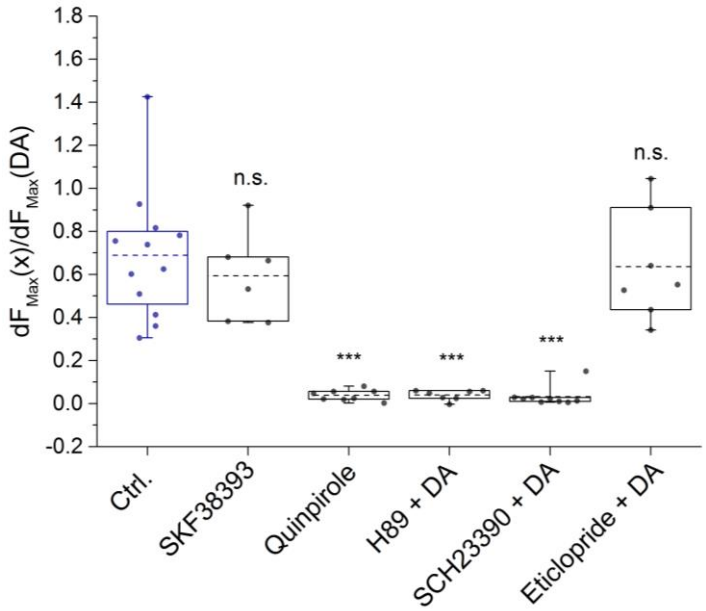

Fig. 3.2.7: The increase in PKA activity was due to activation of D1Rs. The box plot depicts the ratio between the maximal change in YFP/CFP induced by SKF38393, quinpirole or a second DA application in the presence of the blockers H89, SCH23390 or eticlopride ($dF_{Max}(x)$) and the response amplitude triggered by the first application of DA ($dF_{Max}(DA)$). Each dot represents the ratio $dF_{Max}(x)/dF_{Max}(DA)$ of one cell. The box covers the central 50% of the data. The dashed lines indicate the mean and the whiskers above and below the box the 95th and 5th percentiles, respectively. Student´s t-test or Mann-Whitney Rank Sum Test were used to test for significance. Differences were considered as highly significant at p***≤0.001 and not significant (n.s.) at p>0.5 when compared to control (ctrl.).

The findings of this pharmacological approach are summarized in the box plot in fig. 3.2.7. In all cases, stimulation with DA led to an increase in YFP/CFP. The average amplitude of the DA-induced increase in YFP/CFP was calculated for both stimulations and set into relation to each other ($dF_{Max}(x)/dF_{Max}(DA)$). Cells that were stimulated twice with 5 µM DA served as control (Fig. 3.2.7, ctrl.). The responses triggered by SKF38393 (0.59±0.22; ±95% CI; n=6; t-test: p=0.5) and by DA in the presence of

eticlopride (Eticlopride+DA; 0.64±0.24; ±95% CI; n=7; t-test: 0.7) did not significantly differ from the control (0.69±0.19; ±95% CI; n=12). In contrast to that, the responses induced by quinpirole (0.04±0.02; ±95% CI; n=8; Mann-Whitney Rank Sum Test: p***≤0.001), by DA in the presence of H89 (H89+DA; 0.04±0.02; ±95% CI; n=7; Mann-Whitney Rank Sum Test: p***≤0.001) and by DA in the presence of SCH23390 (SCH23390+DA; mean: 0.03±0.03; ±95% CI; n=9; Mann-Whitney Rank Sum Test: p***≤0.001) were significantly smaller than the control.

These findings support the assumption that the DA-induced increase in YFP/CFP is the consequence of activation of D1Rs leading to an increase in $[cAMP]_i$ followed by a rise in PKA activity and a subsequent phosphorylation of AKAR4.

3.2.2.4. Does the same neuron express both types of DRs?

From the previous experiments, there is only evidence for D1Rs to be expressed in retinal neurons in culture, whose activation by DA leads to an increase in PKA activity. I never observed DA-induced responses that would indicate activation of D2Rs followed by a decrease in $[cAMP]_i$ (decrease in CFP/YFP for EPAC1-camps or YFP/CFP for AKAR4). This can have different reasons: retinal neurons in culture might not express D2Rs or the observed changes in $[cAMP]_i$/PKA activity might already reflect the integration of the responses of both D1 and D2 receptors, being simultaneously activated by DA basal $[cAMP]_i$. Finally, PKA activity levels might already be low and cannot be further reduced by activation of D2Rs. One way to circumvent this problem is to increase PKA activity prior to stimulation of D2Rs. This chapter addresses the question whether the same neuron expresses both types of DRs.

Control experiments were conducted in order to test whether sustained stimulation with the D1R-specific agonist SKF38393 leads to a long lasting augmentation of PKA activity. AKAR4-expressing neurons were stimulated with 50 nM SKF38393 for 7 min. Fig. 3.2.8 A shows the response of four AKAR4-expressing neurons from one culture that all reacted with sustained increase in YFP/CFP. The signal amplitude was reached about 1 min after the stimulus was started and slightly started to decrease until a plateau was reached. About 1 min after the SKF38393 application was stopped YFP/CFP recovered back to baseline.

As PKA activity can permanently be increased by prolonged application of SKF38393, in the next experiments 50-100 nM quinpirole (D2R-specific agonist) was added after 2 min of SKF38393 application. After 3 min, quinpirole was withdrawn and cells were

further stimulated with 50 nM SKF38393 for 2 min. The response patterns of 16 AKAR4-expressing neurons stimulated with this protocol could be divided into three groups.

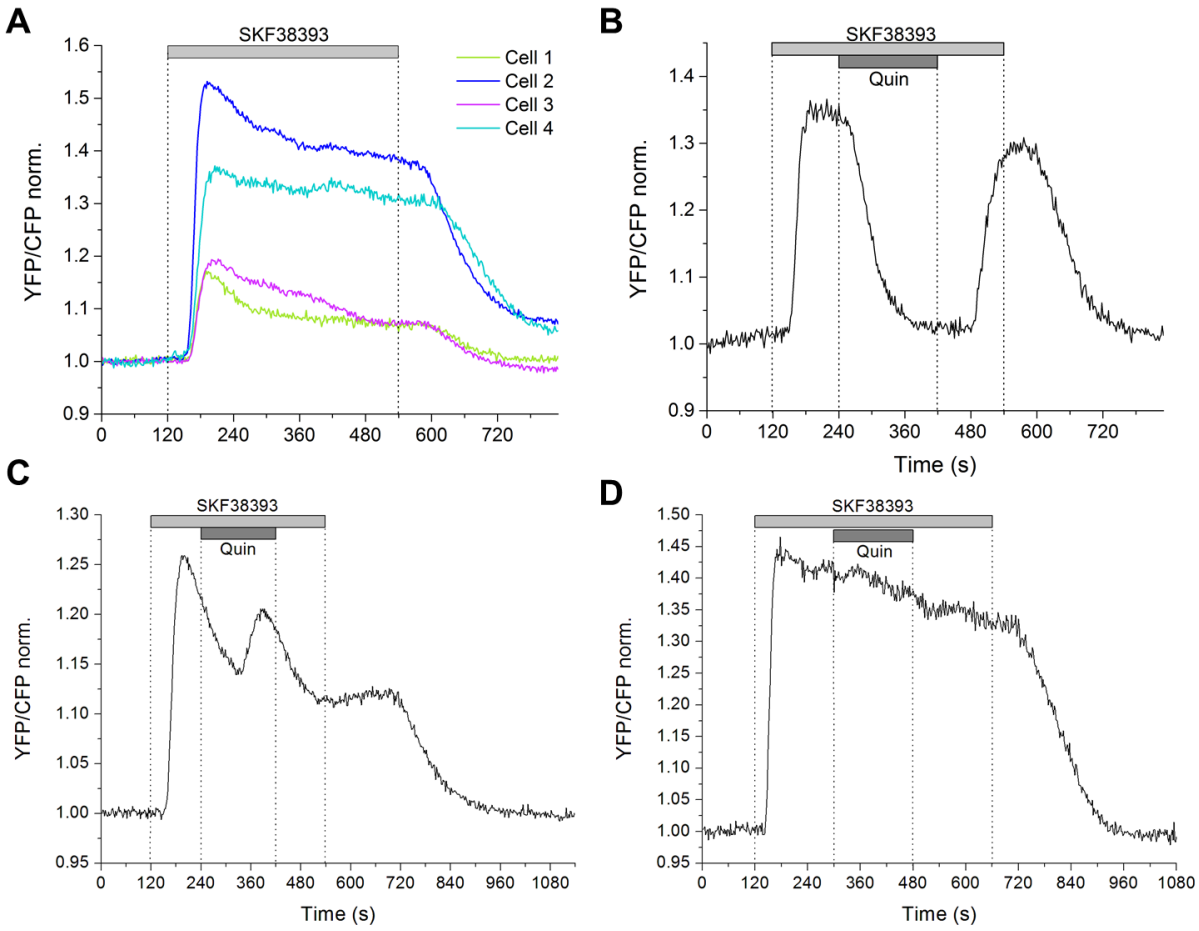

Fig. 3.2.8: Simultaneous stimulation of D1Rs and D2Rs with the specific agonists induced variable responses. Retinal neurons were transiently transfected with cDNA coding for AKAR4. The next day, cells were used for imaging. **(A)** Permanent stimulation with the D1R-specific agonist SKF38393 (50 nM) induced a sustained increase in YFP/CFP. **(B)** Two min after start of the SKF38393 stimulation, the D2R-specific agonist quinpirole (50 nM) was applied. The cell responded with a SKF38393-induced increase in YFP/CFP which was decreased upon application of quinpirole. **(C)** The cell was treated with the same protocol as in B. Application of quinpirole in the presence of SKF38393 induced an increase in YFP/CFP. **(D)** The cell was treated with the same protocol as in B. Quinpirole application did not alter YFP/CFP.

Four cells responded with a SKF38393-induced increase in YFP/CFP and a quinpirole-induced decrease in YFP/CFP. The response from one cell of this group is shown in fig. 3.2.8 B. The increase in YFP/CFP peaked roughly one min after the start of SKF38393 application and reached a plateau during SKF38393 stimulation. This response pattern may be of the same kind as of cell 4 in the control experiments (Fig. 3.2.8 A). Quinpirole application in the presence of SKF38393 induced a decrease in YFP/CFP that started about 0.5 min after the quinpirole stimulus was given. About 2.5 min after the start of quinpirole administration, the YFP/CFP reached a plateau that was less than 10 % of the SKF38393-induced peak amplitude. After withdrawal of quinpirole but still in the

presence of SKF38393, YFP/CFP started to rise again reaching a second peak 2.5 min after the quinpirole application was stopped. About 4 min after washout of SKF38393, the ratio YFP/CFP recovered back to baseline. These findings indicate that stimulation of D2Rs led to a decrease in PKA activity once the basal PKA activity level had been increased by stimulation of D1Rs. This is to be expected, as the classical understanding of DR-signaling includes a D1R-induced increase in PKA activity whereas activation of D2Rs, that are negatively coupled to ACy, would result in a decrease in PKA activity. Ten out of 16 cells responded with an increase in YFP/CFP upon stimulation with quinpirole in the presence of SKF38393. The response of one neuron of this type is shown in fig. 3.2.8 C. Stimulation with SKF38393 induced an increase in YFP/CFP that peaked roughly 1 min after the SKF38393 stimulus was started. Still during SKF38393 application, YFP/CFP started to decrease. This behavior was already observed in control measurements (Fig. 3.2.8 A; Cell 1 and 2). This decrease went on until the ratio YFP/CFP started to rise again 1.5 min after start of the quinpirole application. This increase in YFP/CFP reached a peak 2.5 min after the quinpirole stimulus was started. This second peak was 20% smaller than the first peak induced by SKF38393 stimulation alone. After peaking, YFP/CFP decreased again, reaching a plateau about 2 min after quinpirole administration had been stopped. This plateau was 50% of the response amplitude during the initial SKF38393 stimulation. About 3 min after the SKF38393 stimulus was stopped, YFP/CFP started to recover back to baseline. Compared to control measurements, this decrease back to baseline took longer. These results were quite surprising. It appears that simultaneous stimulation with quinpirole and SKF38393 induced an increase in PKA activity (indicated by the increase in YFP/CFP) which cannot be explained by the well described opposing influences of D1 and D2 receptor activation on ACy activity.

Two out of 16 cells responded with an increase in YFP/CFP to stimulation with SKF38393 but did not show any change in ratio during stimulation with quinpirole indicating the lack of D2Rs (Fig. 3.2.8 D). This response was quite similar to responses of cells from control measurements (Fig. 3.2.8 A).

In summary, there is good evidence for the co-existence of D1 and D2 receptors on the same retinal neuron as some neurons responded to simultaneous stimulation with specific agonists. Surprisingly, this simultaneous activation of both receptors by SKF38393 (D1R) and quinpirole (D2R) led to different effects in the downstream signaling cascades. One fourth of AKAR4-expressing neurons responded with a

quinpirole induced decrease in YFP/CFP indicating a quinpirole induced decrease in PKA activity, 62.5 % of neurons responded with a quinpirole-induced increase in YFP/CFP indicating an increase in PKA activity and 2 neurons (from 16) only responded to SKF38393 stimulation but did not show any change in YFP/CFP upon quinpirole application. These findings again support the assumption that different retinal neurons express variable types, numbers and combinations of DRs.

3.3. Impact of DA on $[Ca^{2+}]_i$ in cultured retinal neurons

Calcium is the central second messenger in the neuronal system that orchestrates intracellular signaling cascades in every single cell. In literature it has been demonstrated that DA-downstream signaling changes $[Ca^{2+}]_i$ in several neuronal tissues (for review see Neve *et al.*, 2004) thereby modulating the release of neurotransmitters or the activity of Ca^{2+}-regulated proteins such as CaM, ACys or phosphatases. So far, little is known about the regulation of $[Ca^{2+}]_i$ in retinal neurons by DA. In this chapter I will investigate whether DA leads to changes in $[Ca^{2+}]_i$ in retinal neurons and also try to decipher the underlying signaling pathways.

3.3.1. DA triggers a change in $[Ca^{2+}]_i$ in cultured retinal neurons

To visualize changes in $[Ca^{2+}]_i$ in retinal neurons in culture, cells were loaded with the chemical Ca^{2+}-indicator Fluo-4-AM. The Fluo-4 fluorescence emission was recorded over time in two second long frames. In the following, an increase in Fluo-4 fluorescence was interpreted as an increase in $[Ca^{2+}]_i$ whereas a decrease in fluorescence was defined as a decrease in $[Ca^{2+}]_i$. The fluorescence was depicted as dF/F normalized (norm.) to the baseline fluorescence at the beginning of the measurement and plotted over time. Under resting conditions, loaded cells exhibited a baseline fluorescence which indicated a balanced $[Ca^{2+}]_i$ (Fig. 3.3.1, ---). This balanced $[Ca^{2+}]_i$ may be the result of the interplay between different parameters like the influx of Ca^{2+} through plasma membrane ion channels, the release of Ca^{2+} ions from internal stores, the export of Ca^{2+} through pumps and exchangers in the plasma membrane and the sequestration of Ca^{2+} ions into internal stores. The contribution of these parameters might be differentially weighted in distinct cell types leading to cell-specific $[Ca^{2+}]_i$.

Stimulation of neurons (DIV 6-11) with 5 µM DA resulted in different types of responses (Fig. 3.3.1). These responses were grouped into cells that reacted with an increase in

fluorescence indicating a rise in $[Ca^{2+}]_i$ (Fig. 3.3.1 A and B) hereafter called the "increase type" and those that reacted with a decrease in fluorescence indicating a decrease in $[Ca^{2+}]_i$ (Fig. 3.3.1, D and E) in the following called the "decrease type". The increase type was further subdivided into cells with a sustained increase in $[Ca^{2+}]_i$ (Fig. 3.3.1 A), with a transient increase in $[Ca^{2+}]_i$ (Fig. 3.3.1 B) and with an increase in $[Ca^{2+}]_i$ displaying oscillations (Fig. 3.3.1 C). In addition, I found cells that exhibited strong Ca^{2+}-oscillations in control conditions that were abolished by DA (Fig. 3.3.1 E). There were also cells in which DA did not elicit any change in fluorescence (Fig. 3.3.1 F).

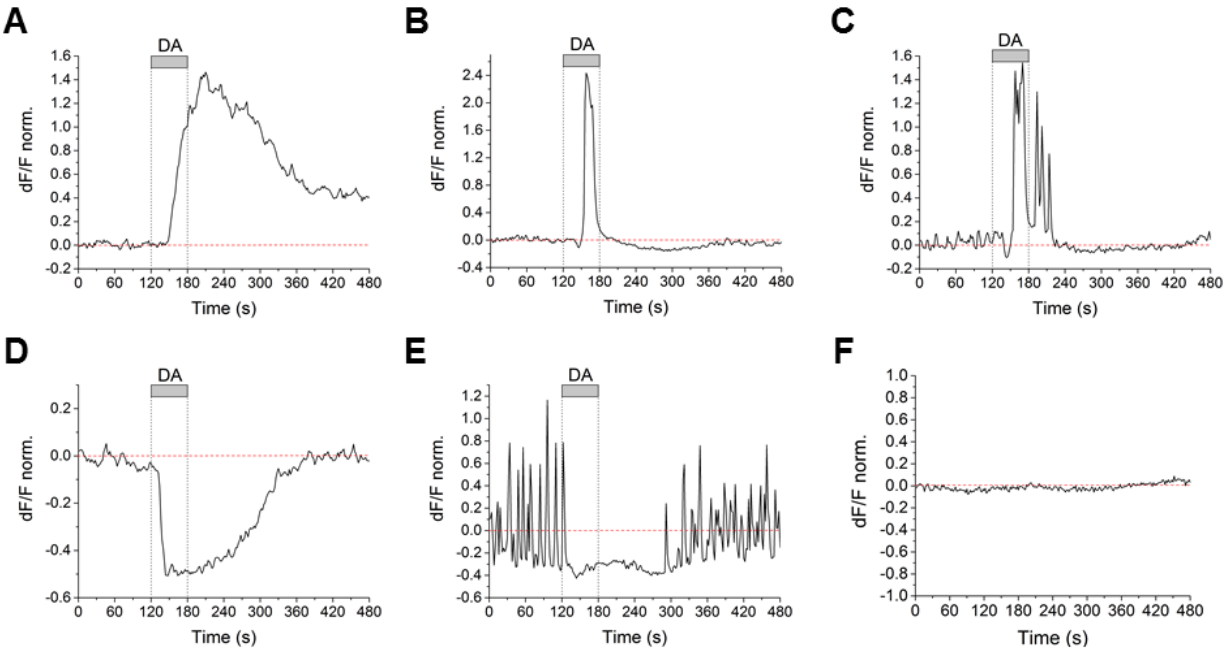

Fig. 3.3.1: DA stimulation of retinal cultured neurons triggered variable response patterns. Retinal dissociated neurons were loaded with the chemical Ca^{2+}-indicator Fluo-4 and stimulated with 5 µM DA for 1 min. Different neurons responded with distinct changes in fluorescence indicating a change in $[Ca^{2+}]_i$. **(A)** Sustained increase **(B)** Transient increase **(C)** Oscillating increase **(D)** Sustained decrease **(E)** Pausing in spontaneous oscillations **(F)** No response.

The different response types were found with different frequencies (Fig. 3.3.2 A). From a total of 876 cells that were analyzed (from 5 cultures), 78% did not respond to DA stimulation or were excluded from analysis (no response > excluded). In the group of responding neurons, 14.5% (n=127) responded with an increase in $[Ca^{2+}]_i$ (including sustained and transient responses; Fig. 3.3.1 A and B). Cells of the decrease type were very rare. Only 5% of neurons (n=45) responded with a decrease in $[Ca^{2+}]_i$ or rather an abolition of spontaneous Ca^{2+}-oscillations (Fig. 3.3.1 D and E). The oscillating increase in fluorescence was observed in a minority of cells (2.3%).

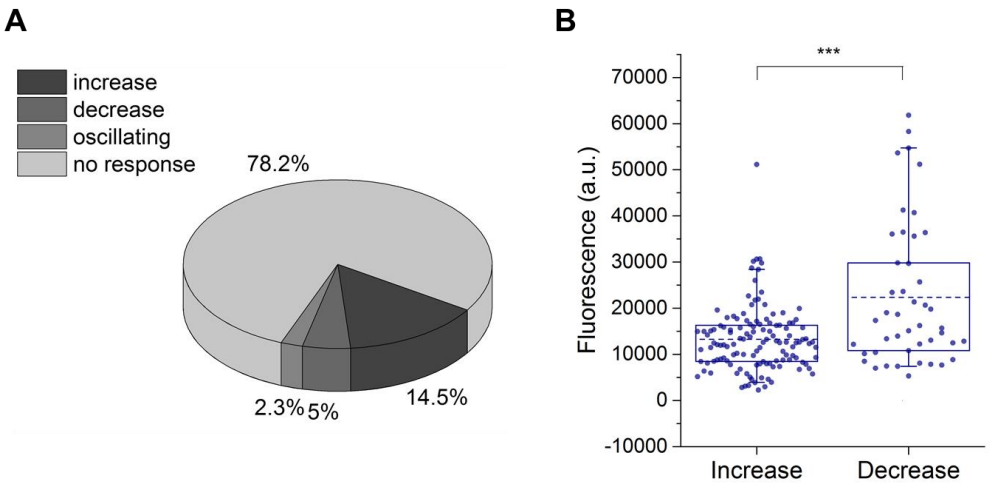

Fig. 3.3.2: Neurons of the different response types were found with different frequencies and exhibited distinct baseline fluorescence levels. (A) Frequency of DA-induced responses in retinal neurons in culture that were loaded with the chemical Ca^{2+}-indicator Fluo-4. The majority of neurons did not respond to stimulation with DA. Fourteen % of neurons responded with an increase and 5% with a decrease in $[Ca^{2+}]_i$. A few cells responded with Ca^{2+}-oscillations. **(B)** Comparison of the background-subtracted average baseline fluorescence of retinal neurons that were loaded with Fluo-4. Each dot represents the baseline fluorescence level of one cell. The box covers the central 50% of the data. The dashed lines indicate the mean (Increase: 13190.1±1254.9; Decrease: 22160.8±4513.8 (±95% CI)) and the whiskers above and below the box the 95th and 5th percentiles, respectively. Neurons of the increase type (n=127) showed significantly lower baseline fluorescence when compared to neurons that responded with a DA-triggered decrease in fluorescence (n=45) (Mann-Whitney Rank Sum Test: p***≤0.001).

In the normalized depiction chosen for fig. 3.3.1, the actual baseline level is not evident. However, during the conductance of experiments it was conspicuous that in most cases neurons that responded to DA with a decrease in fluorescence had a high basal fluorescence. To substantiate this observation, the baseline fluorescence of each neuron was determined by calculating the background-subtracted baseline fluorescence for the time window of 2-12 s of the imaging protocol. Cells of the increase type exhibited a mean baseline fluorescence of 13190.1±1254.9 (±95% CI) while cells of the decrease type had a 69% higher mean baseline fluorescence (22160.8±4513.8; (±95% CI)) (Fig. 3.3.2 B; Mann-Whitney Rank Sum Test: p***≤0.001). It cannot be ruled out that this difference simply reflects differences in the loading efficiency for Fluo-4 between different cell types. On the other hand, this difference in baseline fluorescence might indicate that the two groups of neurons exhibit distinct resting $[Ca^{2+}]_i$ which may be caused by differences *e.g.* in the equipment of Ca^{2+}-channels (CaChs) or their open probability, the activity of plasma membrane Ca^{2+}-ATPase (PMCA) or the export of Ca^{2+} via exchangers such as Na^+/Ca^{2+} exchangers (NCX).

For the following experiments it was quite important to test whether the neurons responded reversibly and repeatedly to subsequent stimulation with DA. Thus, Fluo-4-

loaded cells were stimulated twice with 5 µM DA for 1-3 min and washed in between with ES_{neuro}. Following, the response amplitudes triggered by the first DA stimulus (DA1) and those induced by the second DA stimulus (DA2) were calculated by determination of dF_{Max}/F (for the increase) or dF_{Min}/F (for the decrease) in a time interval of 300 s after start of the stimulus. Following, the response amplitudes were compared with each other by calculating the ratio DA2/DA1.

For the DA-induced increase in fluorescence, 127 cells (from 5 cultures) were analyzed. The cells responded with an average amplitude in fluorescence of about 0.85±0.14 (±95% CI) to the first DA stimulation (DA1). In the second DA stimulation (DA2), the average response amplitude was decreased about one half to 0.38±0.08 (±95% CI; Fig. 3.3.3 A, top). This decrease in the response amplitudes is reflected in the mean ratio of DA2/DA1 which is 0.54±0.1 (±95% CI) for cells responding with an increase in fluorescence upon stimulation with DA (Fig. 3.3.3 B). In the group of cells of the increase type the ratios DA2/DA2 were quite heterogeneous. A few cells exhibited a ratio DA2/DA1 that was larger than 1 indicating that the second response to DA was larger than the first DA-induced response. On the contrary, I found cells with a ratio DA2/DA1 of about zero indicating that the second stimulation with DA did not elicit any increase in $[Ca^{2+}]_i$ in these cells. Thus, cells of the increase type did not originate from a normal distributed population. Thirty-four % of cells had a ratio DA2/DA1 ≥0.54 (which depicts the mean DA2/DA1 for cells of the increase type; "≥0.54" group) and 66% of cells a ratio DA2/DA1 <0.54 ("<0.54" group).

Cells of the decrease type (n=45) showed an average amplitude in fluorescence of about -0.28±0.04 (±95% CI) in the first DA application (DA1) and of about -0.18±0.03 (±95% CI) in the second DA stimulation (DA2; Fig. 3.3.3 A, bottom). The average ratio DA2/DA1 was 0.67±0.07 (±95% CI) (Fig. 3.3.3 B). The ratios DA2/DA1 of cells of the decrease type were not as heterogeneous as those observed for the increase type. I found 58% of cells of the decrease type with DA2/DA1 ≥0.67 (which depicts the mean DA2/DA1 for cells of the decrease type; "≥0.67" group) and 42% of cells exhibiting DA2/DA1 <0.67 ("<0.67" group). A shift in the mean and in the relative frequencies of the two groups, "≥mean" and "<mean", is an indicator for how a pharmacological substance might affect dopaminergic signaling. The relative frequencies for the two groups will be provided in table 3.3.1 at the end of this chapter.

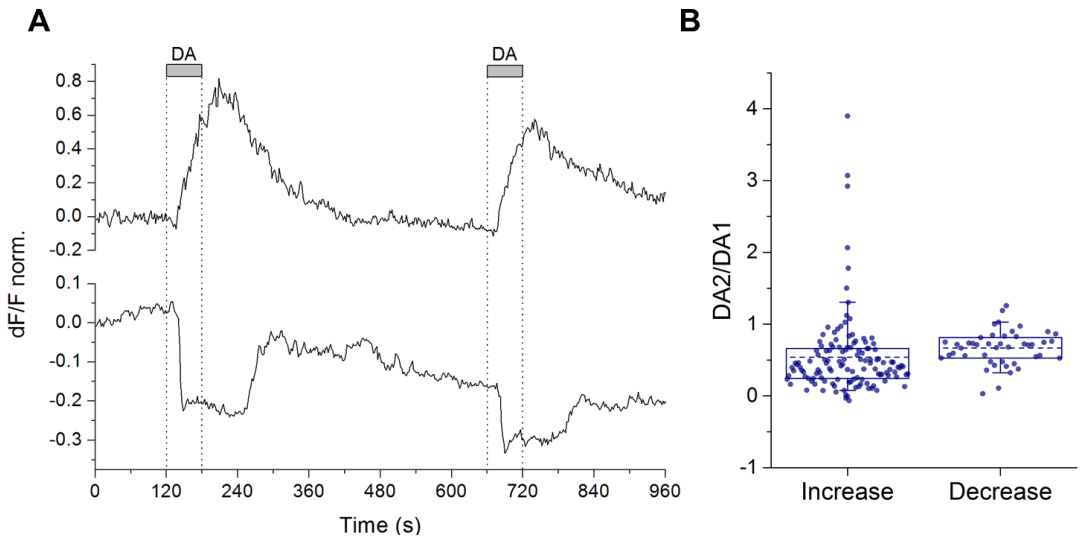

Fig. 3.3.3: Neurons responded reversibly and repeatedly to subsequent stimulation with DA. Retinal dissociated neurons were loaded with Fluo-4 and stimulated twice with 5 µM DA. **(A)** Both stimulations with DA elicited a change in fluorescence in both types of neurons (top: increase type; bottom: decrease type). **(B)** The amplitudes of both DA-induced responses were set in relation to each other (DA2/DA1) and data were plotted as box plot. Each dot represents DA2/DA1 of one cell. The box covers the central 50% of the data. The mean (dashed line) was 0.54±0.1 (±95% CI) for the increase type (n=127) and 0.67±0.07 (±95% CI) for the decrease type (n=45). The whiskers above and below the box indicate the 95th and 5th percentiles, respectively.

In retinal neurons transfected with AKAR4 only one type of response was observed when cells were stimulated with DA, namely an increase in PKA activity (3.2.2). In contrast to that, stimulation of Fluo-4-loaded neurons resulted in various types of responses (Fig. 3.3.1) that were found with different frequencies (Fig. 3.3.2). This finding supports the assumption that different subsets of neurons in my culture exhibited a specific equipment of DRs and downstream signaling molecules. As the increase in fluorescence (sustained and transient (Fig. 3.3.1 A and B)) and the decrease in fluorescence (sustained and pausing in spontaneous oscillations (Fig. 3.3.1 D and E)) were the most often DA-induced effects, the origin of these response types was further investigated in the following subchapters.

3.3.2. Involvement of different dopamine receptor types

There are five different types of dopamine receptors (DRs) all of which could be the mediators for the observed changes in $[Ca^{2+}]_i$. In experiments with the AKAR4 sensor I have demonstrated that the DA-induced increase in PKA activity is due to the activation of D1Rs (3.2.2.3). In addition, it was found by simultaneous stimulation of D1Rs and D2Rs that both receptor subtypes are co-expressed in retinal neurons in culture (3.2.3.4). On the basis of this knowledge, I sought for a correlation between DR subtype and type of Ca^{2+}- response to DA.

3.3.2.1. D1Rs are partly involved in the increase in $[Ca^{2+}]_i$

In order to investigate the role of D1Rs in the generation of DA-induced changes in $[Ca^{2+}]_i$, I used 10 µM of the D1R-specific antagonist SCH23390, a concentration that has also been used in previous studies (Guenther *et al.*, 1994; Hayashida *et al.*, 2009; Ogata *et al.*, 2012). Retinal neurons were stimulated with 5 µM DA for 1 min followed by a washing phase with ES_{neuro}. Then, SCH23390 was superfused for 3 min. Still during SCH23390 application, cells were stimulated with 5 µM DA for 1 min for the second time. After that, cells were washed again with ES_{neuro}.

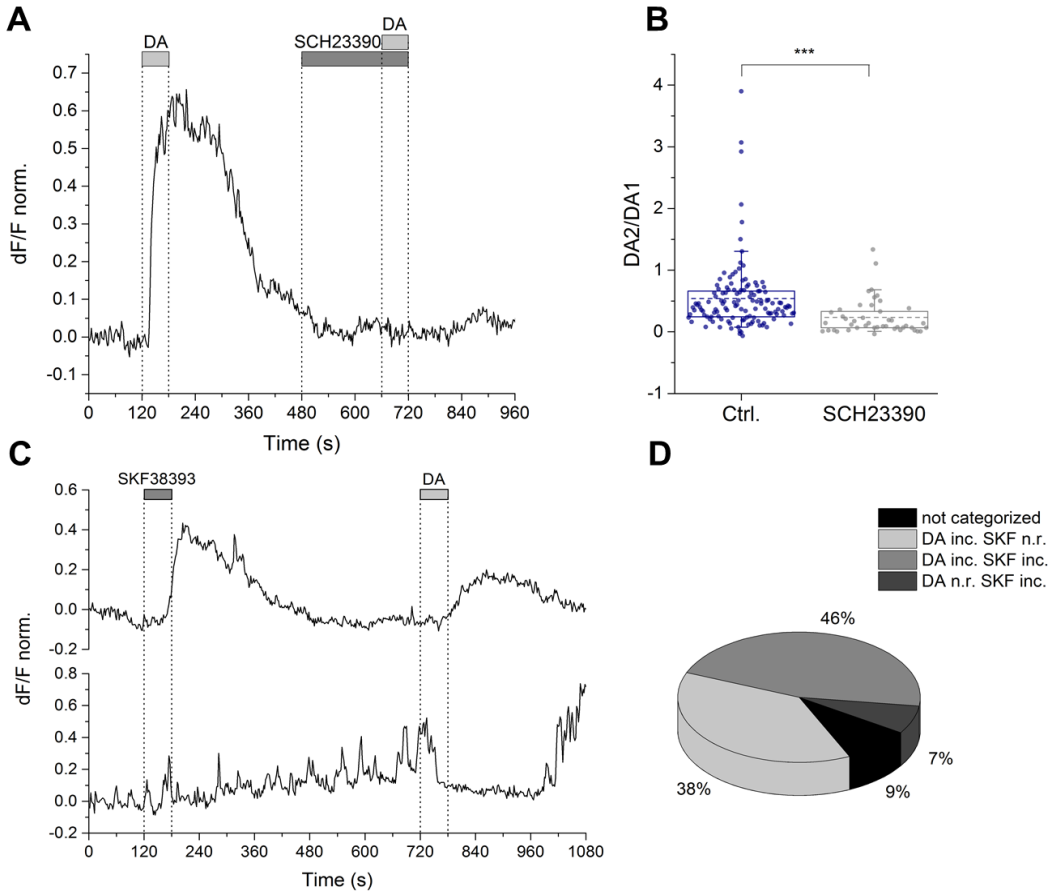

Fig. 3.3.4: Contribution of D1R-signaling to DA-stimulated increases in $[Ca^{2+}]_i$. (A) Retinal dissociated neurons were loaded with Fluo-4 and stimulated twice with 5 µM DA, once in the absence and once in the presence of 10 µM SCH23390, a D1R-specific antagonist. The graph shows the response of one neuron of the increase type. In the presence of 10 µM SCH23390 the DA-induced increase in $[Ca^{2+}]_i$ was abolished. **(B)** The amplitudes of both DA-induced responses were set in relation to each other (DA2/DA1) and data were plotted as box plot. Each dot represents DA2/DA1 of one cell. The box covers the central 50% of the data. The mean (dashed line) was 0.54±0.1 for the control (n=127; blue) and 0.23±0.09 (±95% CI) in the presence of SCH23390 (n=45; grey). The whiskers above and below the box indicate the 95th and 5th percentiles, respectively. The DA-induced increase in $[Ca^{2+}]_i$ in the presence of SCH23390 was less pronounced compared to control (Mann-Whitney Rank Sum Test: p***≤0.001). **(C)** Retinal dissociated neurons loaded with Fluo-4 were stimulated with 100 nM SKF38393 (a D1R-specific agonist) and 5 µM DA. SKF38393 induced an increase in fluorescence in cells of the increase type (top) but had no effect in cells of the decrease type (bottom). **(D)** Relative frequency of SKF38393 responses in respect to the DA response. Abbreviations: inc: increase; n.r.: no response; SKF: SKF38393.

Fig. 3.3.4 A shows the response of one neuron of the increase type. In this particular cell no DA-induced increase in $[Ca^{2+}]_i$ was observed in the presence of 10 µM SCH23390. Statistical analysis of neurons of the increase type revealed that there was a significant difference between cells of the control group (n=127) and cells treated with SCH23390 (n=45) (Mann-Whitney Rank Sum Test: p***≤0.001; Fig. 3.3.4 B). However, there were still a few cells (13%) that exhibited DA2/DA1 ≥0.54 (Fig. 3.3.4 B; Table 3.3.1).
In order to further prove the role of D1Rs in the generation of DA-induced increases in $[Ca^{2+}]_i$, cells were stimulated with the D1R-specific agonist SKF38393. SKF38393 was used at concentrations of 50-100 nM that only activate D1R-family members (Seeman and Van Tol, 1994) and that I have already successfully used in AKAR4-imaging experiments (3.2.2.3). All neurons that responded to stimulation with SKF38393 exhibited an increase in fluorescence indicating an increase in $[Ca^{2+}]_i$. These SKF38393-induced increases in $[Ca^{2+}]_i$ were only found in cells that also responded to DA with an increase in fluorescence, *i.e.* increase type cells (Fig. 3.3.4 C, top) but not in cells of the decrease type (Fig. 3.3.4 C, bottom). In 46% of cells that responded with a DA-induced increase in $[Ca^{2+}]_i$, SKF38393 elicited an increase in $[Ca^{2+}]_i$ (Fig. 3.3.4 D; medium grey). However, there were 38% of cells that responded with an increase in $[Ca^{2+}]_i$ to DA but not to SKF38393 (Fig. 3.3.4 D; light grey). In addition, I found 7% of cells that exhibited a SKF38393-induced increase in $[Ca^{2+}]_i$ but did not react to DA (Fig. 3.3.4 D; dark grey) and 9% that I could not categorize into one of the three groups (Fig. 3.3.4 D; black).

The responses of cells of the decrease type were quite variable during blockade of D1Rs. I found two different types of behaviors during application of SCH23390: in one half of cells of the decrease type, SCH23390 elicited an increase in fluorescence (Fig. 3.3.5 A, bottom) and in the other half of the cells SCH23390 application was without changes in fluorescence (Fig. 3.3.5 A, top). However, in both groups of decrease type cells application of DA in the presence of SCH23390 induced a decrease in $[Ca^{2+}]_i$ indicating that the decrease in $[Ca^{2+}]_i$ does not depend on D1Rs. Statistical analysis revealed that there was no significant difference between cells of the control group (n=45) and cells treated with SCH23390 (n=17) (3.3.5 B; Mann-Whitney Rank Sum Test: p= 0.36).

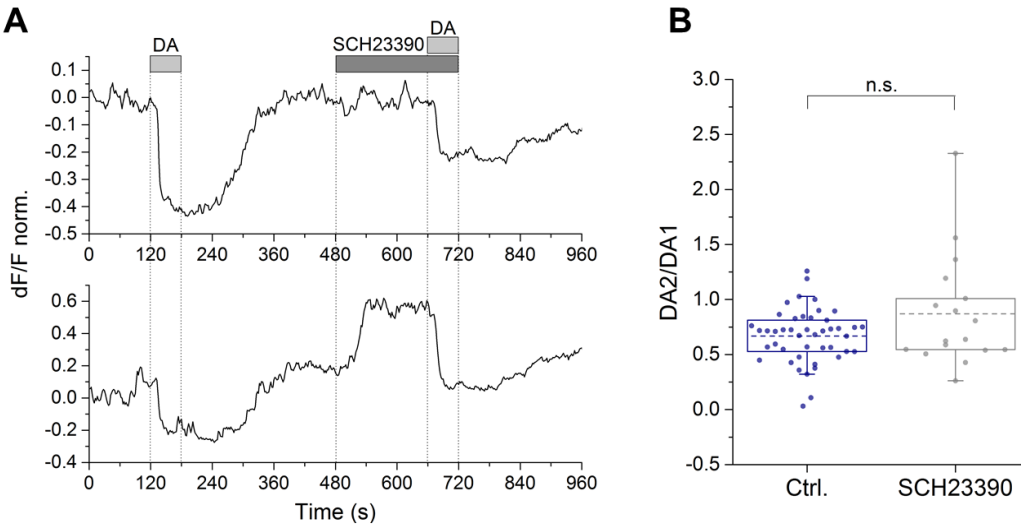

Fig. 3.3.5: The DA-induced decrease in $[Ca^{2+}]_i$ was not blocked by SCH23390. Retinal dissociated neurons were loaded with Fluo-4 and stimulated twice with 5 µM DA, once in the absence and once in the presence of 10 µM SCH23390, a D1R-specific antagonist. **(A)** Temporal responses of two different cells of the decrease type that both responded to stimulation with DA. SCH23390 triggered an increase in $[Ca^{2+}]_i$ in one cell (bottom) whereas the other was unaffected (top). **(B)** The amplitudes of both DA-induced responses were set in relation to each other (DA2/DA1) and data were plotted as box plot. Each dot represents DA2/DA1 of one cell. The box covers the central 50% of the data. The mean (dashed line) was 0.67±0.07 (±95% CI) for the control (n=45; blue) and 0.87±0.26 (±95% CI) in the presence of SCH23390 (n=17; grey). The whiskers above and below the box indicate the 95th and 5th percentiles, respectively. The average of DA2/DA1 in the presence of SCH23390 was not different when compared to control (Mann-Whitney Rank Sum Test: p= 0.36).

In summary, it was shown that D1Rs are involved in the DA-induced increase in $[Ca^{2+}]_i$ as blockade of these receptors by SCH23390 reduced and the D1R-specific agonist SKF38393 mimicked the effects of DA in a subset of cells of the increase type. However, there are two findings that might indicate that alternative pathways distinct from the D1R-pathway are involved in DA-induced increases in $[Ca^{2+}]_i$. First, some of the cells responding to DA did not respond to SKF38393. Second, blockade of D1Rs with SCH23390 did not block the increase in $[Ca^{2+}]_i$ in all cells (Fig. 3.3.4). Results for cells of the decrease type suggest that D1Rs are not involved in the DA-induced decrease in $[Ca^{2+}]_i$ as blockade of D1Rs by SCH23390 did not prevent the response to DA and the D1R-specific agonist SKF38393 never triggered a decrease in $[Ca^{2+}]_i$.

3.3.2.2. Are D2Rs involved in DA-induced changes in $[Ca^{2+}]_i$?

As data presented in the previous chapter suggest that D1Rs are not involved in the DA-mediated decrease in $[Ca^{2+}]_i$, this subchapter focuses on the role of D2Rs in the generation of DA-induced changes in $[Ca^{2+}]_i$. For that reason, retinal neurons were stimulated using the protocol similar to that described in 3.3.2.1. D2Rs were blocked with eticlopride (5 µM), a D2R-specific antagonist that was already used in previous studies at this concentration (Ogata *et al.*, 2012). Responses of both increase and

decrease type were unaffected by eticlopride application (Fig. 3.3.6; (A) Increase: Mann-Whitney Rank Sum Test: p=0.368; (B) Decrease: t-test: p=0.293).

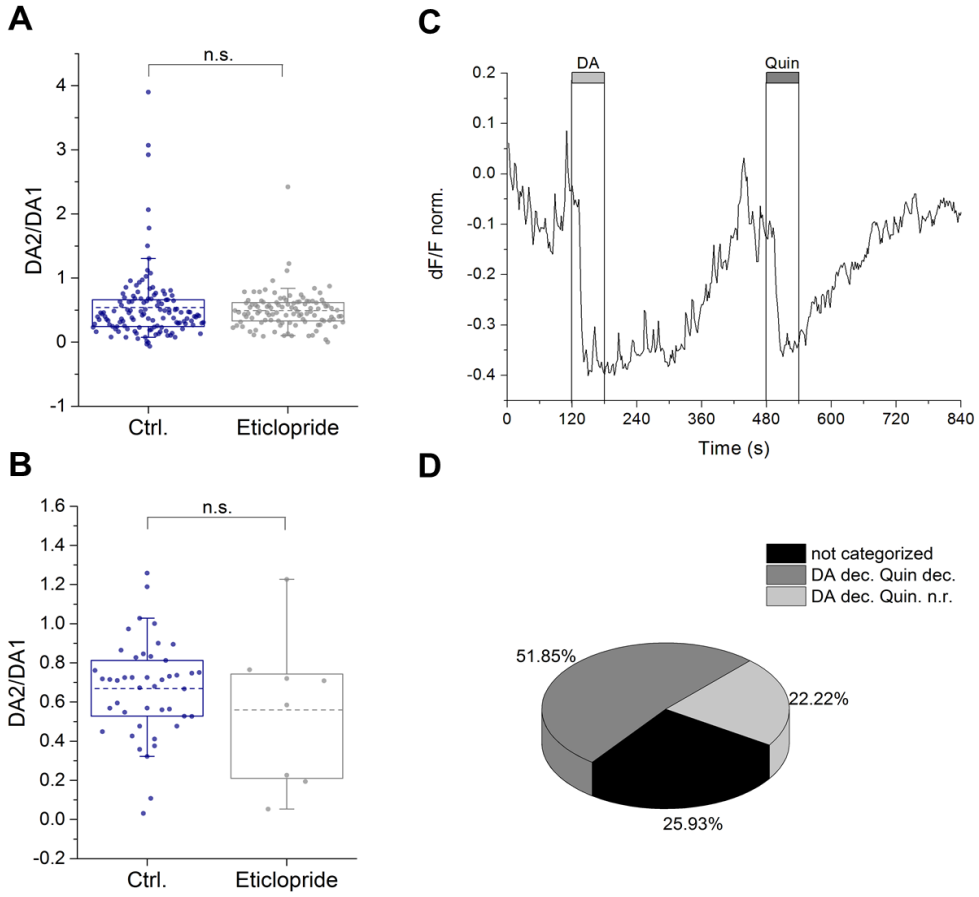

Fig. 3.3.6: The role of D2Rs in the generation of DA-induced decreases in $[Ca^{2+}]_i$ was elusive. (A and B) Retinal dissociated neurons were loaded with Fluo-4 and stimulated with 5 µM DA in the absence as well as in the presence of 5 µM of the D2R-specific antagonist eticlopride. The amplitudes of both DA-triggered responses were set in relation to each other (DA2/DA1) and data were plotted as box plot. Each dot represents DA2/DA1 of one cell. The box covers the central 50% of the data. The whiskers above and below the box indicate the 95th and 5th percentiles, respectively. **(A)** Cells of the increase type. The mean (dashed line) was 0.54±0.1 (±95% CI) for the ctrl. (n=127; blue) and 0.49±0.06 (±95% CI) in the presence of eticlopride (n=109; grey). The DA-induced increase in $[Ca^{2+}]_i$ was not affected by eticlopride (Mann-Whitney Rank Sum Test: p=0.368). **(B)** Cells of the decrease type**.** The mean (dashed line) was 0.67±0.7 (±95% CI) for the ctrl. (n=45; blue) and 0.56±0.32 (±95% CI) in the presence of eticlopride (n=8; grey). The DA-induced decrease in $[Ca^{2+}]_i$ was not affected by eticlopride (t-test: p=0.293). **(C)** The D2R-specific agonist quinpirole reduced $[Ca^{2+}]_i$ in about 52% of cells of the decrease type. **(D)** The quinpirole-induced decrease in $[Ca^{2+}]_i$ was most often found in cells that also responded with a decrease in $[Ca^{2+}]_i$ upon DA stimulation (dark grey). There were also cells that responded with a decrease in fluorescence to stimulation with DA but not to stimulation with quinpirole (light grey). One fourth of cells could be not assigned to one of the other groups (black). Abbreviations: dec: decrease; n.r.: no response; Quin: quinpirole.

To further prove the role of D2Rs in the generation of DA-induced changes in $[Ca^{2+}]_i$, cells were stimulated with the D2R-specific agonist quinpirole. Quinpirole was used at concentrations that only activate D2R-family members (50-100 nM; Seeman and Van Tol, 1994). I found neurons that responded with a quinpirole-induced decrease in

fluorescence (Fig. 3.3.6 C). This quinpirole-induced decrease in $[Ca^{2+}]_i$ was exclusively found in cells of the decrease type (Fig. 3.3.6 C; Fig. 3.3.6 D, dark grey). However, these robust responses to quinpirole were rather unexpected as I never observed a quinpirole-induced change in PKA activity using AKAR4 as a sensor (3.2.2.3). I also found neurons (22%) that responded to DA stimulation with a decrease in $[Ca^{2+}]_i$ but did not respond to stimulation with quinpirole (Fig. 3.3.6 D; light grey).

These results supported the assumption that DA-induced increases in $[Ca^{2+}]_i$ do not rely on D2R-signaling as blockade of D2Rs by eticlopride did not affect the DA-induced increase in $[Ca^{2+}]_i$. For the role of D2Rs in DA-induced decreases in $[Ca^{2+}]_i$, I cannot define a clear conclusion as the experiments with the specific D2R antagonist eticlopride and the specific D2R agonist quinpirole produced contradicting results.

3.3.3. Investigation of the classical DR signaling pathway

In principle, $[Ca^{2+}]_i$ can be altered in various ways. An increase in $[Ca^{2+}]_i$ could result from an increase in the Ca^{2+}-influx through ion channels, a release of Ca^{2+} from internal stores or a reduction in the export of Ca^{2+} from the cytoplasm. On the other hand, a decrease in $[Ca^{2+}]_i$ can be caused by a reduction of Ca^{2+}-influx through ion channels, a sequestration of Ca^{2+} to internal stores or a rise in Ca^{2+} extrusion via PMCA or exchangers. In order to unravel the underlying mechanisms of both response types, I employed different pharmacological approaches. In this chapter, I focused on the dissection of the classical DR/PKA-mediated pathway and its role in DA-induced changes in $[Ca^{2+}]_i$.

3.3.3.1. The role of external Ca^{2+} in DA-induced changes in $[Ca^{2+}]_i$

To find out whether external Ca^{2+} is essential for DA-induced changes in $[Ca^{2+}]_i$, retinal neurons were stimulated with DA in the presence or absence (wo Ca) of external Ca^{2+}. Fig. 3.3.7 shows the responses of three neurons that exhibited different types of responses to stimulation with DA in the presence of extracellular Ca^{2+} (A: no response; B: increase; C: decrease). Withdrawal of extracellular Ca^{2+} led to a reduction in fluorescence in all three neurons that was between 0.2 and 0.3 (Fig. 3.3.7). In the absence of extracellular Ca^{2+} none of the neurons showed a DA-induced change in $[Ca^{2+}]_i$. After re-addition of extracellular Ca^{2+}, neurons of the increase and decrease type again responded to DA stimulation (DA3) with a change in fluorescence (Fig. 3.3.7 B and C).

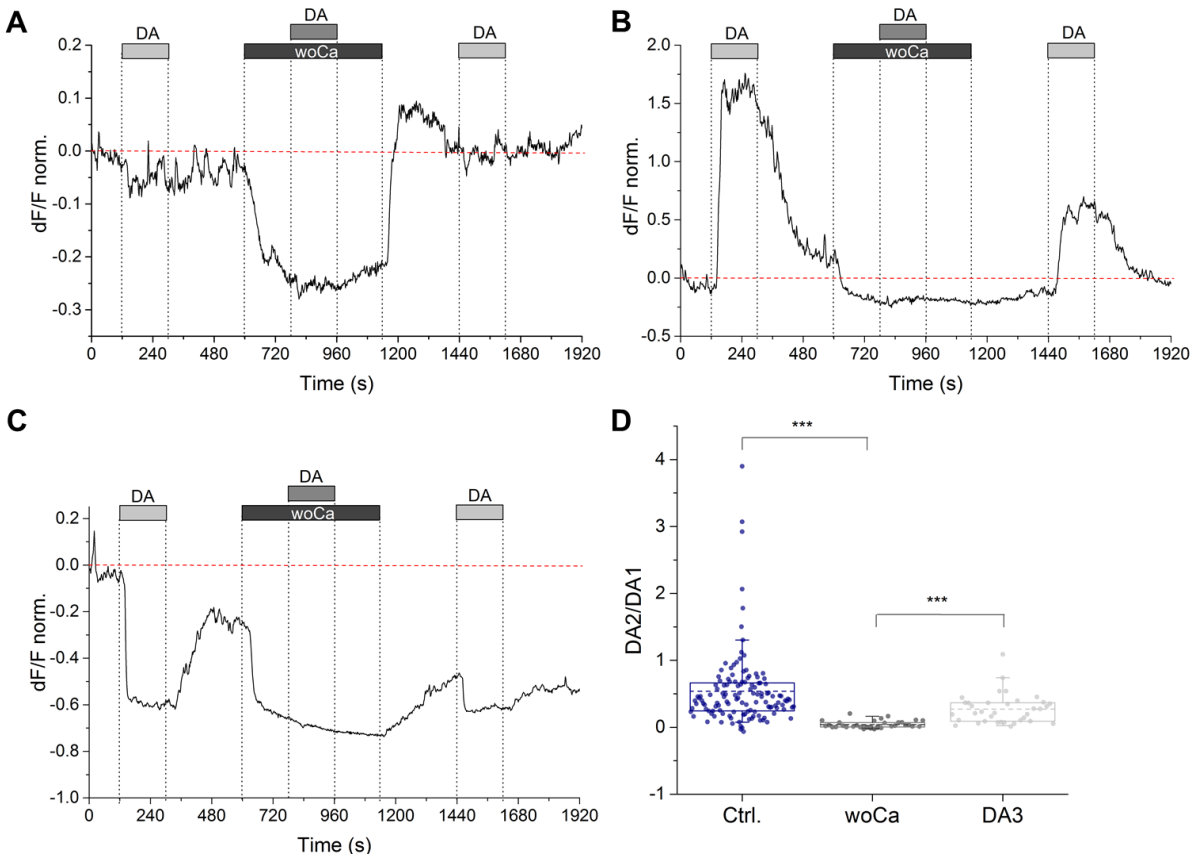

Fig. 3.3.7: DA-induced changes depended on the presence of extracellular Ca^{2+}. Retinal dissociated neurons were loaded with Fluo-4 and stimulated twice with 5 µM DA once in the presence and once in the absence of extracellular Ca^{2+} (woCa) **(A)** No response to DA. **(B)** Cell of the increase type. **(C)** Cell of the decrease type. **(B and C)** In the absence of extracellular Ca^{2+} (woCa) no responses to stimulation with DA were observed. **(D)** The amplitudes of DA-induced responses in cells of the increase type were set in relation to each other (DA2/DA1; DA3/DA1) and data were plotted as box plot. Each dot represents DA2/DA1 or DA3/DA1 of one cell. The box covers the central 50% of the data. The DA-induced increase in $[Ca^{2+}]_i$ was reduced in the absence of extracellular Ca^{2+} (wo Ca; Mann-Whitney Rank Sum Test: p***≤0.001; n=36). After re-addition of external Ca^{2+}, DA triggered an increase in $[Ca^{2+}]_i$ again (DA3). This was higher than in the absence of external Ca^{2+} (Mann-Whitney Rank Sum Test: p***≤0.001). The dashed lines indicate the mean (Ctrl.: 0.54±0.1; woCa: 0.04±0.02; DA3: 0.27±0.08; (±95% CI)) and the whiskers above and below the box indicate the 95th and 5th percentiles, respectively.

The box plot in fig. 3.3.7 D summarizes the results of the statistical analysis of 36 cells (from one culture) of the increase type. In the absence of extracellular Ca^{2+} (wo Ca) the increase in $[Ca^{2+}]_i$ was reduced when compared to control (Mann-Whitney Rank Sum Test: p***≤0.001). After re-addition of external Ca^{2+} DA triggered again an increase in $[Ca^{2+}]_i$ (DA3) that was higher than in the absence of external Ca^{2+} (DA3; Mann-Whitney Rank Sum Test: p***≤0.001). It was impossible to statistically analyze the 6 retinal neurons that responded with a decrease in $[Ca^{2+}]_i$ to stimulation with DA. This was due to the fact that these neurons exhibited a strong rundown in fluorescence as depicted in Fig. 3.3.7 C distorting the evaluation of the ratio DA2/DA1.

The reduction in Fluo-4 fluorescence upon withdrawal of external Ca^{2+} may indicate that in all cell types continuous Ca^{2+}-influx contributes to basal $[Ca^{2+}]_i$. For cells of the

increase type the absence of fluorescence increase during withdrawal of extracellular Ca^{2+} may indicate that under control conditions DA increases Ca^{2+} influx through plasma membrane CaChs. However, the effect of withdrawal of external Ca^{2+} on cells of the decrease type is more difficult to interpret. Removal of extracellular Ca^{2+} mimicked the effects of DA: withdrawal of Ca^{2+} and application of DA both reduced $[Ca^{2+}]_i$ in cells of the decrease type. As $[Ca^{2+}]_i$ is already at minimal levels in the absence of extracellular Ca^{2+}, a further DA-induced decrease in $[Ca^{2+}]_i$ may not be detected.

3.3.3.2. Role of Ca^{2+}-channels in DA-induced changes in $[Ca^{2+}]_i$

In 3.3.3.1 it was shown that both types of DA-induced changes in $[Ca^{2+}]_i$ depend on the presence of external Ca^{2+}, suggesting that Ca^{2+}-channels (CaChs) are a possible targets for dopaminergic modulation. Indeed, it has been described that stimulation of D1Rs or D2Rs leads to variable changes in the physiology of CaChs (reviewed in Neve *et al.*, 2004 and Missale *et al.*, 1998).

In a first attempt it was, therefore, tested whether the blockade of L-type CaChs with the specific blocker nimodipine (10 µM; Chen *et al.*, 2014b; Habermann *et al.*, 2003) results in the modulation of any type of DA-induced change in $[Ca^{2+}]_i$. Retinal neurons loaded with Fluo-4 were stimulated according to the protocol in 3.3.2.1. The response of two different cells is shown in Fig. 3.3.8 A: The neurons responded to stimulation with DA with either an increase (bottom) or a decrease (top) in fluorescence. Both responses were abolished in the presence of 10 µM nimodipine. The box plot in fig. 3.3.8 B summarizes the results of the statistical analysis of 85 neurons of the increase type. In the presence of 10 µM nimodipine the DA-induced increase was strongly reduced (Mann-Whitney Rank Sum Test: $p^{***} \leq 0.001$) when compared to control. Statistical analysis of cells of the decrease type could not be performed as the nimodipine-induced decrease in $[Ca^{2+}]_i$ distorts the evaluation of DA2/DA1.

The finding that blockade of L-type CaChs reduced both types of DA-induced responses may argue for a DA-induced modulation of L-type CaChs. However, the effect of nimodipine on cells of the decrease type is more difficult to interpret. Blockade of L-type CaChs mimicked the effects of DA in a sense that both effectors namely nimodipine and the DA reduced $[Ca^{2+}]_i$. As $[Ca^{2+}]_i$ is already at minimal levels during blockade of L-type CaChs, a further DA-induced decrease in $[Ca^{2+}]_i$ may not be detected.

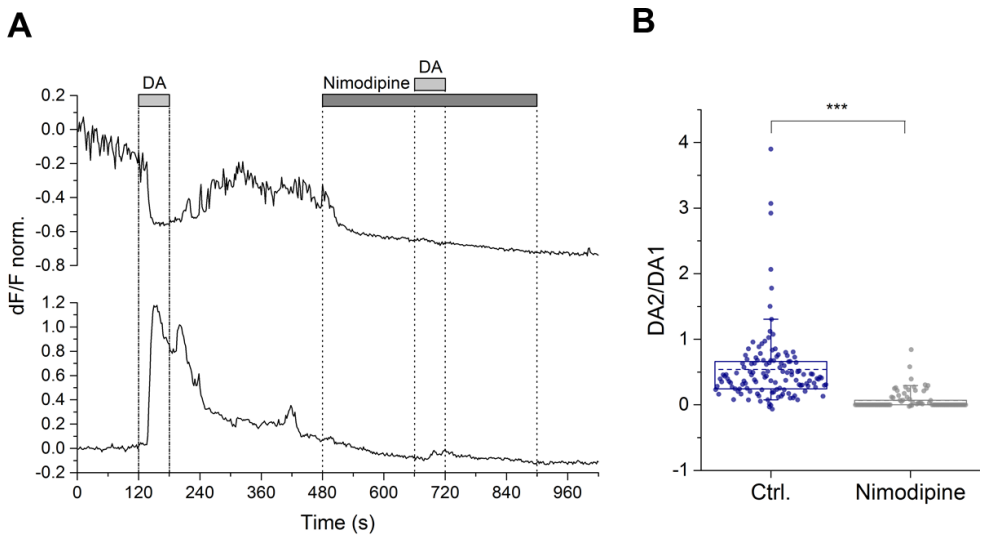

Fig. 3.3.8: Blockade of L-type CaChs led to a reduction in DA-induced response amplitudes. Retinal dissociated neurons were loaded with Fluo-4 and stimulated twice with 5 µM DA once in the presence and once in the absence of the L-type CaCh inhibitor nimodipine (10 µM). **(A)** In the presence of nimodipine the response to DA was abolished in neurons of both response types (top: decrease type; bottom: increase type). **(B)** The amplitudes of both DA-induced responses of cells of the increase type were set in relation to each other (DA2/DA1) and data were plotted as box plot. Each dot represents DA2/DA1 of one cell. The box covers the central 50% of the data. The dashed lines indicate the mean (Ctrl.: 0.54±0.1; Nimodipine: 0.07±0.03; ±95% CI) and the whiskers above and below the box indicate the 95th and 5th percentiles, respectively. The DA-induced increase in $[Ca^{2+}]_i$ was significantly reduced by nimodipine (n=85) when compared to control (n=127) (Mann-Whitney Rank Sum Test: p***≤0.001).

As the L-type channel is not the only CaCh in neurons, it was tested whether another type of CaCh also contributes to the DA-induced changes in $[Ca^{2+}]_i$. N-type CaChs are largely restricted to neurons (Tsien *et al.*, 1991; Fujita *et al.*, 1993) and predominantly found in both synaptic layers of the rat retina (Xu *et al.*, 2002). They were shown to be generally modulated by D1Rs as well as by D2Rs (reviewed in Neve *et al.*, 2004 and Missale *et al.*, 1998). In order to investigate the contribution of N-type channels in DA-induced changes in $[Ca^{2+}]_i$, I made use of the N-type CaCh-specific antagonist ω-conotoxin GVIA. Cells were stimulated according to the protocol described in 3.3.2.1. The neurons responded to stimulation with DA with either an increase (Fig. 3.3.9 A) or a decrease (Fig. 3.3.9 C) in fluorescence. In the group of cells of the increase type I found two types of responses: in some of the cells the DA-induced increase in $[Ca^{2+}]_i$ in the presence of ω-conotoxin GVIA was similar to the second DA response under control conditions (Fig. 3.3.9 A, bottom) while in the other group of cells ω-conotoxin GVIA reduced the DA-induced increase in $[Ca^{2+}]_i$ (Fig. 3.3.9 A, top). Statistical analysis of 196 cells of the increase type (from 6 cultures) revealed that ω-conotoxin GVIA reduced the DA-induced increase in $[Ca^{2+}]_i$ when compared to control (n=127) (Mann-Whitney Rank Sum Test: p***≤0.001; Fig. 3.3.9 B). However, there were still 21% of cells that exhibited a ratio DA2/DA1 that was comparable to the average DA2/DA1 of the control ("≥0.54")

(Table 3.3.1). Omega-Conotoxin GVIA did not affect the DA-induced decrease in fluorescence in cells of the decrease type (n=42; Mann-Whitney Rank Sum Test: p=0.063; Fig. 3.3.9 C and D).

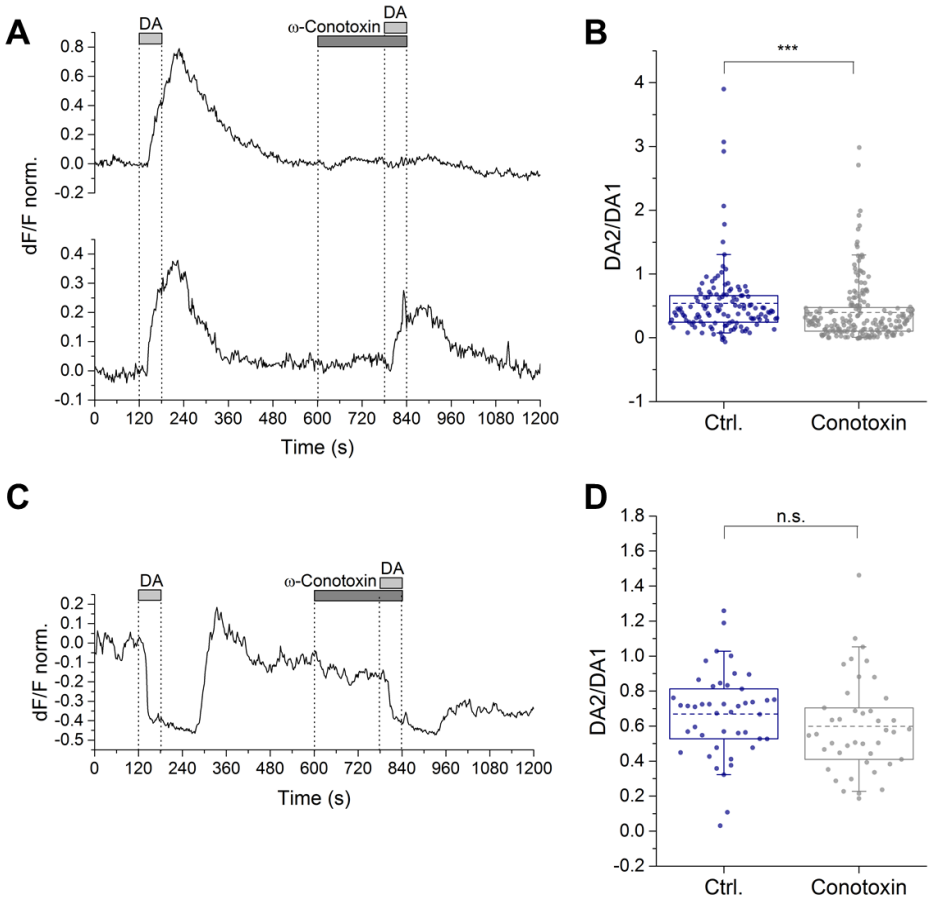

Fig. 3.3.9: Blockade of N-type CaChs affected DA-induced response amplitudes. Retinal dissociated neurons were loaded with Fluo-4 and stimulated twice with 5 µM DA once in the presence and once in the absence of 100 nM ω-conotoxin GVIA, an N-type CaCh inhibitor. **(A)** The responses of two neurons of the increase type. **(B and D)** The amplitudes of both DA-induced responses were set in relation to each other (DA2/DA1) and data were plotted as box plot. Each dot represents DA2/DA1 of one cell. The box covers the central 50% of the data. The whiskers above and below the box indicate the 95th and 5th percentiles, respectively. **(B)** The DA-induced increase in $[Ca^{2+}]_i$ was significantly reduced by ω-conotoxin GVIA (n=196; Mann-Whitney Rank Sum Test: p***≤0.001) when compared to control (n=127). The dashed lines indicate the mean (Ctrl.: 0.54±0.1; Conotoxin: 0.4±0.07; ±95% CI). **(C)** The response of one neuron of the decrease type. **(D)** The DA-induced decrease in $[Ca^{2+}]_i$ was unaffected by ω-conotoxin GVIA (n=42; Mann-Whitney Rank Sum Test: p=0.063) when compared to control (n=45). The dashed lines indicate the mean (Ctrl.: 0.67±0.07; Conotoxin: 0.6±0.08; ±95% CI).

Thus, these findings led to the assumption that not only L-type CaChs but also N-type CaChs contribute to the generation of DA-induced increases in $[Ca^{2+}]_i$. However, in contrast to the experiments with nimodipine, only increase type cells were affected by ω-conotoxin GVIA. N-type CaChs seemed not to be involved in the generation of DA-induced decrease of $[Ca^{2+}]_i$ in retinal neurons in culture.

3.3.3.3. PKA is a mediator of DA-induced increase in $[Ca^{2+}]_i$

In the previous chapter I have demonstrated that L-type and N-type CaChs play a role in the generation of DA-induced changes in $[Ca^{2+}]_i$. One central mechanism by which voltage-gated CaChs can be modulated is by phosphorylation through kinases such as PKA (for review see Neve *et al.*, 2004). Interestingly, I have demonstrated in experiments using AKAR4 as sensor that activation of DRs alters the activity of PKA (3.2.2.1). Thus, it is plausible that PKA is involved in the generation of DA-induced changes in $[Ca^{2+}]_i$. In order to test for this, the PKA-specific antagonist H89 (20 µM) was applied at concentrations that were already used in chapter 3.2.2.4. Retinal neurons were stimulated according to the protocol in 3.3.2.1. It is important to point out that blockade of PKA affects both the D1R-mediated signaling pathway by preventing D1R-mediated increases in PKA activity and the D2R-mediated signaling pathway by mimicking the D2R-triggered reduction in PKA activity.

Fig. 3.3.10 A shows the response of one neuron that responded with an increase in $[Ca^{2+}]_i$ to stimulation with 5 µM DA. The response to DA was abolished in the presence of H89. Statistical analysis of 87 neurons (from 3 cultures) revealed that the DA-induced response amplitude in the presence of H89 was reduced (Mann-Whitney Rank Sum Test: $p^{***} \leq 0.001$) when compared to control (Fig. 3.3.10 B). These findings indicate that PKA plays a role in the generation of DA-induced increases in $[Ca^{2+}]_i$. However, the blockade of PKA by H89 did not reduce DA2/DA1 as strong as did *e.g.* nimodipine (see 3.3.3.2) or the withdrawal of external Ca^{2+} (see 3.3.3.1).

Fig. 3.3.10 C shows the response of two different neurons of the decrease type. In one half of the cells of the decrease type application of H89 induced a pronounced decrease in fluorescence. In these cells, blockade of PKA abolished the response to DA (Fig. 3.3.10 C, bottom). In the other half of neurons of the decrease type the change in fluorescence induced by H89 was less pronounced. In these cells, DA application induced a decrease in $[Ca^{2+}]_i$ during blockade of PKA (Fig. 3.3.10 C, top). As the H89-induced decrease and the rundown in fluorescence distorted the evaluation of dF_{Min}/F of the second DA-induced response, statistical analysis for the decrease type neurons could not be conducted. Nevertheless, these results indicate that in a subgroup of cells of the decrease type blockade of PKA mimicked the effects of DA arguing for a DR/PKA-mediated reduction in $[Ca^{2+}]_i$. However, in the other subgroup of cells the role of PKA in mediating the DA-induced decrease in $[Ca^{2+}]_i$ has to be further examined.

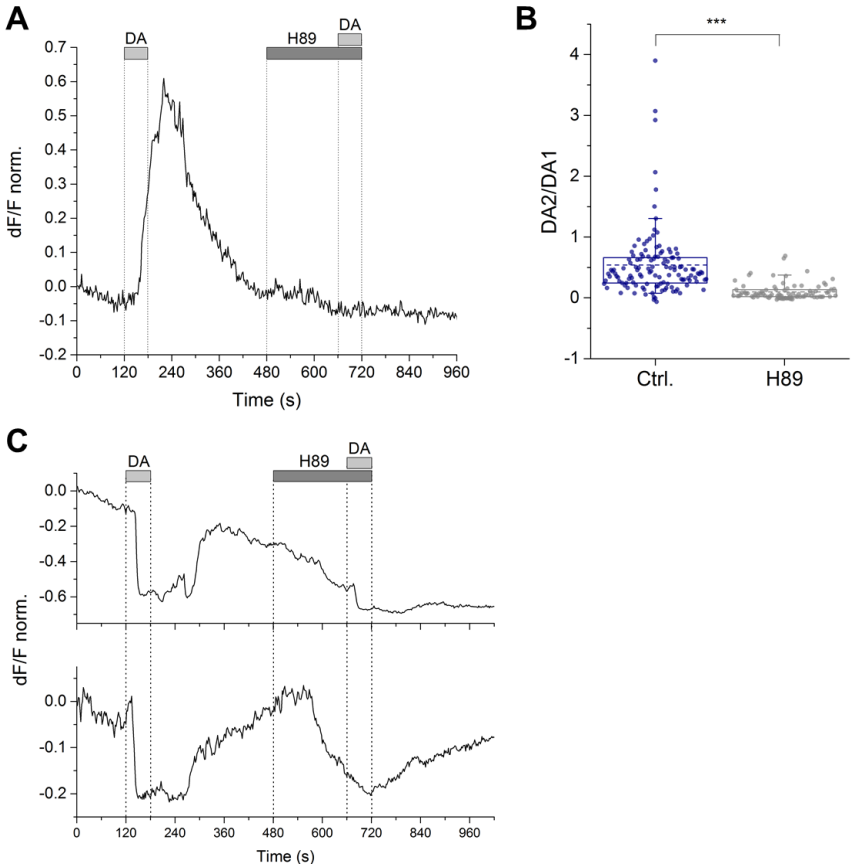

Fig. 3.3.10: Effects of H89 on DA-induced changes in $[Ca^{2+}]_i$. Retinal dissociated neurons were loaded with Fluo-4 and stimulated with 5 µM DA in the absence as well as in the presence of the PKA inhibitor H89 (20 µM). **(A)** Time resolved response of one neuron of the increase type. **(B)** The amplitudes of both DA-induced responses were set in relation to each other (DA2/DA1) and data were plotted as box plot. Each dot represents DA2/DA1 of one cell ($n_{ctrl.}$: 127; n_{H89}: 87). The box covers the central 50% of the data. The response of cells of the increase type was significantly reduced by H89 when compared to control (Mann-Whitney Rank Sum Test: p***≤0.001). The dashed lines indicate the mean (Ctrl.: 0.54±0.1; H89: 0.1±0.03; ±95% CI) and the whiskers above and below the box the 95th and 5th percentiles, respectively. **(C)** Time resolved responses of two different neurons of the decrease type. In some cells blockade of PKA abolished the DA-induced decrease (bottom) whereas in other cells blockade of PKA did not completely abolish the DA-induced decrease in $[Ca^{2+}]_i$ (top).

3.3.3.4. Influence of phosphatases PP1 and PP2A

Phosphatases are opponents of kinases and thus contribute to the regulation of intracellular signal transduction pathways by mediating reversible protein dephosphorylation. Two types of serine-threonine phosphatases, namely PP1 and PP2A, have been shown to be involved in dopaminergic downstream signaling by regulating the activity of DARPP-32. Phosphorylation by PKA converts DARPP-32 into a potent inhibitor of PP1 whereas PP2A is directly activated by phosphorylation through PKA (for review see Svenningsson *et al.*, 2004). In the retina, DARPP-32 immunoreactivity has been found in HCs, Müller cells, AII ACs and ACs of unidentified type (Witkovsky *et al.*, 2007). To investigate whether these two phosphatases are also involved in DA-mediated changes in $[Ca^{2+}]_i$ in retinal cultured neurons, which mainly represent ACs, I

used the PP1/PP2A-specific antagonist calyculin A (25 nM; for review see Herzig and Neumann, 2000). Retinal neurons were stimulated according to the protocol used in 3.3.2.1.

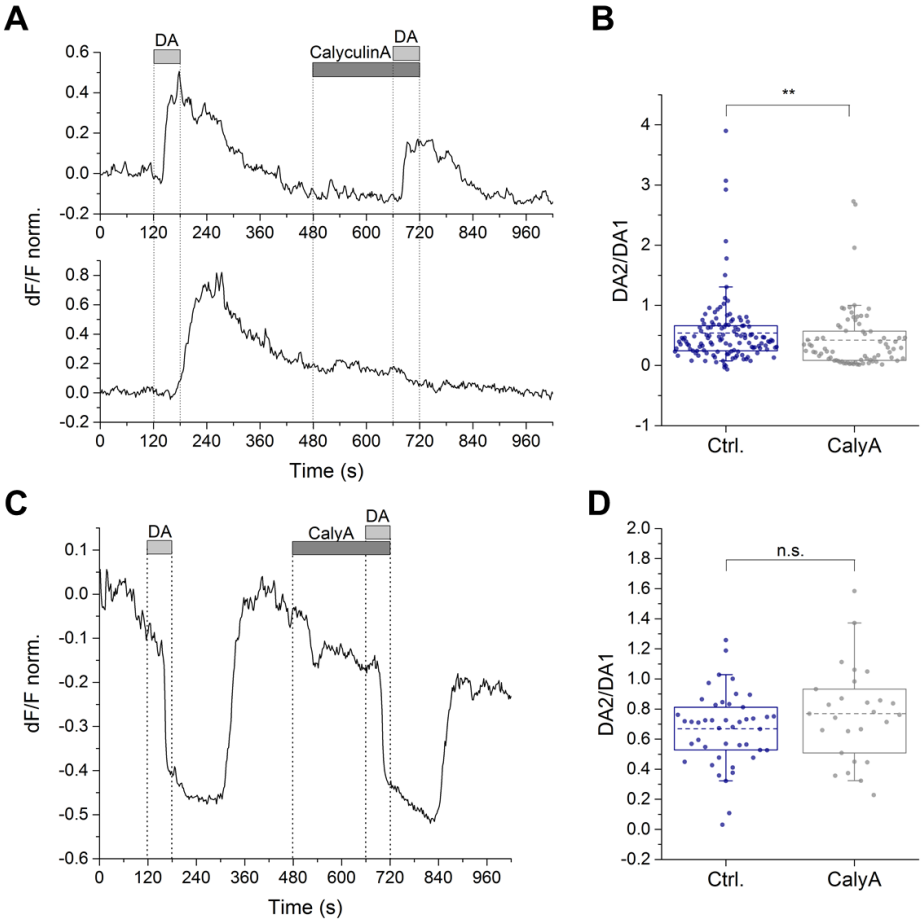

Fig. 3.3.11: Calyculin A only affected the responses of cells of the increase type. Retinal dissociated neurons were loaded with Fluo-4 and stimulated with 5 µM DA in the absence as well as in the presence of the PP1 and PP2A inhibitor calyculin A (25 nM). **(A)** Calyculin A reduced the response to DA in some cells of the increase type (bottom) but did not affect the response in others (top). **(B)** The amplitudes of both DA-induced responses of cells of the increase type were set in relation to each other (DA2/DA1) and data were plotted as box plot. Each dot represents DA2/DA1 of one cell. The box covers the central 50% of the data. The response of cells of the increase type was significantly reduced by calyculin A (CalyA; n=76) when compared to control (n=127)(Mann-Whitney Rank Sum Test: p**≤0.003). The dashed lines indicate the mean (Ctrl.: 0.54±0.1; CalyA: 0.42±0.12; ±95% CI) and the whiskers above and below the box the 95th and 5th percentiles, respectively. **(C)** The time resolved response of one cell of the decrease type. **(D)** The amplitudes of both DA-induced responses of cells of the decrease type were set in relation to each other (DA2/DA1) and data were plotted as box plot. Each dot represents DA2/DA1 of one cell. The box covers the central 50% of the data. The response of cells of the decrease type in the presence of calyA (n=27) was not significantly different when compared to control (n=45) (t-test: p=0.135). The dashed lines indicate the mean (Ctrl.: 0.67±0.07; CalyA: 0.77±0.12; 95% CI) and the whiskers above and below the box the 95th and 5th percentiles, respectively.

In cells of the increase type I found two types of responses to application of calyculin A: in some of the cells the DA-induced increase in $[Ca^{2+}]_i$ in the presence of calyculin A was similar to the second DA response under control conditions (Fig. 3.3.11 A, top) while in the other group of cells calyculin A reduced the DA-induced increase in $[Ca^{2+}]_i$ (Fig.

3.3.11 A, bottom). The box plot in fig. 3.3.11 B depicts the ratio DA2/DA1 of all 76 neurons of the increase type. Comparison between the control group and the group of calyculin A-treated cells revealed that the DA response was reduced in the second group of cells (Mann-Whitney Rank Sum Test: p**≤0.003). However, there were still 27% of cells that exhibited a DA2/DA1 ≥0.54 (Table 3.3.1). In cells of the decrease type the DA-induced response was not blocked by calyculin A (Fig. 3.3.11 C and D; t-test: p=0.135). If one assumes that the DA-induced increase in $[Ca^{2+}]_i$ is due to the stimulation of D1Rs and the activation of PKA in some cells of the increase type, the results obtained with calyculin A are in contradiction to what was expected. Inhibition of PP1 and PP2A should theoretically lead to an inhibition of dephosphorylation processes and thereby favor the phosphorylation of *e.g.* L-type CaChs and thus an increase in $[Ca^{2+}]_i$. However, I found cells of the increase type in which calyculin A reduced the response to DA and others in which the response to DA was not affected. For the decrease type one would have expected that the DA-induced decrease in $[Ca^{2+}]_i$ was completely abolished, if one assumes that the decrease in $[Ca^{2+}]_i$ is due to a dephosphorylation-mediated closure of CaChs. However, the response to DA of cells of the decrease type was not altered by calyculin A.

3.3.3.5. The role of Gβγ in DA-induced changes in $[Ca^{2+}]_i$

G-protein coupled receptors (GPCRs) do not only transduce signals via Gα-subunits but also by Gβγ subunits. Besides others, the activation of D2Rs leads to a reduction in $[Ca^{2+}]_i$ through the action of Gβγ (Beaulieu and Gainetdinov, 2011) or to an increase in K^+-currents and thus a decrease in cell excitability via action of Gβγ (Neve *et al.*, 2004). To test whether Gβγ is involved in mediating DA-induced changes in $[Ca^{2+}]_i$, retinal neurons were stimulated according to the protocol in 3.3.2.1. Gβγ was blocked by 10 µM of the specific inhibitor gallein (Lehmann *et al.*, 2007).

Fig. 3.3.12 shows the response of three neurons of different response types. Application of 10 µM gallein reduced fluorescence by about -0.4 as it can be clearly seen in fig. 3.3.12 A. Control experiments revealed that this decrease in fluorescence is most likely not due to a change in $[Ca^{2+}]_i$ but rather due to an optical artefact caused by quenching of the emission light of Fluo-4. However, gallein seemed to not abolish but rather enhance DA-induced increases in $[Ca^{2+}]_i$ (Fig. 3.3.12 B and D left; Mann-Whitney Rank Sum Test: p***≤0.001). The number of cells that could be grouped into the "≥54" group was higher after gallein application (58%) when compared to control (34%)

(Table 3.3.1). The Ca^{2+}-response of cells of the decrease type was not affected by gallein (Fig. 3.3.12 C and D right; t-test: p= 0.53).

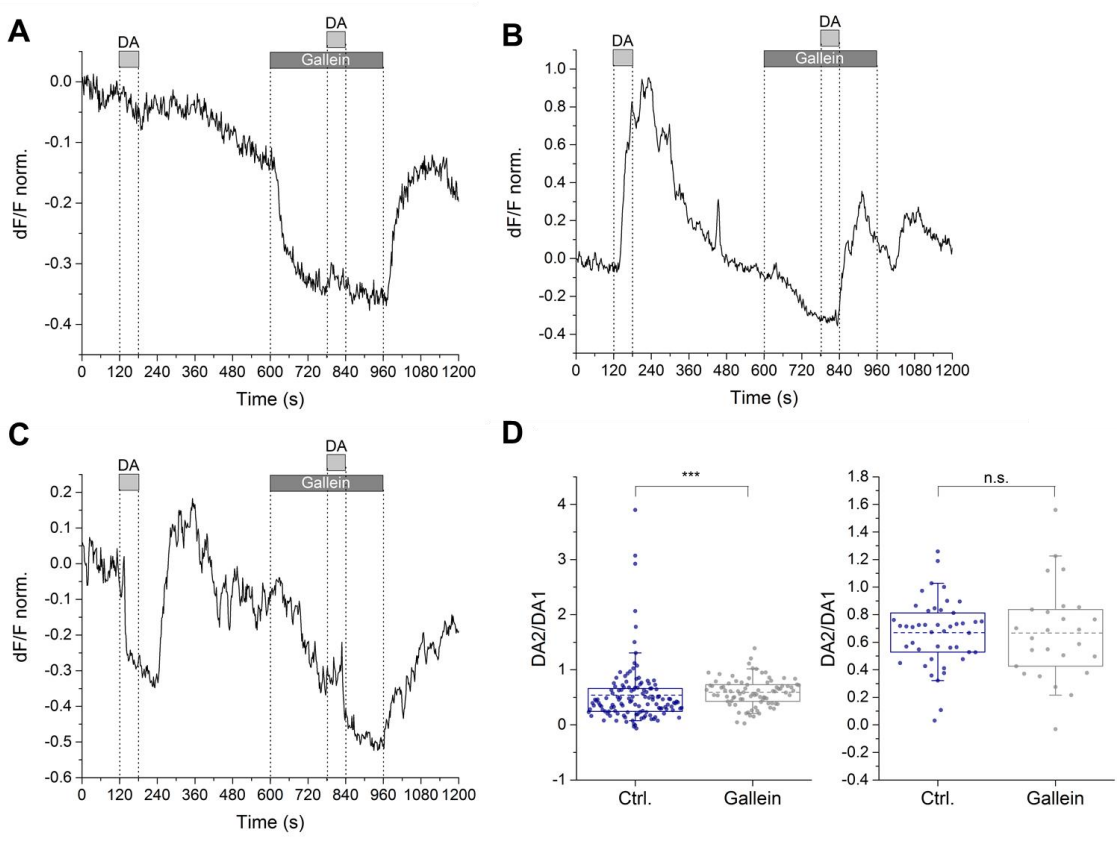

Fig. 3.3.12: Blockade of Gβγ only affected the DA-induced increase in $[Ca^{2+}]_i$. Retinal dissociated neurons were loaded with Fluo-4 and stimulated with 5 µM DA in the absence as well as in the presence of 10 µM gallein, a Gβγ inhibitor. **(A)** Response of one neuron that did not respond to DA application. **(B)** Neuron of the increase type. The response to DA application was not abolished by gallein. **(C)** Neuron of the decrease type. The response to DA application was not blocked by gallein. **(A, B, C)** Gallein induced a decrease in fluorescence in most of the cells measured. **(D)** The amplitudes of both DA-induced responses were set in relation to each other (DA2/DA1) and data were plotted as box plot. Each dot represents DA2/DA1 of one cell. The box covers the central 50% of the data. Left: The response of 84 cells of the increase type in the presence of gallein was significantly different when compared to control (n=127) (Mann-Whitney Rank Sum Test: p***≤0.001). The dashed lines indicate the mean (Ctrl.: 0.54±0.1; Gallein: 0.59±0.06; ±95% CI) and the whiskers above and below the box the 95th and 5th percentiles, respectively. Right: The response of 26 cells of the decrease type in the presence of gallein was not significantly different when compared to control (n=45) (t-test: p=0.53). The dashed lines indicate the mean (Ctrl.: 0.67±0.07; Gallein: 0.67±0.14; ±95% CI) and the whiskers above and below the box the 95th and 5th percentiles, respectively.

3.3.4. Investigation of alternative pathways

The previous chapter focused on the investigation of the classical DR-downstream signaling pathway through PKA and the modulation of CaChs in the plasma membrane which regulate the influx of Ca^{2+} ions. However, $[Ca^{2+}]_i$ is also controlled by the release of Ca^{2+} from internal stores and by sequestration of Ca^{2+} ions into these stores. The aim of this chapter was to investigate the role of internal Ca^{2+} stores in DA-induced changes in $[Ca^{2+}]_i$ via a pharmacological approach.

3.3.4.1. Does blockade of SERCA affect DA-induced changes in $[Ca^{2+}]_i$?

The sarco-/endoplasmatic reticulum Ca^{2+}-ATPase (SERCA) actively pumps Ca^{2+}-ions from the cytoplasm into the lumen of the ER. In order to address the questions whether the DA-induced increase in $[Ca^{2+}]_i$ is due to a release of Ca^{2+} from internal stores and whether the DA-induced decrease in $[Ca^{2+}]_i$ is due to a sequestration of Ca^{2+} into the ER, SERCA was blocked by 5 µM cyclopiazonic acid (CPA), a cell-permeable, reversible inhibitor of SERCA that depletes Ca^{2+} stores and essentially eliminates any further Ca^{2+} release from or uptake into the stores (Thomas and Hanley, 1994). Retinal neurons were stimulated with a protocol similar to the one described in 3.3.2.1.

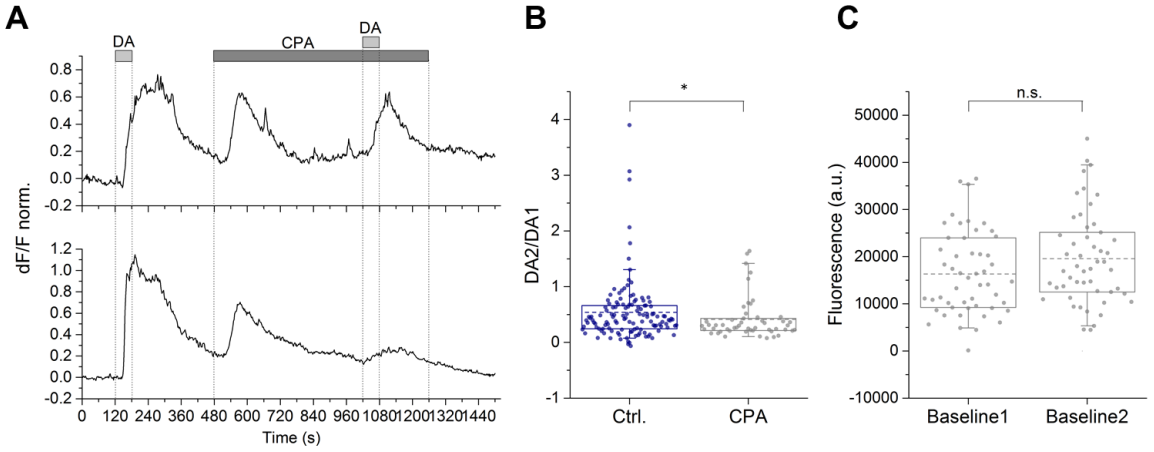

Fig. 3.3.13: Store depletion by CPA weakly affected the DA-triggered increase in $[Ca^{2+}]_i$. Retinal dissociated neurons were loaded with Fluo-4 and stimulated twice with 5 µM DA once in the presence and once in the absence of 5 µM of the SERCA inhibitor CPA. **(A)** Time resolved responses of two neurons of the increase type. Top: CPA no block; Bottom: CPA block. **(B)** The amplitudes of both DA-induced responses were set in relation to each other (DA2/DA1) and data were plotted as box plot. Each dot represents DA2/DA1 of one cell. The box covers the central 50% of the data. The dashed lines indicate the mean (Ctrl.: 0.54±0.1; CPA: 0.41±0.1; ±95% CI) and the whiskers above and below the box the 95th and 5th percentiles, respectively. The response of cells of the increase type was reduced by CPA (n=51) when compared to control (n=127) (Mann-Whitney Rank Sum Test: p*= 0.018). **(C)** Comparison of the background-subtracted average baseline fluorescence of retinal neurons that were loaded with Fluo-4. Each dot represents the baseline fluorescence of one cell. The box covers the central 50% of the data. The dashed lines indicate the mean (Baseline1: 16398.7±2421.3; Baseline2: 19573.3±2753.5; ±95% CI) and the whiskers above and below the box the 95th and 5th percentiles, respectively. Neurons of the increase type did not show significantly different baseline fluorescence levels under control conditions and in the presence of CPA (n=51; Mann-Whitney Rank Sum Test: p= 0.089).

In agreement with the blockade of SERCA, CPA triggered a strong increase in Fluo-4 fluorescence that slowly decayed over time. The responses of two cells of the increase type treated with this protocol are shown in fig. 3.3.13 A. In a group of cells of the increase type the increase in $[Ca^{2+}]_i$ was not blocked by CPA (Fig. 3.3.13 A, top) while in the other group blockade of SERCA reduced the response to DA (Fig. 3.3.12 A, bottom). Statistical analysis revealed that the group of CPA-treated cells (n=51) differed from control (Mann-Whitney Rank Sum Test: p*=0.018). In addition, the number of cells

belonging to the "≥54" group after application of CPA was reduced when compared to control (Table 3.3.1). However, this reduction in DA2/DA1 in the presence of CPA was not as pronounced as found during *e.g.* blockade of L-type CaChs with nimodipine (3.3.3.2). If one inspects the traces of the cell shown in fig. 3.3.13 A, one might interpret this reduction in DA2/DA1 in the presence of CPA as follows: as $[Ca^{2+}]_i$ before the second DA stimulation was higher than $[Ca^{2+}]_i$ before the first DA application, the driving force for Ca^{2+}-influx was lower than before CPA application. However, it was found that there was no significant difference (Fig. 3.3.13 C; Mann-Whitney Rank Sum Test: p= 0.089) between the two fluorescence baseline levels rejecting this hypothesis.

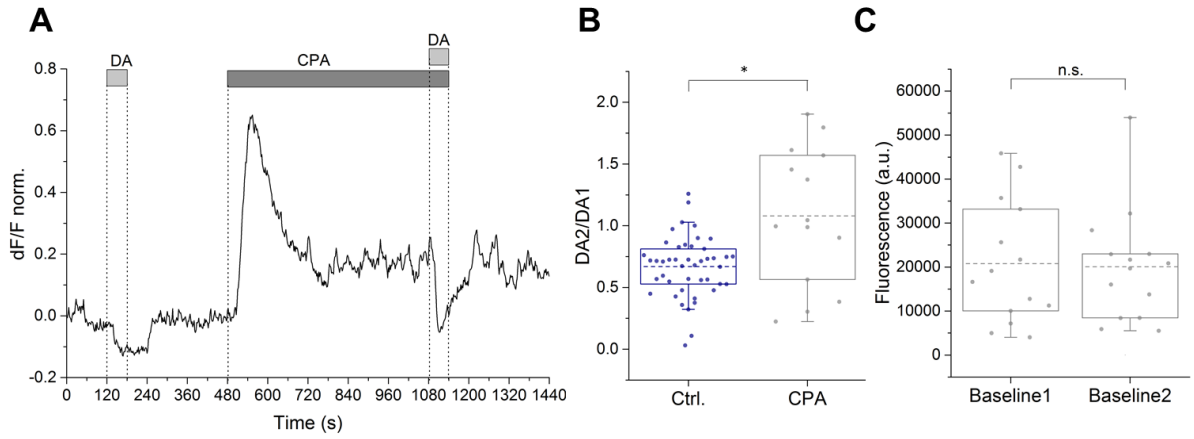

Fig. 3.3.14: Store depletion by CPA affected the DA-triggered decease in $[Ca^{2+}]_i$. Retinal dissociated neurons were loaded with Fluo-4 and stimulated twice with 5 µM DA once in the presence and once in the absence of 5 µM of the SERCA inhibitor CPA. **(A)** Time resolved responses of one neuron of the decrease type. **(B)** The amplitudes of both DA-induced responses were set in relation to each other (DA2/DA1) and data were plotted as box plot. Each dot represents DA2/DA1 of one cell. The box covers the central 50% of the data. The dashed lines indicate the mean (Ctrl.: 0.67±0.07; CPA: 1.08±0.3; ±95% CI) and the whiskers above and below the box the 95th and 5th percentiles, respectively. The response of cells of the decrease type was enhanced in the presence of CPA (n=14) when compared to control (n=45) (Mann-Whitney Rank Sum Test: p*≤0.011). **(C)** Comparison of the background-subtracted average baseline fluorescence of retinal neurons that were loaded with Fluo-4. Each dot represents the baseline fluorescence level of one cell. The box covers the central 50% of the data. The dashed lines indicate the mean (Baseline1: 20776.9±8038.9; Baseline2: 20053.6±7381.7; ±95% CI) and the whiskers above and below the box the 95th and 5th percentiles, respectively. Neurons of the decrease type did not show significantly different baseline fluorescence levels under control conditions and in the presence of CPA (n=14; t-test p=0.887).

In cells of the decrease type CPA did not block the DA-induced decrease in $[Ca^{2+}]_i$ (Fig. 3.3.14 A) but rather enhanced it (Fig. 3.3.14 B; Mann-Whitney Rank Sum Test: p*≤0.011). The number of neurons that could be assigned to the "≥0.67" group was higher in the group of CPA-treated neurons (71%) than in the control group (58%) (Table 3.3.1). Again, the CPA-induced increase in $[Ca^{2+}]_i$ might have an impact on the response to DA: elevated $[Ca^{2+}]_i$ before the second DA stimulation might enhance the driving force for extrusion of Ca^{2+} from the cytoplasm. However, comparison and statistical analysis of the baseline fluorescence levels before the two DA applications

revealed that there was no significant difference (Fig. 3.3.14 C; t-test p=0.887) which rejects this hypothesis.

In summary, these findings suggest that the DA-induced decrease in $[Ca^{2+}]_i$ is not due to a sequestration of Ca^{2+}-ions into the ER because blockade of SERCA by CPA did not abolish but rather enhanced the DA-induced decrease in $[Ca^{2+}]_i$. The reduction of DA2/DA1 in cells of the increase type during blockade of SERCA may indicate that the DA-induced increase in $[Ca^{2+}]_i$ is not only due to the modulation of CaChs but also partly mediated by a release of Ca^{2+}-ions from the ER in some cells of the increase type.

3.3.4.2. The role of phospholipase C

In the previous chapter I have demonstrated that a DA-induced release of Ca^{2+} from the ER might contribute to the increase of $[Ca^{2+}]_i$ in a group of cells of the increase type. As a release of Ca^{2+} from internal stores can be induced by the activation of PLC, I applied the PLC-specific antagonist U73122 (5-10 µM; Sakaki *et al.*, 1996; Contín *et al.*, 2010) to investigate the role of PLC in the generation of DA-induced changes in $[Ca^{2+}]_i$. Retinal neurons were stimulated according to the protocol used in 3.3.2.1.

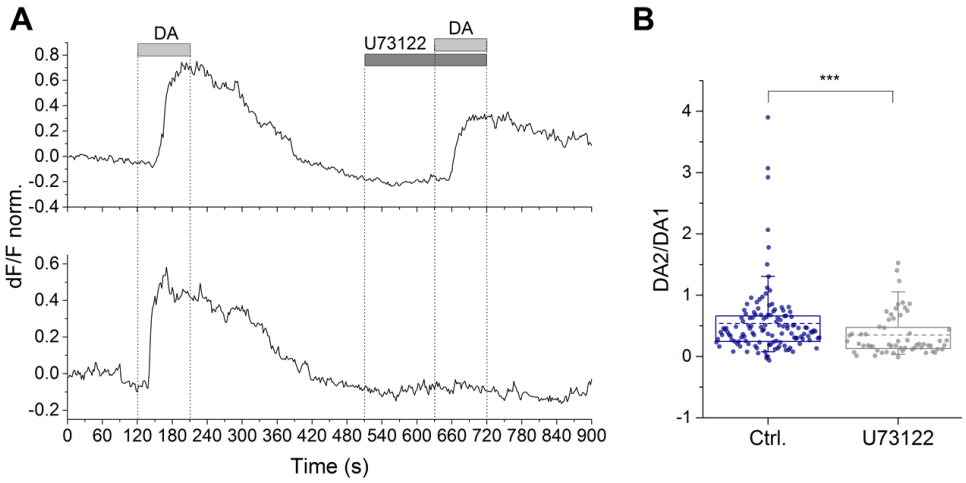

Fig. 3.3.15: Effects of U73122 on DA-induced changes in $[Ca^{2+}]_i$ in cells of the increase type. Retinal dissociated neurons were loaded with Fluo-4 and stimulated with 5 µM DA in the absence as well as in the presence of the PLC inhibitor U73122 (5-10 µM). **(A)** Time resolved responses of two neurons of the increase type. **(B)** The amplitudes of both DA-induced responses were set in relation to each other (DA2/DA1) and data were plotted as box plot. Each dot represents DA2/DA1 of one cell. The box covers the central 50% of the data. The dashed lines indicate the mean (Ctrl.: 0.54±0.1; U73122: 0.35±0.09; ±95% CI) and the whiskers above and below the box the 95th and 5th percentiles, respectively. The response of cells of the increase type was reduced by U73122 (n=60) when compared to control (n=127) (Mann-Whitney Rank Sum Test: p***≤0.001).

Cells of the increase type (n=60) exhibited two different types of DA-induced responses in the presence of U73122. In one group of cells blockade of PLC with U73122 did not affect the DA-induced increase in $[Ca^{2+}]_i$ (Fig. 3.3.15 A, top), while in the other group of cells inhibition of PLC reduced the Ca^{2+}-response to DA (Fig. 3.3.15 A, bottom). The DA-

induced Ca^{2+}-responses in cells treated with U73122 differed from control (Fig. 3.3.15 B; Mann-Whitney Rank Sum Test: p***≤0.001). From the U73122-treated neurons 23% still belonged to the "≥0.54" group (Table 3.3.1). These results supported the assumptions made in 3.3.2.3 and 3.3.3.1: it appears as if alternative pathways are involved in DA-induced increases in $[Ca^{2+}]_i$ in different retinal cultured neurons. One of these alternative pathways might be associated with the activation of the PLC-cascade and the release of Ca^{2+} from internal stores.

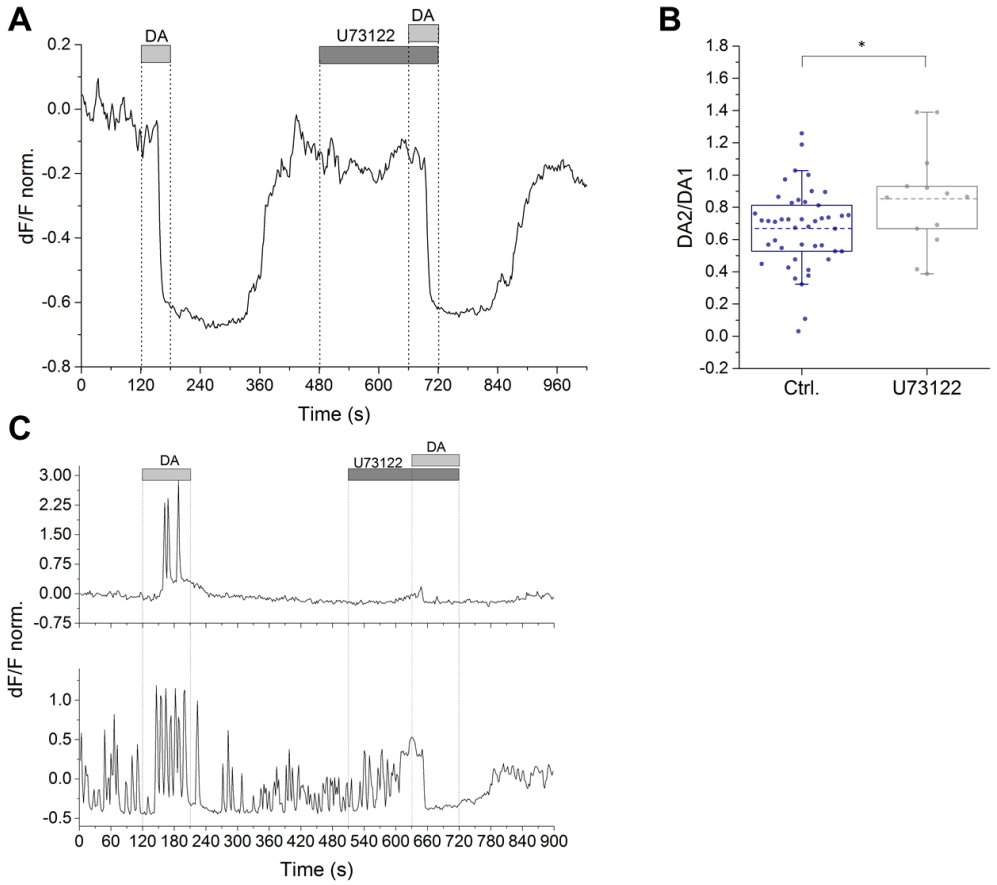

Fig. 3.3.16: Effects of U73122 on DA-induced changes in $[Ca^{2+}]_i$ in cells of the decrease type and cells of the oscillating increase type. Retinal dissociated neurons were loaded with Fluo-4 and stimulated with 5 µM DA in the absence as well as in the presence of the PLC inhibitor U73122 (5-10 µM). **(A)** Time resolved response of one neuron of the decrease type. **(B)** The amplitudes of both DA-induced responses were set in relation to each other (DA2/DA1) and data were plotted as box plot. Each dot represents DA2/DA1 of one cell. The box covers the central 50% of the data. The dashed lines indicate the mean (Ctrl.: 0.67±0.07; U73122: 0.85±0.2; ±95% CI) and the whiskers above and below the box the 95th and 5th percentiles, respectively. The DA-induced response of cells of the decrease type was enhanced by U73122 (n=13) when compared to control (n=45) (t-test: p*=0.03). **(C)** Time resolved response of two neurons responding with an oscillating increase (top) or an enhancement of Ca^{2+}-oscillations (bottom).

The DA-induced decline in $[Ca^{2+}]_i$ in cells of the decrease type was not abolished during blockade of PLC (Fig. 3.3.16 A) but rather enhanced (Fig. 3.3.16 B; t-test: p*=0.03). Interestingly, cultures used for these experiments exhibited a significant number of cells that reacted with Ca^{2+}-oscillations upon stimulation with DA (Fig. 3.3.16 C, top) and cells

displaying spontaneous fluctuations in $[Ca^{2+}]_i$ that were enhanced by DA (Fig. 3.3.16 C, bottom). Blockade of PLC prevented the generation of these oscillations (Fig. 3.3.16 C) and in some cells favored a DA-induced decrease in $[Ca^{2+}]_i$ (Fig. 3.3.16 C, bottom). These findings did not fully dissect the underlying pathways of DR-downstream signaling, but they suggest that PLC is an important mediator in retinal neurons in culture. In summary, it appears that DA does not act via a unique and restrictive pathway. Rather the orchestration of multiple interwoven DA-driven signaling pathways seems to control $[Ca^{2+}]_i$ in cultured retinal neurons. At least two signaling pathways seem to be involved in DA-induced changes in $[Ca^{2+}]_i$: the classical DR/PKA-pathway and another pathway involving PLC and release of Ca^{2+} from internal stores.

Table 3.3.1: Summary of the pharmacological investigation of DA-induced changes in $[Ca^{2+}]_i$.

Substance	Specificity	Increase type			Decrease type		
		Mean DA2/DA1 ± 95% CI	n	DA2/DA1 ≥0.54	Mean DA2/DA1± 95% CI	n	DA2/DA1 ≥0.67
DA	DR agonist	0.54±0.1	127	34%	0.67±0.07	45	58%
SCH23390	D1R antagonist	0.23±0.09	45	13%	0.87±0.26	17	47%
Eticlopride	D2R antagonist	0.49±0.06	109	40%	0.56±0.32	8	50%
w/o Ca	-	0.04±0.02	36	0%	n.a.	6	n.a.
Nimodipine	L-type CaCh antagonist	0.07±0.03	85	2%	n.a.	21	n.a.
ω-conotoxin GVIA	N-type CaCh antagonist	0.4±0.07	196	21%	0.6±0.08	42	33%
H89	PKA inhibitor	0.1±0.03	87	2%	n.a.	22	n.a.
Calyculin A	PP1/PP2A inhibitor	0.42±0.12	76	28%	0.77±0.12	27	63%
Gallein	Gβγ inhibitor	0.59±0.06	84	58%	0.67±0.14	26	50%
CPA	SERCA inhibitor	0.41±0.1	51	18%	1.08±0.3	14	71%
U73122	PLC inhibitor	0.35±0.09	60	23%	0.85±0.2	13	69%

n.a.: not analyzed.

3.4. Investigation of dopaminergic signaling *in vivo*

So far, all investigations were based on single retinal neurons in culture. The results obtained in the previous chapters have demonstrated that the primary retinal culture is

a well suited model system for the examination of D1R downstream signaling that involves changes in $[cAMP]_i$ (3.2.2.1), PKA activity (3.2.2.1) and $[Ca^{2+}]_i$ (3.3). The final aim of the study was to investigate these DA-induced signaling pathways in the intact retinal network in order to contribute to a better understanding of DA's role in complex processes like light-adaptation. Here, I will present my results from experiments conducted to investigate dopaminergic signaling in the intact retina.

3.4.1. Towards the visualization of DA release

Cell type-specific promoters can be used to restrict expression of proteins to specific cell populations. In the murine retina there is only one cell type that produces and releases DA and can be identified due to the expression of the enzyme tyrosine hydroxylase (TH) (Versaux-Botteri *et al.*, 1984; Nguyen-Legros, 1988).

To visualize the release of DA, I attempted to express the sensor synapto-pHluorin exclusively in dopaminergic ACs. For this purpose, by means of molecular cloning, the construct pcTH-EGFP was generated (2.3.10) in which GFP expression is controlled by the TH promoter. In the following it was tested, whether transfection of HEK293 cells and retinal cultured neurons with pcTH-EGFP would yield cell type-specific expression of GFP and whether synapto-pHluorin would be expressed under the control of this promoter.

3.4.1.1. Does the TH promoter yield cell type-specific expression of GFP?

In order to test for the specificity of these constructs, HEK293 cells were transiently transfected with either pcTH-EGFP or pEGFP-N1. The construct pEGFP-N1 served as control as expression of EGFP is driven by the ubiquitously used cytomegalovirus (CMV) promoter.

Cells that were transfected with the CMV-driven GFP exhibited strong fluorescence (Fig. 3.4.1, top, "endoGFP" for endogenous fluorescence of GFP). Immunocytochemistry with an antibody directed against GFP detected the same cells (Fig. 3.4.1, top, "antiGFP"). Using the same microscopic settings, no GFP-fluorescence was found in cells transfected with pcTH-EGFP (Fig. 3.4.1, bottom, "endoGFP"). Only few cells were found to weakly express GFP under the control of the TH promoter after staining with anti-GFP verifying that the construct is functional (Fig. 3.4.1, bottom, "antiGFP"). Staining with TO-PRO®3 (Fig. 3.4.1, blue), a DNA-intercalator, revealed that significantly more HEK293 cells expressed the CMV-driven GFP than the TH-driven GFP.

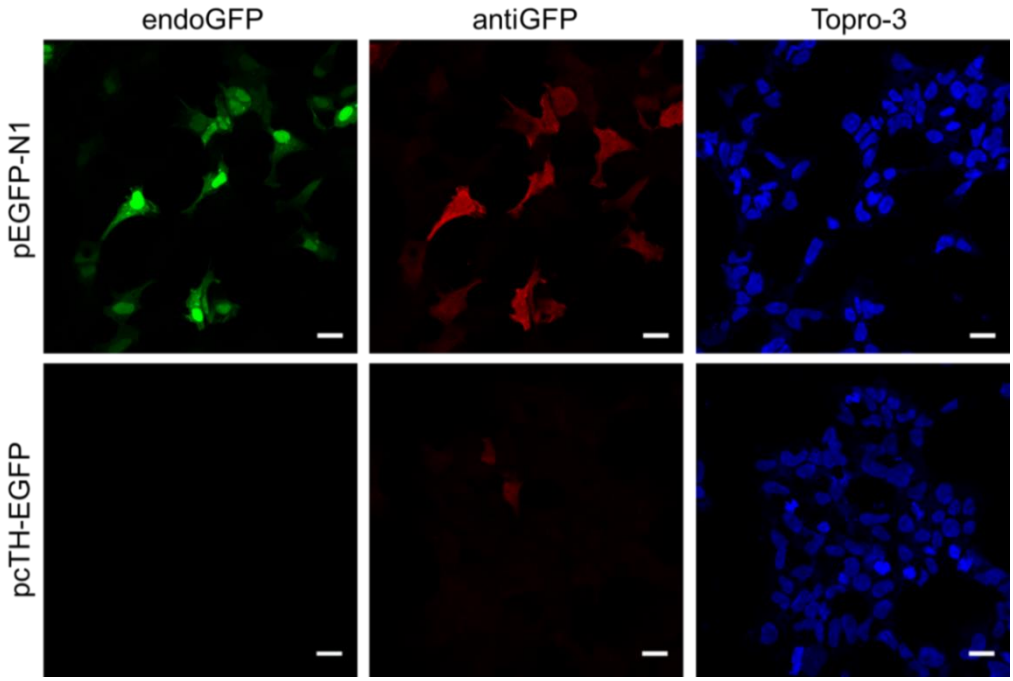

Fig. 3.4.1: The TH promoter did not drive expression of EGFP in HEK293 cells. Confocal pictures of HEK293 cells transiently transfected with cDNA coding for pcTH-EGFP or pEGFP-N1. Expression of pEGFP-N1 served as control. Nuclei were visualized by TO-PRO®3 staining (blue). The endogenous fluorescence of GFP is shown in green, the staining with the GFP-antibody is depicted in red. **(Top)** HEK293 cells expressing pEGFP-N1 which is driven by a CMV promoter. **(Bottom)** HEK293 cells transfected with pcTH-EGFP. Scale bars 20 µm.

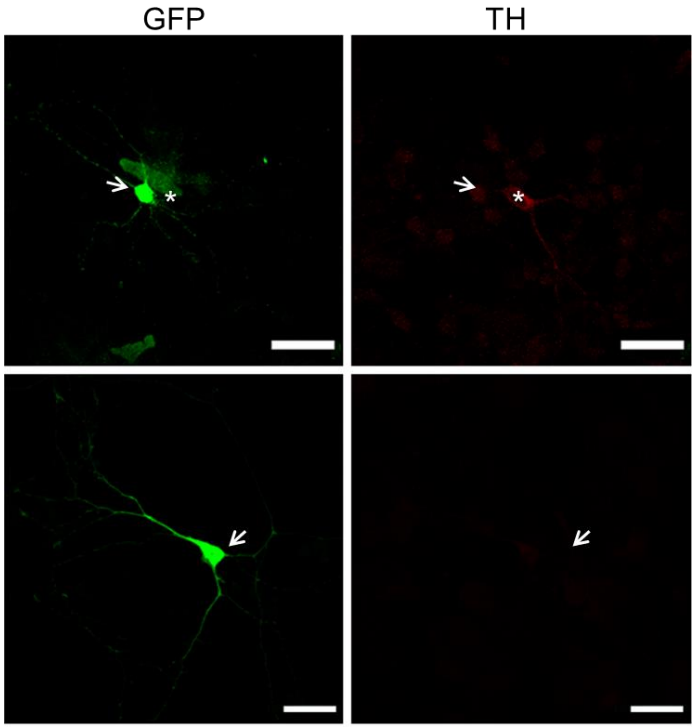

Fig. 3.4.2: TH-positive neurons did not express GFP after transient transfection with pcTH-EGFP. Confocal pictures of retinal cultured neurons transiently transfected with cDNA coding for pcTH-EGFP. Staining with anti-GFP and anti-TH revealed that GFP is expressed in TH-negative neurons. **(Top)** Although the neighboring cell expressed GFP (arrow), the TH-positive neuron did not (asterisk). **(Bottom)** The GFP-positive neuron (arrow) was negative for TH. Scale bars 25 µm.

In order to test for the specificity of the TH promoter in retinal neurons in culture, cells were transiently transfected with pcTH-EGFP using Lipofectamine-transfection. Staining with anti-TH revealed that GFP was expressed in retinal neurons that were negative for TH (Fig. 3.4.2, arrow). Although neighboring cells expressed GFP after transfection with pcTH-EGFP (Fig. 3.4.2, top, arrow) TH-positive neurons did not express GFP (Fig. 3.4.2 top, asterisk). Hence, expression was not as restricted as expected.

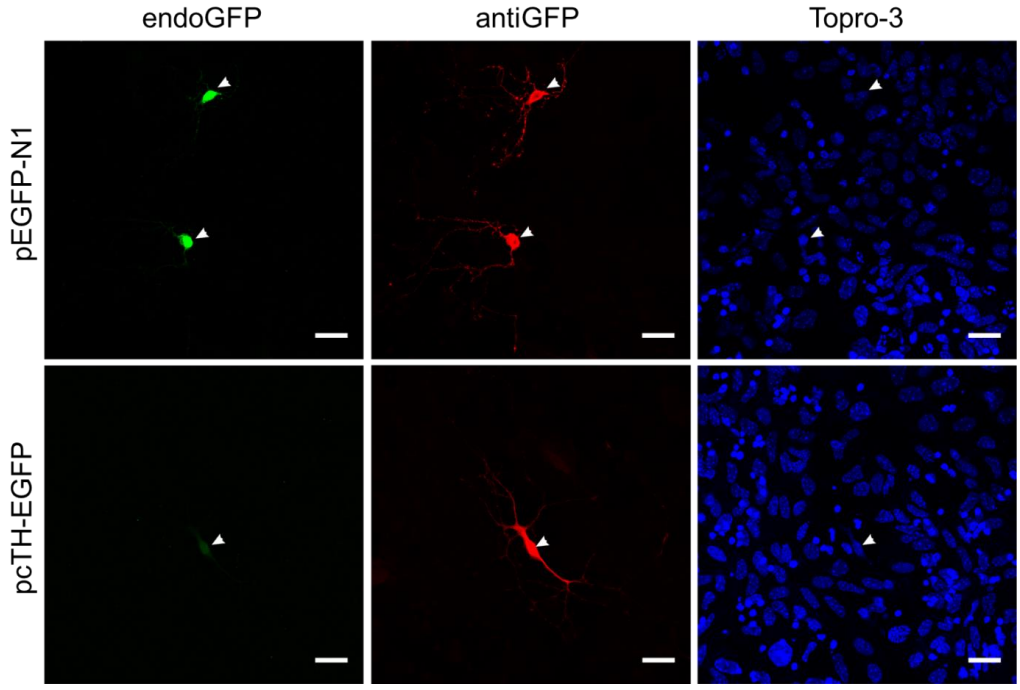

Fig. 3.4.3: EGFP expression under the TH promoter was lower than under the CMV promoter. Confocal pictures of retinal cultured neurons transiently transfected with cDNA coding for pcTH-EGFP or pEGFP-N1. Expression of pEGFP-N1 served as control. Nuclei were visualized by TO-PRO®3 staining (blue). The endogenous fluorescence of GFP is shown in green, the staining with the GFP-antibody is depicted in red. **(Top)** Retinal neurons express pEGFP-N1 which is driven by a CMV promoter (pEGFP-N1). **(Bottom)** Retinal neurons transfected with pcTH-EGFP. Arrowheads indicate the location of the transfected cell. Scale bars 25 µm.

In further experiments I compared the expression pattern of pcTH-EGFP and pEGFP-N1 which again served as control. Two findings rule for a certain specificity of the TH promoter construct: first it was found, that the number of GFP-expressing neurons was lower in cultures transfected with the promoter construct pcTH-EGFP than in cultures transfected with the control construct pEGFP-N1 (data not shown). In cultures that were transfected with pEGFP-N1 a considerable number of glia cells were expressing GFP. This was not the case for cultures transfected with the TH promoter construct. Second, it was found that the GFP fluorescence in cells transfected with the TH-driven EGFP was clearly lower than in neurons transfected with the control construct pEGFP-N1 (Fig. 3.4.3). This is in line with the results described for HEK293 cells (Fig. 3.4.1).

3.4.1.2. The sensor synapto-pHluorin is expressed in retinal neurons

To test whether synapto-pHluorin is suitable to visualize neurotransmitter release from retinal neurons in culture, cells were transiently transfected with cDNA coding for a CMV promoter-driven synapto-pHluorin (p156rrlSybIIpHluorin; 2.4.2.5). This construct was used because the number of p156rrlSybIIpHluorin-transfected neurons was higher than the number of pcTH-SynpH-expressing neurons. Fluorescence was found throughout the cell but puncta of higher fluorescence intensity were regularly observed. Neurons were depolarized by superfusion with a high potassium concentration (20 mM). Puncta were defined as ROIs (Fig. 3.4.4 A). Depolarization induced an increase in fluorescence in all three puncta in accordance with release of vesicles (Fig. 3.4.4 B). The amplitudes and kinetics of the responses differed between different puncta. This may be due to the properties of the synapse, the number of vesicles released and the number of synapto-pHluorin-molecules incorporated into the vesicle membrane.

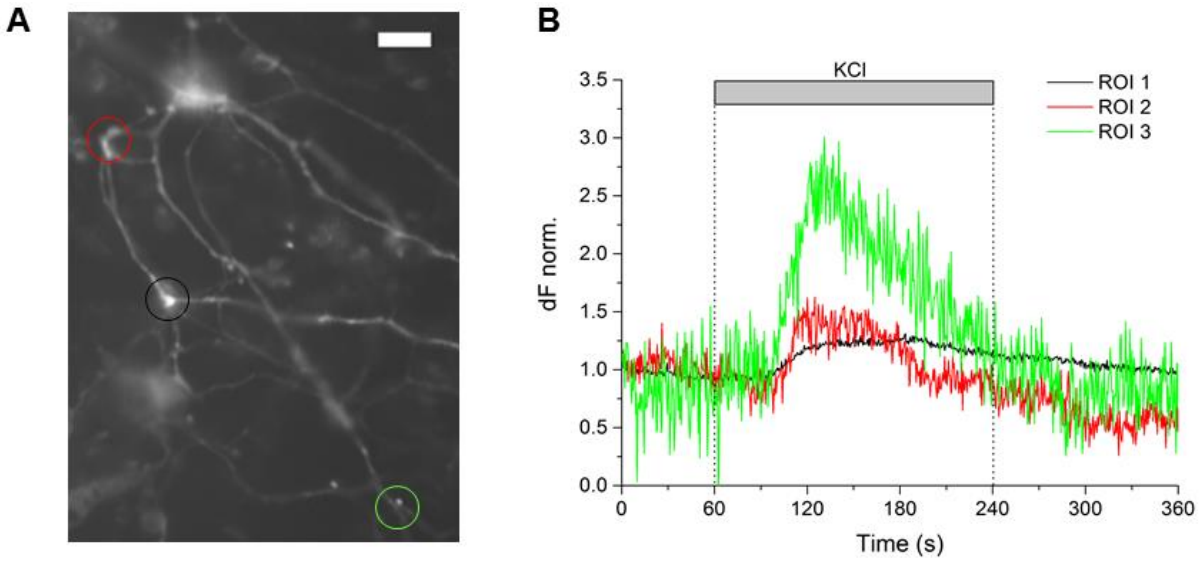

Fig. 3.4.4: Synapto-pHluorin fluorescence in puncta (ROIs) increased upon depolarization. (A) Wide-field image of a neuron expressing synapto-pHluorin after Lipofectamine-transfection with p156rrlSybIIpHluorin. Three different ROIs (black=ROI1; red=ROI2 and green=ROI3) were defined. Scale bar 10 µm. **(B)** Change in synapto-pHluorin fluorescence at three ROIs to stimulation with 20 mM KCl.

In order to test whether the sensor synapto-pHluorin is expressed in retinal neurons under the control of the TH promoter, cells were transiently transfected with cDNA coding for synapto-pHluorin (pcTH-SynpH) or EGFP (pcTH-EGFP) driven by the TH promoter. Synapto-pHluorin fluorescence was found in puncta in the soma as well as in the fine processes (Fig. 3.4.5, arrowheads). From immunocytochemical analysis with synaptic markers it is assumed that the synapto-pHluorin-positive puncta are located at synapses (Lange, 2015). This was different from the expression of pcTH-EGFP which

was found throughout the soma and more evenly distributed in the processes (Fig. 3.4.5, arrow).

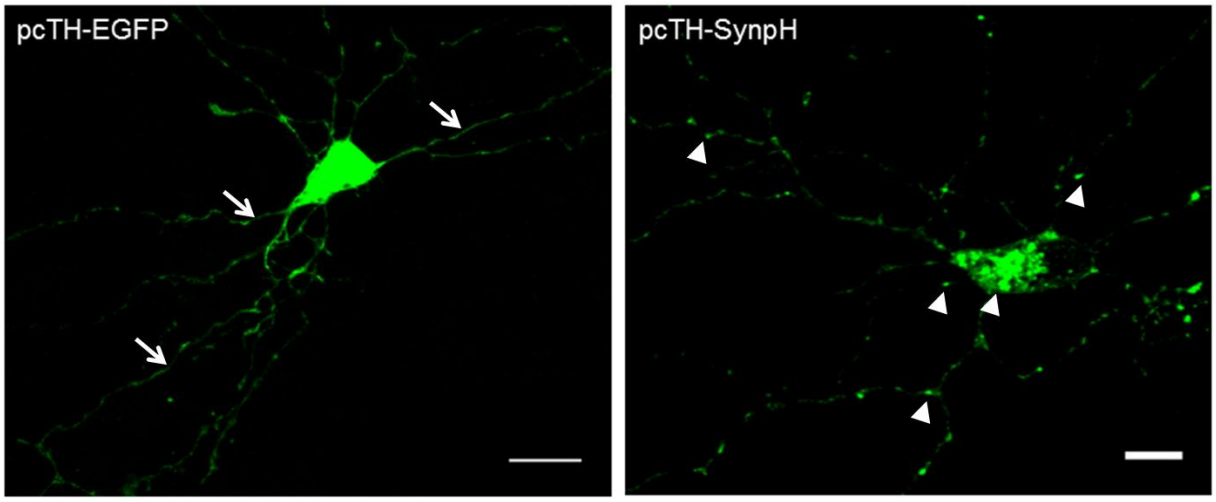

Fig. 3.4.5: Synapto-pHluorin was expressed at puncta in retinal dissociated neurons. Confocal pictures of cultured retinal neurons transiently transfected with cDNA coding for EGFP (left) or synapto-pHluorin (right). Cells were stained with anti-GFP. The expression of both proteins was controlled by the TH promoter. Synapto-pHluorin fluorescence was found in puncta in the soma as well as in the fine processes (arrowheads) while pcTH-EGFP expression was found throughout the soma and more evenly distributed in the processes (arrows). Scale bars 10 µm (pcTH-EGFP) and 5 µm (pcTH-SynpH).

In summary, it was found that the TH promoter did not restrict GFP expression exclusively to TH-positive neurons. However, there was a difference in the expression pattern of the CMV-driven GFP and the TH-driven GFP. In addition, I could show that the synapto-pHluorin sensor is suitable to visualize transmitter release from retinal neurons. The next step would be to test the specificity of the TH-driven constructs *in vivo*. To this end, an appropriate method of gene transfer had to be established.

3.4.2. Using AAVs as gene shuttles to express sensor proteins

To monitor DA-induced signaling in the intact retina, the genetically encoded biosensors had to be expressed. As transfection with *e.g.* Lipofectamine is not applicable for expression *in vivo*, adeno-associated viruses were planned to serve as gene-shuttles. In previous studies we found that AAV serotype 2 (AAV2) was best suited for transduction of retinal neurons both *in vitro* and *in vivo* (own observations; see also Zhao, 2015). This chapter focuses on two main questions: Are target cells for dopaminergic signaling transduced by AAV2 and are FRET-based sensors properly expressed in retinal neurons after viral transduction *in vivo*?

3.4.2.1. AAV2-GFP infects target neurons of dopaminergic signaling in culture

Retinal dissociated neurons were transduced with 1×10^9 vp per well of AAV2-GFP on DIV2. Cultures were fixed on DIV8 and stained with anti-GFP and different other primary antibodies identifying specific cell types in the culture. AAV2-GFP infected different types of neurons which were distinguishable due to their soma size and their morphology (Fig. 3.4.6, GFP). GFP expression was found in cells with large somata and in smaller cells. The expression level of GFP was heterogeneous: there were bright fluorescent cells as well as less fluorescent cells. GFP expression was found throughout the cell including cytoplasm, nucleus and fine processes.

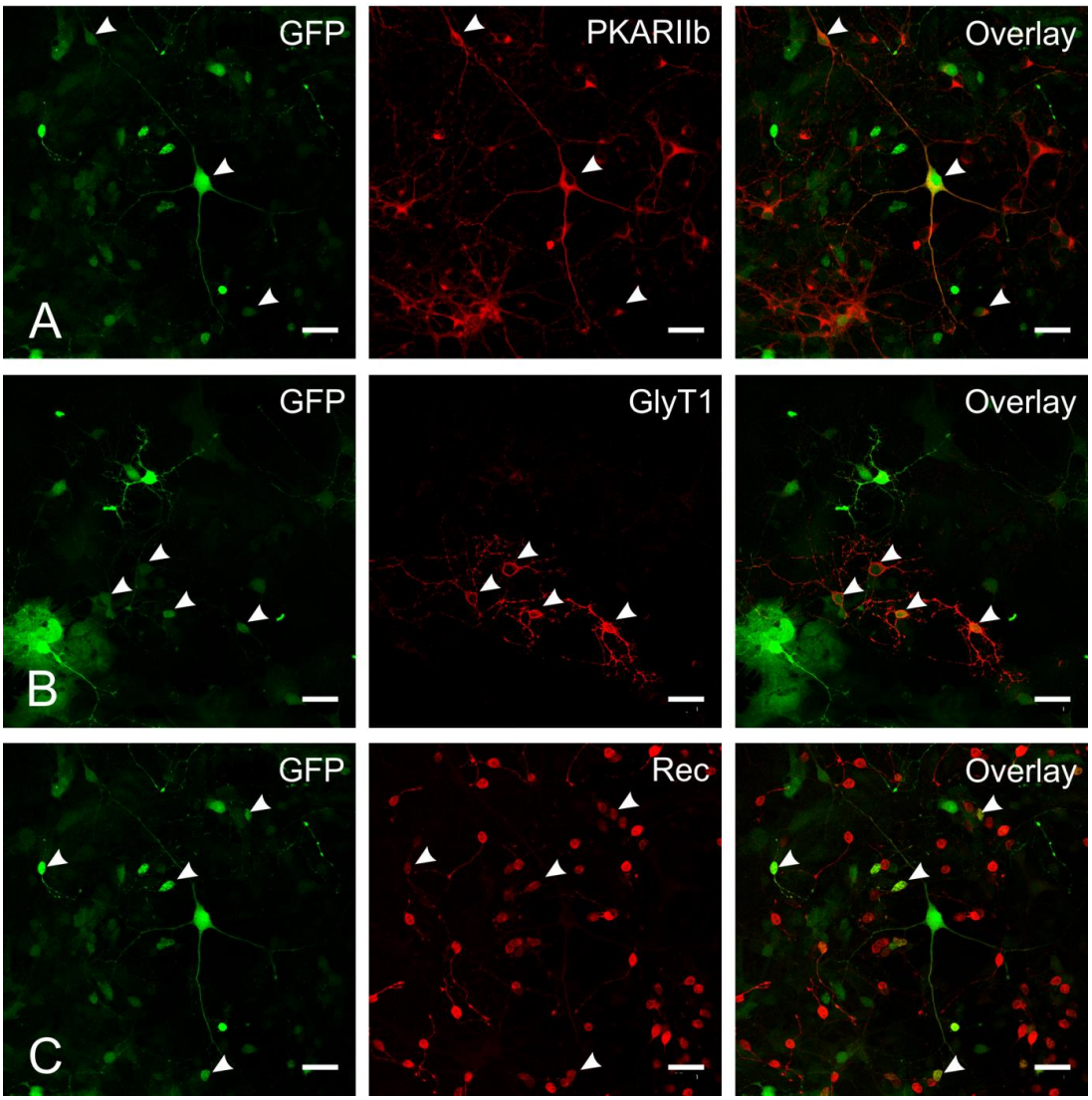

Fig. 3.4.6: AAV2-GFP infected a variety of retinal neurons in culture. Retinal dissociated neurons were transduced with AAV2-GFP on DIV2. After fixation on DIV10, cells were stained with anti-GFP (green) and **(A)** anti-PKARIIβ (ms; red), **(B)** anti-GlyT1 (red) and **(C)** anti-Recoverin (Rec, red). Pictures in A and C were obtained from a triple staining. Arrowheads indicate AAV2-GFP infected cells that are immunoreactive for PKARIIβ (A), GlyT1 (B) or Rec (C). Scale bar 25 µm.

It has been shown in chapter 3.1 that in retinal dissociated culture most D1R-positive neurons are also positive for PKARIIβ. Thus, PKA-positive neurons, namely type 3b BCs and ACs (Mataruga *et al.*, 2007), are of great interest regarding their modulation through DA. For that reason, it was investigated whether AAV2 infects PKARIIβ-positive neurons in retinal dissociated cultures. PKARIIβ immunoreactivity was found in the cytoplasm and the processes but not in the nucleus of retinal neurons in culture (3.4.6 A, red). The overlay of anti-GFP and anti-PKARIIβ revealed that some PKARIIβ-positive neurons were infected by AAV2-GFP (Fig. 3.4.6 A, arrowhead). AII ACs were found to be modulated by DA (Hampson *et al.*, 1992). It is known that AII ACs are glycinergic cells and, hence can be immunochemically labelled by an antibody directed against glycine transporter 1 (GlyT1; Haverkamp and Wässle, 2000). Some glycinergic neurons were infected by AAV2-GFP (Fig. 3.4.6 B, arrowhead). These GlyT1/GFP-positive cells exhibited weaker GFP expression than other infected cells. A third group of neurons known to be influenced by DA are PR cells (Cohen *et al.*, 1992). Some of the GFP-positive neurons were found to be immunoreactive for recoverin (Fig. 3.4.6 C, arrowhead) indicating that PRs are possible targets for AAV2-GFP.

In conclusion, AAV2-GFP infected a variety of different types of retinal neurons in culture including putative target cells for dopaminergic modulation. Thus, AAV serotype 2 meets all the requirements for the application *in vivo*.

3.4.2.2. AAV2-GFP infects target neurons of dopaminergic signaling *in vivo*

As it was shown that AAV2-GFP is well suited to infect those cell types whose activity may be influenced by DA *in vitro*, the same virus was used for *in vivo* expression. Eyes of mice were injected with AAV2-GFP at P5-7. One to two weeks after injection, retinae were fixed and analyzed immunohistochemically.

In order to test whether AAV2-GFP successfully infects neurons *in vivo*, intact retinae of injected mice were immunohistochemically stained with anti-GFP. The retina of the injected eye showed bright green fluorescence indicating successful infection with AAV2-GFP (Fig. 3.4.7 A). The close-up revealed that plenty of somata and fine processes were positive for GFP. In some regions of the retina the number of infected neurons was high whereas in other regions only few GFP-positive neurons were found (Fig. 3.4.7 A). This phenomenon has already been observed in previous studies (own observations; see also Zhao, 2015). The region of high GFP expression is most likely the region where the virus suspension was injected and thus viruses were highly concentrated. In comparison

to that, no green fluorescence was found in the contralateral control eye which had not been injected (Fig. 3.4.7 B and B1).

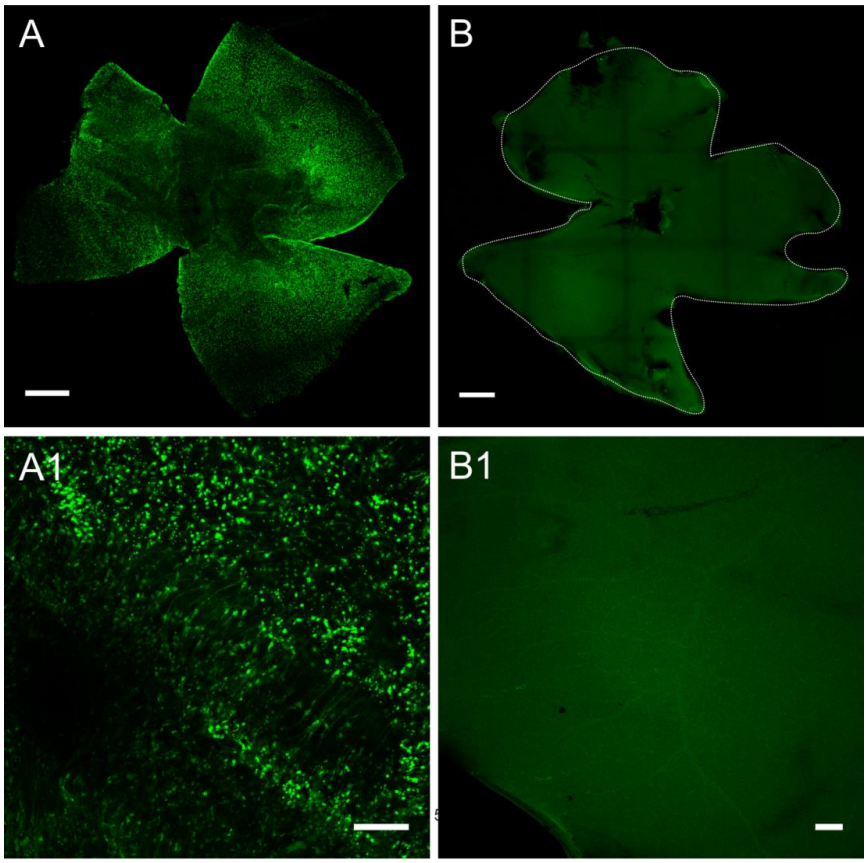

Fig. 3.4.7: Retinae of AAV2-GFP injected eyes expressed GFP. Confocal images from two wholemounted retinae stained with anti-GFP. **(A)** Retina of the injected eye. Many green-fluorescent areas could be observed. Scale bar 500 µm. **(A1)** Zoom from A. GFP was expressed in somata and fine processes. Scale bar 100 µm. **(B)** Retina of the control eye. No fluorescent areas and cells were found. Scale bar 500 µm. **(B1)** Zoom from B. Scale bar 100 µm.

In order to identify neurons that were infected by AAV2-GFP *in vivo*, retinae were cut into 18 µm thick vertical cryosections and stained with cell type-specific antibodies. Figure 3 shows such a vertical cyrosection of an AAV2-GFP injected retina (Fig. 3.4.8). Different types of cells characterized by their location and morphology were infected by the virus (Fig. 3.4.8, GFP): Müller cells that are spanning through the whole thickness of the retina (a), BCs (b), GCs (c), HCs (d) and many ACs (arrowheads and asterisks). Staining with anti-Glycine (Fig. 3.4.8, red) revealed that AAV2-GFP successfully infected glycinergic ACs (Fig. 3.4.8, overlay, arrowhead). Some of the glycine/GFP-positive cells could be identified as AII ACs (Fig. 3.4.8, arrowhead) due to the morphology of their dendritic tree that was composed of multi-branched, beaded and appendage-bearing dendrites as it had been described to be characteristic for AII ACs in the mammalian retina (Kolb, 1997). AAV2-GFP did not infect all glycine-positive ACs (Fig. 3.4.8, arrow) but infected other types of ACs (Fig. 3.4.8, asterisk).

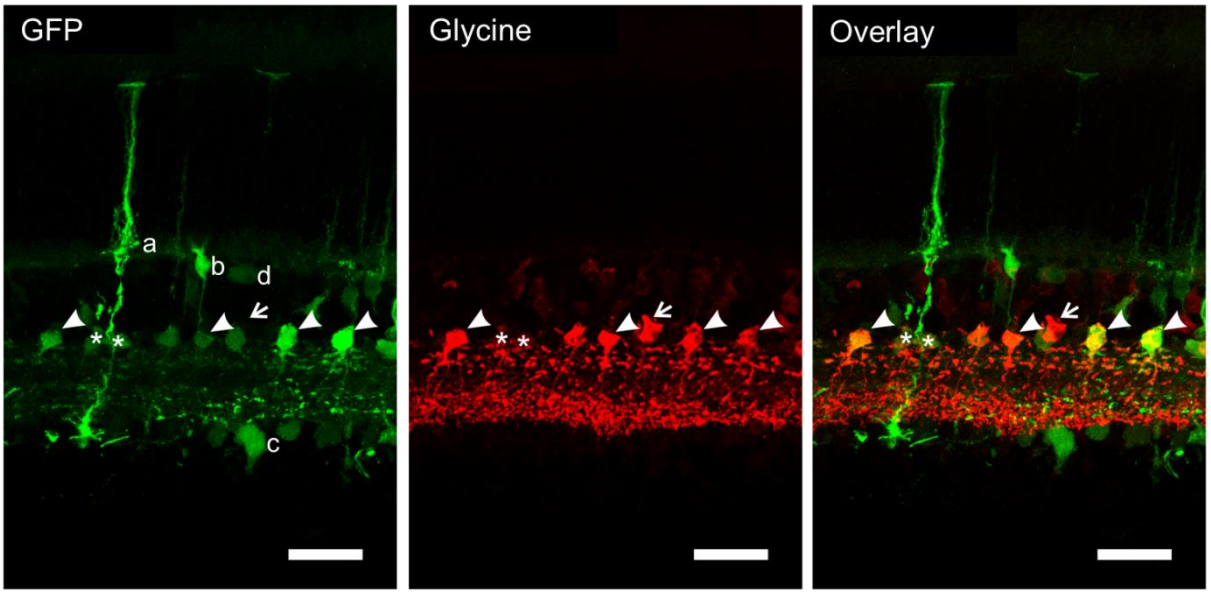

Fig. 3.4.8: AAV2-GFP infected a variety of retinal neurons including glycinergic ACs. Confocal pictures of cryosections from AAV2-GFP injected retinae. GFP fluorescence was strong enough to be detected without staining by an antibody. Glycinergic ACs were labeled with anti-Glycine (red). GFP expression was found in almost all retinal cell classes: a) Müller cell b) BC c) GC d) HC. Some glycinergic ACs, most likely AII ACs, were infected by AAV2-GFP (arrowhead). Other glycinergic ACs were negative for GFP (arrow) while other glycine-negative ACs had been infected (asterisk). Scale bar 25 µm.

As it was already mentioned in chapter 3.1, the coupling between PRs is modulated by DA most likely through D4Rs. Thus, one goal was to express the FRET-based sensors EPAC1-camps or AKAR4 in PR cells. In order to investigate whether AAV2 is suitable to infect PR cells in the intact retinal tissue, vertical sections of AAV2-GFP injected retinae were stained with anti-Recoverin. AAV2-GFP infected some PR cells in mouse retina (Fig. 3.4.9). GFP fluorescence was found in the somata of PR cells (Fig. 3.4.9, asterisk), the inner and outer segments (Fig. 3.4.9, arrowhead) and the synaptic endfeet (Fig. 3.4.9, arrow).

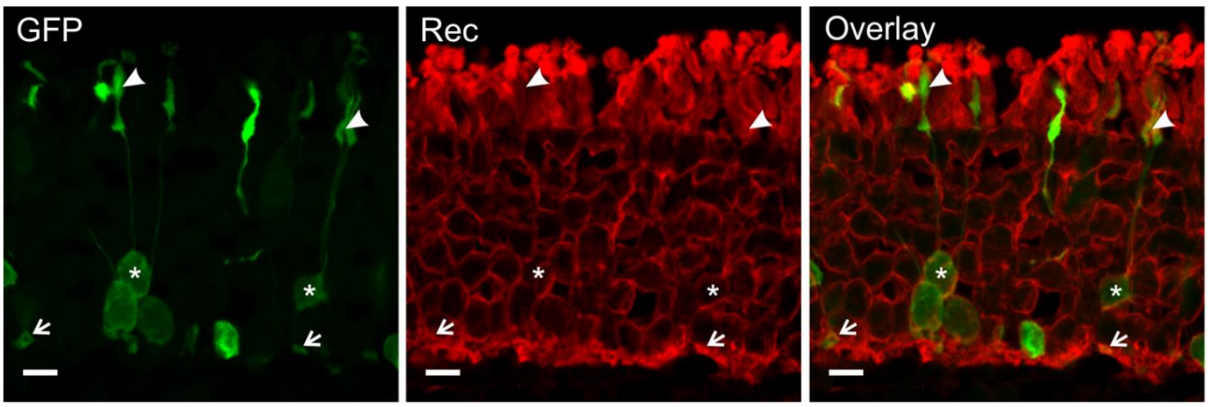

Fig. 3.4.9: AAV2-GFP transduced PRs *in vivo*. Confocal pictures of the PR layer in a cryosection from an AAV2-GFP injected retina. GFP fluorescence was strong enough to be detected without staining by an antibody. PR cells were labeled with anti-Recoverin (Rec, K2; red). GFP fluorescence was found in the somata of PR cells (asterisk), the inner and outer segments (arrowhead) and the synaptic endfeet (arrow). Scale bar 5 µm.

In summary, AAV2 infected retinal neurons whose activity had been shown to be modulated by DA (*e.g.* AII ACs, PRs) not only *in vitro* but also *in vivo*. This founds the basis for the viral expression of EPAC1-camps and AKAR4 in retinal neurons.

3.4.2.3. Does AAV2 infect dopaminergic neurons *in vivo*?

A precondition for the expression of the synapto-pHluorin in dopaminergic ACs in the retina *in vivo* is that AAV2 infects TH-positive ACs. It has already been shown that AAV2-GFP is capable of infecting neurons in the AC layer of the INL (Fig. 3.4.8). To find out whether dopaminergic ACs are amongst the infected cells, injected retinae were fixed and stained with antibodies directed against GFP and TH. Many different cells, located at the border between INL and IPL, were infected by AAV2-GFP (Fig. 3.4.10, green). TH-positive ACs were found in the same retinal layer (Fig. 3.4.10, red). A colocalization between anti-GFP and anti-TH was not found in any of the immunohistochemically analyzed retinae (n_{retina}=7; n_{THcell}=19; always surrounded by other GFP-expressing ACs) as demonstrated in the overlay pictures in fig. 3.4.10. Thus, viral gene transfer via AAV2-GFP seemed not to be the tool of choice for the expression of synapto-pHluorin in dopaminergic ACs in the intact retina.

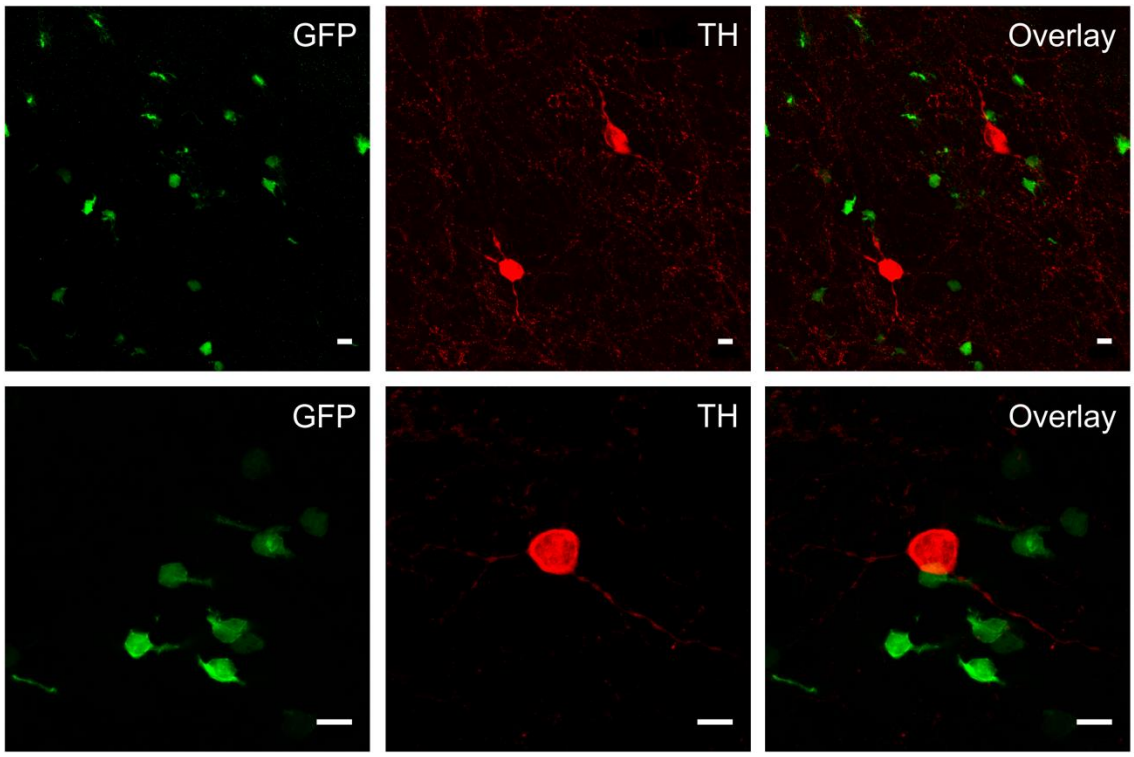

Fig. 3.4.10: AAV2-GFP did not infect dopaminergic ACs. Maximal projections of stacks of confocal pictures made at the border of INL and IPL in wholemounts of AAV2-GFP injected retinae. Endogenous fluorescence of the GFP indicator was enhanced by anti-GFP (green). Dopaminergic ACs were labeled with the anti-TH (red). **(Top)** Stack of 9 focal planes. **(Bottom)** Stack of 6 focal planes at higher magnification. Although neighboring cells were infected by AAV2-GFP, none of the TH-positive ACs expressed GFP. Scale bars 10 µm.

3.4.3. Viral expression of the FRET-based cAMP sensor EPAC1-camps

In chapters 3.4.2.1 and 3.4.2.2 it has been shown that AAV2 is well suited to transfer sensor-DNA to cell types that are of main interest in the context of dopaminergic signaling in the retina. Thus, in the next subchapters it was investigated whether EPAC1-camps is functionally expressed after viral transduction.

3.4.3.1. AAV2-mediated expression of EPAC1-camps in cultured cells

In a first approach it was tested whether AAV2-EPAC1-camps successfully infected HEK293 cells. To this end, HEK293 cells were transduced with AAV2-EPAC1-camps and used for imaging experiments one week later. As it was shown that HEK293 cells express adrenergic receptors (Sumi *et al.*, 2010; Friedman *et al.*, 2002), norepinephrine (NA) was used to increase $[cAMP]_i$. In order to prevent the immediate degradation of cAMP, phosphodiesterases (PDE) were blocked by 100 µM 3-isobutyl-1-methylxanthine (IBMX).

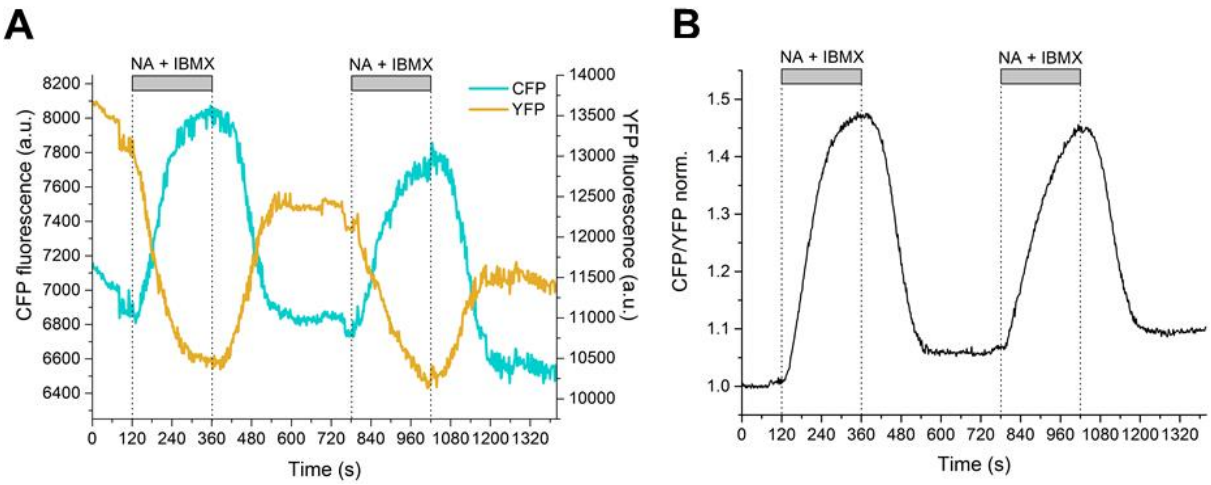

Fig. 3.4.11: EPAC1-camps was functionally expressed in HEK293 cells after infection with AAV2-EPAC1-camps. HEK293 cells were transduced with AAV2-EPAC1-camps. One week later, cells were stimulated twice with 5 µM NA in the presence of 100 µM IBMX for 2 min. HEK293 cells responded with an increase in $[cAMP]_i$. **(A)** The CFP and YFP fluorescence plotted over time. **(B)** The normalized ratio CFP/YFP plotted over time.

HEK293 cells were stimulated twice with 5 µM NA and 100 µM IBMX for 2 min. About 30 s after the stimulus started, a change in fluorescence of the two fluorophores CFP and YFP was observed. The YFP fluorescence decreased whereas the CFP fluorescence mirror-reversely increased (Fig. 3.4.11 A). The change in fluorescence of both fluorophores peaked about 2 min after the stimulus started. While the CFP fluorescence returned to baseline, the YFP fluorescence did not fully recover back to baseline (Fig. 3.4.11 A). The second stimulation revealed that the induced effects were reproducible. It

has to be noted that the YFP showed stronger bleaching effects than CFP (YFP bleaching: 0.14; CFP bleaching: 0.1; Fig. 3.4.11 A). This bleaching effect could cause the incomplete recovery back to baseline (Fig. 3.4.11 B).

As I confirmed that AAV2-EPAC1-camps successfully infected HEK293 cells resulting in the expression of a functional sensor that detects changes in $[cAMP]_i$ upon stimulation with NA, I used the same virus to express EPAC1-camps in retinal neurons in culture. Neurons were infected with virus at DIV2 and further incubated for 7 days in order to provide the neurons with enough time to properly express the sensor. At DIV9, neurons were fixed and confocal pictures of the CFP and YFP fluorescence were taken.

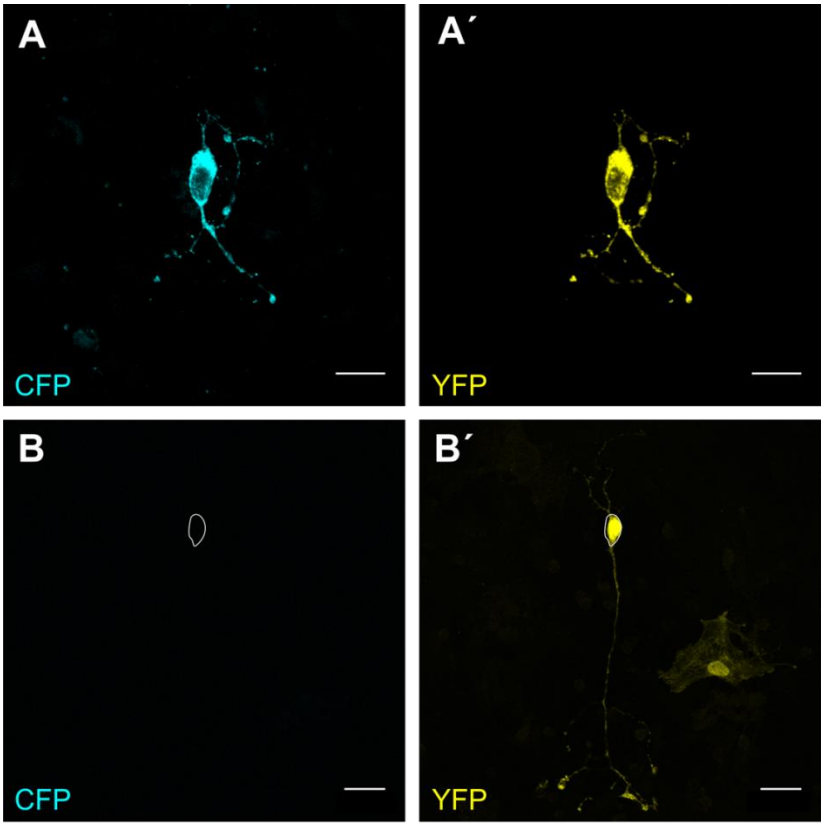

Fig. 3.4.12: Transduction of retinal neurons with AAV2-EPAC1-camps only rarely resulted in proper expression of the EPAC1-camps sensor. Retinal dissociated neurons were transduced with AAV2-EPAC1-camps at DIV2 and further incubated until DIV9. Cells were fixed and analyzed with confocal microscopy. Two groups of infected neurons could be found: **(A, A´)** neurons that exhibited CFP and YFP fluorescence only in the cytoplasm and the processes and **(B, B´)** neurons that displayed YFP fluorescence but no CFP fluorescence in the cytoplasm, processes and in the nucleus. Scale bar 25 µm.

Some of the infected neurons were found to express the sensor exclusively in the cytoplasm and processes but not in the nucleus (Fig. 3.4.12 A and A´). Those neurons exhibited CFP (Fig. 3.4.12 A) as well as YFP fluorescence (Fig. 3.4.12 A´). In addition, there was a second group of infected neurons that displayed YFP fluorescence but lacked CFP fluorescence (Fig. 3.4.12 B and B´). These YFP^+/CFP^- neurons displayed

fluorescence in the cytoplasm, the processes and the nucleus. Two observations led to the conclusion that the expressed protein in the second group of neurons is not expressed properly. First, the protein seemed to lack the CFP domain which could be due to degradation or improper folding of the CFP. The existence of two functional fluorophores is the precondition for an energy transfer in a FRET-based sensor. Second, the protein was found in the nucleus although it did not harbor a nucleus-targeting sequence. This implies that the protein was smaller than the intact sensor protein and thus could enter the nucleus by passive diffusion.

Only those neurons fulfilling both quality criteria, that is to say the expression of both fluorophores and a free nucleus, were used for subsequent imaging experiments. To increase $[cAMP]_i$, retinal neurons were superfused with 40 µM NKH477, a potent activator of adenylyl cyclase (Tatee *et al.*, 1996). In order to prevent immediate degradation of cAMP, PDEs were inhibited with 100 µM IBMX. Only a few EPAC1-camps-expressing neurons responded to stimulation with NKH477 in the presence of IBMX with a change in fluorescence. The response of one neuron, that was judged to be the best response of all, is shown in fig. 3.4.13.

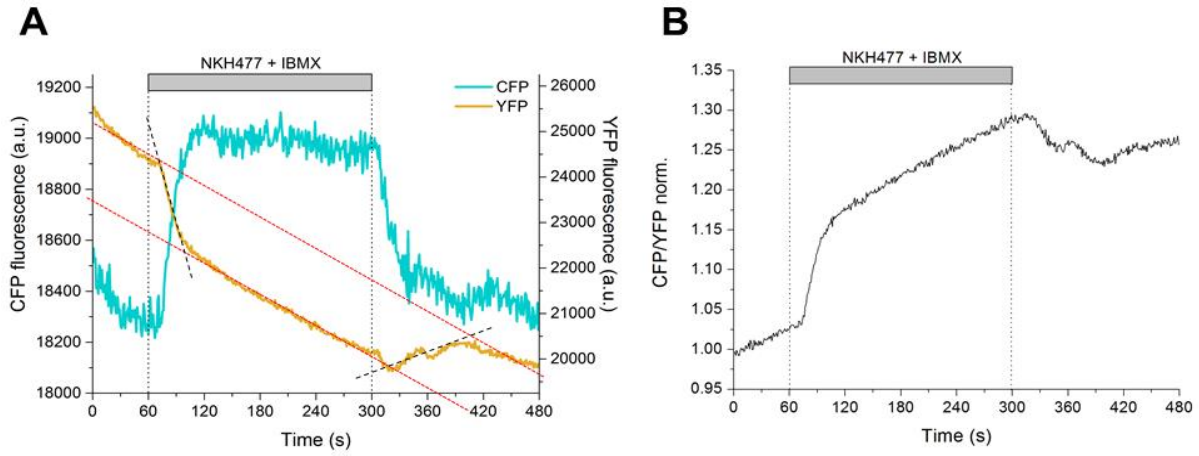

Fig. 3.4.13: A few retinal neurons expressing EPAC1-camps after viral infection responded to stimulation of ACy. The neuron was infected with AAV2-EPAC1-camps on DIV2 and was used for imaging at DIV9. Stimulation of ACy with 40 µM NKH477 in the presence of 100 µM IBMX increased $[cAMP]_i$. **(A)** The CFP and YFP fluorescence plotted over time. **(B)** The normalized ratio CFP/YFP plotted over time.

The CFP fluorescence increased and reached a plateau about 1 min after the stimulus started and recovered back to baseline immediately after stop of the stimulus. The stimulus-induced change in YFP fluorescence is more complex: the two parallel red lines in fig. 3.4.13 (---) demonstrate that YFP fluorescence underwent strong bleaching of about 0.27. If one neglects this bleaching, the stimulus-induced onset of the change in YFP fluorescence (---) reached plateau about 45 s after the stimulus started and began to

recover 0.5 min after the stop of the stimulus (---). The change in CFP fluorescence was about 0.04 compared to a change in YFP fluorescence of about 0.06, when bleaching is neglected (Fig. 3.4.13 A). When the ratio of CFP/YFP was calculated, a strong increase of ~0.27 was observed over the time course of the experiment (Fig. 3.4.13 B). This steady increase in CFP/YFP most likely does not represent an increase in $[cAMP]_i$ but may be the result of the strong bleaching of the YFP fluorophore. This conclusion is supported by the fact that the ratio increased by the same extend as the YFP fluorescence decreased.

Due to the weak expression of the EPAC1-camps sensor after viral transduction I had to excite the sensor at high LED-intensities. This may have caused the strong bleaching of the YFP. Compared to the EPAC1-camps sensor expressed after Lipofectamine-transfection (3.2.2.1), the virally-expressed sensor exhibited lower expression levels and improper processing as I often found truncated versions of the virally-expressed protein lacking CFP fluorescence. In addition, it appeared as if the virally-expressed EPAC1-camps sensor was less functional compared to the Lipfectamine-expressed sensor as CFP and YFP fluorescence did not change in a mirror-reversed way as expected for a clear FRET change. Despite these described drawbacks of the virally expressed EPAC1-camps sensor it was judged to be worth testing its function *in vivo*.

3.4.3.2. Is EPAC1-camps expressed *in vivo* after viral infection with AAV2?

To investigate whether EPAC1-camps is expressed in retinal neurons after viral infection *in vivo*, mouse pups were injected with AAV2-EPAC1-camps at P7. Mice were sacrificed 2 months later and retinal wholemounts were used for immunohistochemical analysis. Fig. 3.4.14 shows a z-stack of two positions (A and B) in the wholemounted AAV2-EPAC1-camps injected retina. The endogenous fluorescence of the EPAC1-camps sensor could laboriously be detected (Fig. 3.4.14 A and B, endoEPAC). There were some somata of neurons weakly expressing EPAC1-camps (Fig. 3.4.14, arrow). In addition, some brighter green fluorescent star-like structures, most likely Müller-cell processes, were found (Fig. 3.4.14, arrowhead). The antibody against GFP labeled much more EPAC1-camps-expressing neurons than were revealed by the endogenous fluorescence of the sensor (Fig. 3.4.14, compare endoEPAC and antiGFP; asterisks). Only a small fraction of these EPAC1-camps-positive neurons exhibited a free nucleus (Fig. 3.4.14, arrow with filled head) which was previously shown to be a criterion for the functional expression

of the EPAC1-camps sensor (3.4.3.1). Due to the low endogenous expression of EPAC1-camps *in vivo*, imaging experiments could not be conducted on intact retinae.

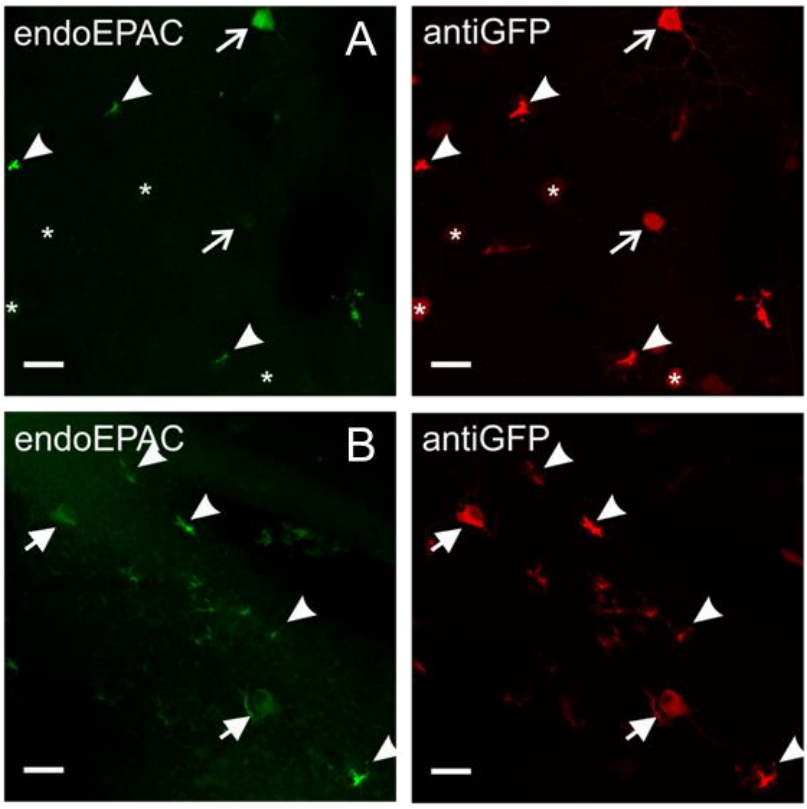

Fig. 3.4.14: The endogenous EPAC1-camps fluorescence after viral expression was quite low. Eyes of mouse pups at the age of P7 were injected with AAV2-EPAC1-camps and fixed 2 months later. Endogenous fluorescence of the EPAC1-camps sensor (green) was low. Staining with anti-GFP (red) revealed that there were many more EPAC1-camps-positive cells (asterisk). EPAC1-camps expression was found in star-like structures, resembling Müller cell processes (arrowhead). Only rarely, neurons with a free nucleus were found (arrow with filled head). Other neurons exhibited EPAC1-camps expression in the nucleus (arrow). **(A)** and **(B)** show a z-projection of the retinal wholemount at different positions. Scale bar 25 µm.

The result that EPAC1-camps was barely functionally expressed in retinal neurons *in vitro* and *in vivo* upon AAV2-mediated gene transfer was an unexpected finding. As a control, expression of another sensor was tested by injection of AAV2-GCaMP3.0 in eyes of mouse pups. Two weeks after injection, mice were sacrificed and the retinae used for either $[Ca^{2+}]_i$ imaging experiments or immunohistochemical analysis. For immunohistochemical analysis, retinal wholemounts were stained with an antibody directed against GFP that is also suitable for the detection of GCaMP3.0. AAV2-GCaMP3.0 successfully infected retinal neurons *in vivo* (Fig. 3.4.15). Plenty of somata and fine processes were positive for GCaMP3.0. In some regions of the retina the number of infected neurons was high whereas in other regions only few GCaMP3.0- positive neurons were found. Regions of high GCaMP3.0 expression probably indicate the neighboring areas of the virus-suspension injection site. This phenomenon has already

been observed in AAV2-GFP injected retinae (Fig. 3.4.7) and in a previous study (Zhao, 2015).

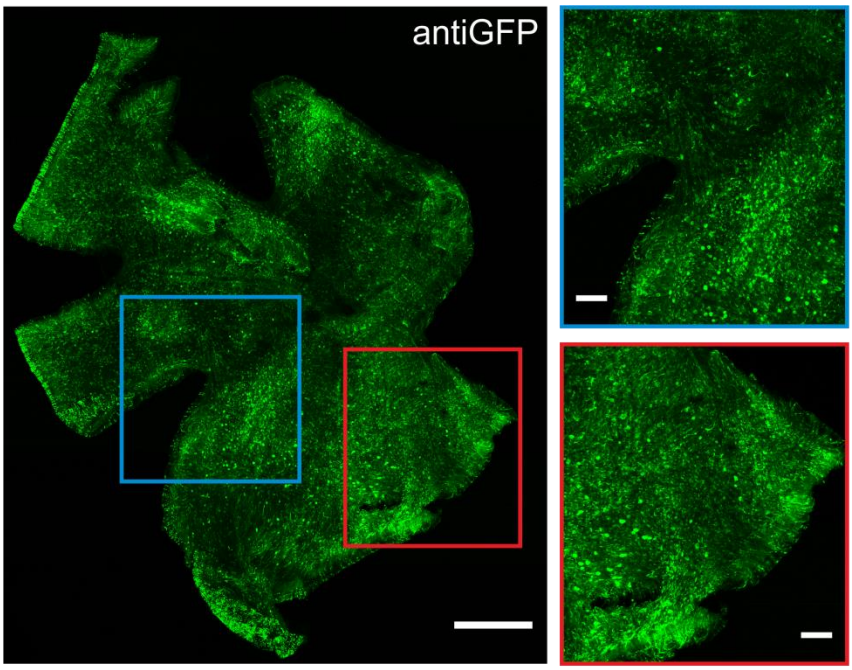

Fig. 3.4.15: GCaMP3.0 was expressed in retinal neurons *in vivo* after intraocular injection of AAV2-GCaMP3.0. Eyes of mouse pups at the age of P7 were injected with AAV2-GCaMP3.0 and fixed 2 weeks later. Retinal wholemounts were stained with an antibody directed against GFP that also detects the GCaMP3.0 sensor. GCaMP3.0 was strongly expressed in the retina. **(A)** Confocal image of a z-projection of the retinal wholemount. Scale bar 500 µm. **(B)** and **(C)** show a zoom-in of different positions in the wholemount. Scale bar 120 µm.

In order to test the functionality of the Ca^{2+}-sensor GCaMP3.0 after transduction with viruses *in vivo*, injected retinae were used for Ca^{2+}-imaging experiments. Two months after infection of the retina with AAV2-GCaMP3.0, the mouse was sacrificed, the injected retina embedded into low melt agarose and subsequently cut into 200 µm thick vertical slices. After a short recovery time, the slice was transferred into the imaging chamber and perfused with oxygenated Ames. In the unstimulated condition, almost no GCaMP3.0 fluorescence was observed in the retinal slice, which is in agreement with low GCaMP 3.0 fluorescence at low $[Ca^{2+}]_i$. Only some bright fluorescent spots were detected that were most likely dead cells filled with Ca^{2+}. Exactly those positions, where bright fluorescent spots had been located, were chosen for imaging experiments, as this was a good indicator for an AAV2-GCaMP3.0 transduced region. Strongly fluorescent spots were excluded from the analysis as they were most likely dead cells flooded with Ca^{2+}. After measuring the baseline fluorescence for 1 min, the retinal slice was superfused with Ames containing 20 mM KCl for 2 min followed by a 1 min wash out phase. The response of one ROI in such a retinal slice is shown in fig. 3.4.16. About 20 s after start of

the stimulus a rise in GCaMP3.0 fluorescence could be detected. This increase in fluorescence reached a plateau after roughly 1min and started to decay after 1.5 min of KCl application. The fluorescence went almost back to baseline during the wash out phase.

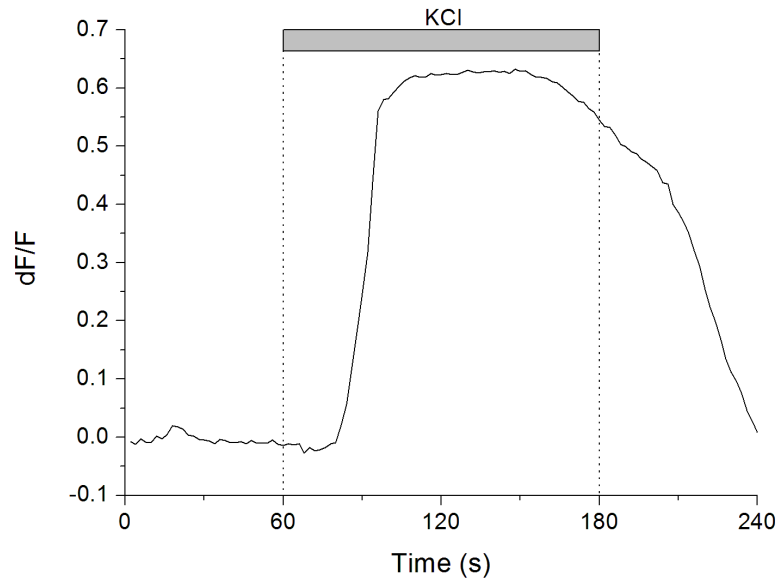

Fig. 3.4.16: Changes in $[Ca^{2+}]_i$ were visualized in retinal slices from AAV2-GCaMP3.0 injected retinae. Retinae from AAV2-GCaMP3.0 injected mice were cut into 200 µm thick slices and stimulated with 20 mM KCl. Cells that were infected by AAV2-GCaMP3.0 and still intact responded with an increase in fluorescence indicating a depolarization-induced increase in $[Ca^{2+}]_i$.

These findings illustrated that AAV2 is suitable to not only transfer GFP marker proteins into retinal neurons *in vivo* but also fluorescent sensor proteins such as GCaMP3.0. It was further demonstrated that the retinal network is still intact and responsive after the injection and slicing procedure. Based on these findings it is hard to understand why EPAC1-camps was not functionally expressed in the retina *in vivo* after viral gene transfer with AAV2.

3.4.4. Alternative approach: *in vivo* electroporation

As the virally-mediated transduction did not result in strong and proper expression of the EPAC1-camps sensor protein *in vivo* and as AAV2 does not infect dopaminergic neurons, an alternative approach was pursued. Matsuda and Cepko were the first who successfully expressed GFP in the retina of rodent pups after *in vivo* electroporation (Matsuda and Cepko, 2004).

Based on this protocol, eyes of mouse pups at the age of P7-8 were injected with 0.5 µl of cDNA coding for GFP (pEGFP-N1; 1.8 µg/µl). Immediately after injection, the head of the pup was placed between two tweezer electrodes and subjected to 5 square-wave pulses with a voltage of 80 V or 100 V and 50 ms duration. Best results were obtained when

100 V were used for electroporation. There was no significant difference found between the expression of GFP in retinae fixed one or three weeks after electroporation. Fig. 3.4.17 A shows a confocal picture of a retina successfully electroporated with pEGFP-N1 and fixed 3 weeks later. GFP expression was found in a restricted area of the retina which amounted to one fourth of the entire retinal tissue. Fig. 3.4.17 B shows confocal pictures of another retina that was successfully electrofected with pEGFP-N1. Neurons that received cDNA after electroporation expressed the GFP marker protein brightly in their soma. In addition, some fine process-like structures could be detected (Fig. 3.4.17 B, green). Staining with anti-GFP revealed that there were many more electrofected neurons than suspected from the endogenous fluorescent picture. Furthermore, many fine structures like processes and axons were found (Fig. 3.4.17 B´, red).

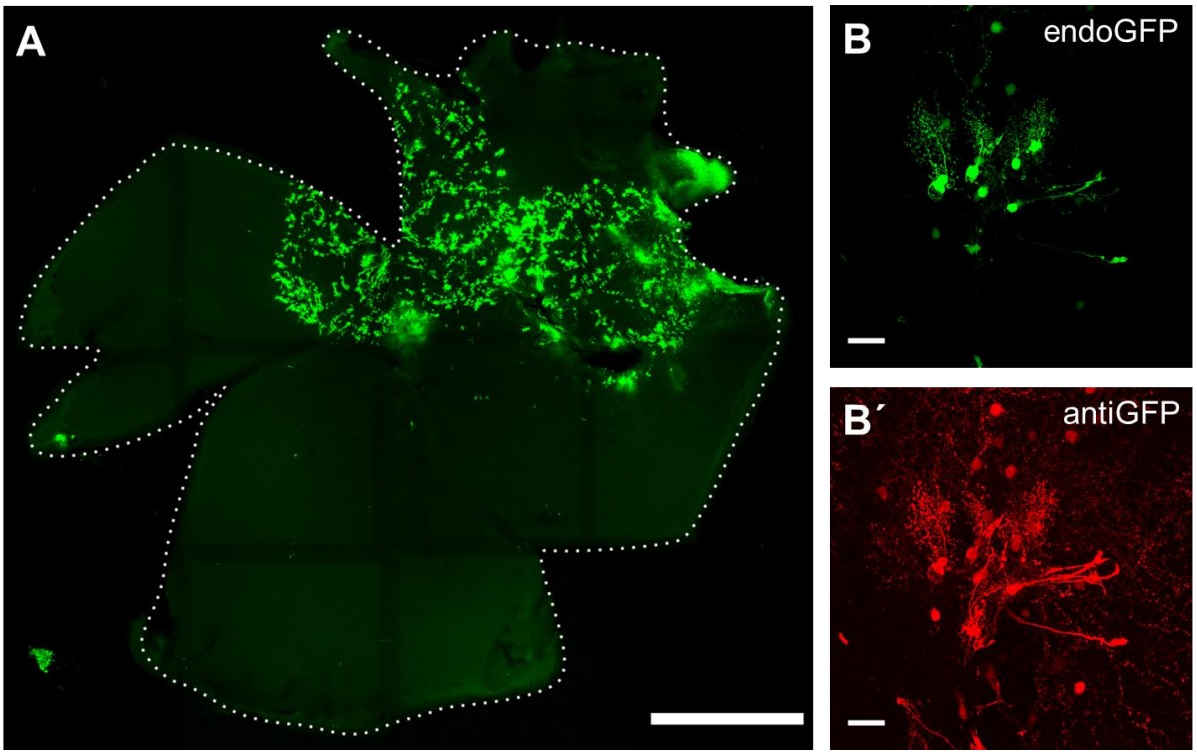

Fig. 3.4.17: GFP is expressed in the retina after *in vivo* electroporation. (A) Confocal image of a retinal wholemount from a mouse injected at the age of P8. cDNA coding for GFP (0.5 µl ; 1.8 µg/µl) was injected into the eye followed by electroporation. The retina was fixed 3 weeks later and stained with an antibody directed against GFP. Scale bar 1 mm. Bright GFP fluorescence was found in a restricted area of the retina. **(B, B´)** Confocal image zoom into a retinal wholemount from another mouse injected at the age of P7. cDNA coding for GFP (0.5 µl; 1.8 µg/µl) was injected into the eye followed by electroporation. Retina was fixed 4 weeks later. Endogenous fluorescence (green) was lower than fluorescence observed after staining with an antibody directed against GFP (red). Scale bar 25 µm.

Despite the successful expression of GFP shown in fig. 3.4.17, the majority of electroporated retinae showed no GFP expression or only a few electrofected neurons that were distributed all over the retinae (Fig 3.4.18 A) or localized in a minimal region of the retina (Fig. 3.4.18 B).

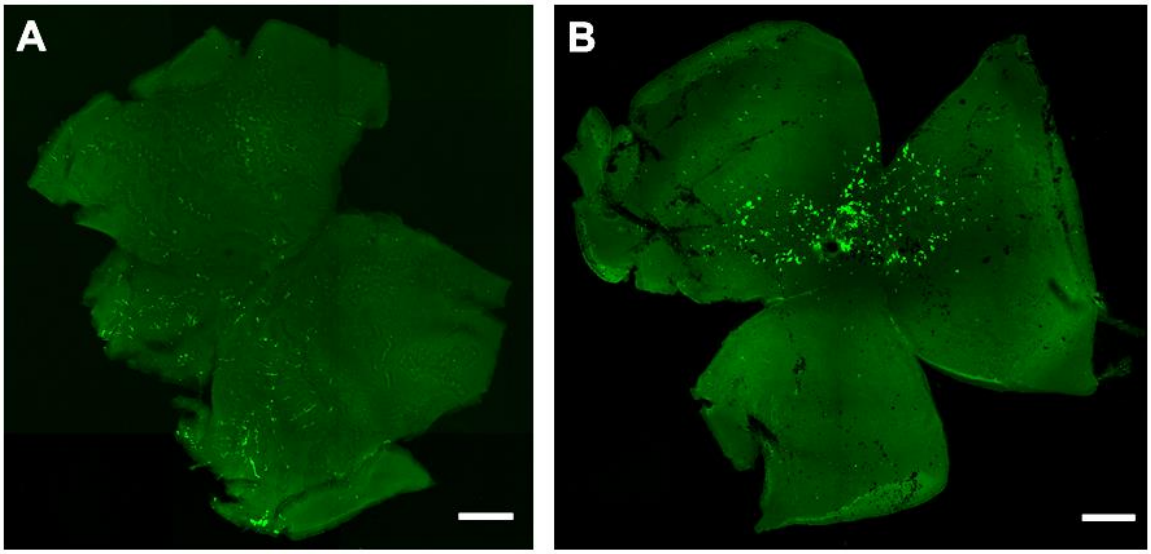

Fig. 3.4.18: GFP expression after electroporation was quite variable. Confocal images of retinal wholemounts from two mice injected at the age of P8. cDNA coding for GFP (0.5 µl; 1.8 µg/µl) was injected into the eye followed by electroporation. The retina was fixed 2 weeks later and stained with an antibody directed against GFP. **(A)** A few electrofected neurons exhibited GFP expression and were distributed all over the retina. **(B)** GFP-expressing neurons were found in a small restricted area of the injected retina. Scale bars 500 µm.

In summary it was shown that the *in vivo* electrofection method yielded expression in restricted areas in a few injected retinae. Unfortunately, these results were inadequately reproducible. Expression of sensor proteins such as AKAR4 and EPAC1-camps via electroporation failed. Thus, the method of *in vivo* electroporation has to be further improved.

3.4.5. Impact of dopaminergic signaling on $[Ca^{2+}]_i$ in GCs of the intact retina

This chapter focuses on the investigation of DA-induced effects in GCs of the intact retina. GCs are the retinal output neurons that collect and integrate all information coming from the retinal network. Estimates of the number of GC types in the mouse retina differ between 10 and 32 functional types (Kong *et al.*, 2005; Farrow and Masland, 2011; Sümbül *et al.*, 2013; Baden *et al.*, 2016).

In order to monitor DA-triggered changes in $[Ca^{2+}]_i$ in GCs, I made use of a transgenic mouse line (Heim *et al.*, 2007) that expresses the FRET-based Ca^{2+}-sensor TN-L15 in the majority of GCs (80%; F. Müller, personal communication). In TN-L15, an increase in the ratio YFP/CFP reflects an increase in $[Ca^{2+}]_i$. In the retina of this transgenic mouse line, TN-L15 expression is found in the somata and processes of GCs and in a few ACs. The TN-L15-expressing GCs can be differentiated by their soma size (Fig. 3.4.19). Cells were grouped into cells with a large soma (Fig. 3.4.19, asterisk), medium sized soma (Fig.

3.4.19, arrow) and small soma (Fig. 3.4.19, arrowhead). TN-L15-positive GC processes are found in both ON- and OFF-layer of the IPL indicating that both ON- and OFF-GCs express the sensor. In the following, I will demonstrate that DA changes $[Ca^{2+}]_i$ in GCs and that the TN-L15-positive GCs not only differ in their morphology but also in their response to DA.

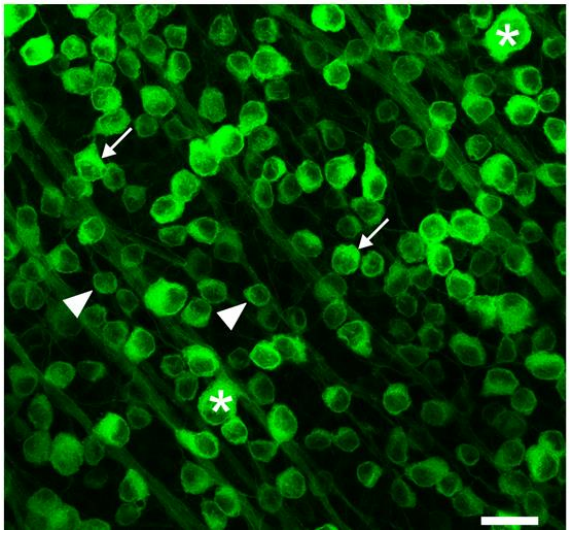

Fig. 3.4.19: TN-L15 is expressed in GCs of the mouse retina. Confocal image of the GC layer from a TN-L15 mouse retina. TN-L15-fluorescence was strong enough to be detected without staining the sensor with an antibody. Cells were grouped into cells with a large soma (asterisk), medium sized soma (arrow) and small soma (arrowhead). Scale bar 25 µm.

3.4.5.1. DA altered $[Ca^{2+}]_i$ in TN-L15-positive GCs

In order to find out whether DA influences $[Ca^{2+}]_i$ of retinal GCs, acutely isolated TN-L15 retinae were superfused three times with 20 µM DA for 3 min. In between, retinae were washed for 5 min with Ames solution. Four general types of Ca^{2+}-responses to stimulation with 20 µM DA were observed: GCs that responded with an increase in YFP/CFP indicating an increase in $[Ca^{2+}]_i$ (Fig. 3.4.20 B, "increase type"), cells that reacted with a decrease in YFP/CFP indicating a decrease in $[Ca^{2+}]_i$ (Fig. 3.4.20 C, "decrease type") and others that responded with an initial drop in YFP/CFP followed by a peaking increase in YFP/CFP (Fig. 3.4.20 D, "biphasic type") indicating a biphasic change in $[Ca^{2+}]_i$. In addition, there were TN-L15-positive GCs that did not respond to DA application at all (Fig. 3.4.20 A). These cells were shown to be still responsive as depolarization with 20 mM KCl elicited an increase in YFP/CFP reflecting an increase in $[Ca^{2+}]_i$.

These general types of Ca^{2+}-responses could be further subdivided. Both, the increase type and the decrease type encompassed a sustained response type (Fig. 3.4.20 B bottom and C top) and a transient response type (Fig. 3.4.20 B top and C bottom). In the

sustained increase response type, increase in $[Ca^{2+}]_i$ started about 30 s after the DA stimulus was given and lasted until a plateau was reached. The change in $[Ca^{2+}]_i$ recovered slowly back to baseline after the DA application was stopped (Fig. 3.4.20 B, bottom). In contrast, the transient responses started about 20 s after DA was washed in, rapidly reached a peak and started to recover back to baseline during DA application (Fig. 3.4.20 B, top). However, the transient kinetics of the increase in $[Ca^{2+}]_i$ was lost in the third application of DA and the response became quite similar to the third response of the sustained increase type cell.

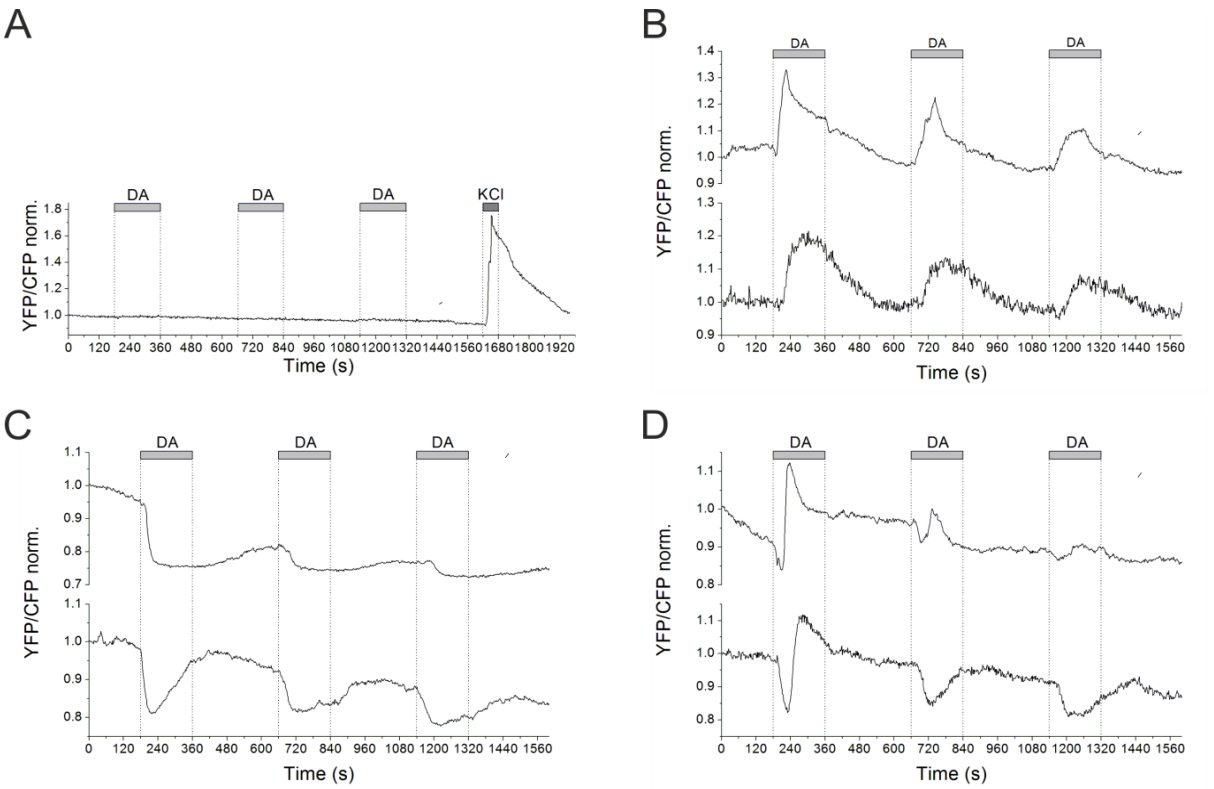

Fig. 3.4.20: TN-L15-positive GCs responded differently and repeatedly to DA. DA-induced changes in YFP/CFP of GCs shown in dependence of time. **(A)** Response of a GC that did not respond to stimulation with DA. The cell was still intact as depolarization with 20 mM induced an increase in $[Ca^{2+}]_i$. **(B)** Response of two GCs reacting with an increase in $[Ca^{2+}]_i$ upon stimulation with 20 µM DA. **(C)** Response of two GCs that reacted with a reduction in $[Ca^{2+}]_i$. **(D)** Response of two GCs that showed a biphasic change in $[Ca^{2+}]_i$.

Both the transient and sustained response of cells of the decrease type started promptly after the DA stimulus was given. Cells of the sustained decrease type exhibited a long-lasting decrease in $[Ca^{2+}]_i$ which did not recover back to baseline during washout (Fig. 3.4.20 C, top). This was observed in almost all cells of this response type. In contrast to that, cells of the transient decrease type recovered back to baseline about 1 min after the DA stimulus was stopped (Fig. 3.4.20 C, bottom). However, the transient nature of the response converted into a more sustained one in the following DA applications similar

to the findings described for cells of the transient increase type. The responses of cells belonging to the biphasic type were quite variable. There were cells that in two of three DA applications responded with a biphasic change in $[Ca^{2+}]_i$ (Fig. 3.4.20 D, top) and others in which the second and third DA application triggered only a transient decrease in $[Ca^{2+}]_i$.

Quantification of the different types of $[Ca^{2+}]_i$ responses to DA revealed that about half of the cells analyzed (n_{cells}=270, n_{mice}=8) did not respond to application of 20 µM DA (Fig. 3.4.21). The majority of reacting cells responded with an increase in $[Ca^{2+}]_i$ (~33%) and the decrease type and biphasic type could be found equally often (~7% and ~9%, respectively) (Fig. 3.4.21).

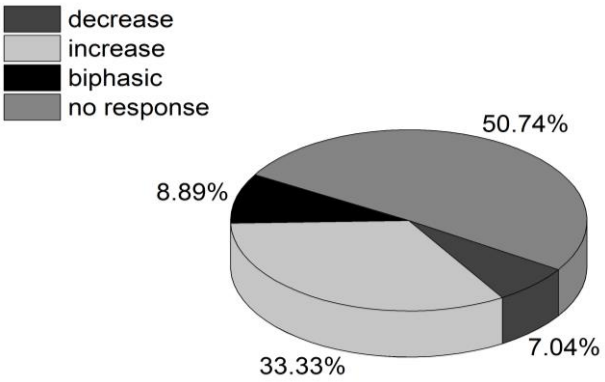

Fig. 3.4.21: Frequency of different DA-induced changes in $[Ca^{2+}]_i$. The majority of reacting cells responded with an increase in $[Ca^{2+}]_i$ upon stimulation with DA. The decrease in $[Ca^{2+}]_i$ and the biphasic change in $[Ca^{2+}]_i$ were found equally often. Total number of cells: 270.

These different types of responses to DA can be explained in various ways. Based on the fact that the mammalian retina comprises at least 10-15 types of GCs (Masland, 2001; Wässle, 2004), different responses to DA could be attributed to distinct types of GCs. GC types might differ in their inventory and in the expression level of DRs. In the following chapter I will investigate the correlation between GC types and response types.

3.4.5.2. Is there a correlation between the type of GC and type of response to DA?

3.4.5.2.1. Large GCs responded with a decrease in $[Ca^{2+}]_i$

In order to search for a correlation between the type of response to DA and the type of GC, the soma size was used. Regions of interest (ROI) were drawn around the somata of recorded cells and the area of the ROI was calculated (ImageJ, NIH). For simplification, somata of GCs were assumed to be circular so that known parameters (image size: 502x501 pixels; physical size: 200x200 µm) could be used to determine the radius of the

soma with the equation $r = \sqrt{\frac{A}{\pi}}$. Based on their soma size, GCs were grouped into three clusters: cells with a soma radius of 4-6 µm which accounted for one third of cells (Fig. 3.4.22 A, medium grey), ~53% of analyzed cells with a soma radius of 6-8 µm (Fig. 3.4.22 A, light grey) and about 15% of cells with a radius of 8-12 µm (Fig. 3.4.22 A, dark grey).

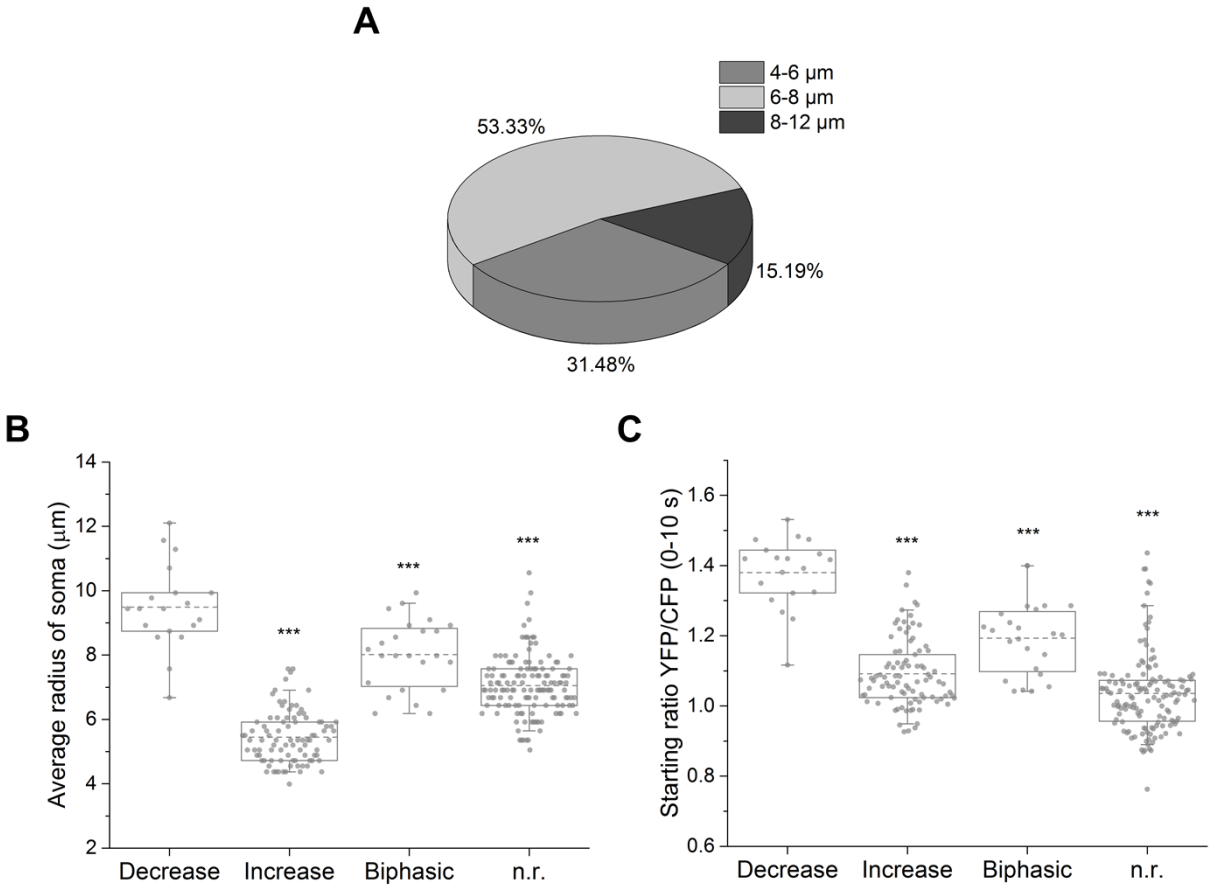

Fig. 3.4.22: GCs of the decrease type exhibited larger somata and a higher starting ratio. (A) Three groups of GCs were identified due to the size of their soma. The radius of the soma of each cell was calculated using the equation $r = \sqrt{\frac{A}{\pi}}$. **(B)** The soma radius for each GC of each response type was calculated and data were plotted as box plot. Each dot represents the soma radius of one cell. The box covers the central 50% of the data. The dashed lines indicate the mean (decrease: 9.49±0.63 µm; increase: 5.45±0.17 µm; biphasic: 8.02±0.46 µm and no response (n.r.): 7.05±0.15 µm; ±95% CI) and the whiskers above and below the box indicate the 95th and 5th percentiles, respectively. Significance of differences between the increase type, biphasic type and no response cells compared to the decrease type was tested with either t-test or Mann-Whitney Rank Sum Test (p***≤0.001). Cells that showed a decrease in $[Ca^{2+}]_i$ upon DA stimulation had the largest somata of all cells. **(C)** The average YFP/CFP ratio of the time interval 0-10 s of the measurement was calculated for each cell of each response type and data were plotted as boxplot. Each dot represents the starting ratio YFP/CFP of one cell. The box covers the central 50% of the data. The dashed lines indicate the mean (decrease: 1.38±0.05; increase: 1.09±0.02; biphasic: 1.19±0.04 and no response (n.r.): 1.04±0.02; ±95% CI) and the whiskers above and below the box indicate the 95th and 5th percentiles, respectively. Significance of differences between the increase type, biphasic type and no response type compared to the decrease type was tested with either t-test or Mann-Whitney Rank Sum Test. p***≤0.001. Neurons of the decrease type had the highest YFP/CFP ratio at the beginning of the measurements.

A more detailed analysis of the soma radius of specific response types revealed that the group of GCs that responded with a decrease in $[Ca^{2+}]_i$ upon stimulation with DA showed the largest average soma radius with 9.49±0.63 µm (±95% CI; n=19), followed by GCs responding with a biphasic response (8.02±0.46 µm; ±95% CI; n=24) (Fig. 3.4.22 B). GCs of the increase type exhibited the smallest average soma radius with 5.45±0.17 µm (±95% CI; n=90). GCs that did not respond to stimulation with DA had an average soma radius of 7.05±0.15 µm (±95% CI; n=137). Statistic tests (t-test or Mann-Whitney Rank Sum Test) revealed that differences in soma size were significant (Fig. 3.4.22 B). Another noticeable difference between the GCs of the different response types was the ratio of YFP/CFP at the beginning of the measurements (t=0-10s). Statistical analysis revealed that GCs of the decrease type exhibited an average starting ratio of 1.38±0.05 (±95% CI), which was significantly higher than the average starting ratios of all other response types (increase: 1.09±0.02; biphasic: 1.19±0.04; no response: 1.04±0.02; ±95% CI) (Fig. 3.4.22 C). The higher YFP/CFP of GCs of the decrease type may indicate that these cells had a higher $[Ca^{2+}]_i$ than the other groups of cells.

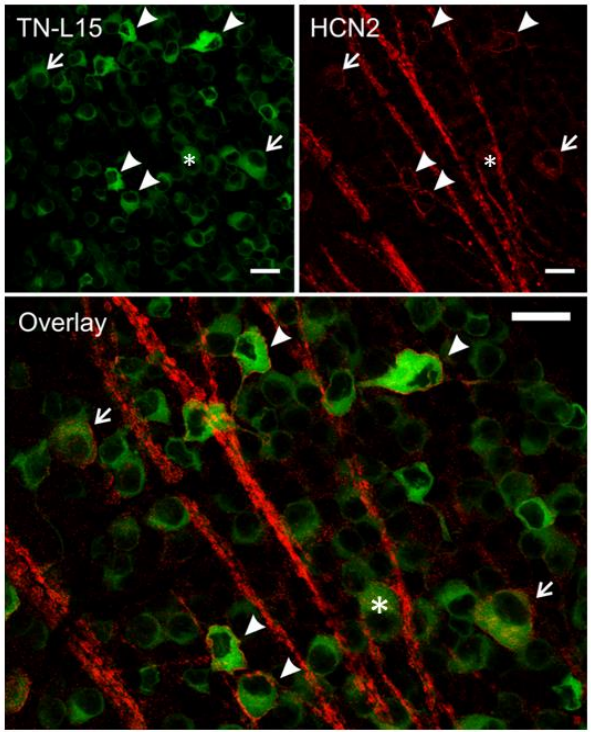

Fig. 3.4.23: Some large TN-L15-expressing GCs were immunoreactive for HCN2. One retina of a TN-L15 mouse was fixed and stained with an antibody directed against the HCN2 channel (red). The confocal image shows the GCL. Endogenous fluorescence (green) of the TN-L15 sensor was bright enough to be detected without staining. Some TN-L15-positive GCs exhibited plasma membrane staining of HCN2 (arrowhead), others showed cytoplasmic HCN2 immunoreactivity (arrow). In addition, some large TN-L15-positive GCs were negative for HCN2 (asterisk). Scale bar 25 µm.

In immunohistochemical studies of mouse retina it was found that one type of OFF-GC is immunoreactive for the ion channel HCN2 (hyperpolarization-activated and cyclic nucleotide-gated channel 2). These HCN2-positive GCs exhibited a soma diameter of 20-30 µm and stratified in the OFF sublamina (Mataruga *et al.*, 2007). In order to find out whether those large TN-L15-positive GCs, that react with a DA-induced decrease in $[Ca^{2+}]_i$, are positive for HCN2, one TN-L15 retina was stained as a wholemount with an antibody against HCN2. Some TN-L15-positive GCs showed HCN2 immunoreactivity throughout the cytoplasm (Fig. 3.4.23, arrow) and others exhibited HCN2 label exclusively at the plasma membrane (Fig. 3.4.23, arrowhead). In addition, there were TN-L15-positive GCs with a large soma that were not positive for HCN2 (Fig. 3.4.23, asterisk). The average soma radius of eleven $HCN2^+$/$TN\text{-}L15^+$ GCs was 11.8±0.7 µm (±95% CI) which was larger than the average soma radius of GCs responding with a DA-induced decrease in $[Ca^{2+}]_i$ (t-test; p***≤0.001).

In summary, it was found that GCs of the decrease type exhibited distinct properties: they had a larger soma and a higher $[Ca^{2+}]_i$ at the beginning of the experiments when compared to the GCs of the other response types. In immunohistochemical analysis with the antibody directed against HCN2 I found that $HCN2^+$/$TN\text{-}L15^+$ GCs had a larger soma than cells of the decrease type. Thus, one can assume that GCs of the decrease type are not the HCN2-positive OFF-GCs found by Mataruga and colleagues (Mataruga *et al.*, 2007). In order to further characterize the different response types, the next chapter focuses on the pharmacological identification of ON- and OFF-GCs.

3.4.5.2.2. Differentiation between ON- and OFF-GCs via L-AP4

One physiological characteristic of GCs is their response to light. As for BCs, ON-GCs depolarize whereas OFF-GCs hyperpolarize at light onset. Two-amino-4-phosphonobutyric acid (L-AP4) is a selective group III metabotropic glutamate receptor agonist and thus a well-suited pharmacological tool to block the ON pathway in the retina that depends on the metabotropic glutamate receptor 6 (mGluR6) (Shiells *et al.*, 1981; Slaughter and Miller, 1981; Schiller, 1982; Nakajima *et al.*, 1993). Stimulation of ON-BCs with L-AP4 mimics scotopic conditions (= glutamate release from PRs) resulting in a hyperpolarization of ON-BCs and in turn a hyperpolarization of ON-GCs. As rod BCs synapse onto AII ACs, AII ACs are also hyperpolarized. The hyperpolarization of the AII AC additionally causes a reduction in glycine release resulting in the loss of inhibition of OFF-BCs and in turn a depolarization of OFF-GCs (Fig. 3.4.24). Thus, application of L-AP4

can be used for the distinction between ON- and OFF-GCs in the retina (Massey *et al.*, 1983; Müller *et al.*, 1988).

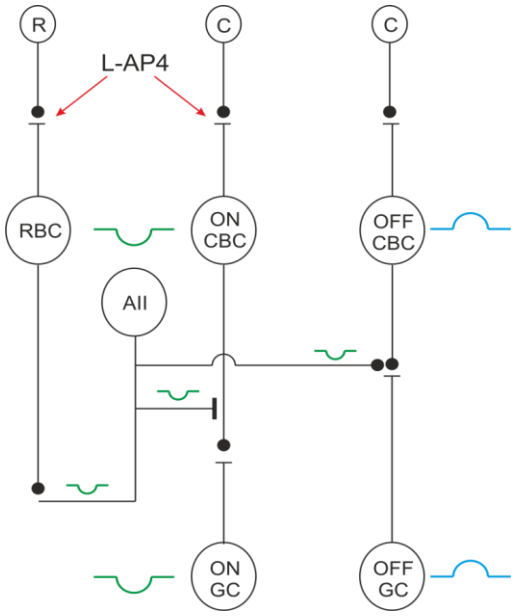

Fig. 3.4.24: Action of L-AP4 in the retina. Rods (R) and cones (C) are connected to ON-BCs (rod BC (RBC) and ON cone BCs (ON CBC)). Upon binding of L-AP4, these ON-BCs are hyperpolarized (green curve). As RBCs make synapses to AII ACs, AIIs are also hyperpolarized. AII are coupled to ON CBC via gap junctions thus enhancing the L-AP4-induced hyperpolarization in ON CBCs. In addition, AIIs make inhibitory synapses onto OFF CBC. Through the diminished release of the inhibitory transmitter glycine, OFF CBC and following OFF-GCs become depolarized (blue curve). Scheme modified from Müller *et al.*, 1988.

Application of 20 µM DA for 3 min was followed by a washing phase of 5 min with Ames. Following, 100 µM L-AP4 was applied for 3 min. After another washing phase of 10 min duration, cells were stimulated again with 20 µM DA for 3 min. Six of eight GCs that responded with a decrease in $[Ca^{2+}]_i$ upon stimulation with DA also reacted with a decrease in $[Ca^{2+}]_i$ upon L-AP4 application (Fig. 3.4.25 A, bottom). The other two GCs that responded with a decrease in $[Ca^{2+}]_i$ upon DA application did not react to L-AP4 (Fig. 3.4.25 A, top). However, after washout of L-AP4 cells of both groups often reacted with an increase in $[Ca^{2+}]_i$ resembling the overshoot in the electrical activity of light-adapted ON-GCs observed after removal of L-AP4 (Wässle *et al.*, 1986; Müller *et al.*, 1988). After this "overshoot" in $[Ca^{2+}]_i$ the second stimulation with DA resulted in a fall in $[Ca^{2+}]_i$ (Fig. 3.4.25 A). These observations would suggest that cells responding with a DA-induced decrease in $[Ca^{2+}]_i$ are ON-GCs, namely those cells that show a decrease in $[Ca^{2+}]_i$ upon stimulation with L-AP4. On the other hand, there were cells that responded with an increase in $[Ca^{2+}]_i$ upon stimulation with DA (Fig. 3.4.25 B). In 65% of these cells, L-AP4 did not elicit any change in $[Ca^{2+}]_i$ (Fig. 3.4.25 B, top). In another 20% of cells

L-AP4 caused an increase in $[Ca^{2+}]_i$ (Fig. 3.4.25 B, bottom) giving rise to the assumption that they are OFF-GCs.

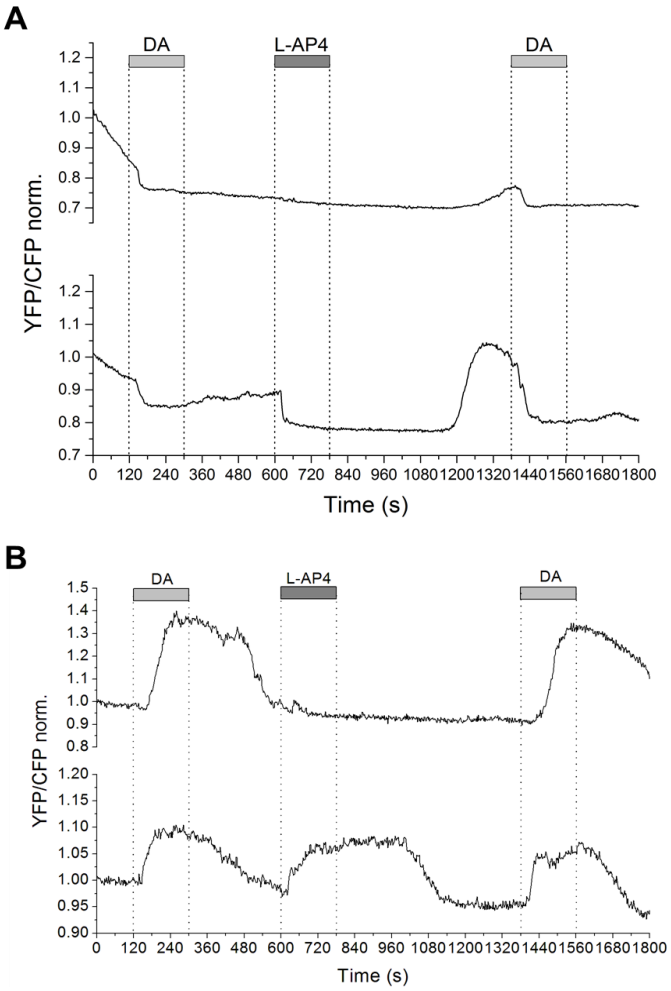

Fig. 3.4.25: Inhibition of the ON pathway by L-AP4 led to a reduction in $[Ca^{2+}]_i$ in some cells of the decrease type and to a rise in $[Ca^{2+}]_i$ in some cells of the increase type. Acutely isolated retinae from a TN-L15 transgenic mouse were stimulated with 20 µM DA followed by the application of 100 µM L-AP4 and a second DA application. **(A)** The responses of two TN-L15-expressing GCs of the decrease type. **(B)** The responses of two TN-L15-expressing GCs of the increase type.

In summary, three things have to be pointed out: First, in the L-AP4 experiments only a few cells responded to stimulation with 20 µM DA (n_{cells}: 66 of 390; $n_{animals}$: 4). This is only 16% of all cells tested in the L-AP4 experiments and clearly less than previously found in control experiments (~50%). Second, it was quite surprising that only a few GCs responded to superfusion with 100 µM L-AP4 as it would be expected that ca. 50% of cells respond with a decrease in $[Ca^{2+}]_i$ (ON-GCs) and the other 50% with an increase in $[Ca^{2+}]_i$ (OFF-GCs). However, from the results of the L-AP4 experiments it can be assumed that cells of the decrease type are most likely ON-GCs and some cells of the increase type are OFF-GCs.

3.4.5.3. Are the DA-induced changes in $[Ca^{2+}]_i$ due to a network response or due to direct action at GCs?

The heterogeneity of the responses triggered by DA might be further increased by a combination of direct effects of DA on the GCs themselves and on presynaptic cells. Indeed, in chapter 3.3 I have shown that DA induces different types of $[Ca^{2+}]_i$ responses in retinal neurons in culture which most likely represent ACs. DA also modulates the physiology of BCs (Heidelberger and Matthews, 1994; Wellis and Werblin, 1995; Smith *et al.*, 2015) which make glutamatergic synapses to GCs (reviewed in Massey, 1990). Thus, DA might alter the excitatory or inhibitory input from presynaptic cells onto GCs and thus lead to a de- or hyperpolarization of GCs concomitant with changes in $[Ca^{2+}]_i$. This chapter focuses on the question whether inhibition of the presynaptic input reduces or abolishes the DA-induced change in $[Ca^{2+}]_i$ in GCs.

3.4.5.3.1. Role of the excitatory input in DA-induced changes in $[Ca^{2+}]_i$

Using the glutamate receptor antagonists CNQX (20 µM; AMPA/kainate receptor antagonist) and AP5 (20 µM; NMDA receptor antagonist) I attempted to dissect the contribution of the glutamatergic input from BCs to the generation of the DA-induced changes in $[Ca^{2+}]_i$.

A first application of 20 µM DA for 3 min was followed by a washing phase of 5 min with Ames. The glutamatergic input was inhibited by a 3 min application of a blocker cocktail composed of CNQX and D-AP5. Still during glutamatergic blockade, cells were stimulated for 3 min with 20 µM DA. The different types of response patterns are summarized in table 3.4.1. Amongst various types of responses, one was found in retinae of all 4 animals tested. About 12% of GCs responded with an increase in $[Ca^{2+}]_i$ upon stimulation with DA that was not blocked in the presence of AP5 and CNQX. In 4.7% of GCs, DA triggered an increase in $[Ca^{2+}]_i$ that was abolished in the presence of AP5 and CNQX. The response to AP5 and CNQX was quite diverse in these cells. In another 3.5% of GCs, DA induced an increase in $[Ca^{2+}]_i$ with a pronounced peak as did CNQX and AP5. The blockade of the glutamatergic input did not abolish the DA-induced increase in $[Ca^{2+}]_i$ in these cells. In another 3.5% of GCs DA induced a biphasic change in $[Ca^{2+}]_i$ that was blocked by AP5 and CNQX. In these cells, blockade of the glutamatergic input induced a decrease in $[Ca^{2+}]_i$. In 5% of GCs, DA induced a decrease in $[Ca^{2+}]_i$. AP5 and CNQX reduced $[Ca^{2+}]_i$ and abolished the response to DA in one half of these cells. In the other 50% of the decrease type GCs, DA induced a decrease in YFP/CFP that was not reversible. AP5 and CNQX or DA in the presence of the blocker cocktail did not induce a

further decrease in $[Ca^{2+}]_i$. Almost 10% of cells could not be categorized into a specific response type.

Table 3.4.1: Inhibition of the glutamatergic input by AP5 and CNQX resulted in variable response patterns. Acutely isolated retinae from TN-L15 transgenic mice were stimulated twice with 20 µM DA in the absence as well as in the presence of the glutamate receptor antagonists CNQX (20 µM) and AP5 (20 µM). The relative frequency of $[Ca^{2+}]_i$ responses (↑: increase; ↓: decrease; ↓↑ biphasic; x: no response) to stimulation with DA, AP5+CNQX and DA in the presence of AP5 and CNQX is depicted in this table. Four animals were used for these experiments, but not all types of responses were found in all animals as depicted in N_{animal}.

Rel. Frequency	DA	CNQX + AP5	DA on CNQX+AP5	N_{animal}	Example
12%	↑	↓	↑	4/4	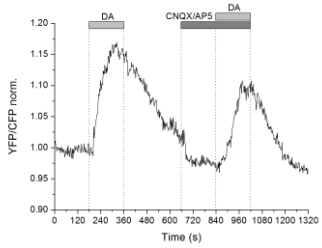
4.7%	↑	x	x	3/4	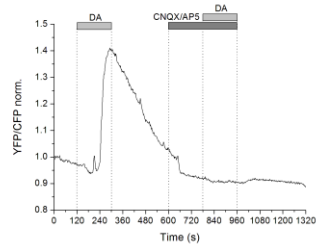
3.5%	↑	↑	↑	3/4	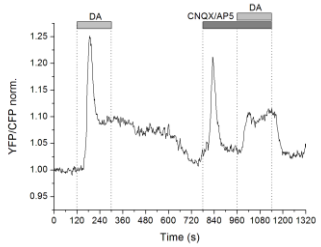
3.5%	↓↑	↓	x	3/4	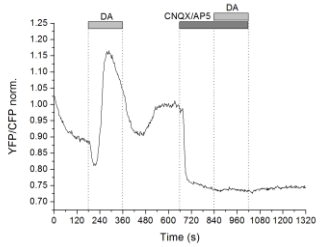
2.5%	↓	↓	x	2/4	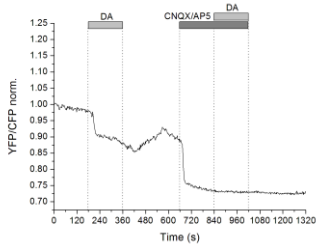

Rel. Frequency	DA	CNQX + AP5	DA on CNQX+AP5	N_{animal}	Example
2.5%	↓	x	x	2/4	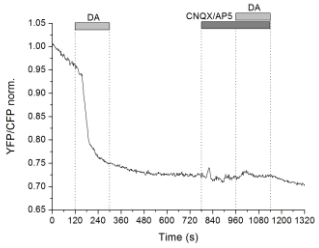
62%	x	x	x	4/4	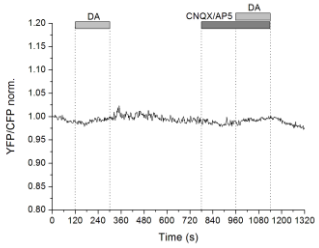

As table 3.4.1 demonstrates, the results obtained from this pharmacological approach resulted in further subdivisions of the Ca^{2+}-responses. Inhibition of the glutamatergic input abolished the DA-induced change in $[Ca^{2+}]_i$ in some TN-L15-positive GCs indicating that in these cells DA mostly acted presynaptically via the modulation of the glutamatergic input from BCs. On the other hand, there were cells that despite the presence of the blockers CNQX and AP5 responded to stimulation with DA with a change in $[Ca^{2+}]_i$. In these cells, DA-induced changes might reflect a direct action of DA at the GC itself or a DA-induced modulation of the inhibitory input from ACs. The impact of the inhibitory input on the DA-induced changes in $[Ca^{2+}]_i$ in GCs was investigated in the following experiments.

3.4.5.3.2. Role of the inhibitory input in DA-induced changes in $[Ca^{2+}]_i$

To investigate the portion of the inhibitory input in the DA-induced changes in $[Ca^{2+}]_i$ in retinal GCs, glycine- and GABA-receptors were blocked by an inhibitor cocktail composed of 10 µM strychnine (glycine-receptor antagonist), 100 µM picrotoxin ($GABA_A$-receptor antagonist), 2 µM CGP54626 ($GABA_B$-receptor antagonist) and 20 µM TPMPA ($GABA_C$-receptor antagonist). Experiments were conducted according to the protocol used in 3.4.5.3.1. Again, DA induced responses with increase, decrease or biphasic changes in $[Ca^{2+}]_i$. Inhibition of the inhibitory input induced an increase in $[Ca^{2+}]_i$ in all GCs but response patterns were quite diverse as demonstrated in table 3.4.2.

In some cells blockade of the inhibitory input induced an increase in $[Ca^{2+}]_i$ that exhibited oscillations, others responded with an increase in $[Ca^{2+}]_i$ that peaked and started to recover still during perfusion of the inhibitor cocktail and some cells exhibited a mixture of both Ca^{2+}-responses. In 4% of GCs DA still elicited an increase in $[Ca^{2+}]_i$ or an increase in the amplitudes of Ca^{2+}-oscillations in the presence of the inhibitor cocktail while in 12% of GCs the inhibitor cocktail seemed to block the DA-induced increase in $[Ca^{2+}]_i$. About 9% of cells responded with a DA-induced decrease in $[Ca^{2+}]_i$ which also varied in signal amplitude and kinetics from cell to cell. Like in chapter 3.4.5.3.1, two sub-groups could be identified: in 5.6% of GCs the DA-induced decrease in $[Ca^{2+}]_i$ was not blocked by blockade of the inhibitory input while in 3.2% of GCs the DA-induced decrease in $[Ca^{2+}]_i$ seemed to be blocked by the inhibitor cocktail. Only 3 cells of the biphasic type were found (2.4%). Blockade of the inhibitory input induced a biphasic change in $[Ca^{2+}]_i$ in these cells. However, it was hard to qualify the response to DA in the presence of the inhibitor cocktail in these three cells. The majority of GCs (73%) did not respond to stimulation with DA.

Table 3.4.2: Inhibition of the glycingeric and GABAergic input resulted in variable response patterns. Acutely isolated retinae from TN-L15 transgenic mice were stimulated twice with 20 µM DA in the absence as well as in the presence of the inhibitor cocktail containing 10 µM strychnine, 100 µM picrotoxin, 2 µM CGP54626 and 20 µM TPMPA. The relative frequency of $[Ca^{2+}]_i$ responses (↑: increase; ↓: decrease; ↓↑ biphasic; x: no response) to stimulation with DA and DA in the presence of the inhibitor cocktail is depicted in this table.

Rel. Frequency	DA	DA on inhibitor cocktail	Example
4%	↑	↑	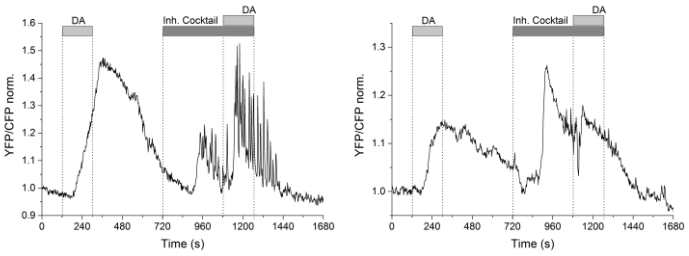
12%		x	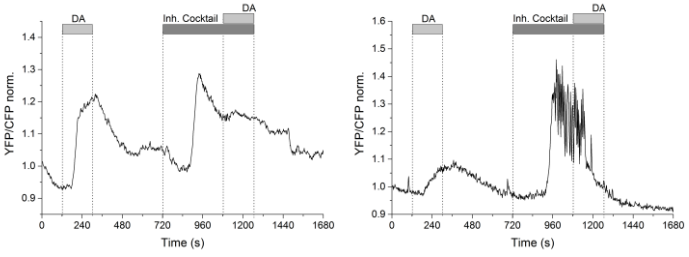

Rel. Frequency	DA	DA on inhibitor cocktail	Example
5.6%	↓	↓	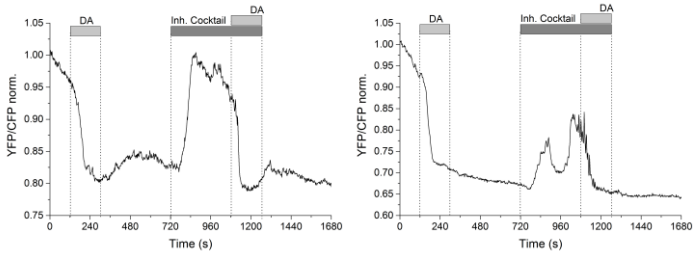
3.2%		x	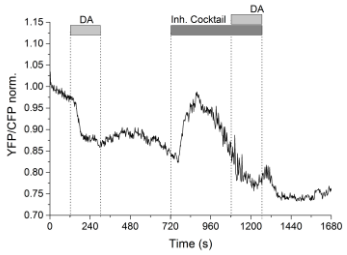
2.4%	↓↑	x	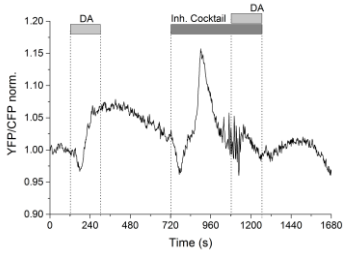
73%	x	x	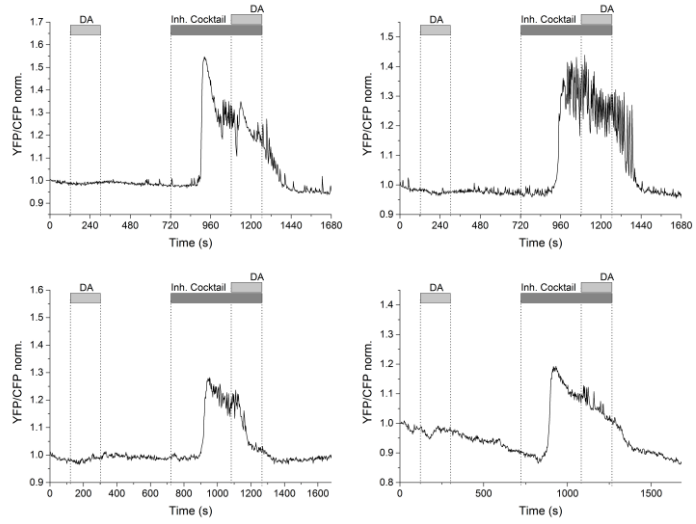

As summarized in table 3.4.2, blockade of the inhibitory input induced variable responses. In some GCs the blockade of the inhibitory input abolished the DA-induced change in $[Ca^{2+}]_i$ arguing that in these cells DA acts mostly presynaptically via the modulation of the inhibitory input from ACs. On the other hand, there were cells that despite the presence of the inhibitor cocktail responded to stimulation with DA with a change in $[Ca^{2+}]_i$. This may be due to a direct action of DA at the GC itself but could also be due to a DA-induced modulation of the glutamatergic input of BCs.

Comparison and combination of the relative frequencies of the two sub-groups of the increase type from 3.4.5.3.1 and this chapter may lead to the conclusion that the DA-induced increase in $[Ca^{2+}]_i$ in a small sub-group of cells (~4%) of the increase type is due to DA-triggered changes in the glutamatergic input whereas in a bigger sub-group of cells (~12%) the increase is due to a modulation of the inhibitory input.

I also found two subgroups of GCs of the decrease type. These two subgroups had in common that the Ca^{2+}-response to DA was blocked in the presence of CNQX and AP5. However, they are assumed to constitute two different groups of cells as CNQX and AP5 alone triggered different responses in the two subgroups (3.4.5.1). During blockade of the inhibitory input (this chapter) two subgroups could be identified on the basis of their responses to DA: one group of cells still responded to DA in the presence of the blockers while the other group of cells did not.

4. Discussion

Dopamine plays a key role in light adaptation processes in the retina and has been shown to influence the physiology of different cell types in various ways. However, the underlying signaling pathways are still elusive. This project was conducted in order to contribute to the comprehension of dopaminergic signaling in the retina on the level of second messenger cascades. Immunocytochemical analysis of the retinal culture revealed that this model system is well suited for the investigation of dopaminergic signaling in single retinal neurons (3.1). Using the two FRET-based biosensors EPAC1-camps and AKAR4 it was shown in this culture system, that DA affects single neurons by changing the intracellular concentration of cAMP and the activity of PKA (3.2). As changes in cAMP or PKA activity trigger further signaling cascades such as the phosphorylation of target proteins or opening of nucleotide-gated ion channels - many of which will affect $[Ca^{2+}]_i$ - DA's effects on the $[Ca^{2+}]_i$ were examined (3.3). It was shown, that DA changes $[Ca^{2+}]_i$ in single retinal neurons in culture (3.3) as well as in GCs in the intact retinal network (3.4.5). Pharmacological dissection of the underlying pathways identified the involvement of specific types of DRs as well as other signaling molecules. Furthermore, it could be demonstrated that there is a correlation between the type of response to DA and the type of GC (3.4.5). However, the underlying pathways emerged to be more complex than expected.

4.1. DA modulates the intracellular concentration of second messengers

4.1.1. Activation of D1Rs induces an increase in $[cAMP]_i$ and PKA activity

Immunocytochemical analysis of my culture system revealed that most of the neurons that are present at DIV7-9 are ACs (3.1). This finding fits to previous reports that demonstrated a time-dependent reduction of PRs and BCs in retinal primary culture (Politi *et al.*, 1988). Thus, imaging experiments carried out in the culture most likely investigated DA-induced signaling in retinal ACs.

Using the sensors EPAC1-camps and AKAR4 I found that DA increases $[cAMP]_i$ and PKA activity in cultured retinal neurons (3.2.2.1). Pharmacological investigation revealed that the DA-triggered increase in PKA activity was due to the activation of D1R but not D2Rs (3.2.2.3). These findings are in line with the classical way of D1R downstream signaling (for review see Missale *et al.*, 1998 and Neve *et al.*, 2004). However when applying DA or the D2R-specific agonist quinpirole alone, I never observed a decrease in

PKA activity which would be expected after activation of D2Rs. The most likely explanation for this finding is that the basal cAMP concentration and PKA activity in the cells are that low that they cannot be further decreased by stimulation of D2Rs. In order to test this, I conducted experiments in which I increased PKA activity by the D1R-specific agonist SKF38393 prior to the application of the D2R-specific agonist quinpirole. Interestingly, I observed three different response types in this experiment. I found cells that only responded to stimulation with SKF38393 indicating that they expressed D1Rs but not D2Rs. Other cells responded with a SKF38393-induced increase in PKA activity (activation of D1Rs) that was reduced by application of quinpirole (stimulation of D2Rs) being in agreement with the classical downstream signaling of DRs (for review see Missale *et al.*, 1998 and Neve *et al.*, 2004).

Furthermore, I found cells that showed a quinpirole-triggered increase in PKA activity. This D2R-induced increase in PKA activity cannot be explained by the classical understanding of D1R- and D2R-signaling. It has been reported that the βγ complex of $G\alpha_{i/o}$-coupled D2Rs enhances the activity of type II and type IV ACys in dependence on coincidental activation by $G\alpha_s$ proteins (reviewed in Sunahara *et al.*, 1996 and Neve *et al.*, 2004; Tang and Gilman, 1991). On the assumption that some retinal neurons express type II or type IV ACy, this action of βγ could account for the quinpirole- and thus D2R-induced increase in PKA activity. It is also known from co-expression studies of D1Rs and D2Rs in HEK293 cells that simultaneous activation of co-expressed D1Rs and D2Rs by their specific agonists SKF81297 (D1R) and quinpirole (D2R) evokes an increase in intracellular $[Ca^{2+}]_i$ (Lee *et al.*, 2004). The authors proposed that this increase in $[Ca^{2+}]_i$ is mediated via a PLC-dependent pathway (Lee *et al.*, 2004). Interestingly, Dunn and colleagues found that increases in PKA-activity are mediated by a combination of transmembrane and soluble Ca^{2+}-dependent ACys in the somata of developing GCs of mice. Using dual imaging with AKAR3 and Fura-2 they revealed that Ca^{2+}-transients reliably preceded all PKA activity transients (Dunn *et al.*, 2009). Thus, the quinpirole-induced increase in PKA activity in the presence of a D1R agonist I observed in my experiments might also be due to stimulation of a D1R-D2R heteromeric complex inducing a PLC-dependent increase in $[Ca^{2+}]_i$ which in turn stimulates Ca^{2+}-dependent ACys resulting in a rise in PKA activity.

In order to proof these hypotheses, future experiments should investigate the role of Ca^{2+}-dependent ACys, PLC and Gβγ in the generation of quinpirole-induced increases of PKA activity in AKAR4-expressing retinal neurons. In order to unravel the interplay

between Ca^{2+} and cAMP signaling cascades, dual imaging with Fura-2 and AKAR4 should be applied as already used by Dunn and colleagues. However, independent of these open questions, my studies suggest that the majority of retinal neurons in culture co-expressed D1Rs and D2Rs leading to variable downstream signaling cascades.

4.1.2. DA changes $[Ca^{2+}]_i$ in retinal cultured neurons

In chapter 3.3 I investigated the impact of DA on $[Ca^{2+}]_i$. I found that stimulation of retinal neurons in culture with DA triggered different types of responses. The majority of neurons that were responsive to DA responded with an increase in $[Ca^{2+}]_i$ whereas cells that exhibited a DA-induced decrease in $[Ca^{2+}]_i$ were very rare (3.3.1). I applied a pharmacological approach to dissect the signaling cascades underlying the observed DA-induced changes in $[Ca^{2+}]_i$.

4.1.2.1. The DA-induced increase in $[Ca^{2+}]_i$ is caused by the interplay of different parameters

Using a pharmacological approach I found that the increase in $[Ca^{2+}]_i$ is mediated via two distinct pathways at least. The first one is the classical D1R/PKA pathway and the second one most likely involves DA-triggered store-depletion through the activation of PLC. In the following, I will discuss these two pathways in more detail.

Classical pathway. The assumption that the DA-induced increase in $[Ca^{2+}]_i$ is due to the activation of the D1R/PKA signaling cascade is based on the following findings. Using the D1R-specific antagonist SCH23390 I found that the DA-induced increase in $[Ca^{2+}]_i$ was blocked in the majority of neurons of the increase type. Furthermore, the D1R-specific agonist SKF38393 mimicked the effects of DA (3.3.2.1). SKF38393-induced increases in $[Ca^{2+}]_i$ were exclusively found in cells that also responded to DA with an increase in $[Ca^{2+}]_i$. In about 46% of cells both SKF38393 and DA induced an increase in $[Ca^{2+}]_i$ underlining the role of D1Rs in the generation of the DA-induced increase in $[Ca^{2+}]_i$. As withdrawal of extracellular Ca^{2+} prevented the generation of increases in $[Ca^{2+}]_i$ in the presence of DA (3.3.3.1), I assumed that this type of Ca^{2+}-response is amongst others induced by a modulation of Ca^{2+}-influx through ion channels in the plasma membrane. Indeed, it has been shown that voltage-gated CaChs are generally modulated by D1Rs and D2Rs (reviewed in Neve *et al.*, 2004 and Missale *et al.*, 1998) and that they are expressed in the retina (Xu *et al.*, 2002). I found that L-type CaChs make a major contribution to the generation of DA-induced increases in $[Ca^{2+}]_i$ in retinal neurons in

culture (3.3.3.2). This finding is consistent with findings in HCs in which DA has been demonstrated to amplify L-type Ca^{2+}-currents (Pfeiffer-Linn and Lasater, 1993). In addition, it has been shown that the DA-induced increase in $[Ca^{2+}]_i$ in isolated retinal GCs was blocked by SCH23390 (Ogata *et al.*, 2012).

I also found that N-type CaChs seemed to be partly involved in the generation of the DA-induced increase in $[Ca^{2+}]_i$ in retinal neurons in culture (3.3.3.2). In 1990, Gross and colleagues demonstrated that Ca^{2+}-currents through N- and L-type CaChs were enhanced by phosphorylation through PKA (Gross *et al.*, 1990). But these findings are in conflict with another publication that rather argues for a D1R-mediated decrease in N-type Ca^{2+}-currents through a PKA/PP1-pathway (Surmeier *et al.*, 1995). As I have shown that stimulation of D1Rs induced an increase in PKA activity in cultured neurons using AKAR4 as sensor (3.2.2.3) and as phosphorylation by PKA is a known regulation mechanism of N- and L-type CaChs (Gross *et al.*, 1990; for review see Missale *et al.*, 1998 and Neve *et al.*, 2004), I investigated the impact of PKA on the DA-induced increase in $[Ca^{2+}]_i$. In fact, blockade of PKA by the specific antagonist H89 reduced the DA-triggered increase in $[Ca^{2+}]_i$ in the majority of cells of the increase type (3.3.3.3) indicating that PKA is a key player in the DA-triggered increase in $[Ca^{2+}]_i$.

Quite interestingly, I also found a reduction in the response amplitudes of some cells of the increase type after treatment with the PP1/PP2A inhibitor calyculin A (3.3.3.4). PP1 and PP2A have been demonstrated to be involved in DA-signaling in the retina as they are key players in the DA-induced closure of gap junctions in ACs of the retina (Kothmann *et al.*, 2009). Based on the assumption that the DA-induced increase in $[Ca^{2+}]_i$ is due to the stimulation of D1Rs (3.3.2.1) and partly due to activation of PKA (3.3.3.3), the results obtained with calyculin A are in contradiction to what was expected. Inhibition of PP1 and PP2A should theoretically lead to an inhibition of dephosphorylation processes and thereby favor the phosphorylation of *e.g.* L-type CaChs and NCX. Both these effects should induce an increase in $[Ca^{2+}]_i$ rather than a decrease in $[Ca^{2+}]_i$ (Lin *et al.*, 1994; Gross *et al.*, 1990). However, the complex regulatory network of kinases and phosphatases might provide an explanation for the observed reduction in the DA-induced increase in $[Ca^{2+}]_i$ upon inhibition of PP1 and PP2A. Both phosphatases are involved in DARPP-32 signaling pathways. Phosphorylation at Thr75 converts DARPP-32 into a potent inhibitor of PKA. Dephosphorylation of DARPP-32 by PP2A counteracts this modulation. Thus, PP2A indirectly controls PKA activity. If PP2A is blocked by calyculin A, the phosphorylated form of DARPP-32-Thr75 dominates, thus

driving inactivation of PKA. If now D1Rs are activated by DA, D1R-driven activation of PKA must counteract DARPP-32-driven inhibition. If the D1R/PKA-mediated phosphorylation of L-type CaChs is already reduced by DARPP-32-driven inhibition of PKA, a calyculin A-induced blockade of dephosphorylation might not profoundly amplify the increase in Ca^{2+}-flux through L-type CaChs. Coming from this standpoint, the interpretation from Surmeier and colleagues might need to be rethought. As the authors blocked PP1 and PP2A by okaidic acid, they also favored the inhibition of PKA through PP2A inhibition. If one now assumes that PKA activity in their cells was quite high, the PP2A-induced inhibition of PKA might result in less phosphorylation and thus a closure of N-type CaChs. However, to elucidate the role of phosphatases PP1 and PP2A, DARPP-32 and N-type CaChs in DA-induced increases in $[Ca^{2+}]_i$, further experiments with well-chosen agonists and antagonists have to be conducted.

Alternative pathways. There were a number of results indicating that the DA-induced increase in $[Ca^{2+}]_i$ might also be mediated by alternative pathways. First, I found that some cells (38%) responding to DA with an increase in $[Ca^{2+}]_i$ did not respond to stimulation with the D1R-specific agonist SKF38393 (3.3.2.1). Second, I found a small number of cells in which blockade of D1Rs by SCH23390 did not abolish the response to DA (3.3.2.1). Third, I found a few cells that despite the blockade of PKA by H89 responded to DA with an increase in $[Ca^{2+}]_i$ (3.3.3.3). Fourth, in experiments with the SERCA-inhibitor CPA I found that release of Ca^{2+} from the ER might contribute to the DA-induced increase in $[Ca^{2+}]_i$ in some cells of the increase type (3.3.4.1). From literature it is known that the emptying of intracellular Ca^{2+} stores activates Ca^{2+} influx through ion channels in the plasma membrane. This mechanism is called store-operated Ca^{2+} entry (SOCE) (for review see Parekh and Putney Jr., 2005). Thus, blockade of SERCA might prevent the DA-induced SOCE in some neurons of the increase type. This could explain why I did not detect a DA-induced increase in $[Ca^{2+}]_i$ in the absence of external Ca^{2+}: there were no external Ca^{2+} ions available that could enter into the cytoplasm after induction of SOCE. Although Ca^{2+} was withdrawn from the extracellular solution, I would have still expected to observe a minimal increase in $[Ca^{2+}]_i$ upon stimulation with DA, as this should induce a release of Ca^{2+} from internal stores. However, this was not the case. The finding that nimodipine inhibited the DA-induced increase in $[Ca^{2+}]_i$ in most of the cells is hard to explain in the context of SOCE as L-type CaChs are not CaChs typically involved in SOCE (for review see Parekh and Putney Jr., 2005). However, CPA-evoked Ca^{2+}-release from internal stores might trigger the modulation of L-type CaChs via the

activation of CaM-kinase (CaMK) (Zühlke *et al.*, 1999). The finding that release of Ca^{2+} from internal stores might cause the increase in $[Ca^{2+}]_i$ in some cells of the increase type is supported by the finding that inhibition of PLC by U73122 reduced the response to DA in some cells of the increase type (3.3.4.2). At least two alternative pathways whose activation results in an increase in $[Ca^{2+}]_i$ independent of the cAMP/PKA cascade are known in literature (for review see Neve *et al.*, 2004). One such alternative pathway might be the activation of DR hetero-oligomers (D1R-D2R) and the other the activation of a novel SCH23390-binding receptor which both have been proposed to be linked to PLC-signaling (Lee *et al.*, 2004; Chun *et al.*, 2013; Undie and Friedman, 1990; for review see Neve *et al.*, 2004). Both alternative pathways are blocked by SCH23390 (Undie and Friedmann, 1990; Lee *et al.*, 2004). Hence, this would argue against contribution of these pathways to the increase in $[Ca^{2+}]_i$. In my experiments I found cells that in the presence of SCH23390 still responded to DA stimulation with an increase in $[Ca^{2+}]_i$ (3.3.2.1). Amongst others, this finding led to the assumption that there must be an alternative pathway for the DA-induced increase in $[Ca^{2+}]_i$ (see above).

4.1.2.2. The origin of the DA-induced decrease in $[Ca^{2+}]_i$ is still undefined

The interpretation of the results obtained for cells of the decrease type is even more difficult. In order to identify the DR type mediating this DA-induced decrease in $[Ca^{2+}]_i$, I made use of specific DR agonists and antagonists. I can rule out that activation of D1Rs is responsible for the decrease in $[Ca^{2+}]_i$ as blockade of D1Rs with SCH23390 did not abolish the response to DA and stimulation with the D1R-specific agonist SKF38393 never elicited a decrease in $[Ca^{2+}]_i$ (3.3.2.1). The results obtained for the role of D2Rs were contradicting: blockade of D2Rs with eticlopride did not abolish the response to DA but stimulation of D2Rs with the specific agonist quinpirole induced a decrease in about 52% of cells (3.3.2.2). This quinpirole-induced decrease in $[Ca^{2+}]_i$ was exclusively found in cells of the decrease type. However, there were also 26% of cells that responded to DA stimulation with a decrease in $[Ca^{2+}]_i$ but were not affected by quinpirole application (3.3.2.2). Thus, it will need further experiments to identify the DR-type responsible for the DA-induced decrease in $[Ca^{2+}]_i$.

A decrease in $[Ca^{2+}]_i$ can be caused by different mechanisms: by closure of CaChs in the plasma membrane, by enhancing Ca^{2+}-export via exporters or by sequestration of Ca^{2+} ions into internal Ca^{2+}-stores. I found that blockade of L-type channels (3.3.3.2) or inhibition of Ca^{2+}- influx (3.3.3.1) mimicked the effects of DA in cells of the decrease

type. However, the results are not as clear as expected and can be explained in two different ways at least. First, the activation of DRs might induce a closure of L-type CaChs resulting in decrease in $[Ca^{2+}]_i$. Second, the blockade of Ca^{2+}-influx into these cells might reduce $[Ca^{2+}]_i$ to its minimum level making the observation of a further DA-induced decrease in $[Ca^{2+}]_i$ impossible. If one assumes that DA triggers the closure of L-type CaChs, this might be achieved by reduced phosphorylation of these channels. In the classical pathway, a D2R-mediated decrease in PKA activity might account for this reduction in phosphorylation of L-type CaChs. Indeed, I found in some cells of the decrease type that application of the PKA inhibitor H89 reduced basal $[Ca^{2+}]_i$ and abolished the DA-triggered decrease in $[Ca^{2+}]_i$ indicating that inhibition of PKA might be the reason for the DA-induced decrease in $[Ca^{2+}]_i$ (3.3.3.3). This finding would presuppose that basal PKA-activity is quite high in these cells. A high PKA activity might also be the explanation for the finding that cells of the decrease type exhibit a higher $[Ca^{2+}]_i$ than cells of the increase type (3.3.1). If these assumptions were true, I should have found two things: a DA-induced decrease in YFP/CFP of neurons expressing AKAR4 (provided that this group of cells can be transfected by lipofectamine) and a stronger nimodipine-induced reduction in $[Ca^{2+}]_i$ in cells of the decrease type when compared to cells of the increase type. However, I never observed a decrease in PKA activity when I stimulated neurons that expressed AKAR4 with DA or quinpirole alone (3.2.2.3) and I did not find a difference in the nimodipine-induced decrease in $[Ca^{2+}]_i$ between cells of the increase type and cells of the decrease type (3.3.3.2).

On the other hand, in the other half of neurons of the decrease type I found that blockade of PKA did not abolish the DA-induced decrease in $[Ca^{2+}]_i$ (3.3.3.3). This can again be explained in two different ways at least: either H89 did not completely block PKA making it possible to detect a further DA-induced reduction in PKA-activity resulting in a decrease in $[Ca^{2+}]_i$ or PKA is not involved in this particular DA-induced pathway and the decrease in $[Ca^{2+}]_i$ is mediated by alternative pathways. One of these alternatives might involve the activation of DR heterodimers leading to the activation of the PLC/PKC-cascade and thus to phosphorylation and modulation of other downstream targets such as PMCA (for review see Carafoli, 1991) or NCX (Soma *et al.*, 2009) resulting in an increased Ca^{2+}-export. If this were the case, I would expect that blockade of PLC reduces the response to DA. However, in experiments with the PLC-inhibitor U73122 I found that blockade of PLC enhanced rather than reduced the DA-induced decrease in $[Ca^{2+}]_i$ (3.3.4.2). Another alternative pathway might be the modulation of downstream

targets via the Gβγ subunit that is released by receptor activation of $G\alpha_i$-linked proteins (for review see Neve *et al.*, 2004). It has been shown that L-type CaChs in striatal medium spiny neurons are modulated via a Gβγ-induced activation of PLC, the release of Ca^{2+} from internal stores and thus the activation of the Ca^{2+}-regulated phosphatase calcineurin (Hernández-López *et al.*, 2000). However, in experiments with the Gβγ-antagonist gallein I did not find significant changes in the response of cells of the decrease type indicating that Gβγ is not involved in the generation of DA-induced changes in $[Ca^{2+}]_i$ (3.3.3.5).

If the decrease in $[Ca^{2+}]_i$ were caused by a sequestration of Ca^{2+} into internal stores such as the ER blockade of SERCA in store-depletion experiments (3.3.4.1) should block the DA-induced decrease in $[Ca^{2+}]_i$. In contrast, the DA-induced decrease in $[Ca^{2+}]_i$ was amplified when SERCA was blocked by CPA. One might expect that if $[Ca^{2+}]_i$ was increased by store-operated-Ca^{2+}-entry (SOCE), extrusion mechanisms via NCX or PMCA were elevated. Indeed, it has been shown that SOCE and Ca^{2+}-extrusion are intermingled mechanisms. Bautista and colleagues found that PMCA activity was increased after a rise in $[Ca^{2+}]_i$ and only slowly recovered from modulation (Bautista *et al.*, 2002). However, the underlying signaling pathways resulting in a decrease in $[Ca^{2+}]_i$ are far from solved and need further experiments investigating the role of pumps and exchangers in the plasma membrane.

4.2. Application of genetically encoded sensors *in vivo*

4.2.1. Expression of FRET-based biosensors in the intact retina

In this study, virally mediated gene transfer was applied to express FRET-based biosensors in the intact retinal tissue. In previous work it was demonstrated that amongst all tested serotypes AAV2 was best suited for the *in vivo* application as it exhibited the highest transduction efficiency and targeted a variety of retinal neurons in all major cell classes (own observations; see also Zhao, 2015). In my study I investigated AAV2-GFP-injected retinae via immunohistochemistry. I found that AAV2 targeted cell types in the inner and outer retina that are known to be affected by dopaminergic modulation such as PRs and AII ACs (3.4.2.2). Thus, I judged AAV2 to be the serotype of choice for the transfer of sensor DNA to target neurons of dopaminergic signaling.

AAVs have been successfully applied in the retina in order to restore vision in different mouse models of blindness by delivering channelrhodopsin 2 to ON-BCs (Dorouchi *et al.*,

2011) or ACs and GCs (Bi *et al.*, 2006). Despite these successful applications of AAVs in the intact retina, AAV2-mediated expression of the EPAC1-camps sensor was not successful in my experiments (3.4.3.2). Based on the fluorescence of EPAC1-camps, only few neurons could be detected in wholemounts of infected retinae. Staining with an antibody against GFP revealed a higher number of EPAC1-camps-expressing neurons. Only some of these EPAC1-camps-expressing neurons had a free nucleus which was found to be an indicator for the functional expression of the sensor (3.4.3.1). Based on these results, I could not conduct imaging experiments using EPAC1-camps in the retina. Interestingly, as to my knowledge there are no publications using AAV-mediated expression of FRET-based sensors in the intact retina. Either this lack of data reflects the low number of studies that apply FRET-based sensors in the intact retina or it is due to problems in the expression of virally introduced FRET-sensors. There are a few papers about viral expression of FRET-based sensors in neurons in the brain. Mironov and colleagues illustrated that EPAC1-camps is expressed in the pre-Bötzinger complex after viral transduction with AAV (Mironov *et al.*, 2009). Unfortunately, they did not mention which AAV serotype they used. The same holds true for a publication that showed expression of a virally delivered AKAR sensor into the striatum of a transgenic mouse (Chen *et al.*, 2014a) or another report about the expression of a FRET-based voltage sensor in dendrites of Purkinje neurons after AAV-injection (Gong *et al.*, 2014). All three papers conducted proof-of-principle experiments which verified the functionality of the sensors but did not investigate beyond that.

In 2004, Matsuda and Cepko described an alternative approach for gene-transfer into the retina *in vivo* (Matsuda and Cepko, 2004). When a GFP expression vector driven by the cytomegalovirus-actin-globin hybrid (CAG) promoter was electroporated into the retina on postnatal day 0 (P0) using 80 V pulses, an average of ~80% of the electrofected rat retinae and ~50% of electrofected mouse retinae expressed GFP. In a good transfection, GFP expression was observed in a wide area of the retina (Matsuda and Cepko, 2004). In preliminary electroporation experiments (3.4.4) I found that a voltage of 100 V yields a better transfection-efficiency in retinae of mouse pups (P5-7) that were electroporated with cDNA coding for a CMV-driven GFP. Critical parameters for efficient electrofection are the concentration of DNA that is injected, the promoter that controls expression, targeting of the DNA to the specific location in the eye and placement of the tweezer electrodes (for review see Venkatesh *et al.*, 2013). Due to restriction in DNA preparation, I could only use a DNA concentration of 1.8 µg/µl in my

experiments. This was significantly lower than the concentrations used by Matsuda and Cepko who injected DNA solution of 3~6 µg/µl (Matsuda and Cepko, 2004) and may be one parameter worth to test in future experiments. However, as I obtained robust expression in one retina that was injected with this low DNA concentration, this parameter cannot be the only reason for the relatively low number of successfully electrofected retinae.

Another alternative approach for the expression of FRET-based sensors in the intact tissue is the application of transgenic mouse lines. The Lohse group generated a transgenic mouse line (CAG-Epac1-camps) that exhibited EPAC1-camps expression in almost all tissues, *e.g.* the eye, skin, brain, heart, kidney, and ileum (Calebiro *et al.*, 2009). I investigated retinae of this transgenic mouse line using immunohistochemistry with antibodies against GFP (data not shown). Due to three reasons this transgenic mouse was not suitable for my project: first due to their genetic background, the mice exhibited a retinal degeneration – they lacked PRs. Second, the strong expression of EPAC1-camps in Müller cells would make it almost impossible to identify and measure single neurons that are relevant for my project. Third, the expression of EPAC1-camps in neurons was quite low. The transgenic mouse approach would therefore only make sense if EPAC1-camps expression in neurons is high and expression is restricted to specific cell populations by using cell type-specific promoters.

4.2.2. Cell-specific expression of sensor proteins

One of my aims was to visualize DA release from dopaminergic ACs in the intact retina. In order to do so, the sensor synapto-pHluorin had to be specifically expressed in dopaminergic ACs, the only retinal cell type positive for the enzyme tyrosine hydroxylase (TH) (Nguyen-Legros, 1988). Thus, cell type specific-expression should be achieved by controlling the expression of synapto-pHluorin by the TH promoter. From immunocytochemical studies of HEK293 cells and cultured retinal neurons that were transfected with a control plasmid and a plasmid that would drive GFP expression under the TH promoter (pcTH-EGFP) I concluded that the promoter construct pcTH-EGFP yielded a more restricted expression level when compared to the control construct (3.4.1). However, after Lipofectamine-transfection I only found GFP expression in TH-negative neurons in my culture system, indicating that the TH promoter did not restrict expression to dopaminergic cells.

Another method for the cell type specific expression of sensor proteins would be the

generation of transgenic mouse models. Regarding the expression of synapto-pHluorin it was demonstrated that this sensor can specifically be expressed in presynaptic terminals of sensory neurons in glomeruli of the olfactory bulb using a cell-specific promoter (Bozza *et al.*, 2004). Furthermore, Araki and co-workers generated six transgenic mouse lines in which synapto-pHluorin was expressed under the control of the *Thy1* promoter (Araki *et al.*, 2005). In order to express proteins specifically in dopaminergic neurons, three research groups generated transgenic mouse lines using the rat promoter of the TH gene (Gustincich *et al.*, 1997; Matsushita *et al.*, 2002; Zhang *et al.*, 2004). In the retina of these TH-transgenic mice two types of ACs were identified expressing the respective reporter protein: type 1, which was large and positive for TH and type 2, which was smaller than type 1 and negative for TH (Gustincich *et al.*, 1997; Zhang *et al.*, 2004; Knop *et al.*, 2011). Thus, generating a transgenic mouse line that expresses synapto-pHluorin under the control of the TH promoter might be an interesting approach for future studies of DA release in the retina but it is difficult to speculate about the specificity of sensor protein expression in these models.

4.2.3. AAV troubleshooting

In order to express synapto-pHluorin in dopaminergic ACs in the retina, I tested whether AAV2 is suitable to transduce this specific cell type. Unfortunately, in all retinae investigated AAV2 never targeted dopaminergic ACs although neighboring cells were infected (3.4.2.3).

Different AAV serotypes vary in their tropism. This difference in tropism is *inter alia* based on the interaction of the virus capsid with cell surface receptors (for review see Wu *et al.*, 2006). For AAV2 it has been demonstrated that heparin sulfate proteoglycans mediate both AAV2 attachment to and infection of target cells (Summerford and Samulski, 1998). Amongst others, Müller cells are transduced by AAV2 (Fig. 3.4.8) which may be due to the expression of heparin sulfate proteoglycan as it has been demonstrated for immortalized cultured Müller cells from rat (Liang *et al.*, 2003). To my knowledge there are no data whether dopaminergic ACs in the retina possess heparin sulfate proteoglycans on their cells surface and may thus be targets for transduction by AAV2. However, the binding to specific cell surface receptors is not the only critical step determining the tropism of a given AAV serotype. Other factors include cellular uptake, intracellular processing, nuclear delivery of vector genomes, uncoating, and second-strand DNA conversion (for review see Wu *et al.*, 2006). Although AAV2 has been tested

to yield high efficient transduction in the *in vivo* retina (Fig. 3.4.8; Zhao, 2015), it may be worth to investigate the suitability of genetically modified viruses (Petrs-Silva *et al.*, 2008) in regard to the infection of dopaminergic ACs in the intact retina. The usage of serotypes different from AAV2 did not yield high transduction efficiencies in intact mouse retina (own observations; see also Zhao, 2015).

The problems encountered in the AAV2-mediated expression of EPAC1-camps in retinal neurons *in vitro* and *in vivo* are quite difficult to interpret. I could demonstrate that transduction of HEK293 cells with AAV2-EPAC1-camps resulted in a functional sensor that monitored NA-induced changes in $[cAMP]_i$. In addition, control experiments with using AAV2 to express the Ca^{2+}-sensor GCaMP3.0 resulted in functional sensor protein (3.4.3.2). A major limitation of AAVs is their cargo capacity which is limited to ~4.7 kb (for review see Trapani *et al.*, 2014). However, the cDNA of EPAC1-camps has a size of ~1.9 kb (Börner *et al.*, 2011), the CMV promoter of 0.63 kb. Thus, the cDNA of EPAC1-camps should fit into the AAV capsid. For future experiments it is therefore questionable whether it is worth to test for viral expression of AKAR4 (~ 2 kb).

4.3. DA modulates $[Ca^{2+}]_i$ in GCs of the intact retina

For the studies of dopaminergic regulation of $[Ca^{2+}]_i$ in GCs of the retina I used the transgenic mouse line TN-L15 (Heim *et al.*, 2007). Expression of the TN-L15 sensor is driven by the *Thy1* promoter (Heim *et al.*, 2007), which has also been used for other transgenic mouse lines (Chen *et al.*, 2012; Asrican *et al.*, 2013; Araki *et al.*, 2005). In the retina of the TN-L15 mouse line, sensor expression is found in about 80% of GCs and in a few ACs. Immunohistochemical analysis of cryosections of the TN-L15 retina revealed that TN-L15 is expressed in ON- and OFF-GCs which could be identified due to their stratification pattern in the IPL (F. Müller, personal communication). In my studies I could show that DA changes $[Ca^{2+}]_i$ in TN-L15-positive GCs, that specific responses can be correlated to distinct types of GCs, and that the observed responses are due to the action of DA directly at the GCs as well as in the retinal network.

4.3.1. GCs of the decrease type

4.3.1.1. Are GCs of the decrease type ON-alpha-GCs?

In chapter 3.4.5 I described that a subpopulation of TN-L15-positive GCs responded to DA application with a decrease in $[Ca^{2+}]_i$. These GCs were quite rare, were the largest

amongst other TN-L15-positive GCs and exhibited the highest $[Ca^{2+}]_i$ at the beginning of the measurements. In the following I will discuss that these cells could represent the ON-alpha-GCs that in mouse are also intrinsically photosensitive.

Morphological characterization of GCs in other studies. The mammalian retina comprises a variety of GC types that have been identified by their electrophysiological or morphological characteristics (stratification pattern, receptive field or soma size). Morphological classification led to different numbers of GC types. Using a horseradish peroxidase assay, Doi and colleagues classified GCs of the mouse retina into three types: type 1 cells exhibited a large soma and large dendritic field, type 2 cells had a small-to-medium soma and a small dendritic field and type 3 cells exhibited a small-to-medium soma and a large dendritic field. Each type was further subdivided according to the termination level of dendrites in the IPL and the dendritic branching pattern (Doi *et al.*, 1995). Another survey of morphological distinct types of mouse retinal GCs was conducted in 2002. Using the DiOlistic method, GCs were classified into four groups based on soma size, dendritic field size, pattern and level of stratification (Sun *et al.*, 2002). Monostratified cells were classified into three groups: RG_A with large somata and large dendritic fields, RG_B with small to medium-sized somata and small to large dendritic fields and RG_C with small to medium-sized somata and medium-sized to large dendritic fields. Bistratified cells were classified as RG_D (Sun *et al.*, 2002). Comparison of the Sun study with the Doi study revealed that subtype 1 of type 1 (Doi *et al.*, 1995) is qualitatively similar to RG_{A2} from the Sun study and that subtype 2 of type 1 (Doi *et al.*, 1995) is similar to RG_{A1} (Sun *et al.*, 2002). In 2005, Kong and colleagues published a study using a combination of different methods to identify GC types in the mouse retina (Kong *et al.*, 2005). They came up with 13 types of GCs classified on the basis of the level of stratification, extent of the dendritic field and the density of branching. In another study, examination of the coupling pattern of different GC subtypes in the dark-adapted mouse retina by injection with neurobiotin led to the identification of 22 morphologically distinct GC populations (Völgyi *et al.*, 2009). Völgyi and co-workers identified G_1 GCs that displayed a large soma diameter of about 21 µm, one of the largest dendritic arbors and stratification in the ON-sublamina. These G1 GCs showed strong homology with mouse GCs described in the studies mentioned above, including RG_{A1} cells (Sun *et al.*, 2002) and cells of cluster 11 (Kong *et al.*, 2005).

Alpha GCs. Based on their large soma size (3.4.5.2.1; Fig. 3.4.22) and their low frequency (3.4.5.2; Fig. 3.4.21), GCs of the decrease type found in the present study may reflect RG_A cells (Sun *et al.*, 2002), which in the Doi study are classified as type 1 GCs (Doi *et al.*, 1995). Sun and colleagues argued that RG_A cells are equivalent to alpha cells, which are found in retinae of all twenty species examined by Peichl and colleagues (Peichl *et al.*, 1987). Alpha cells characteristically have the largest somata and large dendritic fields and make up 2-4% of the GC population in rat retina (for review see Peichl, 1991). The relative frequencies of decrease type GCs obtained in the present study were variable (5-9%), thus making a comparison with the frequencies for alpha-GCs determined in other studies (Peichl, 1991; Sun *et al.*, 2002; Kong *et al.*, 2005) difficult. Things become even more complicated as only 80% of GCs in the retina of the transgenic mouse line express TN-L15 (F. Müller, personal communication). However, it seems as if the relative frequency between 5% and 9% found for decrease type GCs in the present study was in the same range as found for alpha-GCs by others (Peichl, 1991; Sun *et al.*, 2002).

ON-alpha-GCs. Alpha-GCs can further be subdivided in ON- and OFF-alpha-GCs (Peichl, 1987). Pang and colleagues found three types of alpha-GCs in the mouse retina: ON-alpha-GCs, transient OFF-alpha-GCs and sustained OFF-alpha-GCs (Pang *et al.*, 2003). Cells of the decrease type were found to respond to L-AP4 with a decrease in $[Ca^{2+}]_i$ indicating that they are ON-GCs (3.4.5.2.2). In 2007, Mataruga and colleagues found a HCN2-positive GC that accounted for less than 3% of the GCs and exhibited the largest somata found in the GCL (Matargua *et al.*, 2007). In agreement with the studies from Mataruga and colleagues, I found large HCN2-positive GCs that expressed TN-L15 (3.4.5.2.1; Fig. 3.4.23). However, these TN-L15/HCN2-positive GCs were larger than GCs of the decrease type (3.4.5.2.1). Besides that, there were also large TN-L15-positive GCs that were not labeled by the HCN2 antibody. Based on the soma size and stratification level, Mataruga and colleagues concluded that these HCN2-positive OFF-GCs might correspond to the RG_{A2}-GCs identified by Sun and colleagues (Sun *et al.*, 2002). On the assumption, that RG_A cells are equivalent to alpha-GCs (Sun *et al.*, 2002) and that GCs of the decrease type are ON-GCs, my findings can be interpreted as follows: $HCN2^+$/TN-$L15^+$ GCs might represent OFF-alpha-GCs whereas the $HCN2^-$/TN-$L15^+$ GCs might be ON-alpha-GCs.

Intrinsically photosensitive GCs. ON-alpha-GCs of the mouse retina exhibit no spike activity in darkness, an increase in spiking in light and a sustained light-evoked inward

cation current (Pang *et al.*, 2003). In 2011, Margolis and colleagues illustrated that at light onset dendritic $[Ca^{2+}]_i$ in ON-alpha-GCs increased (Margolis *et al.*, 2011). Furthermore, in mouse retina ON-alpha-GCs have been brought into association with the group of intrinsically photosensitive GCs (ipGC) (Estevez *et al.*, 2012; Hu *et al.*, 2013) which in total comprises five morphologically distinct types (M1-M5) (Berson *et al.*, 2010; Hu *et al.*, 2013). ON-alpha-GCs are identified as type M4 ipGC which exhibit an average soma diameter of 21±0.4 µm and smaller melanopsin-based intrinsic photocurrents compared to other ipGCs (Estevez *et al.*, 2012). Immunohistochemically, melanopsin can only be detected with strong amplification in M4 cells (Estevez *et al.*, 2012). These physiological properties of ON-alpha-GCs might be the explanation for the high starting $[Ca^{2+}]_i$ I found in cells of the decrease type GCs (3.4.5.2.1) as my experiments were conducted using 1-photon excitation at a wavelength of 420 nm (2.7.4.). Because retinae were prepared at ambient room light levels, rhodopsin was most likely bleached during the preparation procedure. Hence, it is unlikely that rods contribute much to the light response during the imaging experiments. However, cone-mediated light responses can be recorded from GCs of retinae prepared under these conditions (F. Müller, personal communication). Blue cone opsins (for review see Bowmaker, 1998) and melanopsin (Hankins *et al.*, 2008) absorb at the excitation wavelength (420 nm; 2.7.4.4). Besides the excitation light there is also emission light from the two fluorophores, albeit much weaker in intensity: CFP mostly emits in the range of 460 to 530 nm and YFP in the range of 520 to 550 nm (Fluorescence SpectraViewer, Thermo Fisher Scientific) which are wavelengths that can be detected by all types of PRs and the ipGCs. Stimulation of melanopsin activates a PLC/transient receptor potential channel (TRP)-channel cascade resulting in depolarization of the cell membrane and an increase in $[Ca^{2+}]_i$ of ipGCs (for review see Hankins *et al.*, 2008 and Davies *et al.*, 2012). Thus, it is reasonable to assume that the GCs of the decrease type responded to the excitation light of 420 nm resulting in Ca^{2+} influx.

Interestingly, it has been demonstrated that DA attenuates the photocurrent in ipGCs via activation of D1Rs in rat retina (Van Hook *et al.*, 2012) probably leading to phosphorylation of melanopsin by PKA (Blasic *et al.*, 2012). Thus, the observed DA-induced decrease in $[Ca^{2+}]_i$ in cells of the decrease type in the TN-L15 retina might reflect the D1R/PKA-mediated attenuation in Ca^{2+}-influx through TRP-channels. Melatonin is a neuromodulator that is released by PRs. In contrast to DA, it is assumed to play a central role in dark-adaptation by *e.g.* enhancing the input from rods to rod BCs or

to increase light-sensitivity of HCs (for review see Wiechmann and Sherry, 2013). Melatoninergic and dopaminergic systems are intermingled: DA suppresses melatonin synthesis in light while melatonin suppresses DA synthesis in darkness (for review see Huang *et al.*, 2013). In this aspect, it is quite interesting that M4-type ipGCs (ON-alpha-GCs) are also modulated by melatonin, albeit in the opposite direction than DA does (Pack *et al.*, 2015).

Evidence for a direct action of DA on GCs also comes from other studies. In 1994, two groups demonstrated that DA affects Ca^{2+}-currents in isolated GCs (Liu and Lasater, 1994; Guenther *et al.*, 1994). These electrophysiological findings were supported by Ca^{2+}-imaging experiments conducted in isolated GCs that showed a DA-mediated increase in $[Ca^{2+}]_i$ (Ogata *et al.*, 2012). Others found a D1R-mediated reduction of retinal GC-excitability in dissociated GCs of the mouse retina (Hayashida *et al.*, 2009) as well as a D1R-mediated reduction in photocurrent in isolated ipGCs of rats (Van Hook *et al.*, 2012).

4.3.1.2. Is the DA-triggered decrease in $[Ca^{2+}]_i$ in GCs due to a network response?

Using a pharmacological approach blocking either the excitatory (glutamatergic) input from BCs or the inhibitory (GABAergic/glycinergic) input from ACs, I attempted to find out whether DA exerts it´s effects at the GC itself, in the retinal network or both.

Glutamatergic input. Cells of the decrease type responded to DA either in a transient or in a sustained fashion (Fig. 3.4.20). In the experiments in which glutamatergic transmission was inhibited (3.4.5.3.1), the blockers were applied after the first application of DA (Table 3.4.1). In cells of the transient decrease type, by this time, $[Ca^{2+}]_i$ had mostly recovered back to baseline. Blockade of the glutamatergic input from BCs via CNQX and D-AP5 resulted in a decrease in $[Ca^{2+}]_i$. In the presence of these blockers, $[Ca^{2+}]_i$ could not be further reduced, leading to the suspicion that in these GCs the DA-induced decrease in $[Ca^{2+}]_i$ is mediated via the modulation of the glutamatergic input from BCs. In cells of the sustained decrease type, the role of the glutamatergic input remains elusive as blockade by CNQX and AP5 did not elicit any Ca^{2+}-response in these cells. However, as $[Ca^{2+}]_i$ barely recovered in these cells, it cannot be ruled out that $[Ca^{2+}]_i$ was already at minimum after the application of DA so that a further reduction in $[Ca^{2+}]_i$ triggered by either the blocker cocktail or a second application of DA could not be detected. However, these findings have to be interpreted with caution as the number of

analyzed neurons was quite low.

On the assumption that GCs of the decrease type are ON-GCs (3.4.5.2.2), the DA-induced decrease in $[Ca^{2+}]_i$ can be explained in different ways. It has been shown that ON-alpha-GCs receive glutamatergic (excitatory) input from BCs and inhibitory input from ACs (Pang *et al.*, 2003; Freed and Sterling, 1988). To my knowledge distinct presynaptic partners have not been identified for the mouse retina to date. However, from the stratification of ON-alpha-GCs in the IPL (71%-77% of IPL depth; Völgyi *et al.*, 2005) one might assume that they receive input from type 6, 7, and 8 BCs that all stratify at this level of the IPL (Ghosh *et al.*, 2004). Interestingly, it has been demonstrated that type 6 and 7 ON-BCs express D1Rs (Farshi *et al.*, 2015; Usai, 2014). In tiger salamander retina activation of D1Rs modulates sodium channels as demonstrated for transient ON-BCs (Ichinose and Lukasiewicz, 2007). If this holds true for mammalian BCs, too, it could in turn reduce the release of glutamate from BCs resulting in a decrease in $[Ca^{2+}]_i$ in ON-alpha-GCs. From my studies in retinal cultured neurons I assumed that DA modulates L-type CaChs resulting in an alteration of Ca^{2+}-flux through the plasma membrane (3.3.3.2). Thus, a reduction in glutamate release from the BC could also be caused by a DA-induced modulation of L-type CaChs leading to a reduction in $[Ca^{2+}]_i$ and, thus, a decrease in glutamate release. However, there is also another explanation for the DA-induced decrease in glutamatergic input from BCs. In my Ca^{2+}-imaging studies in the retinal culture, which most likely harbors ACs, I found a number of cells that responded with a DA-induced decrease in $[Ca^{2+}]_i$ (3.3.1.). Although the underlying pathway could not be fully deciphered in the present study, some evidence suggests that this decrease in $[Ca^{2+}]_i$ may partly be due to the activation of D2Rs (3.3.2.2.). For rat retina it has been shown that D2Rs are - besides the D2-autoreceptor in dopaminergic ACs - found in the IPL and in cells amongst the AC layer (Derouiche and Asar, 1999). This finding is in agreement with immunohistochemical studies conducted in mouse (Usai, 2014) and by Wagner and colleagues in different species (Wagner *et al.*, 1993). If one assumes that DA via D2Rs induces a decrease in $[Ca^{2+}]_i$ in ACs that are electrically coupled to ON-BCs, this could in turn result in a reduction in glutamate release from the ON-BCs and thus a decrease in glutamatergic input to the GC.

Inhibitory input. In one group of decrease type GCs (3.2%) blockade of the inhibitory input seemed to abolish the DA-induced decrease in $[Ca^{2+}]_i$ while cells of the other group (5.6%) still responded to DA in the presence of the inhibitor cocktail (3.4.5.3.2). Unfortunately, it was impossible to assign one of the two groups to the transient

decrease type or the sustained decrease type.

The glycinergic AII ACs have been shown to be modulated by DA via the activation of D1Rs (for review see Witkovsky, 2004). In addition, it has been demonstrated that they express L-type CaChs at their output synapses (Habermann *et al.*, 2003) which are important for the glycinergic synaptic inputs to GCs (Bieda and Copenhagen, 2004). Glycinergic ACs were found to stratify in all sub-layers of the IPL (Menger *et al.*, 1998; Haverkamp and Wässle, 2000). In Fluo-4 experiments I have shown that DA induced an increase in $[Ca^{2+}]_i$ in some neurons of my culture system. This DA-induced increase in $[Ca^{2+}]_i$ was partly due to a D1R-mediated modulation of L-type CaChs (3.3.3.2). Thus, one might assume that in the intact TN-L15 retina stimulation of D1Rs induces an increase in $[Ca^{2+}]_i$ in ACs, an increase in glycine release from their output synapses and thus an inhibition of the postsynaptic GC. This would be in line with the observation that blockade of the inhibitory input abolished the DA-induced decrease in $[Ca^{2+}]_i$ in a small population of GCs (3.4.5.3.2).

From the results discussed above it may be speculated that the population of cells of the decrease type encompasses two different cell types. Both cell types would have in common that they exhibit a high YFP/CFP starting ratio at the beginning of the measurement, respond to DA stimulation with a decrease in $[Ca^{2+}]_i$ and are the largest cells amongst the TN-L15-positive GCs (3.4.5.2). The following observations support the idea that two distinct cell types might belong to the group of decrease type GCs: First, in one group of cells the DA effect was short lasting and mostly reversible (Fig. 3.4.20 C, bottom; transient decrease type), while in the second group of cells, the DA-mediated decrease in $[Ca^{2+}]_i$ was long lasting and a recovery was barely observed (Fig. 3.4.20 C, top; sustained decrease type). Second, on the basis of this differentiation, I found differences between these two groups of cells in L-AP4 experiments. The cells of the transient decrease type responded with a decrease in $[Ca^{2+}]_i$ upon stimulation with L-AP4, whereas L-AP4 did not elicit a change in $[Ca^{2+}]_i$ in cells of the sustained decrease type. As both groups of cells exhibited an “overshoot”-like increase in $[Ca^{2+}]_i$ after washout of L-AP4, I assumed that both types of cells represent ON-GCs (3.4.5.2.2). Third, blockade of the glutamatergic input reduced $[Ca^{2+}]_i$ in cells of the transient decrease type while it did not affect $[Ca^{2+}]_i$ in cells of the sustained decrease type (3.4.5.3.1). However, I cannot rule out that this difference is owed to the fact that cells of the sustained decrease type were already at minimum $[Ca^{2+}]_i$ so that a further decrease induced by the glutamatergic blocker cocktail could not be detected. Fourth, I found that

blockade of the inhibitory input abolished the DA-induced response in one group of cells of the decrease type while the other group of cells still responded to DA stimulation (3.4.5.3.2). In the case that two distinct cell types could be assigned to the group of decrease type GCs, only one of them might represent the M4 ipGC/ON-alpha GC I discussed in the previous chapter.

It needs further experiments to substantiate the suspicion that the group of decrease type GCs harbors two distinct cell types. First, it has to be investigated whether cells of the transient decrease type and cells of the sustained decrease type can be morphologically discriminated (soma size, dendritic tree, stratification level). This may be achieved by filling the cells with fluorescent dyes after recording their DA-induced Ca^{2+}-responses. Second, it has to be tested whether the assumptions made from the L-AP4 experiments can be verified electrophysiologically. This may be achieved by a combination of TN-L15 imaging and electrophysiological recordings of large TN-L15-positive GCs. Finally, using the knowledge obtained from the experiments suggested above, it needs to be investigated whether there is a correlation between the GC type and the type of response triggered in blocker experiments.

4.3.2. GCs of the increase type

4.3.2.1. Are GCs of the increase type W3 GCs?

The response most often found in TN-L15-positive GCs upon stimulation with DA was an increase in $[Ca^{2+}]_i$ (3.4.5.1; Fig. 3.4.21). These cells exhibited the smallest soma radius (Fig. 3.4.22) amongst all other response types.

Based on the soma size, GCs of the increase type may represent type II subtype 2 and/or type III subtype GCs in the Doi study (Doi *et al.*, 1995) and type RG_B and/or type RG_C GCs in the Sun study (Sun *et al.*, 2002). In the study of Völgyi and colleagues two types of small soma GCs were identified: G_5 GC, which stratifies in the inner half of the IPL, most likely being an ON-GC, and the quite rare G_{19} GC that stratifies in the OFF-sublamina of the IPL (Völgyi *et al.*, 2009). Using a transgenic mouse line, Zhang and colleagues found that a specific type of GC, which they called W3, is the most numerous GC type of the mouse retina (Zhang *et al.*, 2012). In another study it was assumed that W3 cells correspond to RG_{B2} of the Sun study and to type G_5 of the Völgyi study (Kim *et al.*, 2010). W3 cells have been demonstrated to be ON-OFF center GCs suggesting that they receive excitation from both ON- and OFF-BCs, which is in agreement with their stratification in the middle of the IPL (Zhang *et al.*, 2012). I showed that in the majority of GCs of the

increase type L-AP4 did not elicit any change in $[Ca^{2+}]_i$ (3.4.5.2.2). One might argue that in ON-OFF type of GCs the hyperpolarizing input from ON-BCs, which is triggered by L-AP4 stimulation (Müller *et al.*, 1988), becomes counterbalanced by the depolarizing input of OFF-BCs resulting in a zero net change in $[Ca^{2+}]_i$ (Fig. 3.4.24).

However, there were also few GCs of the increase type that responded with a Ca^{2+}-increase to stimulation with L-AP4 suggesting that they are OFF-GCs (Müller *et al.*, 1988; 3.4.5.2.2). This group of GCs might reflect the G_{19} GCs identified by Völgyi and colleagues (Völgyi *et al.*, 2009), which have been shown to be quite sparse OFF-GCs.

4.3.2.2. Is the DA-triggered increase in $[Ca^{2+}]_i$ in GCs due to a network response?

As already discussed for GCs of the decrease type, a DA-induced change in $[Ca^{2+}]_i$ can originate from a direct action of DA at the GC itself or from DA-action in the retinal network. Using a pharmacological approach I tried to investigate which of the two ways induced an increase in $[Ca^{2+}]_i$ in GCs.

Inhibitory input. In a group of GCs (12%) the response to DA (increase in $[Ca^{2+}]_i$) was blocked by inhibition of the GABAergic and glycinergic input (3.4.5.3.2). In the previous chapter I made the assumption that GCs of the increase type might reflect the W3 GCs identified by Zhang and colleagues (Zhang *et al.*, 2012). Brüggen and colleagues used a transgenic mouse line to identify presynaptic partners for W3 GCs in the retina (Brüggen *et al.*, 2014). They found one type of AC to make GABAergic synapses to W3 GCs. I found that DA decreases $[Ca^{2+}]_i$ in some cells in my culture (3.3.1). This might result in a reduction in GABA-release from these cells. A reduction in GABA-release can affect GCs in two ways: First, a relief of GABAergic inhibition directly at the GCs. Second, an increase in glutamatergic input from BCs due to less inhibition of BCs by GABA. Both these effects would cause an increase in $[Ca^{2+}]_i$ in GCs.

Glutamatergic input. In a smaller group of GCs of the increase type (4%) I found that blockade of the glutamatergic input resulted in abolition of the DA-induced increase in $[Ca^{2+}]_i$ (3.4.5.3.1). It can be assumed that DA modulates the glutamate release from BCs which have been shown to express D1Rs (Farshi *et al.*, 2015; Usai, 2014) leading to a rise in glutamatergic input to GCs and thus an increase in $[Ca^{2+}]_i$.

Direct action at the GC. As for the GCs of the decrease type, it cannot be ruled out that DA also exerts effects via DRs at the GCs themselves.

4.4. How do changes in second messenger concentrations affect signal processing in the retinal network?

Light adaptation involves two major processes. First, the sensitivity of the retina to a given light stimulus is reduced by ambient background light, *i.e.* a given stimulus produces a smaller response in the light-adapted retina, than in the dark-adapted retina. Second, adaptation to photopic light conditions is concomitant with the transition from rod-mediated to cone-mediated vision. In both processes DA seems to be involved.

The sensitivity of PRs is regulated by intrinsic Ca^{2+}-dependent feedback mechanisms that can work independently of dopaminergic modulation (for review see Müller and Kaupp, 1998). This regulation of sensitivity may account for large fraction of the sensitivity shift observed during light adaptation. Within the retinal network, DA seems to further modulate sensitivity. It has been shown that DA shifts the stimulus-response curve of retinal GCs to higher stimulus intensities (Thier and Alder, 1984; Jensen and Daw, 1986; Usai, 2014). A DA-induced change in the balance between excitatory and inhibitory transmission would change the magnitude of cellular responses to a given light stimulus. This can be achieved by modulation of transmitter release or by changing the density of receptors or their sensitivity in the postsynaptic membrane. The impact of the rod pathway also seems to be regulated by DA. In the rod pathway, information flow not only relies on chemical, but also on electrical synapses in form of gap junctions. The coupling efficiency of gap junctions is controlled by DA.

In this project I have demonstrated that DA modulates the intracellular concentration of the two central second messengers cAMP and Ca^{2+} in different types of retinal neurons. In the following, I will discuss how these changes relate to other findings and how they might contribute to the above mentioned mechanisms of light adaptation.

Neurotransmitter release. Changes in $[Ca^{2+}]_i$ can result in the modulation of neurotransmission as the release of neurotransmitters is controlled by Ca^{2+}. The most commonly observed response in $[Ca^{2+}]_i$ to DA in my study was an increase in $[Ca^{2+}]_i$ which may result in an increase in neurotransmitter release, whereas the less often observed decrease in $[Ca^{2+}]_i$ may prevent or reduce the release of neurotransmitters. Most ACs are inhibitory cells using either GABA or glycine as neurotransmitter (for review see Masland, 2012b). In a quite early study it has been demonstrated that glycine is released from the retina upon light stimulation (Ehinger and Lindberg, 1974). In a later study it was demonstrated that DA reduces the release of $[^3H]$-glycine from isolated

rat retina (Pycock and Smith, 1983.). As the release of glycine from ACs in the salamander retina is regulated by L- and N-type CaChs (Bieda and Copenhagen, 2004), one might assume that the DA-induced reduction in glycine release observed by Pycock and Smith might be caused by the modulation of L- and N-type CaChs through DA resulting in a decrease in $[Ca^{2+}]_i$. A reduction in glycine release might disinhibit cone-driven OFF-BCs and OFF-GCs that are under strong glycinergic inhibition.

From store-depletion experiments I assumed that in some cells of my culture the release of Ca^{2+} from internal stores is involved in DA-induced increases in $[Ca^{2+}]_i$ (3.3.4). Interestingly, in a publication from 2005 it was demonstrated that Ca^{2+}-release from internal stores after stimulation of metabotropic receptors enhanced both spontaneous and evoked GABA-release from ACs in culture (Warrier *et al.*, 2005.). Thus, it may be possible that DA-triggered increases in $[Ca^{2+}]_i$ might result in changes of GABA release from ACs. The GABAergic A17 AC makes reciprocal synapses onto rod BCs and has been shown to receive synapses from dopaminergic ACs (for review see Witkovsky, 2004). If a DA-induced increase in $[Ca^{2+}]_i$ triggers GABAergic inhibition of rod BCs this would not only reduce retinal activity but would also prevent rod signals from entering the cone-pathways via AII ACs.

There are also ACs – the so-called starburst ACs - utilizing the excitatory neurotransmitter acetylcholine (ACh) (Masland and Mills, 1979; Haverkamp *et al.*, 2003). In a study using a co-culture of rat striated muscle cells and rat retinal neurons it was found that DA increases the glutamate-induced Ach-release from rat retinal ACs (Yeh *et al.*, 1984). Studies in intact retina revealed that the increase in Ca^{2+}-dependent ACh-release is controlled by D1Rs (Hensler and Dubocovich, 1986). Interestingly, the neuromodulator melatonin, which is discussed to play a role in dark adaptation, was shown to have opposite effects: it inhibits ACh-release from ACs in the intact rabbit retina (Mitchell and Redburn, 1991). Release of ACh from ACs induces GABA release from A17 ACs leading to an inhibition of rod BCs, again preventing rod signals from entering the cone-pathways via AII ACs (Elgueta *et al.*, 2015). In conclusion, DA-induced changes in $[Ca^{2+}]_i$ might result in the modulation of the release of neurotransmitters such as GABA, glycine and ACh from ACs in the retina thereby also effectively reducing rod signals.

Phosphorylation-induced modulation of neurotransmitter receptors. In order to reduce the amplitude of light responses, it would be straight forward if DA reduced excitatory transmission and increased inhibitory transmission. However, dopaminergic

modulation seems to be not as simple as that. DA was shown to enhance glutamate-gated currents in OFF-BC dendrites thereby modulating synaptic transmission from cones to OFF-BCs (Maguire and Werblin, 1994). Phosphorylation processes also control surface expression of neurotransmitter receptors. In cultures of chick amacrine-like neurons it was found that the D1R-induced rise in PKA activity increases kainate-induced Ca^{2+}-influx which may be caused by an increase in trafficking of the receptors to the membrane (Gomes *et al.*, 2004). This is in line with a finding in postnatal rat *nucleus accumbens* neurons where it was demonstrated that stimulation of D1Rs increases GluR1 surface expression (Wolf *et al.*, 2003). In the end, an increase in glutamatergic transmission from cones to BCs and cone-driven BCs to GCs by phosphorylation of neurotransmitter receptors will favor cone-mediated vision through action of DA. Furthermore, it has been demonstrated that DA reduces $GABA_C$ receptor sensitivity at BC terminals in tiger salamander retina, thereby relieves the inhibitory effects of GABA and, thus, increases Ca^{2+}-entry into and transmitter release from BC terminals (Wellis and Werblin, 1995). The authors hypothesized that PKA phosphorylates the $GABA_C$ receptor which reduces the conductance of its associated channel similar to the finding that $GABA_A$ receptor conductance is reduced by phosphorylation (Wellis and Werblin, 1995; Moss *et al.*, 1992). Intracellular Ca^{2+} also down-modulates $GABA_A$-evoked currents through the intermediation of one or more Ca^{2+}-dependent enzymes in GCs of the turtle retina (Akopian *et al.*, 1998). Thus, while DA on one hand increases GABA release from certain ACs (see above), it reduces the effect of GABA at certain GABA-receptors. While this seems contradictory, it is in line with the fact that dopaminergic modulation may differ from cell to cell in a significant way, as also exemplified for the dopaminergic regulation of $[Ca^{2+}]_i$ shown in the present study.

Spike firing in GCs. Using the transgenic mouse line that expresses the FRET-based Ca^{2+}-sensor TN-L15 in GCs, I found that DA changes $[Ca^{2+}]_i$ in about 50% of GCs (3.4.5). In studies conducted on isolated turtle retinal GCs it was found that DA either facilitated or reduced Ca^{2+}-currents (Liu and Lasater, 1994). In current-clamp experiments the authors demonstrated that the voltage-dependent Ca^{2+}- currents in turtle retinal GCs participate in shaping the spiking pattern of these cells. The direct result of the modulation of Ca^{2+}-currents by DA was an alteration in the spiking properties of the GC (Liu and Lasater, 1994). GCs express potassium channels that are regulated by Ca^{2+} (for review see Zhong *et al.*, 2013). These channels are known to contribute to a substantial fraction to the repolarizing current during action potentials (Adams *et al.*, 1982), to

affect the inter-spike-intervals and to induce spike frequency adaptation. It has also been reported that elevation of $[Ca^{2+}]_i$ either through influx or by release from intracellular stores reduces light-evoked excitatory postsynaptic currents (EPSCs) in salamander retinal neurons (Akopian and Witkovsky, 2001). The authors assumed that NMDA-receptors are the primary targets for a Ca^{2+}-induced modulation and concluded that the Ca^{2+}-mediated reduction in the EPSC will help to shape the spike pattern of the GCs. Thus, DA-induced changes in $[Ca^{2+}]_i$ in GCs might affect the generation of action potentials and thus modulate the retina´s information transfer to the brain.

Gap junctional coupling. In each of the five major neuronal cell classes of the retina (PR, BC, HC, AC, GC) electrical coupling via gap-junctions can be observed (for review see Bloomfield and Völgyi, 2009). The regulation of these gap-junctions is mainly controlled by the circadian clock and by light-adaptation processes involving DR-signaling via cAMP. Regulation of gap junctional coupling is particularly important in controlling the impact of the rod pathway. In 2008, Ribelayga and colleagues demonstrated that rod-cone coupling is maximal in darkness and minimal in light (Ribelayga *et al.*, 2008). The proposed uncoupling mechanism is mediated via a D4R-induced reduction in $[cAMP]_i$, a decrease in PKA activity and a reduction in Cx35 phosphorylation (for review see Bloomfield and Völgyi, 2009). Under scotopic conditions, the extensive coupling between rods and cones facilitates the detection of dim objects. Under mesopic conditions, this coupling may result in fast saturation of the network. Thus, uncoupling ensures that the saturated rod signals are not conveyed to cones (for review see Bloomfield and Völgyi, 2009).

Light adaptation was found to affect the coupling between AII ACs in a triphasic manner: AII ACs are weakly coupled under scotopic and photopic conditions whereas they are extensively coupled under mesopic conditions (for review see Bloomfield and Völgyi, 2009). In order to not attenuate small signals, under scotopic conditions coupling between AII ACs must be kept minimal. Under mesopic conditions, a higher number of photons reaches the retina making it necessary to increase signal-to-noise ratio by synchronizing AII ACs. There are two competing and conflicting hypotheses concerning the DA-driven uncoupling mechanism in AII ACs: First, Urschel and colleagues proposed that PKA-induced phosphorylation of Cx36 decreases gap junction conductance (Urschel *et al.*, 2006). In contrast, Kothmann and colleagues proposed that the uncoupling results from a D1R-driven activation of PKA, PKA-induced activation of PP2A and PP2A-induced dephosphorylation of Cx36 (Kothmann *et al.*, 2009).

Opposite to the light-induced effects on PR and AII ACs, Hu and colleagues found that light adaptation results in a dramatic increase in the coupling of OFF-alpha-GCs to both neighboring GCs and ACs (Hu *et al.*, 2010). ON-alpha-GCs were never found to be coupled to one another (Hu *et al.*, 2010). The control of the coupling between GCs seems to be rather complex as, depending on the light intensity, either D2Rs or D1Rs are thought to be activated and thus control phosphorylation of connexins (Hu *et al.*, 2010). Interestingly, the findings from the Hu study contradict an earlier study (Mills *et al.*, 2007) in two aspects: first, Mills and colleagues proposed that gap junctional coupling between GCs is reduced during light adaptation. Second, the authors proposed a D2R-mediated control of gap junctional coupling between GCs (Mills *et al.*, 2007; for review see Bloomfield and Völgyi, 2009). However, the overall proposed function for GC electrical coupling is to provide for correlated activity of neighboring cells (Völgyi *et al.*, 2009). This would promote detection of visual signals by increasing the temporal summation at central targets (for review see Bloomfield and Völgyi, 2009).

Changes in gene transcription. Through the modulation of gene expression, DA-induced changes in $[Ca^{2+}]_i$ and PKA might induce longer-lasting modifications in retinal neurons. The transcription factor Ca^{2+}/cAMP-response element binding protein (CREB) is activated by phosphorylation of Ser133 through PKA and CaMKII, both of which are regulated by DA (Bito *et al.*, 1997). Phosphorylation of CREB induces the formation of a stable complex with the CREB-binding protein (CBP), a co-activator of transcription and, in turn, induces recruitment of the RNA polymerase II holoenzyme (for review see Bito *et al.*, 1997). CREB binds to the cAMP response element (CRE) which is typically found upstream of genes within promoter or enhancer regions and thereby regulates the transcription of specific genes (for review see Carlezon Jr. *et al.*, 2005). Thus, DA-induced changes in PKA-activity and in $[Ca^{2+}]_i$ might alter the expression of neurotransmitter receptors or intracellular signaling molecules during day time, leading to an alteration in synaptic transmission between retinal neurons.

4.5. Outlook

In this thesis I demonstrated, by using optogenetic sensors and pharmacological as well as immunochemical methods, that DA has variable effects on single cells in the culture as well the intact retinal network. Stimulation of DRs led to profound changes in the intracellular concentration of the two central second messengers cAMP and Ca^{2+}. The

interplay between various complex DR-triggered pathways was quite hard to dissect. However, all of these processes can result in the modulation of neurotransmission, the alteration of a neurons´ activity and, thus, the output from the retinal network to the brain.

To unravel DA´s role in light adaptation, further experiments have to be conducted. The retinal primary culture is a well-suited model system to dissect DA-signaling in isolated ACs of the retina. Simultaneous Ca^{2+}-imaging and cAMP/PKA-imaging in the same neuron may be an elegant way to further dissect the underlying mechanisms for the processes I have observed in Fluo-4-loaded and in AKAR4-expressing neurons. As for the investigation of dopaminergic signaling in GCs in the TN-L15 retina, it might be helpful to combine TN-L15 imaging with electrophysiological recording to get a dual read-out for the DA-induced changes in the physiology of GCs. Furthermore, immunohistochemical analysis of imaged GCs could contribute to the identification of GCs of the different response types I observed in my experiments. However, to get a real clue about DA´s role in light adaptation, it is of great necessity to establish a read-out system that visualizes light-induced changes in DA-release. This may be achieved by a combination of synapto-pHluorin expression in dopaminergic ACs and the read-out of DA-induced changes in the physiology of target cells by means of suitable optogenetic sensors. By combining synapto-pHluorin with *e.g.* the genetically-encoded Ca^{2+}-sensor RCaMP, that can be used for imaging in the far-red spectrum (Akerboom *et al.*, 2013), DA release and effects in target cells could be studied simultaneously. These experiments should be conducted using two-photon-excitation imaging to exclude light responses triggered by the excitation light during image acquisition. Taken together, the present study has created a foundation for further investigations of dopaminergic signaling in the retina by optogenetic sensor-based visualization of second messenger signaling.

References

Adams *et al.*, 1982. Intracellular Ca^{2+} activates fast voltage-sensitive K^+ current in vertebrate sympathetic neurons. *Nature*, 296(5859):746-749.

Ai, 2015. Green-to-red photoconversion of GCaMP. *PLoS One,* 10(9):e0138127.

Akerboom *et al.*, 2013. Genetically encoded calcium indicators for multi-color neural activity imaging and combination with optogenetics. *Front. Mol. Neurosci*., 6:2.

Akopian and Witkovsky, 2001. Intracellular calcium reduces light-induced excitatory post-synaptic responses in salamander retinal ganglion cells. *J. Physiol*., 532(Pt 1): 43–53.

Akopian *et al.*, 1998. Calcium released from intracellular stores inhibits $GABA_A$-mediated currents in ganglion cells of the turtle retina. *J. Neurophysiol.*, 80(3):1105-1115.

Araki *et al.*, 2005. Transgenic mouse lines expressing synaptopHluorin in hippocamous and cerebellar cortex. *Genesis*, 42(2):53-60.

Asrican *et al.*, 2013. Next-generation transgenic mice for optogenetic analysis of neural circuits. *Front. Neural Circuits*, 7:160.

Baden *et al.*, 2016. The functional diversity of retinal ganglion cells in the mouse. *Nature*, 529(7586):345-350.

Baird *et al.*, 1999. Circular permutation and receptor insertion within green fluorescent proteins. *Proc. Natl. Acad. Sci. USA,* 96(20):11241-11246.

Bauer *et al.*, 1980. [^{3}H]-dopamine release from the rabbit retina. *Albrecht von Graefes Arch. Klin. Opthalmol.*, 215(2):71-78.

Bautista *et al.*, 2002. Enhancement of calcium signalling dynamics and stability by delayed modulation of the plasma-membrane calcium-ATPase in human T cells. *J. Physiol.*, 541(Pt 3):877-894.

Baylor, 1996. How photons start vision. *Proc. Natl. Acad. Sci. USA*, 93(2):560-565.

Beaulieu and Gainetdinov, 2011. The physiology, signaling and pharmacology of dopamine receptors. *Pharmacol. Rev*., 63(1):182-217.

Berson *et al.*, 2010. Morphology and mosaics of melanopsin-expressing retinal ganglion cell types in mice*. J. Comp. Neurol*., 518(13):2405-2422.

Bi *et al.*, 2006. Ectopic expression of a microbial-type rhodopsin restores visual responses in mice with photoreceptor degeneration. *Neuron*, 50(1):23-33.

Bieda and Copenhagen, 2004. N-type and L-type calcium channels mediate glycinergic synaptic inputs to retinal ganglion cells of tiger salamanders. *Vis. Neurosci.*, 21(4):545-550.

Biswas *et al.*, 2014. Pharmacological analysis of intrinsic neuronal oscillation in *rd10* retina. *PLoS One,* 9(6):e99075.

Bito *et al.*, 1997. Ca^{2+}-dependent regulation in neuronal gene expression. *Curr. Opin. Neurobiol.*, 7(3):419-429.

Blasic *et al.*, 2012. Phosphorylation of mouse melanopsin by protein kinase A. *PLoS One*, 7(9):e45387.

Bloomfield and Völgyi, 2009. The diverse functional roles and regulation of neuronal gap junctions in the retina. *Nat. Rev. Neurosci.,* 10(7):495-506.

Börner *et al.*, 2011. FRET measurements of intracellular cAMP concentrations and cAMP analog permeability in intact cells. *Nat. Prot.*, 6(4):427-428.

Bowmaker, 1998. Evolution of colour vision in vertebrates. *Eye (Lond).*, 12 (Pt 3b):541-547.

Bozza *et al.*, 2004. *In vivo* imaging of neuronal activity by targeted expression of a genetically encoded probe in the mouse. *Neuron*, 42(1):9-21.

Brandstätter and Hack, 2001. Localization of glutamate receptors at a complex synapse - The mammalian photoreceptor synapse. *Cell Tissue Res.,* 303(1):1-14.

Broussard *et al.*, 2013. Fluorescence resonance energy transfer microscopy as demonstrated by measuring the activation of the serine/threonine kinase Akt. *Nat. Protoc.,* 8(2):265-281.

Brüggen *et al.*, 2014. Type 2 wide-field amacrine cells in TH::GFP mice show a homogenous synapse distribution and contact small ganglion cells. *Eur. J. Neurosci.*, 41(6):734-747.

Calebiro *et al.*, 2009. Peristent cAMP-signals triggered by internalized G-protein-coupled receptors. *PLos Biol*., 7(8):e1000172.

Carafoli, 1991. Calcium pump of the plasma membrane. *Physiol. Rev*., 71(1):129-153.

Carlezon Jr. *et al.*, 2005. The many faces of CREB. *Trends Neurosci*., 28(8):436-445.

Chen *et al.*, 2012. Imaging neural activity using *Thy1*-GCaMP transgenic mice. *Neuron*, 76(2):297-308.

Chen *et al.*, 2014a. A PKA activity sensor for quantitative analysis of endogenous GPCR signaling via 2-photon FRET-FLIM imaging. *Front. Pharmacol.*, 5:56.

Chen *et al.*, 2014b. Somatostatin receptor-mediated suppression of GABAergic synaptic transmission in cultured rat retinal ACs. *Neuroscience,* 273:118-127.

Chun *et al.*, 2013. D1-D2 dopamine receptor synergy promotes calcium signaling via multiple mechanisms. *Mol. Pharmacol.,* 84(2):190-200.

Cohen *et al.*, 1992. Photoreceptors of mouse retinas possess D4 receptors coupled to adenylate cyclase. *Proc. Natl. Acad. Sci. USA,* 89(24):12093-12097.

Contín *et al.*, 2010. Light activation of the phosphoinositide cycle in intrinsically photosensitive chicken retinal ganglion cells. *Invest. Ophthalmol. Vis. Sci.*, 51(11):5491-5498.

Davies *et al.*, 2012. Focus on molecules: melanopsin. *Exp. Eye Res.*, 97(1):161-162.

Depry *et al.*, 2011. Visualization of PKA activity in plasma membrane microdomains. *Mol. BioSyst.,* 7(1):52-58.

Derouiche and Asar, 1999. The dopamine D2 receptor subfamily in rat retina: ultrastructural immunogold and *in situ* hybridization studies. *Eur. J. Neurosci.*, 11(4):1391-1402.

Djamgoz *et al.*, 2000. Light-adaptive role of nitric oxide in the outer retina of lower vertebrates: a brief review. *Philos. Trans. R. Soc. Lond. B. Biol. Sci,.* 355(1401):1199-1203.

Doi *et al.*, 1995. Morphological classification of retinal ganglion cells in mice. *J. Comp. Neurol.,* 356(3):368-386.

Dorouchi *et al.*, 2011. Virally delivered channelrhodopsin-2 safely and effectively restores visual function in multiple mouse models of blindness. *Mol. Ther.*, 19(7):1220-1229.

Dunn *et al.*, 2009. Calcium-dependent increases in protein kinase-A activity in mouse retinal ganglion cells are mediated by multiple adenylate cyclases. *PLoS One*, 4(11):e7877.

Dunn, 2006. Imaging of cAMP levels and protein kinase A activity reveals that retinal waves drive oscillations in second-messenger cascades. *J. Neurosci.*, 26(49):12807-12815.

Ehinger and Lindberg, 1974. Light-evoked release of glycine from the retina. *Nature*, 251:727-728.

Elgueta *et al.*, 2015. Acetylcholine induces GABA release onto rod bipolar cells through heteromeric nicotinic receptors expressed in A17 amacrine cells. *Front. Cell. Neurosci.*, 9:6.

Estevez *et al.*, 2012. Form and function of the M4 cell, an intrinsically photosensitive retinal ganglion cell type contributing to geniculocortical vision. *J. Neurosci.*, 32(39):13608-13620.

Euler *et al.*, 2014. Retinal bipolar cells: elementary building blocks of vision. *Nat. Rev. Neurosci.*, 15(8):507-519.

Farrow and Masland, 2011. Physiological clustering of visual channels in the mouse retina. *J. Neurophysiol.*, 105(4):1516-1530.

Farshi *et al.*, 2015. Dopamine D1 receptor expression is bipolar cell type-specific in the mouse retina. *J. Comp. Neurol*., doi: 10.1002/cne.23932. [Epup ahead of print]

Feigenspan and Bormann, 1994. Facilitation of GABAergic signaling in the retina by receptors stimulating adenylate cyclase. *Proc. Natl. Acad. Sci. USA*, 91(23):10893-10897.

Freed and Sterling, 1988. The ON-alpha ganglion cell of the cat retina and its presynaptic cell types. *J. Neurosci*., 8(7):2303-2320.

Friedman *et al.*, 2002. Beta(2)-adrenergic receptor lacking the cyclic AMP-dependent protein kinase consensus sites fully activates extracellular signal-regulated kinase 1/2 in human embryonic kidney 293 cells: lack of evidence for G(s)/G(i) switching. *Mol. Pharmacol*., 62(5):1094-1102.

Fujita *et al.*, 1993. Primary structure and functional expression of the ω-conotoxin-sensitive N-type calcium channel from rabbit brain. *Neuron*, 10(4):585-598.

Gallego, 1971. Horizontal and amacrine cells in the mammal´s retina. *Vision Res.,* 11:33-50.

Ghosh *et al.*, 2004. Types of bipolar cells in the mouse retina. *J. Comp. Neurol*., 469(1):70-82.

Gomes *et al.*, 2004. Metabotropic glutamate and dopamine receptors co-regulate AMPA receptor activity through PKA in cultured chick retinal neurons: effect on GluR4 phosphorylation and surface expression. *J. Neurochem*., 90(3):673-682.

Gong *et al.*, 2014. Imaging neural spiking in brain tissue using FRET-opsin protein voltage sensors. *Nat. Commun*., 5:3674.

Gorshkov and Zhang, 2014. Visualization of cyclic nucleotide dynamics in neurons. *Front. Cell Neurosci.,* 8:395.

Graham *et al.*, 1977. Characteristics of a human cell line transformed by DNA from a human adenovirus type 5. *J. Gen. Virol*., 36(1):59-74.

Gross *et al.*, 1990. The cyclic AMP-dependent protein kinase catalytic subunit selectively enhances calcium currents in rat nodose neurons. *J. Physiol*., 429: 483–496.

Guenther *et al.*, 1994. Inhibitory action of haloperidol, spiperone and SCH23390 on calcium currents in rat retinal ganglion cells. *NeuroReport*, 5(11):1373-1376.

Gustincich *et al.*, 1997. Control of dopamine release in the retina: a transgenic approach to neural networks. *Neuron*, 18(5):723-736.

Habermann *et al.*, 2003. AII amacrine cells express L-type calcium channels at their output synapses. *J. Neurosci.,* 23(17):6904-6913.

Hampson *et al.*, 1992. Dopaminergic modulation of gap junction permeability between amacrine cells in mammalian retina. *J. Neurosci.*, 12(12):4911-4922.

Hankins *et al.*, 2008. Melanopsin: an exciting photopigment. *Trends Neurosci.*, 31(1):27-36.

Haverkamp and Wässle, 2000. Immunocytochemical analysis of the mouse retina. *J. Comp. Neurol.,* 424(1):1-23.

Haverkamp *et al.*, 2003. A comparison of immunocytochemical markers to identify bipolar cell types in human and monkey retina. *Vis. Neurosci.,* 20(6):589-600.

Hayashida *et al.*, 2009. Inhibition of adult rat retinal ganglion cells by D1-type dopamine receptor activation. *J. Neurosci.,* 29(47):15001-15016.

Heidelberger and Matthews, 1994. Dopamine enhances Ca^{2+} responses in synaptic terminals of retinal bipolar neurons. *NeuroReport,* 5(6):729-732.

Heim and Griesbeck, 2004. Genetically encoded indicators of cellular calcium dynamics based on troponin C and green fluorescent protein. *J. Biol. Chem.,* 279(14):14280-14286.

Heim *et al.*, 2007. Improved calcium imaging in transgenic mice expressing a troponin C-based biosensor. *Nat Methods*. 4(2):127-129.

Hensler and Dubocovich, 1986. D_1-dopamine receptor activation mediates [^{3}H]-acetylcholine release from rabbit retina. *Brain Res.*, 398(2):407-412.

Hernández-López *et al.*, 2000. D2 dopamine receptors in striatal medium spiny neurons reduce L-type Ca^{2+} currents and excitability via a novel PLCβ1-IP_3-calcineurin signaling cascade. *J. Neurosci*., 20(24):8987-8995.

Herzig and Neumann, 2000. Effects of Serine/Threonine protein phosphatases on ion channels in excitable membranes. *Physiol. Rev.*, 80(1):173-210.

Hille, 1994. Modulation of ion-channel function by G-protein-coupled receptors. *Trends Neurosci.,* 17(12):531-536.

Hu *et al.*, 2010. Light increases the gap junctional coupling of retinal ganglion cells. *J. Physiol.*, 588(Pt 21):4145-4163.

Hu *et al.*, 2013. Intrinsic physiological properties of the five types of mouse ganglion-cell photoreceptors. *J. Neurophysiol*., 109(7):1876-1889.

Huang *et al.*, 2013. Neuromodulatory role of melatonin in retinal information processing. *Prog. Retin. Eye Res*., 32:64-87.

Ichinose and Lukasiewicz, 2007. Ambient light regulates sodium channel activity to dynamically control retinal signaling. *J. Neurosci.*, 27(17):4756-4764.

Jensen and Daw, 1986. Effects of dopamine and its agonists and antagonists on the receptive field properties of ganglion cells in the rabbit retina. *Neurosci.*, 17(3):837-855.

Johnson *et al.*, 2004. Vesicular glutamate transporter 3 expression identifies glutamatergic amacrine cells in the rodent retina. *J. Comp. Neurol.,* 477(4):386-398.

Kim *et al.*, 2010. Laminar restriction of retinal ganglion cell dendrites and axons: subtype-specific developmental patterns revealed with transgenic markers. *J. Neurosci.*, 30(4):1452-1462.

Kimura *et al.*, 1995. Coupling of human D-1 receptors to different guanine nucleotide binding proteins. *J. Biol. Chem.,* 270(24):14672-14678.

Knop *et al.*, 2011. Inputs underlying the ON-OFF light response of type 2 wide-field amacrine cells in TH::GFP mice. *J. Neurosci*., 31(13):4780-4791.

Kong *et al.*, 2005. Diversity of ganglion cells in the mouse retina: unsupervised morphological classification and its limits. *J. Comp. Neurol.,* 489(3):293-310.

Kothmann *et al.*, 2009. Dopamine-stimulated dephosphorylation of connexin 36 mediates AII amacrine cell coupling. *J. Neurosci.*, 29(47):14903-14911.

Kramer, 1971. Dopamine: A retinal neurotransmitter. I. Retinal uptake, storage, and light-stimulated release of H3-dopamine *in vivo*. *Invest. Ophthalmol*., 10(6):438-452.

Lange, 2015. Imaging von pHluorin-basierten Sensoren für Neurotransmitter-freisetzung in dissoziierter Kultur. Masterarbeit am ICS-4 (FZ-Jülich) in der AG-Müller.

Lee *et al.*, 2004. Dopamine D1 and D2 receptor co-activation generates a novel phospholipase C-mediated calcium signal. *J. Biol. Chem.*, 279(34):35671-35678.

Lehmann *et al.*, 2007. Small molecule disruption of G protein βγ subunit signaling inhibits neutrophil chemotaxis and inflammation. *Mol. Pharmacol.*, 73(2):410-418.

Lelito and Shafer, 2012. Imaging cAMP dynamics in the drosophila brain with the genetically encoded sensor Epac1-camps. *Springer Science*, Genetically encoded functional indicators, ISBN 978-1-62703-014-4, pp 149-168.

Li and O'Brien, 2012. Regulation of gap junctional coupling in photoreceptors. *Nova Science Publishers Inc.,* In: PRs: physiology, types and abnormalities. ISBN 978-1-61942-619-1, pp 97-112.

Liang *et al.*, 2003. Müller cell transduction by AAV2 in normal and degenerative retinas. *Adv. Exp. Med. Biol.*, 533:439-445.

Lin *et al.*, 1994. Agents that promote protein phosphorylation inhibit the activity of the Na^+/Ca^{2+} exchanger and prolong Ca^{2+} transients in bovine chromaffin cells. *J. Neurochem*., 63(5):1941-1947.

Liu and Lasater, 1994. Calcium currents in turtle retinal ganglion cells. II. Dopamine modulation via a cyclic AMP-dependent mechanism. *J. Neurophysiol*., 71(2):743-752.

Maguire and Werblin, 1994. Dopamine enhances a glutamate-gated ionic current in OFF bipolar cells of the tiger salamander retina. *J. Neurosci*., 14(10):6094-6101.

Margolis *et al.*, 2011. Dendritic calcium signaling in ON and OFF mouse retinal ganglion cells. *J. Neurosci*., 30(21):7127-7138.

Masland and Mills, 1979. Autoradiographic identification of acetylcholine in the rabbit retina. *J. Cell Biol*., 83(1):159-178.

Masland, 2001. The fundamental plan of the retina. *Nat. Neurosci.*, 4(9):877-886.

Masland, 2012a. The neuronal organization of the retina. *Neuron*, 76(2):266-280.

Masland, 2012b. The tasks of amacrine cells. *Vis. Neurosci*., 29(1):3-9.

Massey *et al.*, 1983. The effects of 2-amino-4-phosphonobutyric acid (APB) on the ERG and ganglion cell discharge of rabbit retina. *Vision Res.*, 23(12):1607-1613.

Massey, 1990. Cell types using glutamate as neurotransmitter in the vertebrate retina. *Prog. Ret. Res.*, 9:399-425.

Mataruga *et al.*, 2007. Type 3a and 3b OFF-cone bipolar cells provide for the alternative rod pathway in the mouse retina. *J. Comp. Neurol.,* 502(6):1123-1137.

Matsuda and Cepko, 2004. Electroporation and RNA interference in the rodent retina *in vivo* and *in vitro*. *Proc. Natl. Acad. Sci. USA*,101(1):16-22.

Matsushita *et al.*, 2002. Dynamics of tyrosine hydroxylase promoter activity during midbrain dopaminergic neuron development. *J. Neurochem*., 82(2):295-304.

Menger *et al.*, 1998. Glycinergic amacrine cells of the rat retina. *J. Comp. Neurol.,* 401(1):34-46.

Miesenböck *et al.*, 1998. Visualizing secretion and synaptic transmission with pH-sensitive green fluorescent proteins. *Nature,* 394(6689):192-195.

Mills *et al.*, 2007. Dopaminergic modulation of tracer coupling in a ganglion-amacrine cell network. *Vis. Neurosci.*, 24(4):593-608.

Mironov *et al.*, 2009. Imaging cytoplasmic cAMP in mouse brainstem neurons. *BMC Neurosci.,* 10:29.

Missale *et al.*, 1998. Dopamine receptors: from structure to function. *Physiol. Rev.*, 78(1):189-225.

Mitchell and Redburn, 1991. Melatonin inhibits ACh release from rabbit retina. *Vis Neurosci*., 7(5):479-486.

Moss *et al.*, 1992. Functional modulation of GABAA receptors by cAMP-dependent protein phosphorylation. *Science*, 257(5070):661-665.

Müller and Kaupp, 1998. Signaltransduktion in Sehzellen. *Naturwissenschaften*, 85(2):49-61.

Müller *et al.*, 1988. Pharmacological modulation of the rod pathway in the cat retina. *J. Neurophysiol.*, 59(6):1657-1672.

Nakai *et al.*, 2001. A high signal-to-noise Ca^{2+} probe composed of a single green fluorescent protein. *Nat. Biotechnol.,* 19(2):137-141.

Nakajima *et al.*, 1993. Molecular characterization of a novel retinal metabotropic glutamate receptor mGluR6 with a high agonist selectivity for L-2-amino-4-phosphonobutyrate. *J. Biol. Chem.,* 268(16):11868-11873.

Nelson *et al.*, 1978. Intracellular staining reveals different levels of stratification for On- and Off-center ganglion cells in cat retina. *J. Neurophysiol.*, 41(2):472-483.

Neve *et al.*, 2004. Dopamine receptor signaling. *J. Recept. Signal Transduct. Res.,* 24(3):165-205.

Nguyen-Legros *et al.*, 1997. Immunocytochemical localization of dopamine D1 receptors in the retina of mammals. *Vis. Neurosci.*, 14(3):545-551.

Nguyen-Legros *et al.*, 1999. Dopamine receptor localization in the mammalian retina. *Mol. Neurobiol.*, 19(3):181-204.

Nguyen-Legros, 1988. Morphology and distribution of catecholamine-neurons in mammalian retina. *Prog. Ret. Res.,* 7:112-147.

Nikolaev *et al.*, 2004. Novel single chain cAMP sensors for receptor-induced signal propagation. *J. Biol. Chem,* 279(36):37215-37218.

Nowicki *et al.*, 2000. Dopamine-induced translocation of protein kinase C isoforms visualized in renal epithelial cells. *Am. J. Physiol. Cell Physiol.,* 279(6):C1812-C1818.

Ogata *et al.*, 2012. Dopamine and full-field illumination activate D1 and D2-D5-type receptors in adult rat retinal GCs*. J. Comp. Neurol.,* 520(17):4032-4049.

Pack *et al.*, 2015. Melatonin modulates M4-type ganglion-cell photoreceptors. *Neuroscience*, 303:178-188.

Pang *et al.*, 2003. Light-evoked excitatory and inhibitory synaptic inputs to ON and OFF alpha ganglion cells in the mouse retina. *J. Neurosci*., 23(14):6063-6073.

Pang *et al.*, 2008. Comparative analysis of *in vivo* and *in vitro* AAV vector transduction in the neonatal mouse retina: Effects of serotype and site of administration. *Vision Res.*, 48(3):377-385.

Parekh and Putney Jr., 2005. Store-operated calcium channels. *Physiol. Rev.*, 85(2):757-810.

Peichl *et al.*, 1987. Alpha ganglion cells in mammalian retinae. *Proc. R. Soc. Lond. B Biol. Sci.*, 231(1263):169-197.

Peichl, 1991. Alpha ganglion cells in mammalian retinae: Common properties, species differences and some comments on other GCs. *Vis. Neurosci.*, 7(1-2):155-169.

Peichl, 1992. Prinzipien der Bildverarbeitung in der Retina der Säugetiere. *Biologie in unserer Zeit,* 22(1):45-53.

Perreault *et al.*, 2011. The dopamine D1-D2 receptor heteromer in striatal medium spiny neurons: evidence for a third distinct neuronal pathway in basal ganglia. *Front. Neuroanat.,* 5:31.

Petrs-Silva *et al.*, 2008. High-efficiency transduction of the mouse retina by tyrosine-mutant AAV serotype vector. *Mol. Ther.*, 17(3):463-471.

Pfeiffer-Linn and Lasater, 1993. Dopamine modulates in a differential fashion T- and L-type calcium currents in bass retinal horizontal cells*. J. Gen. Physiol*., 102(2):277-294.

Piccolino *et al.,* 1984. Decrease of gap junction permeability induced by dopamine and cyclic adenosine 3':5'-monophosphate in horizontal cells of turtle retina. *J. Neurosci.,* 4(10):2477-2488.

Politi *et al.*, 1988. Development of neonatal mouse retinal neurons and photoreceptors in low density culture. *Invest. Ophthalmol. Vis. Sci.*, 29(4):534-543.

Ponsioen *et al.*, 2004. Detecting cAMP-induced Epac activation by fluorescence resonance energy transfer: Epac as a novel cAMP indicator. *EMBO Rep.,* 5(12):1176-1180.

Pow *et al.*, 1995. The immunocytochemical detection of amino-acid neurotransmitters in paraformaldehyde-fixed tissues. *J. Neurosci. Methods*, 56(2):115-123.

Preißel, 2006. Zur vollständig antagonisierbaren Anästhesie von neugeborenen Mäusen mit Midazolam, Medetomidin und Fentanyl- eine experimentelle Dosierungsstudie. Doktorarbeit an der Tierärztlichen Fakultät der LMU München. Dr. Hut-Verlag, ISBN-10: 3899633997.

Pycock and Smith, 1983. Interactions of dopamine and the release of [^{3}H]-taurine and [^{3}H]-glycine from the isolated retina of the rat. *Br. J. Pharmac.*, 78:395-404.

Rashid *et al.*, 1993. Evidence for D2 receptor regulation of dopamine release in the goldfish retina. *J. Neurochem.,* 61(6):2025-2033.

Ribelayga and Mangel, 2005. A circadian clock and light/dark adaptation differentially regulate adenosine in the mammalian retina. *J. Neurosci.*, 25(1):215-222.

Ribelayga *et al.*, 2008. The circadian clock in the retina controls rod-cone coupling. *Neuron*, 59(5):790-801.

Rodieck, 1998. The first steps in seeing. *Sinnauer Associates Inc*. ISBN 0-87893-757-9.

Royle *et al.*, 2008. Imaging pHluorin-based probes at hippocampal synapses. *Methods Mol. Biol.*, 457:293-303.

Sakaki *et al.*, 1996. Muscarinic and purinergic Ca^{2+} mobilizations in the neural retina of early embryonic chick. *Int. J. Dev. Neurosci.*, 14(6):691-9.

Samulski *et al.*, 1987. A recombinant plasmid from which an infectious adeno-associated virus genome can be excised *in vitro* and its use to study viral replication. *J. Virol.*, 61(10):3096-3101.

Schiller, 1982. Central connections of the retinal ON and OFF pathways. *Nature*, 297:580-583.

Seeman and Van Tol, 1994. Dopamine receptor pharmacology. *Trends Pharmacol. Sci.*, 15(7):264-270.

Sekar and Periasamy, 2003. Fluorescence resonance energy transfer (FRET) microscopy imaging of live cell protein localizations. *J. Cell. Biol.,* 160(5):629-633.

Shiells *et al.*, 1981. Action of glutamate and aspartate analogues on rod horizontal and bipolar cells. *Nature*, 294:592–594.

Shigetomi *et al.*, 2013. Imaging calcium microdomains within entire astrocyte territories and endfeet with GCaMPs expressed using adeno-associated viruses. *J. Gen. Physiol*., 141(5):633-647.

Slaughter and Miller, 1981. 2-amino-4-phosphonobuyric acid: a new pharmacological tool for retina research. *Science*, 211(4478):182-185.

Smith *et al.*, 2015. D1 dopamine receptors modulate cone ON bipolar cell Nav channels to control daily rhythms in photopic vision. *Chronobiol. Int.*, 32(1):48-58.

Snyder *et al.*, 1998. A dopamine/D1 receptor/protein kinase A/dopamine- and cAMP-regulated phosphoprotein (Mr 32 kDa)/protein phosphatase-1 pathway regulates dephosphorylation of the NMDA receptor. *J. Neurosci.,* 18(24):10297-12303.

So *et al.*, 2005. D1 and D2 dopamine receptors form heterooligomers and co-internalize after selective activation of either receptor. *Mol. Pharmacol.,* 68(3):568-578.

Soma *et al.*, 2009. Involvement of protein kinase C in the regulation of Na^{+}/Ca^{2+} exchanger in bovine adrenal chromaffin cells. *Clin. Exp. Pharmacol. Physiol*., 36(7):717-723.

Sprenger and Nikolaev, 2013. Biophysical techniques for detection of cAMP and cGMP in living cells. *Int. J. Mol. Sci.,* 14(4):8025-8046.

Strange and Neve, Tocris, 2013. Dopamine receptors. *Tocris Scientific Reviews.*

Sümbül *et al.*, 2013. A genetic and computational approach to structurally classify neuronal types. *Nat. Commun.*, 5:3512.

Sumi *et al.*, 2010. Adrenergic receptor activation involves ATP release and feedback through purinergic receptors. *Am. J. Physiol. Cell Physiol.*, 299(5):C1118-C1126.

Summerford and Samulski, 1998. Membrane-associated heparan sulfate proteoglycan is a receptor for adeno-associated virus type 2 virions. *J. Virol.*, 72(2):1438-1445.

Sun *et al.*, 2002. Large-scale morphological survey of mouse retinal ganglion cells. *J. Comp. Neurol.,* 451(2):115-126.

Sunahara *et al.*, 1996. Complexity and diversity of mammalian adenylyl cyclases. *Annu. Rev. Pharmacol. Toxicol.,* 36:461-480.

Surmeier *et al.*, 1995. Modulation of calcium currents by a D1 dopaminergic protein kinase/phosphatase cascade in rat striatal neurons. *Neuron*, 14(2):385-397.

Svenningsson *et al.*, 2004. DARPP-32: An integrator of neurotransmission. *Annu. Rev. Pharmacol. Toxicol.,* 44:269-296.

Tang and Gilman, 1991. Type-specific regulation of adenylyl cyclase by G protein βγ subunits. *Science,* 254(5037):1500-1503.

Tatee *et al.*, 1996. Forskolin derivatives. I. Synthesis, and cardiovascular and adenylate cyclase-stimulating activities of water-soluble forskolins. *Chem. Pharm. Bull.*, 44(12):2274-2279.

Thier and Alder, 1984. Action of iontophoretically applied dopamine on cat retinal ganglion cells. *Brain Res.*, 292(1):109-121.

Thomas and Hanley, 1994. Pharmacological tools for perturbing intracellular calcium storage. *Methods Cell Biol*., 40:65-89.

Thoreson and Mangel, 2012. Lateral interactions in the outer retina. *Prog. Retin. Eye Res*., 31(5):407-441.

Tian *et al.*, 2009. Imaging neural activity in worms, flies and mice with improved GCaMP calcium indicators. *Nat. Methods.* 6(12):875-881.

Trapani *et al.*, 2014. Vector platforms for gene therapy of inherited retinopathies. *Prog. Retin. Eye Res.*, 43:108-128.

Tsien *et al.*, 1991. Molecular diversity of voltage-dependent Ca^{2+} channels. *Trends Pharmacol. Sci.*, 12(9):349-354.

Undie and Friedman, 1990. Stimulation of a dopamine D1 receptor enhances inositol phosphates formation in rat brain*. J. Pharmacol. Exp. Ther.*, 253(3):987-992.

Urschel *et al.*, 2006. Protein kinase A-mediated phosphorylation of connexin36 in mouse retina results in decreased gap junctional communication between AII amacrine cells. *J. Biol. Chem.*, 281(44):33163-33171.

Usai, 2014. Die potentielle Rolle des Neuromodulators Dopamin in der Helladaptation der Mausretina. Doktorarbeit am ICS-4 (FZ-Jülich) in der AG-Müller.

Van Hook *et al.*, 2012. Dopaminergic modulation of ganglion-cell photoreceptors. *Eur. J. Neurosci.*, 35(4):507-518.

Varella *et al.*, 1997. Protein kinases selectively modulate apoptosis in the developing retina in vitro. *Neurochem. Int.*, 31(2):217-227.

Venkatesh *et al.*, 2013. Retinal gene delivery by rAAV and DNA electroporation. *Curr. Protoc. Microbiol.*, Chapter 14:Unit 14D.4.

Versaux-Botteri *et al.*, 1984. Morphology, density and distribution of tyrosine hydroxylase-like immunoreactive cells in the retina of mice. *Brain Res.*, 301(1):192-197.

Versaux-Botteri *et al.*, 1997. Molecular identification of a dopamine D1b receptor in bovine retinal pigment epithelium. *Neurosci. Lett.,* 237(1):9-12.

Veruki and Wässle, 1996. Immunohistochemical localization of dopamine D1 receptors in rat retina. *Eur. J. Neurosci.,* 8(11):2286-2297.

Veruki, 1997. Dopaminergic neurons in the rat retina express dopamine D2/3 receptors. *Eur. J. Neurosci.,* 9(5):1096-1100.

Voigt and Wässle, 1987. Dopaminergic innervation of AII amacrine cells in mammalian retina. *J. Neurosci.*, 7(12):4115-4128.

Völgyi *et al.*, 2005. Morphology and tracer coupling pattern of alpha ganglion cells in the mouse retina. *J. Comp. Neurol.,* 492(1):66-77.

Völgyi *et al.*, 2009. Tracer coupling patterns of the ganglion cell subtypes in the mouse retina. *J. Comp. Neurol.,* 512(5):664-687.

Völgyi *et al.*, 2014. Compartment-specific tyrosine hydroxylase positive innervation to AII amacrine cells in the rabbit retina. *Neuroscience.*, 270:88-97.

Wagner *et al.*, 1993. Localization of D2 dopamine receptors in vertebrate retinae with anti-peptide antibodies. *J. Comp. Neurol.,* 331(4):469-481.

Wang *et al.*, 1997. Endogenous activation of dopamine D2 receptors regulates dopamine release in the fish retina. *J. Neurophysiol.,* 78(1):439-449.

Warrier *et al.*, 2005. Calcium from internal stores triggers GABA release from retinal amacrine cells. *J. Neurophysiol.*, 94(6):4196-4208.

Wässle and Boycott, 1991. Functional architecture of the mammalian retina. *Physiol. Rev.,* 71(2):447-480.

Wässle *et al.*, 1986. Analysis of a glycinergic inhibitory pathway in the cat retina. *J. Neurosci.*, 6(2):594-604.

Wässle *et al.*, 2009. Cone contacts, mosaics, and territories of bipolar cells in the mouse retina. *J. Neurosci.*, 29(1):106-117.

Wässle, 2004. Parallel processing in the mammalian retina. *Nat. Rev. Neurosci.*, 5(10):747-757.

Wellis and Werblin, 1995. Dopamine modulates $GABA_C$ receptors mediating inhibition of calcium entry into and transmitter release from bipolar cell terminals in tiger salamander retina. *J. Neurosci.*, 15(7):4748-4761.

Wiechmann and Sherry, 2013. Role of melatonin and its receptors in the vertebrate retina. *Int. Rev. Cell. Mol. Biol.*, 300:211-242.

Witkovsky *et al.*, 2007. Cellular localization and function of DARPP-32 in the rodent retina. *Eur. J. Neurosci.,* 25(11):3233-3242.

Witkovsky *et al.*, 2008. Anatomical and neurochemical characterization of dopaminergic interplexiform processes in mouse and rat retinas. *J. Comp. Neurol.,* 510(2):158-174.

Witkovsky, 2004. Dopamine and retinal function. *Doc. Ophthalmol.,* 108(1):17-40.

Wolf *et al.*, 2003. Mechanisms by which dopamine receptors may influence synaptic plasticity. *Ann. NY Acad. Sci.,* 1003:241-249.

Wu *et al.*, 2006. Adeno-associated virus serotypes: Vector toolkit for human gene therapy. *Mol. Ther.*, 14(3):316-327.

Wulle and Schnitzer, 1989. Distribution and morphology of tyrosine hydroxylase-immunoreactive neurons in the developing mouse retina. *Dev. Brain Res.,* 48(1):59-72.

Xu *et al.*, 2002. Expression of voltage-dependent calcium channel subunits in the rat retina. *Neurosci. Lett.,* 329(3):297-300.

Yeh *et al.*, 1984. Dopamine regulates synaptic transmission mediated by cholinergic neurons of the rat retina. *Neurosci.*, 13(3):901:909.

Yuste, 2005. Imaging in neuroscience and development: A laboratory manual. CSHL Press. Chapter 31: Fritjof Helmchen. Calibration of fluorescent calcium indicators.

Zhang *et al.*, 2001. Genetically encoded reporters of protein kinase A activity reveal impact of substrate tethering. *Proc. Natl. Acad. Sci. USA,* 98(26):14997-15002.

Zhang *et al.*, 2004. Characterization of genetically labeled catecholamine neurons in the mouse retina. *NeuroReport*, 15(11):1761-1765.

Zhang *et al.*, 2011. Light- and dopamine-regulated receptive field plasticity in primate horizontal cells. *J. Comp. Neurol.,* 519(11):2125-2134.

Zhang *et al.*, 2012. The most numerous ganglion cell type of the mouse retina is a selective feature detector. *Proc. Natl. Acad. Sci. USA*. 109(36):E2391-2398.

Zhao, 2015. Towards monitoring nitric oxide mediated cGMP metabolism in mouse retinal neurons using a FRET-based genetically encoded sensor. Doktorarbeit am ICS-4 (FZ-Jülich) in der AG-Müller.

Zhong *et al.*, 2013. Potassium ion channels in retinal ganglion cells. *Mol. Med. Rep.*, 8(2):311-319.

Zühlke *et al.*, 1999. Calmodulin supports both inactivation and facilitation of L-type calcium channels. *Nature*, 399(6732):159-162.

Appendix

Internet source fig. 1.2.4

Scotopic: https://jumk.de/blog/1.jpg (10.04.16)

Mesopic: http://natur-photocamp.de/wp-content/uploads/2013/05/TB019045_1100.jpg (10.04.16)

Photopic: http://oekotherm-daemm.info/wordpress/wp-content/uploads/2013/09/4bc72f9683729Sonne.jpg (10.04.16)

Sequence pcTH-EGFP

aattctgcagtcgacggtaccgcgggcccgggatccaccggtcgccaccatggtgagcaagggcgaggagctgttcaccgggg
tggtgcccatcctggtcgagctggacggcgacgtaaacggccacaagttcagcgtgtccggcgagggcgagggcgatgccacc
tacggcaagctgaccctgaagttcatctgcaccaccggcaagctgcccgtgccctggcccaccctcgtgaccaccctgacctac
ggcgtgcagtgcttcagccgctaccccgaccacatgaagcagcacgacttcttcaagtccgccatgcccgaaggctacgtccag
gagcgcaccatcttcttcaaggacgacggcaactacaagacccgcgccgaggtgaagttcgagggcgacaccctggtgaaccg
catcgagctgaagggcatcgacttcaaggaggacggcaacatcctggggcacaagctggagtacaactacaacagccacaac
gtctatatcatggccgacaagcagaagaacggcatcaaggtgaacttcaagatccgccacaacatcgaggacggcagcgtgc
agctcgccgaccactaccagcagaacaccccccatcggcgacggccccgtgctgctgcccgacaaccactacctgagcacccag
tccgccctgagcaaagaccccaacgagaagcgcgatcacatggtcctgctggagttcgtgaccgccgccgggatcactctcggc
atggacgagctgtacaagtaaagcggccgcgactctagatcataatcagccataccacatttgtagaggttttacttgctttaaa
aaacctcccacacctccccctgaacctgaaacataaaatgaatgcaattgttgttgttaacttgtttattgcagcttataatggtta
caaataaagcaatagcatcacaaatttcacaaataaagcatttttttcactgcattctagttgtggtttgtccaaactcatcaatgt
atcttaagtttaaaccgctgatcagcctcgactgtgccttctagttgccagccatctgttgtttgcccctcccccgtgccttccttgac
cctggaaggtgccactcccactgtcctttcctaataaaatgaggaaattgcatcgcattgtctgagtaggtgtcattctattctggg
gggtggggtggggcaggacagcaagggggaggattgggaagacaatagcaggcatgctggggatgcggtgggctctatggc
ttctgaggcggaaagaaccagctggggctctagggggtatccccacgcgccctgtagcggcgcattaagcgcggcgggtgtgg
tggttacgcgcagcgtgaccgctacacttgccagcgccctagcgcccgctcctttcgctttcttcccttcctttctcgccacgttcgc
cggctttccccgtcaagctctaaatcgggggctcccttagggttccgatttagtgctttacggcacctcgaccccaaaaaacttg
attagggtgatggttcacgtagtgggccatcgccctgatagacggtttttcgccctttgacgttggagtccacgttctttaatagtg
gactcttgttccaaactggaacaacactcaaccctatctcggtctattcttttgatttataagggattttgccgatttcggcctattgg
ttaaaaaatgagctgatttaacaaaaatttaacgcgaattaattctgtggaatgtgtgtcagttagggtgtggaaagtccccagg
ctccccagcaggcagaagtatgcaaagcatgcatctcaattagtcagcaaccaggtgtggaaagtccccaggctccccagcag
gcagaagtatgcaaagcatgcatctcaattagtcagcaaccatagtcccgcccctaactccgcccatcccgcccctaactccgcc
cagttccgcccattctccgccccatggctgactaatttttttatttatgcagaggccgaggccgcctctgcctctgagctattccag

aagtagtgaggaggctttttggaggcctaggcttttgcaaaaagctcccgggagcttgtatatccattttcggatctgatcaaga
gacaggatgaggatcgtttcgcatgattgaacaagatggattgcacgcaggttctccggccgcttgggtggagaggctattcgg
ctatgactgggcacaacagacaatcggctgctctgatgccgccgtgttccggctgtcagcgcaggggcgcccggttctttttgtca
agaccgacctgtccggtgccctgaatgaactgcaggacgaggcagcgcggctatcgtggctggccacgacgggcgttccttgc
gcagctgtgctcgacgttgtcactgaagcgggaagggactggctgctattgggcgaagtgccggggcaggatctcctgtcatct
caccttgctcctgccgagaaagtatccatcatggctgatgcaatgcggcggctgcatacgcttgatccggctacctgcccattcga
ccaccaagcgaaacatcgcatcgagcgagcacgtactcggatggaagccggtcttgtcgatcaggatgatctggacgaagagc
atcaggggctcgcgccagccgaactgttcgccaggctcaaggcgcgcatgcccgacggcgaggatctcgtcgtgacccatggc
gatgcctgcttgccgaatatcatggtggaaaatggccgcttttctggattcatcgactgtggccggctgggtgtggcggaccgcta
tcaggacatagcgttggctacccgtgatattgctgaagagcttggcggcgaatgggctgaccgcttcctcgtgctttacggtatcg
ccgctcccgattcgcagcgcatcgccttctatcgccttcttgacgagttcttctgagcgggactctggggttcgaaatgaccgacc
aagcgacgcccaacctgccatcacgagatttcgattccaccgccgccttctatgaaaggttgggcttcggaatcgttttccggga
cgccggctggatgatcctccagcgcggggatctcatgctggagttcttcgcccaccccaacttgtttattgcagcttataatggtta
caaataaagcaatagcatcacaaatttcacaaataaagcatttttttcactgcattctagttgtggtttgtccaaactcatcaatgt
atcttatcatgtctgtataccgtcgacctctagctagagcttggcgtaatcatggtcatagctgtttcctgtgtgaaattgttatccg
ctcacaattccacacaacatacgagccggaagcataaagtgtaaagcctggggtgcctaatgagtgagctaactcacattaatt
gcgttgcgctcactgcccgctttccagtcgggaaacctgtcgtgccagctgcattaatgaatcggccaacgcgcggggagaggc
ggtttgcgtattgggcgctcttccgcttcctcgctcactgactcgctgcgctcggtcgttcggctgcggcgagcggtatcagctcac
tcaaaggcggtaatacggttatccacagaatcaggggataacgcaggaaagaacatgtgagcaaaaggccagcaaaaggcc
aggaaccgtaaaaaggccgcgttgctggcgtttttccataggctccgccccctgacgagcatcacaaaaatcgacgctcaagt
cagaggtggcgaaacccgacaggactataaagataccaggcgtttcccccctggaagctccctcgtgcgctctcctgttccgacc
ctgccgcttaccggatacctgtccgcctttctcccttcgggaagcgtggcgctttctcatagctcacgctgtaggtatctcagttcg
gtgtaggtcgttcgctccaagctgggctgtgtgcacgaacccccgttcagcccgaccgctgcgccttatccggtaactatcgtct
tgagtccaacccggtaagacacgacttatcgccactggcagcagccactggtaacaggattagcagagcgaggtatgtaggcg
gtgctacagagttcttgaagtggtggcctaactacggctacactagaagaacagtatttggtatctgcgctctgctgaagccagtt
accttcggaaaaagagttggtagctcttgatccggcaaacaaaccaccgctggtagcggttttttgtttgcaagcagcagattac
gcgcagaaaaaaaggatctcaagaagatcctttgatcttttctacggggtctgacgctcagtggaacgaaaactcacgttaagg
gattttggtcatgagattatcaaaaaggatcttcacctagatccttttaaattaaaaatgaagttttaaatcaatctaaagtatatat
gagtaaacttggtctgacagttaccaatgcttaatcagtgaggcacctatctcagcgatctgtctatttcgttcatccatagttgcct
gactccccgtcgtgtagataactacgatacgggagggcttaccatctggccccagtgctgcaatgataccgcgagacccacgct
caccggctccagatttatcagcaataaaccagccagccggaagggccgagcgcagaagtggtcctgcaactttatccgcctcca
tccagtctattaattgttgccgggaagctagagtaagtagttcgccagttaatagtttgcgcaacgttgttgccattgctacaggca
tcgtggtgtcacgctcgtcgtttggtatggcttcattcagctccggttcccaacgatcaaggcgagttacatgatcccccatgttgt
gcaaaaaagcggttagctccttcggtcctccgatcgttgtcagaagtaagttggccgcagtgttatcactcatggttatggcagca

ctgcataattctcttactgtcatgccatccgtaagatgcttttctgtgactggtgagtactcaaccaagtcattctgagaatagtgta
tgcggcgaccgagttgctcttgcccggcgtcaatacgggataataccgcgccacatagcagaactttaaaagtgctcatcattgg
aaaacgttcttcggggcgaaaactctcaaggatcttaccgctgttgagatccagttcgatgtaacccactcgtgcacccaactga
tcttcagcatcttttactttcaccagcgtttctgggtgagcaaaaacaggaaggcaaaatgccgcaaaaaagggaataagggcg
acacggaaatgttgaatactcatactcttccttttcaatattattgaagcatttatcagggttattgtctcatgagcggatacatatt
tgaatgtatttagaaaaataaacaaatagggttccgcgcacatttccccgaaaagtgccacctgacgtcgacggatcgggaga
tctcccgatcccctatggtgcactctcagtacaatctgctctgatgccgcatagttaagccagtatctgctccctgcttgtgtgttgg
aggtcgctgagtagtgcgcgagcaaaatttaagctacaacaaggcaaggcttgaccgacaattgcatgaagaatctgcttagg
gttaggcgttttgcgctgcttcgcgatgtacgggccagatatacgcgtggcgtctccttagagatgtcttcttcagcctcccagggt
cctccacactggacaggtgggccctcctgggacattctggaccccacggggcgagcttgggaagccgctgcaagggccacacc
tgcagggcccgggggctgtgggcagatggcactcctaggaaccacgtctatgagacacacggcctggaatcttctggagaagc
aaacaaattgcctcctgacatctgaggctggaggctggattccccgtcttggggctttctgggtcggtctgccacgaggttctggt
gttcattaaaagtgtgcccctgggctgccagaaagcccctccctgtgtgctctcttgagggctgtggggccaaggggaccctggc
tgtctcagccccccgcagagcacgagcccctggtccccgcaagcccgcgggctgaggatgattcagacagggctggggagtga
aggcaattagattccacggacgagccctttctcctgcgcctccctccttcctcacccacccccgcctccatcaggcacagcaggc
aggggtgggggatgtaaggaggggaaggtgggggacccagagggggctttgacgtcagctcagcttataagaggctgctggg
ccagggctgtggagacggagcccggacctccacactgagccatgcccacccccgacgccaccacgccacaggccaagggctt
ccgcagggccgtgtctgagctggacgccaagcaggcagaggccatcatggtaagagtctagactcgagcggccgccactgtgc
tggatatctgcag

Vector map pcTH-EGFP

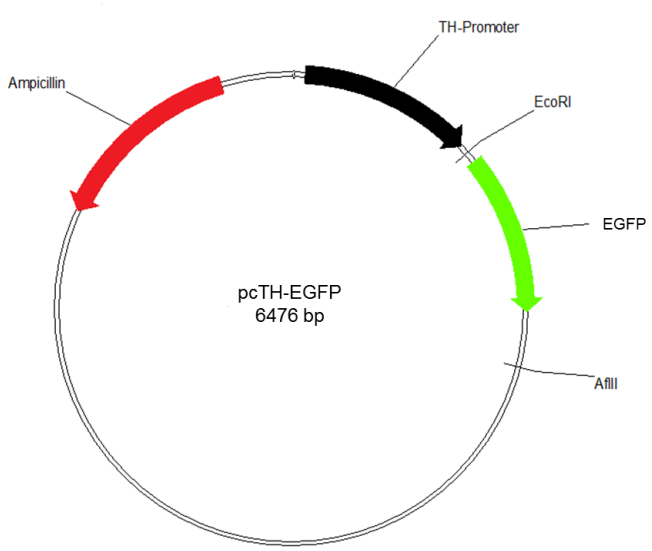

Ampicillin: Ampicillin resistance; EGFP: enhanced GFP; restriction enzymes (*Eco*RI, *Afl*II) are indicated in black.

Sequence pcTH-SynpH

ctagaggatccatgtcggctaccgctgccaccgtcccgcctgccgccccggccggcgagggtggccccccctgcacctcctccaa
accttactagtaacaggagactgcagcagacccaggcccaggtggatgaggtggtggacatcatgagggtgaatgtggacaa
ggtcctggagcgggaccagaagttgtcggagctggatgaccgtgcagatgccctccaggcaggggcctcccagtttgaaacaa
gtgcagccaagctcaagcgcaaatactggtggaaaaacctcaagatgatgatcatcttgggagtgatctgcgccatcatcctcat
catcatcatcgtttacttcagcactagcggcggaagcggcgggaccggtggaagtaaaggagaagaacttttcactggagttgt
cccaattcttgttgaattagatggtgatgttaatgggcacaaattttctgtcagtggagagggtgaaggtgatgcaacatacgga
aaacttacccttaaatttatttgcactactggaaaactacctgttccttggccaacacttgtcactactttaacttatggtgttcaatg
cttttcaagatacccagatcatatgaaacggcatgactttttcaagagtgccatgcccgaaggttatgtacaggaaagaactata
tttttcaaagatgacgggaactacaagacacgtgctgaagtcaagtttgaaggtgatacccttgttaatagaatcgagttaaaag
gtattgattttaaagaagatggaaacattcttggacacaaattggaatacaactataacgatcaccaggtgtacatcatggcaga
caaacaaaagaatggaatcaaagctaacttcaaaattagacacaacattgaagatggaggcgttcaactagcagaccattatc
aacaaaatactccaattggcgatgggcccgtccttttaccagacaaccattacctgtttacaacttctactctttcgaaagatccca
acgaaaagagagaccacatggtccttcttgagtttgtaacagctgctgggattacacatggcatggatgaactatacaaaaccg
ggtaactcgagcggccgccactgtgctggatatctgcagaattccaccacactggactagtggatccgagctcggtaccaagctt
aagtttaaaccgctgatcagcctcgactgtgccttctagttgccagccatctgttgtttgcccctcccccgtgccttccttgaccctg
gaaggtgccactcccactgtcctttcctaataaaatgaggaaattgcatcgcattgtctgagtaggtgtcattctattctgggggggt
ggggtggggcaggacagcaagggggaggattgggaagacaatagcaggcatgctggggatgcggtgggctctatggcttctg
aggcggaaagaaccagctggggctctagggggtatccccacgcgccctgtagcggcgcattaagcgcggcgggtgtggtggtt
acgcgcagcgtgaccgctacacttgccagcgccctagcgcccgctcctttcgctttcttcccttcctttctcgccacgttcgccggct
ttccccgtcaagctctaaatcgggggctccctttagggttccgatttagtgctttacggcacctcgaccccaaaaaacttgattag
ggtgatggttcacgtagtgggccatcgccctgatagacggtttttcgccctttgacgttggagtccacgttctttaatagtggactc
ttgttccaaactggaacaacactcaaccctatctcggtctattcttttgatttataagggattttgccgatttcggcctattggttaaa
aaatgagctgatttaacaaaaatttaacgcgaattaattctgtggaatgtgtgtcagttagggtgtggaaagtccccaggctccc
cagcaggcagaagtatgcaaagcatgcatctcaattagtcagcaaccaggtgtggaaagtccccaggctccccagcaggcaga
agtatgcaaagcatgcatctcaattagtcagcaaccatagtcccgccccctaactccgcccatcccgcccctaactccgcccagtt
ccgcccattctccgccccatggctgactaatttttttttatttatgcagaggccgaggccgcctctgcctctgagctattccagaagt
agtgaggaggcttttttggaggcctaggcttttgcaaaaagctcccgggagcttgtatatccattttcggatctgatcaagagaca
ggatgaggatcgtttcgcatgattgaacaagatggattgcacgcaggttctccggccgcttgggtggagaggctattcggctatg
actgggcacaacagacaatcggctgctctgatgccgccgtgttccggctgtcagcgcaggggcgcccggttctttttgtcaagac
cgacctgtccggtgccctgaatgaactgcaggacgaggcagcgcggctatcgtggctggccacgacgggcgttccttgcgcag
ctgtgctcgacgttgtcactgaagcgggaagggactggctgctattgggcgaagtgccggggcaggatctcctgtcatctcacct
tgctcctgccgagaaagtatccatcatggctgatgcaatgcggcggctgcatacgcttgatccggctacctgcccattcgaccac
caagcgaaacatcgcatcgagcgagcacgtactcggatggaagccggtcttgtcgatcaggatgatctggacgaagagcatca

ggggctcgcgccagccgaactgttcgccaggctcaaggcgcgcatgcccgacggcgaggatctcgtcgtgacccatggcgatg
cctgcttgccgaatatcatggtggaaaatggccgcttttctggattcatcgactgtggccggctgggtgtggcggaccgctatcag
gacatagcgttggctacccgtgatattgctgaagagcttggcggcgaatgggctgaccgcttcctcgtgctttacggtatcgccgc
tcccgattcgcagcgcatcgccttctatcgccttcttgacgagttcttctgagcgggactctggggttcgaaatgaccgaccaagc
gacgcccaacctgccatcacgagatttcgattccaccgccgccttctatgaaaggttgggcttcggaatcgttttccgggacgcc
ggctggatgatcctccagcgcggggatctcatgctggagttcttcgcccaccccaacttgtttattgcagcttataatggttacaaa
taaagcaatagcatcacaaatttcacaaataaagcatttttttcactgcattctagttgtggtttgtccaaactcatcaatgtatctt
atcatgtctgtataccgtcgacctctagctagagcttggcgtaatcatggtcatagctgtttcctgtgtgaaattgttatccgctcac
aattccacacaacatacgagccggaagcataaagtgtaaagcctggggtgcctaatgagtgagctaactcacattaattgcgtt
gcgctcactgcccgctttccagtcgggaaacctgtcgtgccagctgcattaatgaatcggccaacgcgcggggagaggcggttt
gcgtattgggcgctcttccgcttcctcgctcactgactcgctgcgctcggtcgttcggctgcggcgagcggtatcagctcactcaa
aggcggtaatacggttatccacagaatcaggggataacgcaggaaagaacatgtgagcaaaaggccagcaaaaggccagga
accgtaaaaaggccgcgttgctggcgtttttccataggctccgccccccctgacgagcatcacaaaaatcgacgctcaagtcaga
ggtggcgaaacccgacaggactataaagataccaggcgtttcccccctggaagctccctcgtgcgctctcctgttccgaccctgcc
gcttaccggatacctgtccgcctttctcccttcgggaagcgtggcgctttctcatagctcacgctgtaggtatctcagttcggtgta
ggtcgttcgctccaagctgggctgtgtgcacgaaccccccgttcagcccgaccgctgcgccttatccggtaactatcgtcttgagt
ccaacccggtaagacacgacttatcgccactggcagcagccactggtaacaggattagcagagcgaggtatgtaggcggtgct
acagagttcttgaagtggtggcctaactacggctacactagaagaacagtatttggtatctgcgctctgctgaagccagttacctt
cggaaaaagagttggtagctcttgatccggcaaacaaaccaccgctggtagcggtttttttgtttgcaagcagcagattacgcgc
agaaaaaaaggatctcaagaagatcctttgatcttttctacggggtctgacgctcagtggaacgaaaactcacgttaagggattt
tggtcatgagattatcaaaaaggatcttcacctagatccttttaaattaaaaatgaagttttaaatcaatctaaagtatatatgagt
aaacttggtctgacagttaccaatgcttaatcagtgaggcacctatctcagcgatctgtctatttcgttcatccatagttgcctgact
ccccgtcgtgtagataactacgatacgggagggcttaccatctggccccagtgctgcaatgataccgcgagacccacgctcacc
ggctccagatttatcagcaataaaccagccagccggaagggccgagcgcagaagtggtcctgcaactttatccgcctccatcca
gtctattaattgttgccgggaagctagagtaagtagttcgccagttaatagtttgcgcaacgttgttgccattgctacaggcatcgt
ggtgtcacgctcgtcgtttggtatggcttcattcagctccggttcccaacgatcaaggcgagttacatgatcccccatgttgtgcaa
aaaagcggttagctccttcggtcctccgatcgttgtcagaagtaagttggccgcagtgttatcactcatggttatggcagcactgc
ataattctcttactgtcatgccatccgtaagatgcttttctgtgactggtgagtactcaaccaagtcattctgagaatagtgtatgcg
gcgaccgagttgctcttgcccggcgtcaatacgggataataccgcgccacatagcagaactttaaaagtgctcatcattggaaa
acgttcttcggggcgaaaactctcaaggatcttaccgctgttgagatccagttcgatgtaacccactcgtgcacccaactgatctt
cagcatcttttactttcaccagcgtttctgggtgagcaaaaacaggaaggcaaaatgccgcaaaaaagggaataagggcgaca
cggaaatgttgaatactcatactcttccttttcaatattattgaagcatttatcagggttattgtctcatgagcggatacatatttga
atgtatttagaaaaataaacaaatagggttccgcgcacatttccccgaaaagtgccacctgacgtcgacggatcgggagatct
cccgatcccctatggtgcactctcagtacaatctgctctgatgccgcatagttaagccagtatctgctccctgcttgtgtgttggag

gtcgctgagtagtgcgcgagcaaaatttaagctacaacaaggcaaggcttgaccgacaattgcatgaagaatctgcttagggtt
aggcgttttgcgctgcttcgcgatgtacgggccagatatacgcgtggcgtctccttagagatgtcttcttcagcctcccagggtcct
ccacactggacaggtgggccctcctgggacattctggaccccacggggcgagcttgggaagccgctgcaagggccacacctgc
agggcccgggggctgtgggcagatggcactcctaggaaccacgtctatgagacacacggcctggaatcttctggagaagcaaa
caaattgcctcctgacatctgaggctggaggctggattccccgtcttggggctttctgggtcggtctgccacgaggttctggtgttc
attaaaagtgtgcccctgggctgccagaaagcccctccctgtgtgctctcttgagggctgtggggccaaggggaccctggctgtc
tcagccccccgcagagcacgagcccctggtccccgcaagcccgcgggctgaggatgattcagacagggctggggagtgaagg
caattagattccacggacgagccctttctcctgcgcctccctccttcctcacccacccccgcctccatcaggcacagcaggcagg
ggtgggggatgtaaggaggggaaggtgggggacccagagggggctttgacgtcagctcagcttataagaggctgctgggcca
gggctgtggagacggagcccggacctccacactgagccatgcccacccccgacgccaccacgccacaggccaagggcttccg
cagggccgtgtctgagctggacgccaagcaggcagaggccatcatggtaagagt

Vector map pcTH-SynpH

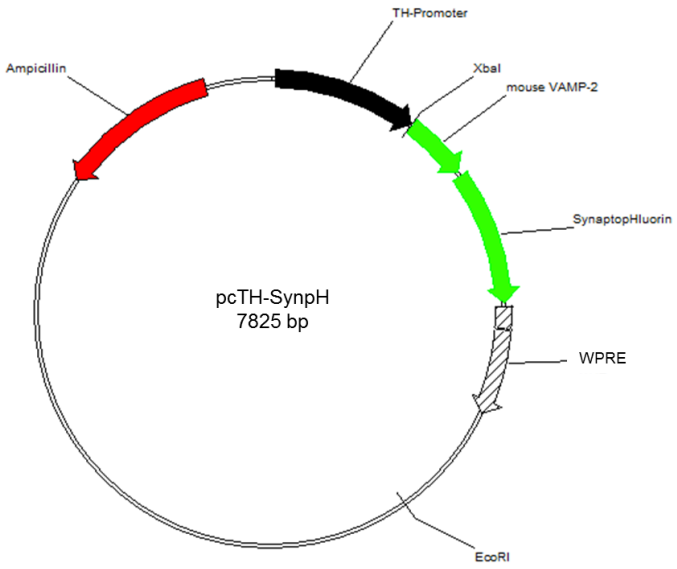

Ampicillin: Ampicillin resistance; WPRE: Woodchuck hepatitis virus (WHP) posttranscriptional regulatory element; restriction enzymes (*Xba*I, *Eco*RI) are indicated in black.

Acknowledgements

Zunächst möchte ich mich bei Herrn Prof. Dr. Frank Müller für die Überlassung des spannenden Themas, die konstruktiven Diskussionen und die gute wissenschaftliche Betreuung bedanken.

Ich danke Herrn Prof. Dr. Marc Spehr für die Übernahme des Zweitgutachtens und Herrn Prof. Dr. Björn Kampa für die Übernahme der Drittprüfer-Funktion.

Ich bedanke mich bei Herrn Prof. Dr. Arnd Baumann und seiner Arbeitsgruppe für die Bereitstellung der Viren.

Mein Dank gilt weiterhin Herrn Prof. Dr. Lohse für die Bereitstellung der CAG-EPAC1-camps transgenen Mäusen zur Entnahme von Gewebeproben.

Weiterer Dank gilt Christoph Aretzweiler, für die Hilfe bei allen erdenklichen Problemen im Labor und beim Erlernen der Immunhistochemie. Arne Franzen danke ich für die Unterstützung bei der Durchführung meines molekularbiologischen Projekts. Desweiteren danke ich Nadine Jordan für ihr gutes Auge bei der Formatierungs-Rechtschreibfehler-Korrektur meiner Arbeit. Ich bedanke mich bei Rudolf (Rudi) Esser für die Verpflegung, sowie die kleinen und großen Späßchen, die wir gemeinsam hatten.

Außerdem bedanke ich mich bei allen Kollegen des ICS-4 für die große Hilfsbereitschaft und die angenehme Arbeitsatmosphäre.

Weiterhin möchte ich mich bei den Beteiligten des „Optogenetics Meetings“ für das Interesse am Fortschritt meiner Arbeit und die hilfreichen Diskussionen bedanken.

Ich danke Dr. Zhijian Zhao für die Unterstützung zu Beginn meiner Arbeit und dafür, dass er mir die chinesische Kultur näher gebracht hat. Ich danke auch Safaa Belaidi, für die gute Zusammenarbeit und die intensiven Gespräche.

Ich bedanke mich ganz herzlich bei Verena Untiet und Rachel Conrad dafür, dass sie als Freundinnen mit mir gelacht, geweint und gearbeitet haben.

Aus tiefstem Herzen bedanke ich mich bei meiner Schwester, meinen Eltern und meinem Freund dafür, dass sie mir immer das Gefühl geben für mich da zu sein, dass sie sich mit mir über jeden kleinen Erfolg freuen, mir Kraft geben, wenn ich selbst mal wenig habe. Danke!

Hiermit erkläre ich, dass ich die hier vorliegende Doktorarbeit selbstständig verfasst habe. Es wurden keine anderen als die in der Arbeit angegebenen Quellen und Hilfsmittel benutzt. Die wörtlichen oder sinngemäß übernommenen Zitate habe ich als solche kenntlich gemacht.

_____ _____

Ort, Datum Unterschrift